



THE UNIVERSITY OF SHEFFIELD

DEPT OF HUMAN METABOLISM, SCHOOL OF MEDICINE & BIOMEDICAL SCIENCES

INVESTIGATING THE ANTI-TUMOUR EFFECTS OF ZOLEDRONIC ACID IN MULTIPLE MYELOMA IN VIVO

DR JAYADEVAN GURUBALAN

2013

ACKNOWLEDGEMENTS

“எந்நன்றி கொன்றார்க்கும் உய்வுண்டாம் உய்வில்லை

செய்ந்நன்றி கொன்ற மகற்கு”

-திருவள்ளுவர்

“For him who's killed all good, escape may be;

But none for him who's killed a kindness done”.

-Thiruvalluvar

I'm in debt of gratitude to **Prof Peter Croucher** for the opportunity to do a PhD under his guidance and supervision. I would like to express my immense thankfulness for the mentoring over the last three years, for teaching me several laboratory techniques, scientific thinking and the trust which made me complete this huge piece of work. I would also like to extend my thanks to **Dr Michelle Anne Lawson** for her guidance in everyday lab work and training me in various laboratory techniques. Also, thanks for the moral support you gave me whenever I needed it. I would also like to extend my special thanks to **Dr Colby L Eaton** for his huge support and guidance which shaped this thesis work.

I would like to thank **Dr Colin Gray**, Core facilities, the University of Sheffield for teaching multiphoton microscopy. I would also like to thank **Dr Allan J Williams** for his help in the field labs. I would like to thank the members of the bone analysis lab **Orla Gallagher, Julia Hough, Holly Evans, Darren Lath and Julie** for their help in histology tissue sectioning and processing. I would like to thank **Dr Leslie Coulton** who not only taught me microCT, but also patiently answered several questions. I would also like to thank the members of flow cytometry core facility **Sue Newton and Kay Hopkinson**. I would like to extend my thanks to **Beka Armstrong** and **Rachel Rodham**, University of Sheffield Field laboratory. I would like to thank **Dr Christopher J Hill**, Electron Microscopy Unit, and Biomedical Sciences. I would like to thank my friends **Dr Clive Buckle** and **Juhi Misra** for their continuous moral support. Finally, I would like to thank my mentor **Dr Ilaria Bellantuono** for mentoring me throughout my Ph.D.

DECLARATION

The work presented in this thesis was carried out by the candidate, with the following exceptions:

Processing of tissue samples for histology was done by **Ms Orla Gallagher, Ms Julia Hough & Mr Darren Lath**, Research Technicians, Mellanby Centre for Bone Research, Sheffield.

Computerised Image Analysis technique for osteolytic lesion detection was designed by **Ms Holly Evans**, Research Technician, Mellanby Centre for Bone Research, Sheffield.

CD138 immunohistochemistry staining protocol for bone was optimised by **Ms Julia Hough**, Research Technician, Mellanby Centre for Bone Research, Sheffield.

Fluorescent activated cell sorting was done by **Mrs Sue Newton and Mrs Kay Hopkinson**, Core Facilities, University of Sheffield.

SUMMARY

Multiple myeloma remains an incurable disease due to the failure of currently available chemotherapies to eradicate all the tumour cells from bone. Tumour cells alter the processes of bone resorption and bone formation to promote the development of osteolytic bone disease. Targeting osteoclastic bone resorption with bisphosphonates, including zoledronic acid has been shown to be effective in preventing tumour-induced bone disease. In addition to preventing bone disease, there is increasing evidence to suggest that altering the bone microenvironment by inhibiting osteoclastic bone resorption reduces tumour burden in bone. However, the mechanisms responsible are not clear. In order to develop effective therapeutic strategies, it is essential to understand the interactions between tumour cells and the bone microenvironment during disease progression from single tumour cells that home to the bone to the development of overt tumour colonies.

In order to characterise the interactions between tumour cells and the bone microenvironment, an *in vivo* murine model of myeloma was utilised by injecting 5TGM1 murine myeloma cells expressing eGFP and labelled with DID into C57BL/KaLwRij mice. Data presented in this thesis show myeloma cells engrafted in the bone as early as 3 days and formed colonies after 10 days post tumour cell injection. Tumour-induced alterations in bone remodelling occurred only at the end-stage of the disease when the mice showed signs of clinical illness. However, development of osteolytic lesions occurred as early as 10 days post tumour cell injection prior to an increase in osteoclast numbers and serum TRACP5b levels or a decrease in osteoblast numbers and serum P1NP levels. Furthermore, this is the first study to identify a subpopulation of quiescent myeloma cells in proximity to bone which suggests the existence of specific niches, which may render cells dormant. However, this warrants further investigation.

Treatment studies showed that early initiation of zoledronic acid treatment (125 µg/kg, subcutaneously, twice-weekly) prior to tumour cell injection is effective not only at inhibiting the development of osteolytic lesions but also at inhibiting the late stage tumour burden in bone. Interestingly, treatment started prior or after tumour cell injection did not affect myeloma colony formation suggesting that the process of expansion from single cells to colonies is not reliant on a so called ‘vicious cycle’ in the 5TGM1 murine model of myeloma. In a separate experiment, zoledronic acid treatment started prior or at the time of tumour cell injection demonstrated a significant increase in disease-free survival when compared with untreated controls (24 vs. 21 days).

Taken together, the data presented in this thesis demonstrate that zoledronic acid treatment, in the 5TGM1 murine model of myeloma started prior to tumour cell arrival in bone is not only able to prevent the development of bone disease but also reduce tumour burden and increase disease-free survival.

CONTENTS

ACKNOWLEDGEMENTS	I
DECLARATION	II
SUMMARY	III
LIST OF FIGURES.....	VIII
ABBREVIATIONS.....	XII
CHAPTER 1 GENERAL INTRODUCTION	1
1.1 MULTIPLE MYELOMA (MM)	2
1.1.1 MYELOMA AETIOPATHOGENESIS & CLINICAL MANIFESTATIONS.....	3
1.2 BIOLOGY OF MULTIPLE MYELOMA	4
1.2.1 NORMAL PLASMA CELL AND MYELOMA CELL DEVELOPMENT.....	4
1.3 STAGES OF MULTIPLE MYELOMA DEVELOPMENT.....	5
1.3.1 MGUS AND SMOLDERING MULTIPLE MYELOMA (SMM).....	6
1.3.2 INTRAMEDULLARY MYELOMA	7
1.3.3 MULTIPLE MYELOMA AND THE BONE MARROW MICROENVIRONMENT	8
1.3.4 MYELOMA BONE DISEASE.....	12
1.3.5 MULTIPLE MYELOMA WITH EXTRAMEDULLARY DISEASE (EMD).....	13
1.4 THE USE OF BISPHOSPHONATES IN MYELOMA MANAGEMENT	14
1.4.1 ZOLEDRONIC ACID (ZA).....	15
1.4.2 ANTI-RESORPTIVE MECHANISM OF ZA.....	15
1.5 THE ANTI-MYELOMA EFFECT OF ZOLEDRONIC ACID.....	17
1.5.1 IN VITRO EVIDENCE OF AN ANTI-MYELOMA EFFECT OF ZA.....	17
1.5.2 PRE-CLINICAL EVIDENCE OF AN ANTI-MYELOMA EFFECT OF ZA	18
1.5.3 EVIDENCE OF AN ANTI-MYELOMA EFFECT OF ZA IN CLINICAL TRAILS.....	18
1.5.4 THE MECHANISMS OF AN ANTI-MYELOMA EFFECT BY ZA.....	19
1.6 AIMS AND OBJECTIVES	25
CHAPTER 2 MATERIALS & METHODS	26
2.1 MATERIALS.....	27

2.1.1 ZOLEDRONIC ACID (ZA)	27
2.1.2 THE 5TGM1 MURINE MYELOMA CELL LINE	27
2.1.3 C57BL/KALWRIJ MICE.....	27
2.2 GENERAL METHODS	28
2.2.1 CELL CULTURE.....	28
2.2.2 CRYOPRESERVATION AND RESUSCITATION OF CELL LINES	28
2.2.3 CELL COUNTING USING A HAEMOCYTOMETER.....	28
2.2.4 DID LABELLING OF 5TMM CELLS.....	29
2.2.5 DETECTION OF FLUORESCENTLY LABELLED 5TGM1 MURINE MYELOMA CELLS (<i>IN VITRO</i>) USING FLOW CYTOMETRY	30
2.2.6 DETECTION OF FLUORESCENTLY LABELLED 5TGM1 MURINE MYELOMA CELLS IN BONE MARROW (EX VIVO) USING FLOW CYTOMETRY.....	31
2.2.7 SORTING OF 5TGM1-EGFP-DID LABELLED CELLS.....	31
2.2.8 INJECTION OF 5TGM1 CELLS INTO MICE UNDER LOCAL ANAESTHESIA.....	32
2.2.9 BLOOD COLLECTION VIA CARDIAC PUNCTURE WHILE MICE ARE UNDER GENERAL ANAESTHESIA.....	32
2.2.10 SERUM COLLECTION & SAMPLE STORAGE.....	32
2.2.11 ADMINISTARTION OF ZOLEDRONIC ACID TO MICE	32
2.2.12 MICRO-COMPUTED TOMOGRAPHY.....	33
2.2.13 CD138 IMMUNOHISTOCHEMISTRY (IHC)	34
2.2.14 SCORING SYSTEM FOR THE QUANTIFICATION OF CD138 POSITIVE CELLS.....	35
2.2.15 HISTOLOGY	36
2.2.16 HAEMATOXYLIN & EOSIN STAINING	37
2.2.17 TRAP STAINING.....	37
2.2.18 SCORING SYSTEM FOR THE QUANTIFICATION OF OSTEOCLASTS & OSTEOBLASTS	38
2.2.19 QUANTIFICATION OF OSTEOLYTIC BONE LESIONS	39
2.2.20 ENZYME LINKED IMMUNOSORBENT ASSAY (ELISA) – SERUM BONE MARKERS	40
2.2.21 OPTIMAL CUTTING TEMPERATURE (OCT) EMBEDDING AND CRYOSTAT SECTIONING.....	42
2.2.22 MULTIPHOTON MICROSCOPY	43
2.2.23 SPECTRAL FINGERPRINTING	45
2.2.24 THREE-DIMENSIONAL IMAGE PROCESSING, VISUALISATION & QUANTITATIVE ANALYSIS USING VOLOCITY SOFTWARE.....	46

2.2.25 STATISTICAL ANALYSIS.....	47
CHAPTER 3 MODULATION OF THE MURINE BONE MICROENVIRONMENT BY ZOLEDRONIC ACID	48
3.1 INTRODUCTION.....	49
3.2 AIMS & OBJECTIVES.....	50
3.3 MATERIALS & METHODS.....	51
3.3.1 IN VIVO EXPERIMENT	51
3.3.2 EXPERIMENTAL DESIGN.....	51
3.4 RESULTS.....	53
3.4.1 CONTINUOUS TREATMENT WITH ZA IS MORE EFFECTIVE AT INHIBITING OSTEOCLASTS AND OSTEOBLASTS THAN SHORT-TERM TREATMENT	53
3.4.2 BOTH SHORT-TERM AND CONTINUOUS ZA TREATMENT REDUCED SERUM LEVELS OF BONE RESORPTION (TRACP5B) AND BONE FORMATION (PINP) MARKERS	58
3.4.3 CONTINUOUS ZA TREATMENT IS MORE EFFECTIVE IN PRESERVING BONE THAN SHORT-TERM TREATMENT	59
3.5 DISCUSSION.....	64
CHAPTER 4 ESTABLISHING THE DEVELOPMENTAL STAGES OF MULTIPLE MYELOMA.....	67
4.1 INTRODUCTION.....	68
4.2 AIMS & OBJECTIVES.....	69
4.3 MATERIALS & METHODS.....	70
4.3.1 DETERMINING THE OPTIMAL CONCENTRATION OF VYBRANT DID DYE TO LABEL 5TMM-EGFP MURINE MYELOMA CELL	70
4.3.2 DETERMINING THE EFFECT OF DID LABELLING ON 5TGM1 MURINE MYELOMA CELL GROWTH.....	70
4.3.3 EXPERIMENTAL DESIGN TO CHARACTERISE THE DEVELOPMENTAL STAGES OF MYELOMA IN BONE	71
4.3.4 STATISTICAL ANALYSIS.....	72
4.4 RESULTS.....	73
4.4.1 OPTIMISING DID LABELLING OF 5TMM-EGFP MURINE MYELOMA CELLS.....	73
4.4.2 5TGM1 CELL PROLIFERATION EFFECTS ON DID LABELLING OVER TIME.....	73
4.4.3 ASSESSMENT OF TUMOUR PROGRESSION IN 5TGM1 MURINE MODEL OF MYELOMA.....	79
4.4.4 THE EFFECT OF MYELOMA DEVELOPMENT ON GROSS MORPHOLOGY	86
4.4.5 THE EFFECT OF MYELOMA DEVELOPMENT ON BONE REMODELLING	87
4.5 DISCUSSION.....	94

CHAPTER 5 THE EFFECT OF ZOLEDRONIC ACID TREATMENT ON THE EARLY STAGES OF MYELOMA DEVELOPMENT IN BONE.....	98
5.1 INTRODUCTION.....	99
5.2 AIMS & OBJECTIVES.....	100
5.3 MATERIALS & METHODS.....	101
5.3.1 EXPERIMENTAL DESIGN TO STUDY THE EFFECT OF ZA TREATMENT INITIATED PRIOR TO TUMOUR CELL INJECTION ON THE EARLY STAGES OF MYELOMA DEVELOPMENT (PRE-TREATMENT EXPERIMENT).....	101
5.3.2 EXPERIMENTAL DESIGN TO STUDY THE EFFECT OF ZA INITIATED AFTER TUMOUR CELL INJECTION ON THE EARLY STAGES OF MYELOMA DEVELOPMENT (POST-TREATMENT EXPERIMENT)	102
5.4 RESULTS	103
5.4.1 ZA TREATMENT EITHER PRE OR POST INJECTION OF 5TGM1 MURINE MYELOMA CELLS SIGNIFICANTLY SUPPRESSED BOTH OSTEOCLASTS AND OSTEOBLASTS IN THE 5TGM1 MURINE MODEL OF MYELOMA DURING THE EARLY STAGES OF MYELOMA DEVELOPMENT.....	103
5.4.2 THE EFFECT OF ZA TREATMENT ON TUMOUR BURDEN IN BONE DURING THE EARLY STAGES OF MYELOMA DEVELOPMENT	112
5.5 DISCUSSION.....	120
CHAPTER 6 THE EFFECT OF ZOLEDRONIC ACID TREATMENT ON THE LATE STAGES OF MYELOMA DEVELOPMENT IN BONE.....	124
6.1 INTRODUCTION.....	125
6.2 AIMS AND OBJECTIVES	126
6.3 MATERIALS AND METHODS	127
6.3.1 EXPERIMENTAL DESIGN TO STUDY THE EFFECT OF ZA TREATMENT INITIATED PRIOR TO TUMOUR CELL INJECTION ON THE LATE STAGES OF MYELOMA DEVELOPMENT IN BONE (PRE-TREATMENT EXPERIMENT)	127
6.3.2 EXPERIMENTAL DESIGN TO STUDY THE EFFECT OF ZA TREATMENT INITIATED AFTER TUMOUR CELL INJECTION ON THE LATE STAGES OF MYELOMA DEVELOPMENT IN BONE (POST-TREATMENT EXPERIMENT)	128
6.3.3 EXPERIMENTAL DESIGN TO STUDY THE EFFECT OF ZA TREATMENT ON DISEASE-FREE SURVIVAL	129
6.4 RESULTS	130
6.4.1 ZA TREATMENT EITHER PRE OR POST INJECTION OF 5TGM1 MURINE MYELOMA CELLS SIGNIFICANTLY SUPPRESSED BOTH OSTEOCLASTS AND OSTEOBLASTS IN THE 5TGM1 MURINE MYELOMA MODEL DURING THE LATE STAGE OF MYELOMA DEVELOPMENT.....	130
6.4.2 THE EFFECT OF ZA TREATMENT ON TUMOUR BURDEN IN BONE DURING THE LATE STAGES OF MYELOMA DISEASE DEVELOPMENT.....	139
6.4.3 THE EFFECT OF ZA TREATMENT ON DISEASE-FREE SURVIVAL IN 5TGM1 TUMOUR-BEARING MICE	149
6.5 DISCUSSION.....	150
CHAPTER 7 DISCUSSION	154
BIBLIOGRAPHY.....	164

LIST OF FIGURES

Figure 1.1-1: First recorded case of MM - Sarah Newbury with fractured femur and humerus.....	2
Figure 1.1-2: Normal and myeloma BM aspirate.	4
Figure 1.2-1: Biology of plasma cell development.....	5
Figure 1.3-1: Stages of myeloma development.....	6
Figure 1.3-2: Interactions of the myeloma cells with the BM	11
Figure 1.4-1: Tridentate configuration of bone binding by bisphosphonates.....	14
Figure 1.4-2: The inhibition of the mevalonate pathway in osteoclasts by ZA.....	16
Figure 1.5-1: Possible anti-tumour mechanisms of ZA in MM.....	21
Figure 2.2-1: Cell counting using a Neubauer haemocytometer.....	29
Figure 2.2-2: DID dye labelling cell membrane.	30
Figure 2.2-3: eGFP and DID excitation and emission spectra.....	31
Figure 2.2-4: Principle of micro-computed tomography imaging.....	33
Figure 2.2-5: MicroCT image analysis and quantification.	34
Figure 2.2-6: Principles of 'sandwich' or 'bridge' immunohistochemical staining of CD138.....	35
Figure 2.2-7: Scoring system for CD138 IHC.	36
Figure 2.2-8: Scoring of Ocs and Obs in TRAP and H&E stained slides	39
Figure 2.2-9: Quantification of cortical defects using Image J software.	40
Figure 2.2-10: Principles of the TRACP5b immunoassay.	41
Figure 2.2-11: Principles of P1NP competitive immunoassay.	42
Figure 2.2-12: Design of Hexane-methanol freezing bath	43
Figure 2.2-13: Principles of multiphoton microscopy and fluorescence imaging.	44
Figure 2.2-14: Principles of spectral fingerprinting.	45
Figure 2.2-15: Velocity image processing for quantitation and analysis.....	46
Figure 3.3-1: Experimental design to study the effect of short-term and continuous ZA treatment.....	52

Figure 3.4-1: The effect of short-term ZA treatment on bone in C57BL/KalwRij mice.....	55
Figure 3.4-2: The effect of continuous ZA treatment on bone in C57BL/KalwRij mice.....	56
Figure 3.4-3: The effect of short-term and continuous ZA treatment on the number of trabecular and cortical osteoclasts and osteoblasts.....	57
Figure 3.4-4: Changes in serum levels of TRACP5b and P1NP following short-term and continuous ZA treatment.....	58
Figure 3.4-5: The microCT changes in tibia following short-term ZA treatment.....	60
Figure 3.4-6: The microCT changes in tibia following continuous ZA treatment.....	61
Figure 3.4-7: Quantitative microCT analysis following short-term and continuous ZA treatment.....	63
Figure 4.3-1: Experimental design for determining the effect of DID labelling on cell proliferation.....	71
Figure 4.3-2: Experimental Design for longitudinal assessment of myeloma development in the 5TGM1 murine model of myeloma.....	72
Figure 4.4-1: DID concentration versus 5TGM1-eGFP-DID cell viability.....	73
Figure 4.4-2: Effect of DID labelling on the proliferation of 5TGM1-eGFP cells <i>in vitro</i>	74
Figure 4.4-3: Flow cytometric analysis of DID labelling of 5TGM1-eGFP cells over time.....	75
Figure 4.4-4: The effect of proliferation on DID labelled 5TGM1-eGFP cells as assessed by flow cytometry.....	76
Figure 4.4-5: <i>In vitro</i> spectral imaging of 5TGM1-eGFP-DID cell.....	77
Figure 4.4-6: Effect of 5TGM1-eGFP-DID cell proliferation on DID labelling by multiphoton microscopy.....	78
Figure 4.4-7: Flow cytometric profiles of 5TGM1-eGFP-DID tumour cells in the BM over time.....	79
Figure 4.4-8: Quantitative flow cytometry analysis of 5TGM1-eGFP-DID tumour development in bone over time.....	80
Figure 4.4-9: Changes in CD138 positive cells in the BM over time post injection of 5TGM1 cells.....	81
Figure 4.4-10: CD138 immunohistochemistry staining showing the developmental stages of 5TGM1 murine myeloma in bone ..	82
Figure 4.4-11: <i>In vivo</i> spectral fingerprinting.....	83
Figure 4.4-12: Multiphoton microscopy images showing the development of 5TGM1-eGFP-DID murine myeloma cells in bone.	84
Figure 4.4-13: Quantitative assessment of tumour burden in 5TGM1 murine model of myeloma using multiphoton microscopy.	85
Figure 4.4-14: Effect of 5TGM1 tumour development on gross morphology.....	86
Figure 4.4-15: Trabecular changes in osteoclast and osteoblast numbers following 5TGM1 myeloma development	87
Figure 4.4-16: Endocortical changes in osteoclast and osteoblast number following 5TGM1 myeloma development.....	88

Figure 4.4-17: Structural changes in tibia following 5TGM1 myeloma development over time.....	89
Figure 4.4-18: Quantitative microCT analysis following 5TGM1 murine myeloma development.....	90
Figure 4.4-19: Changes in systemic bone remodelling markers following 5TGM1 myeloma development.	91
Figure 4.4-20: 5TGM1 myeloma induced development of osteolytic lesions.	92
Figure 4.4-21: Quantification of myeloma induced osteolytic bone lesions in the 5TGM1 model over time.	93
Figure 5.3-1: Experimental design to study the effect of ZA treatment initiated prior to tumour cell injection on the early stages of myeloma.	101
Figure 5.3-2: Experimental design to study the effect of ZA treatment initiated after the tumour cell injection on the early stages of myeloma.	102
Figure 5.4-1: The effect of ZA treatment on Oc numbers in the 5TGM1 murine model of myeloma 10 days post tumour cell injection.....	104
Figure 5.4-2: The effect of ZA treatment on Ob numbers in 5TGM1 murine model of myeloma 10 days post tumour cell injection.....	105
Figure 5.4-3: MicroCT changes following ZA (pre or post) treatment in the 5TGM1 murine model of myeloma assessed 10 days post tumour cell injection.....	107
Figure 5.4-4: The effect of ZA treatment on serum TRACP5b and P1NP levels in the 5TGM1 murine model of myeloma 10 days post tumour cell injection.....	109
Figure 5.4-5: The effect of ZA treatment on the onset of tumour-induced osteolysis in the 5TGM1 murine model of myeloma. .	111
Figure 5.4-6: Flow cytometry profiles of BM cells from naïve C57BL/KaLwRij mice and 5TGM1 tumour-bearing mice treated with VEH or ZA.	112
Figure 5.4-7: The effect of ZA treatment on tumour burden in the 5TGM1 model of myeloma assessed 10 days post tumour cell injection.....	113
Figure 5.4-8: The effect of ZA treatment on CD138 positive colonies assessed by IHC, 10 days post tumour cell injection.	114
Figure 5.4-9: The effect of ZA pre-treatment on the CD138 positive tumour cell population 10 days post tumour cell injection.	115
Figure 5.4-10: The effect of ZA post-treatment on the CD138 positive tumour cell population, 10 days post tumour cell injection.	116
Figure 5.4-11: Representative examples of multiphoton images showing bone and 5TGM1-DID cells assessed 10 days post tumour cell injection.....	117
Figure 5.4-12: The effect of ZA pre or post-treatment on 5TGM1 tumour cell colonisation 10 days post tumour cell injection assessed by multiphoton microscopy.	118
Figure 5.4-13: The effect of ZA on the early stages of myeloma development using multiphoton microscopy.....	119

Figure 6.3-1: Experimental design to study the effect of ZA treatment initiated prior to tumour cell injection on the late stages of myeloma in bone.....	127
Figure 6.3-2: Experimental design to study the effect of ZA treatment initiated after the tumour cell injection on the late stages of myeloma development.	128
Figure 6.3-3: Schematic representation to study the effect of ZA treatment on the onset of illness.	129
Figure 6.4-1: The effect of ZA treatment on Oc numbers in the 5TGM1 murine model of myeloma, 21 days post tumour cell injection.....	131
Figure 6.4-2: The effect of ZA treatment on Ob numbers in the 5TGM1 murine model of myeloma, 21 days post tumour cell injection.....	133
Figure 6.4-3: MicroCT analysis following pre and post ZA treatment in the 5TGM1 murine model of myeloma, 21 days post tumour cell injection	135
Figure 6.4-4: The effect of ZA treatment on serum bone turn over markers in the 5TGM1 murine model of myeloma 21 days post tumour cell injection.	136
Figure 6.4-5: Effect of ZA treatment on the onset of tumour-induced osteolysis assessed 21 days post tumour cell injection.....	138
Figure 6.4-6: Flow cytometric profiles of BM cells positive for DID, eGFP and dual labelled 5TGM1-eGFP-DID cells	139
Figure 6.4-7: The effect of ZA treatment on 5TGM1 tumour burden 21 days post tumour cell injection.....	140
Figure 6.4-8: Effect of ZA on CD138 positive population on the late stages (21 day) of myeloma development in 5TGM1 murine model of myeloma.....	142
Figure 6.4-9: The effect of ZA pre-treatment on CD138 positive tumour cells 21 days post tumour cell injection.	143
Figure 6.4-10: The effect of ZA post-treatment on CD138 positive cells 21 days post tumour cell injection.....	144
Figure 6.4-11: Multiphoton images of bones showing bone structures DID and eGFP labelling 21 days post tumour cell injection.	146
Figure 6.4-12: The effect of ZA on the late stages of myeloma development using multiphoton microscopy.....	147
Figure 6.4-13: The effect of ZA pre or post-treatment on 5TGM1 tumour cell colonisation assessed 21 days post tumour cell injection.....	148
Figure 6.4-14: The effect of ZA treatment on the onset of morbidity.....	149

ABBREVIATIONS

5TGM1-eGFP	eGFP expressing 5TGM1 murine myeloma cell
5TGM1-eGFP-DID	DID labeled eGFP expressing 5TGM1 murine myeloma cell
AF	Amplifier Offset
ALN	Alendronate
AOTF	Acousto-Optic Tunable Filters
Appl	Triphosphoric acid 1-adenosin- 5'-yl ester 3-(3-methyl-but-3-enyl) ester
APRIL	A proliferation-inducing ligand
ASCT	Autologous stem cell transplantation
ATP	Adenosine triphosphate
AU	Arbitrary Unit
BAFF	B-cell activating factor
BM	Bone Marrow
BMD	Bone Mineral Density
BMEC	Bone Marrow Endothelial Cell
BMSC	Bone Marrow Stromal Cell
BP	Bisphosphonate
BV/TV	Percentage Bone Volume
C ₃ H ₃ NaO ₃	Sodium Pyruvate
Ca ²⁺ R	Calcium sensing receptor
CAM	Cell Adhesion Molecule
CLO	Clodronate
Ct. V	Cortical Volume
CTX	C Terminal Telopeptide
DG	Detector Gain
DID dye	1, 1'-dioctadecyl-3, 3, 3', 3'-tetramethylindodicarbocyanine, 4-chlorobenzenesulfonate dye
Ec.	Endocortical/Cortico-endosteal
EFS	Event-free survival
eGFP	Enhanced Green fluorescent protein
ELISA	Enzyme Linked Immuno Sorbent Assay
Em	Emission
EMD	Multiple myeloma with extramedullary disease
EMP	Extramedullary plasmacytoma (solitary & multiple)
FACS	Fluorescent activated cell sorting
FCS	Foetal Calf Serum
FPPS	Farnesyl diphosphate synthase
GC	Germinal centre
H&E	Haematoxylin and eosin
HGF	Hepatocyte growth factor
HSC	Hematopoietic stem cell

IBN	Ibandronate
ICAM	Interstitial Cell Adhesion Molecule
Ig	Immunoglobulin
IHC	Immunohistochemistry
IL	Interleukin
IMDM	Iscove's Modified Dulbecco's Media
IPP	Isopentenyl diphosphate
JK	Janus Kinase
LSM	Laser Scanning Microscope
MAPK	Mitogen-activated protein kinase
MBD	Myeloma Bone Disease
MGUS	Monoclonal gamopathy of undetermined significance
MicroCT	Micro-computed tomography
MIP	Macrophage inflammatory protein
MM	Multiple Myeloma
MM-CSC	Multiple Myeloma-Cancer stem cells
MMSET	Multiple myeloma SET domain containing protein
MZB	Marginal zone B cell
NBP	Nitrogen containing bisphosphonate
NEAA	Non-essential Amino Acid
NIH	National Institute of Health
NIR	Near Infra-Red
NZM	New Zealand mixed mice
OAF	Osteoclast activation factor
Ob	Osteoblast
Oc	Osteoclast
OCT	Optimal Cutting Temperature
OPG	Osteoprotogerin
OS	Overall survival
P1NP	Pro-Collagen I N terminal Pro-peptide
PBS	Phosphate buffered saline
PDGF	Platelet Derived Growth Factor
Pen-Strep	Penicillin-Streptomycin
PI-3K	Phosphatidylinositol-3 Kinase
PMT	Photomultiplier
pNPP	p-Nitrophenyl Phosphate
RANK	Receptor Activator of Nuclear Transcription Factor - kB
RANKL	Receptor Activator of Nuclear Transcription Factor – kB Ligand
ROI	Region of Interest
RT	Room temperature
SCID	Severe combined immunodeficient mice

SDF	Stromal derived factor
SHG	Second harmonic generation
SM	Smoldering myeloma
SMI	Structural Model Index
STAT-3	Signal Transducer and Activator of Transcription 3
TA	Tissue Area (mm ²)
Tb. N	Trabecular Number
Tb. Pf	Trabecular Pattern Factor
Tb. Th	Trabecular Thickness
TGF- β	Transforming growth factor β
TMB	Tetramethylbenzidine
TNF	Tumour necrosis factor
TP	Trypan blue
TRACP	Tartrate Resistant Acid Phosphatase
u-PA	Urokinase-type Plasminogen Activator
u-PAR	Urokinase-type Plasminogen Activator Receptor
VCAM	Vascular Cell Adhesion Molecule
VEGF	Vascular endothelial growth factor
VLA	Very Late Antigen
VOI	Volume of Interest
ZA	Zoledronic Acid

CHAPTER 1 GENERAL INTRODUCTION

1.1 MULTIPLE MYELOMA (MM)

Multiple myeloma (also known as myeloma, Kahlers'disease or myelomatosis) is an incurable malignancy of antibody producing plasma cells. It is the second most common cancer of the blood and accounts for 1-2% of all cancers excluding non-melanoma skin cancer and 10-15% of all haematological malignancies (Becker 2011). Plasma cells are terminally differentiated B lymphocytes which reside in the bone marrow (BM), the soft and spongy tissue found inside the bone. Malignant transformation occurs in the plasma cell that results in uncontrolled proliferation of a single clone which forms tumour in multiple locations in the BM. MM cells, like the normal plasma cells, also produce immunoglobulins (Ig) but in excessive quantities of homogenous forms of Ig. MM is characterised by multi-organ damage and dysfunction which includes bone pain, pathological bone fractures, anaemia and pancytopenia resulting in increased susceptibility to infections, clotting abnormalities, hypercalcaemia, renal failure and hyperviscosity syndrome.

Although archaeological evidence suggests the existence of MM from skeletal defects observed from dinosaur skeletons of the Mesozoic era (Capasso 2005), the first well-documented case of myeloma was recorded by Solly in 1844 as a case of 'mollities ossium' (pathological softness and fragility of bones) (figure 1.1-1) (Solly 1844). Currently, there are 86000 new cases of myeloma diagnosed annually and it is responsible for 63000 deaths worldwide (Becker 2011). Although a relatively rare cancer, it is estimated that there are lifetime risks of 1 in 115 for men and 1 in 155 for women of developing myeloma in the UK. MM is primarily a disease of the elderly with incidence rates increasing with age and currently the median age at diagnosis is 65 years although it remains rare under the age of 40 (Myeloma incidence statistics 2011, Cancer Research UK).

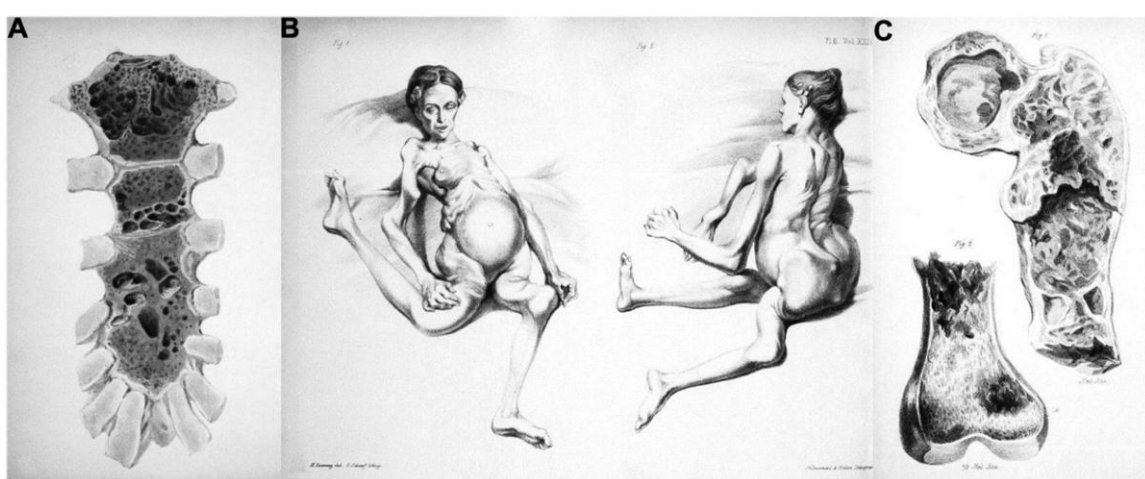


Figure 1.1-1: First recorded case of MM - Sarah Newbury with fractured femur and humerus.

The first well-documented case of MM, Sarah Newbury a 39 yr. old female described by Dr. Samuel Solly in his "Remarks on the Pathology of Mollities Ossium with cases" published in 1843. (A) Diseased sternum from the myeloma patient where there is patchy replacement of the red marrow substance. (B) Sarah Newbury showing MM fractures in both femurs and the right humerus. (C) Extensive bone destruction in the femur following advanced MM. Adapted from (Solly 1844) with permission.

1.1.1 MYELOMA AETIOPATHOGENESIS & CLINICAL MANIFESTATIONS

The aetiology of MM is not known. Multiple chromosomal abnormalities have been identified in MM patients and in some monoclonal gamopathy of undetermined significance (MGUS) patients, an asymptomatic premalignant condition that may progress to myeloma (Drach et al 1995; Zandecki et al 1995; Winter et al 2008). Karyotypic abnormalities include chromosomal gain (in about 30% of cases) such as trisomy's in 1q, 3q, 9q, 11q and 15q and chromosomal loss (about 50% of cases) with the most common being a deletion in 13q (monosomy 13) (Hallek et al 1998). Reciprocal translocations involving the Ig locus that affect B-cell specific DNA remodelling mechanisms has been identified in both the early and the late stages of MM. Reciprocal translocations that put an oncogene next to an Ig loci (Ch. 14q32) may result in defective DNA modification mechanisms like VDJ recombination, somatic hypermutation of B lymphocytes in the germinal centres (GC) and Ig heavy chain (IgH) recombination. The most frequent oncogene translocation sites include the cyclin D loci (11q13 and 6p21), multiple myeloma SET domain containing protein (MMSET) and fibroblast growth factor receptor 3 (4p16), c-MAF (16q23) and c-MYC (8q24) (Gutierrez et al 2007; Anderson 2011).

Although several karyotypic abnormalities were identified in myeloma patients, the precise aetiological factors responsible for the development of the disease remain unknown. No significant association was found between MM and common cancer risk factors like smoking, alcohol, dietary habits and physical activity. However, studies have shown an increased incidence of MM in people exposed to ionising radiations, agricultural workers, miners, farmers, wood and metal workers (Dittel et al 1993). Furthermore, there is also evidence suggesting a genetic predisposition to the condition with an increased incidence in the first-degree relatives of myeloma patients (Vachon et al 2009).

The clinical signs and symptoms seen in MM are due to the infiltration of the BM with myeloma cells, secretions of the myeloma cell and their interaction with the host cells in the BM environment. As myeloma cells are malignant and clonally identical, they grow extensively in the BM (figure 1.1-2) which produces excessive levels of monoclonal Ig. Bone pain and pathological fractures are the most common clinical manifestation of MM. The expanding myeloma cells inside the BM activate osteoclasts, the bone destroying cells resulting in multiple osteolytic lesions causing bone pain and fractures. Infiltration and expansion of the neoplastic plasma cells in the BM also causes haemolysis, decreased erythropoietin levels and reduced red cell production which causes anaemia and fatigue. Furthermore, increased synthesis of monoclonal Ig results in low levels of normal antibodies due to decreased production and increased destruction of normal antibodies. This results in an immunocompromised state causing recurrent infections. In addition, the accumulations of Ig in the kidneys result in amyloidosis and renal failure. Patients also have hypercalcaemia due to excessive bone damage. A small proportion of patients also show signs of bleeding or clotting disorders due to myeloma cell induced damage to platelets, clotting factors and endothelial cells (Fauci 2008).

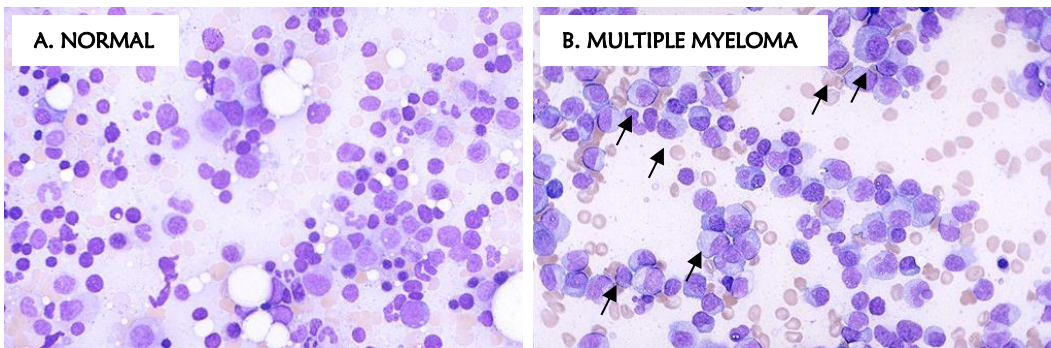


Figure 1.1-2: Normal and myeloma BM aspirate.

(A) A normal BM aspirate showing erythroid and granulocytic precursors. **(B)** A BM aspirate from a patient with MM showing numerous myeloma cells (black arrows) with eccentric nuclei and perinuclear halos of clearer cytoplasm. Reproduced with permission from The Internet Pathology Laboratory for Medical Education, Mercer University School of Medicine, The University of Utah Eccles Health Sciences Library©.

1.2 BIOLOGY OF MULTIPLE MYELOMA

Myeloma cells are malignant clones of terminally differentiated post-GC long-lived memory B cells that home and grow inside the BM.

1.2.1 NORMAL PLASMA CELL AND MYELOMA CELL DEVELOPMENT

Pre-B cells and naïve B lymphoblasts migrate from the BM to peripheral lymphoid tissues like the spleen, lymph nodes and Peyer's patches where they transform into mature lymphoblasts upon antigenic recognition and stimulation. Terminal plasmacytic differentiation of mature B cells is dependent on the temporo-spatial arrangement within the B cell compartment inside the lymphoid tissue. Marginal zone B cells (MZB) of the lymphoid follicles correspond to the first wave of the immune response following antigenic stimulation. MZB cells migrate to the extra-follicular region where they proliferate and provide “T cell independent immune response” by producing IgM antibodies to fight infection. MZB are short-lived plasma cells and usually die after 3 days undergoing apoptosis. However, B cells located in the follicular zone (follicular B cells) migrate into the GCs of the spleen and undergo “T cell dependent antigen recognition and stimulation”. Inside the GCs the follicular B cells proliferate, undergo extensive somatic hypermutation, antigenic selection and VDJ recombination to produce long-lived IgG antibody secreting plasmablasts and non-secreting memory B cells. These plasmablasts migrate from the GCs into the circulation where they terminally mature into plasma cells. Some non-secreting plasma cells migrate to the BM where they reside as memory B cells or as the BM Ig secreting plasma cells (Figure 1.2-1) (Hallek et al 1998; Rogers et al 1999). However, in MM, malignant transformation occurs in the post GC phase following damage to the B cell specific DNA remodelling mechanisms. As mentioned earlier, several chromosomal abnormalities have been identified in MM which damages genes within Ig loci which regulates the sequential DNA modification

processes such as VDJ recombination, somatic hypermutation and isotype switching that are involved in the terminal differentiation of mature plasma cell (Hallek et al 1998).

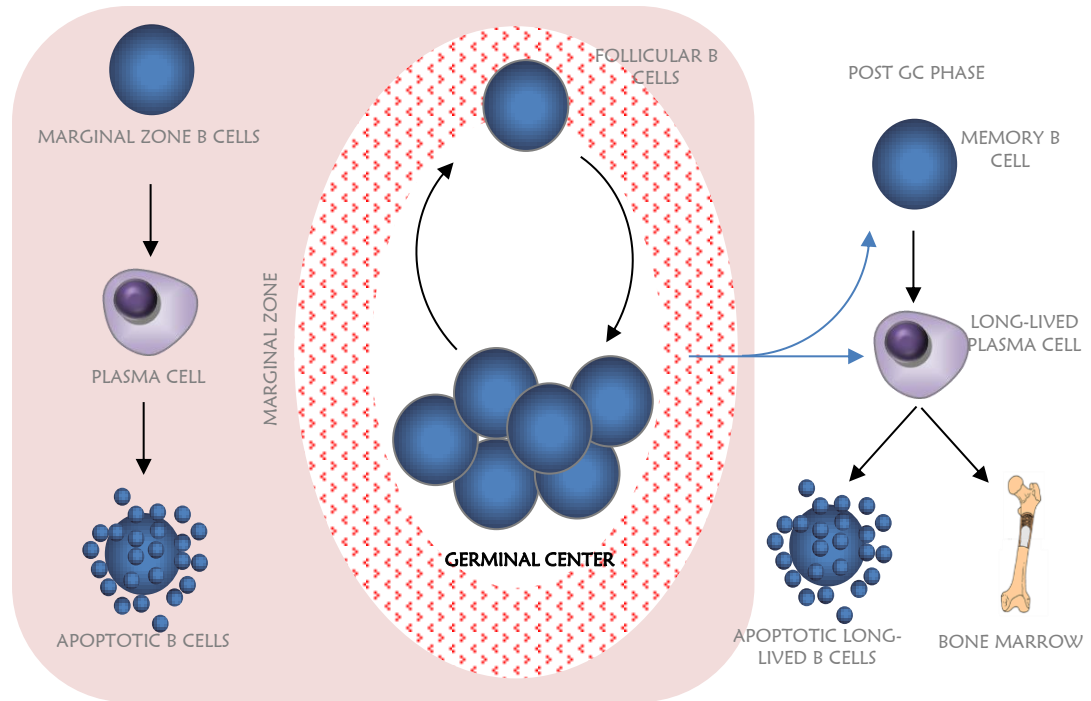


Figure 1.2-1: Biology of plasma cell development.

Immature B cells from the BM migrate to the site of infection and upon antigenic stimulation transform to mature B cells: the plasmablasts and memory B cells. Plasmablasts transform to short-lived plasma cells where they eventually terminate, while memory B cells migrate to the GC and upon antigenic stimulation undergo isotype-switching to become long-lived plasma cells. In MM, mutations of certain oncogenes cause malignant transformation (isotype-switching and extensive somatic hypermutation of the VH gene) of the long-lived plasma cells which mature into myeloma cells that home to the BM (Hallek et al 1998).

1.3 STAGES OF MULTIPLE MYELOMA DEVELOPMENT

Unlike other haematological malignancies, the early stages of MM development are strictly confined to the intramedullary compartments of the bone where the disease becomes symptomatic. Recently studies have shown that all MM patients are preceded by MGUS, a premalignant asymptomatic condition characterised by elevated serum monoclonal protein levels ($<3\text{g/dl}$), elevated plasma cells ($<10\%$) and no end-organ damage (Uchiyama et al 1992; Van Driel et al 2002). Smouldering MM (SMM) is the next stage of progression where the disease still remains asymptomatic although there are elevated levels of serum monoclonal protein ($>3\text{g/dl}$) and elevated plasma cells ($>10\%$) (Menu et al 2004). Following an increase in the proportion of the BM plasma cells and serum M protein the disease becomes clinically evident with tissue and organ involvement causing elevated serum calcium, impairment in renal functions, anaemia and bone involvement (CRAB acronym) Published by the International Myeloma Working Group (2003). In some MM patients, there is extension of myeloma cell growth outside the BM either by local extension through cortical damage or by haematogenous

spread where it is called extramedullary disease (EMD) in MM. EMD can involve organs such as skin, lungs, liver, lymph nodes and breast resulting in multi-organ damage (Varettoni et al 2010). Figure 1.3-1 shows the different stages of myeloma development.

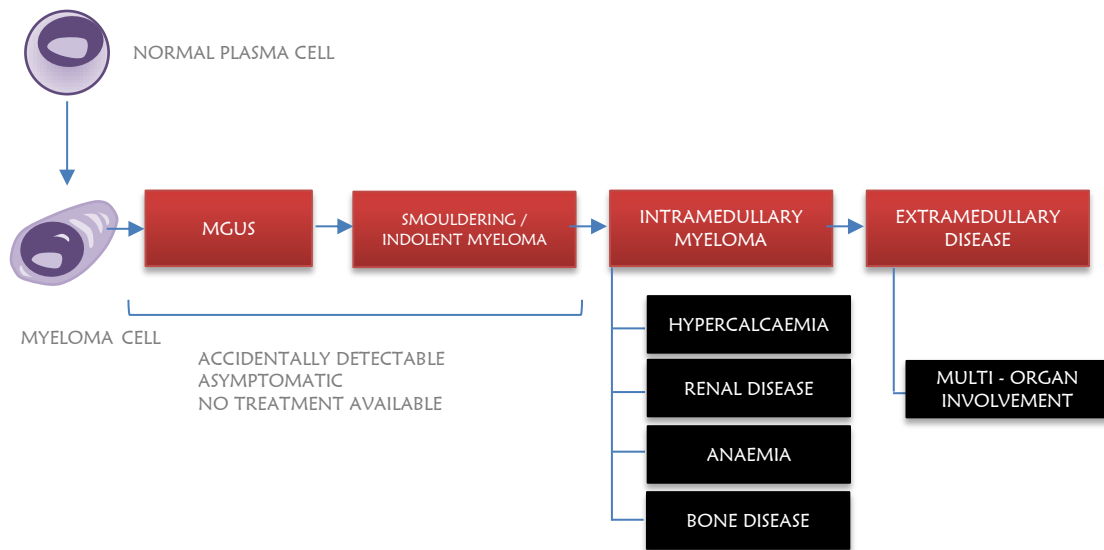


Figure 1.3-1: Stages of myeloma development.

1.3.1 MGUS AND SMOLDERING MULTIPLE MYELOMA (SMM)

Both MGUS and SMM are asymptomatic, premalignant plasma cell dyscrasias characterised by continuous monoclonal plasma cell expansion with no associated end-organ damage. MGUS is prevalent in 3% of the population above 50 years of age (with an age associated increase in prevalence) whereas SMM accounts for 15% of newly diagnosed cases of MM (Rajkumar 2005). Currently, as these conditions remain asymptomatic, no specific treatment is recommended until symptoms develop. These patients are at a life-time risk for progression to overt MM or other malignancies and require life-long monitoring. However, a number of clinical trials are currently underway, testing the effects of early administration of anti-myeloma chemotherapy to these patients. Rajkumar and colleagues (2003) showed that thalidomide treatment in SMM or indolent myeloma patients delayed progression to overt disease. Moreover, Mateos and colleagues (2013) recently showed that a combination of lenalidomide and dexamethasone in patients with high risk SMM successfully delayed the onset of symptomatic MM and also improved their overall survival (OS). In another phase III randomised trial, it was shown that a combination of thalidomide and zoledronic acid (ZA) prolonged the development time to symptomatic MM when compared with a ZA only treatment group (Witzig et al 2013). Taken together, these studies support the early intervention of myeloma using newer chemotherapeutic agents with tolerable toxicity compared to older alkylating agents which were either ineffective or led to long-term toxicity.

1.3.2 INTRAMEDULLARY MYELOMA

The interaction between the myeloma cell and the BM microenvironment has been implicated in the homing and survival of myeloma cells in the BM. Stromal dependency of myeloma cells is seen during the early and the main course of the disease. In the later stages of the disease, myeloma cells may become stromal-independent and may migrate to extramedullary sites (Van Riet et al 1998; Damaj et al 2004). Several studies have indicated that myeloma cells show immunophenotypic and histological similarities to normal B lymphocytes at a particular stage of differentiation (Kubagawa et al 1979). It is the intrinsic feature of B cells to migrate to the BM following maturation to long-lived plasma cells. B cells express a diverse range of adhesion molecules during their maturation phase allowing them to migrate into different compartments. This is coordinated by various cytokines and chemokines which play a critical role in guiding plasma cells to specific BM niches (Dittel et al 1993; Kaisho et al 1994; Koenig et al 2002). As myeloma cells are malignant clones of normal plasma cells, the BM stromal dependency for survival might be a feature acquired from their non-malignant counterpart.

Chemokines like stromal cell-derived factor 1 (SDF-1, also known as CXCL-12) and monocyte chemoattractant protein-1 (MCP-1) plays a critical role in the initial attraction of myeloma cells to the BM. MCP-1 expression by the BM endothelial cells (BMEC) causes the initial attraction of the circulating myeloma cell which express CXCR-2 receptors to adhere to the vascular endothelium of the BM while SDF-1 secreted by the BMSCs binds with the CXCR-4 receptor expressed on the myeloma cell (Lee et al 2001; Sanz-Rodriguez et al 2001; Vanderkerken et al 2002; Alsayed et al 2007). CXCR-4 is a chemokine receptor expressed by haematopoietic progenitor cells (HPC) and plasma cells that play a critical role in the homing of cells to the BM (Aiuti et al 1997; Aparicio et al 1998; Shipman et al 1998; Kawabata et al 1999; Fooksman et al 2010). Studies have shown there is enhanced expression of CXCR-4 by the terminally differentiated post GC phase plasma cells (Iguchi et al 2003). CXCR-4 expressing cells migrate in response to CXCL-12, the unique ligand to CXCR-4. Erickson and colleagues (2003) demonstrated the selective inability of plasma cells to home to the BM in CXCL-12 deficient New Zealand Mixed (NZM) lupus mice. Myeloma cells express various adhesion molecules like very late antigen 4 and 5 (VLA-4 and VLA-5), CD44v, intercellular adhesion molecule 1 (ICAM-1), leukocyte function associated antigen (LFA-1), syndecan 1 (also known as CD138) and cadherins which promote the binding of the myeloma cells to the BM milieu (Diel 2000; Asosingh et al 2001; Van Driel et al 2002; Guenther et al 2010). Studies have demonstrated that SDF-1/CXCR-4 interaction results in an up-regulation of VLA-4 expression in MM cells, which promotes adhesion to fibronectin and VCAM-1 (Sanz-Rodriguez et al 2001; Parmo-Cabañas et al 2004).

Several groups have reported a diverse expression of matrix metalloproteinases (MMPs) in various myeloma cell lines and patient cells. MMPs are zinc-dependent end peptidases that are involved in tissue degradation. MM cells were shown to produce MMP-8, 9 and 13 (Barille et al 1997; Wahlgren et al 2001; Parmo-Cabañas et al 2006) while BMSCs produce MMP-1 and 2 (Barille et al 1997). MMP expression and activation in MM BM milieu is regulated by several cytokines and the interaction of the

MM cells with cells of the BM microenvironment. Syndecan-1, a trans-membrane heparin sulphate glycoprotein plays a critical role in binding the MM cells to the collagen thereby activating the production of MMP-1 (Catlett-Falcone et al 1999). Urokinase-type plasminogen activator (uPA) is another serine protease, which converts plasminogen to its active form plasmin. Plasmin plays a very important role in activating MMPs and induces extracellular matrix degradation (Wong et al 1992; Carmeliet et al 1997; Noel et al 1997; Lijnen et al 1998). Primary myeloma cells and certain myeloma cell lines were also shown to express both uPA and uPAR (Hjertner et al 2000).

1.3.3 MULTIPLE MYELOMA AND THE BONE MARROW MICROENVIRONMENT

The interactions between MM cells and the BM microenvironment are thought to provide necessary survival signals for the proliferation of myeloma cells. Invasion of myeloma cells through BMECs and the basement membrane exposes myeloma cells to the BM microenvironment. The term BM microenvironment includes both the extracellular matrix proteins and the stromal components which include BMSCs, osteoclasts, osteoblasts, sinusoidal endothelial cells, macrophages and adipocytes. The tumour-host interactions influence several elements in the development of intramedullary myeloma: homing and survival of the myeloma cells in the BM; colonisation and intramedullary spread of tumour cells; paracrine secretions that ascertain survival advantage and drug resistance of the myeloma cells; osteoclastogenesis, inhibited osteogenesis and development of lytic lesions and tumour-induced angiogenesis (Thomas et al 2004).

Interactions of the myeloma cells with the bone microenvironment are mediated by direct cell to cell contact or paracrine secretions. Myeloma cells express various adhesion molecules and integrins which mediates their interactions with ECM proteins and BMSCs (Komori 2010). Subsequently, the BM microenvironment produces several cytokines and chemokines after interacting with myeloma cells which helps tumour cell growth and protects them from apoptosis. Tumour cells interact with BMSCs or extracellular matrix proteins by direct cell to cell or cell to matrix contact through the expression of adhesion molecules such as VLA-4, VLA-5 and CD40 (figure 1.3-2).

The interactions of myeloma cells with BMSCs

The BM microenvironment produces several cytokines and chemokines after interacting with the myeloma cells which helps their growth and protects them from apoptosis. Various adhesion molecules including VLA-4 and ICAM-1 mediate the adhesion of the myeloma cell to the BMSCs (Uchiyama et al 1992; Uchiyama et al 1993). Studies have shown that the adhesion of myeloma cells to BMSCs results in enhanced expression of IL-6 by both cell types, which supplies survival and proliferative signals and confers drug resistance to myeloma cells by paracrine and autocrine mechanisms (Uchiyama et al 1993; Chauhan et al 1996). Adhesion of myeloma cells to BMSCs triggers the activation of the nuclear factor kappa B (NF- κ B) pathway which further enhances adhesion by upregulating more adhesion molecules in both cell types (Uchiyama et al 1993; Chauhan et al 1996). Moreover, IL-6 expression in BMSCs is

also up-regulated via an NF- κ B dependent pathway (Hideshima et al 2001). IL-6 was shown to trigger phosphorylation of the signal transducer and activation of transcription 3 (STAT3) pathway via Janus-kinase 1 (JK-1), activation of Ras/mitogen-activated protein kinase (MAPK) pathway and the phosphatidylinositol-3 kinase (PI-3K) pathway which results in the production of anti-apoptotic and proliferative signals for myeloma cells (Ogata et al 1997; Hideshima et al 2001; Brocke-Heidrich et al 2004; van de Donk et al 2005). However, IL-6 blockade did not evoke a substantial anti-myeloma effect and myeloma cells were found to survive when co-cultured with BMSCs (Tripathi et al 2003; Chatterjee et al 2004). This suggests that interactions between the myeloma cells and the BM microenvironment additionally stimulate IL-6 independent mechanisms for the survival of the myeloma cell. Chatterjee and colleagues (2004) demonstrated that the interactions of BMSC with myeloma cells stimulates Ras/MAPK pathway in myeloma cells which is independent of IL-6R blockade.

Insulin like growth factor-I (IGF-1) is another important chemokine produced by BMSCs upon interacting with myeloma cells. It was shown to have a synergistic effect on myeloma cell survival and proliferation through an IL-6 independent mechanism by activating both MAPK and PI-3K pathways (Ferlin et al 2000). Various other cytokines have been identified that play an important role in the anti-apoptotic effects which include interleukin IL-1 α , IL-1 β , basic fibroblast growth factor (bFGF), hepatocyte growth factor (HGF) and vascular endothelial growth factor (VEGF) (Mitsiades et al 2007). Although myeloma cell interaction with the BMSCs, either by direct adhesion mediated interaction or production of chemokines and cytokines, was shown to activate a number of different pathways in the myeloma cell, they all converged to a common downstream event enhancing anti-apoptotic signals and degrading pro-apoptotic signals giving a survival advantage to the myeloma cell in the BM microenvironment.

The interactions of myeloma cells with BMECs & neovascularisation

Tumour angiogenesis is an important event responsible for the growth and expansion in solid tumours. Myeloma cells produce several pro-angiogenic and angiogenic molecules like VEGF, b-FGF, transforming growth factor- β (TGF- β), platelet derived growth factor (PDGF), HGF and IL-1 both by autocrine and paracrine mechanisms upon interaction with BMSCs and BMECs (Vacca et al 1999; Gupta et al 2001; Ria et al 2003; Hideshima et al 2007). All these factors are involved in the growth and differentiation of vascular endothelial cells and the recruitment of new vessels in the BM. Vacca and colleagues (2003) demonstrated that myeloma BMECs express various adhesion molecules and receptors which confers them to have high angiogenic and vasculogenic ability compared to human umbilical vein endothelial cells (HUVEC). Furthermore, adhesive interaction of BMECs with the myeloma cells enhance the invasiveness of myeloma cells by stimulating the production of MMP-2 and MMP-9 which in turn release bone growth factors favouring myeloma growth (Vande Broek et al 2004).

The interactions of myeloma cells with osteoblasts

Studies showed that certain myeloma cell lines upon interaction with osteoblasts via direct cell to cell contact release IL-6 which in turn enhances the survival potential of myeloma cells (Barille et al 1995; Franchimont et al 2000). However, at present the direct role of osteoblasts on myeloma cell survival is not known. Interestingly, myeloma cells have an inhibitory effect on osteoblastogenesis both by direct adhesive interaction with osteoblast progenitors, causing down regulation of RUNX2 transcription factor which plays an important role in osteoblast differentiation, and by the production of soluble Wnt inhibitory factors like dickkopf 1 (DKK1) and frizzled ring protein 2 (FRP2) (Tian et al 2003; Thomas et al 2004; Oshima et al 2005; Abe et al 2006; Giuliani et al 2006a; Chim et al 2007; Komori 2010). Osteoblasts also regulate the expression of the receptor for activation of nuclear factor kappa B ligand (RANKL) and osteoprotogerin (OPG), which are positive and negative mediators of osteoclast differentiation respectively. Therefore, myeloma cells, in addition to their direct effect on osteoclastogenesis, also regulate osteoclasts indirectly through osteoblast inhibition (Glass Li et al 2005; Spencer et al 2006).

The interactions of myeloma cells with osteoclasts

MM cells produce several cytokines and growth factors for the activation and maturation of osteoclasts in the BM microenvironment. Studies have shown that the interaction of myeloma cells with BMSCs and osteoclasts results in a coordinated increase in osteoclastogenic factors such as IL-6, IL-1 β , macrophage-colony stimulating factor (M-CSF), tumour necrosis factor- α (TNF- α), VEGF, and MIP-1 α , 1 β (Sati et al 1999; Oyajobi et al 2003; Mitsiades et al 2007) and suppression of negative regulators of osteoclastogenesis such as OPG (Qiang et al 2008) resulting in uncontrolled osteoclastogenesis and bone resorption. Hecht et al (2008) using an *in vitro* coculture system demonstrated that interactions of myeloma cells with osteoclasts resulted in activation of p44/p42 MAPK STAT3 and Akt signalling and promoted the growth of the myeloma cell. Furthermore, they also showed that these interactions also resulted in an up-regulation of p38 MAPK and NF- κ B signalling pathways which are involved in osteoclastogenesis. Another group showed that the interactions between myeloma cells and osteoclasts resulted in an increased secretion of chondroitin synthase 1, a soluble protein prominently seen in myeloma cells and osteoclast cocultures which support myeloma cell survival by stimulating notch-2 signalling (Yin 2005). Abe et al (2004) demonstrated that the binding of myeloma cells to osteoclasts through cell surface receptors promoted myeloma cell growth and also enhanced the release of IL-6 and osteopontin which in turn promoted myeloma cell survival. Anti-IL-6 and anti-OPN neutralising antibodies were not able to fully abrogate the osteoclast mediated survival of the myeloma as it was suggested to be more dependent on a direct physical contact with the osteoclasts. Furthermore, the same group also showed that myeloma-osteoclast interactions had a more potent growth promoting effect than myeloma-BMSC interactions (Vanderkerken et al 2003b). Two other molecules, B cell activating factor (BAFF) and a proliferation inducing ligand (APRIL), produced by osteoclasts were shown to promote growth and anti-apoptosis in certain myeloma cell

lines (Moreaux et al 2004; Abe et al 2006). In addition, Tanaka et al (2007) showed that the interactions between myeloma cells and osteoclasts resulted in enhanced angiogenesis by secreting proangiogenic factors, VEGF and osteopontin.

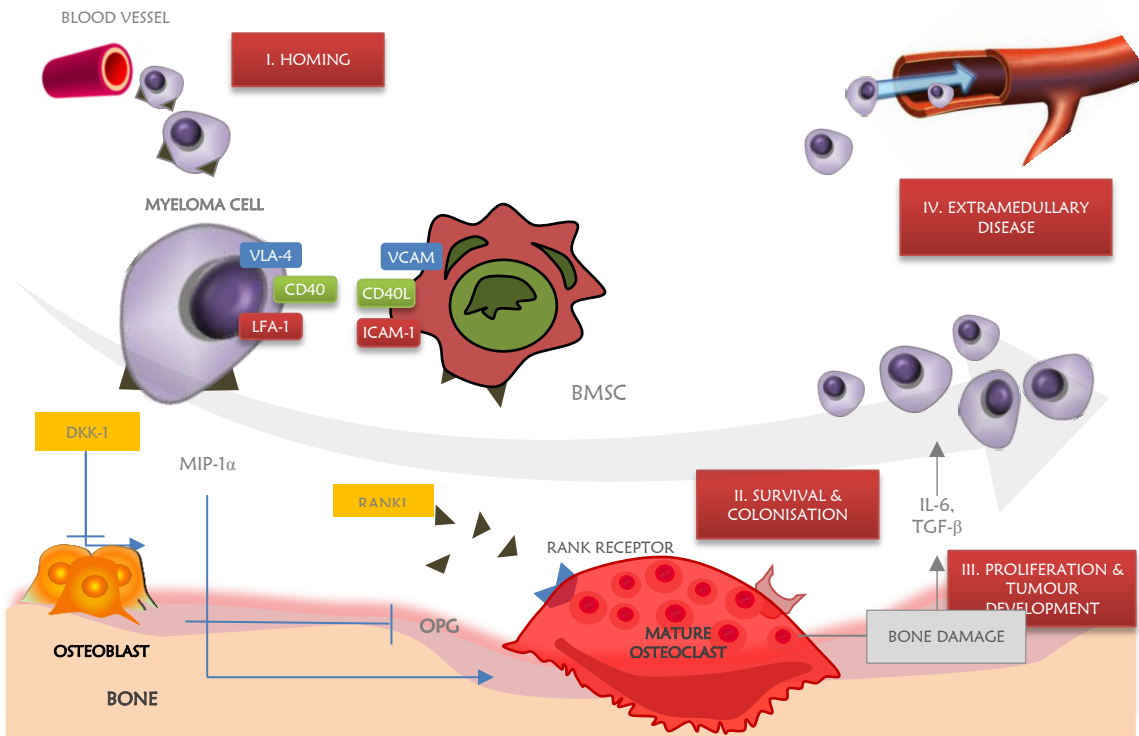


Figure 1.3-2: Interactions of the myeloma cells with the BM

Myeloma cells interact with the BMSCs via expression of molecules such as VLA-4, CD40, and LFA-1. Close cell to cell contact with the BMSC results in the secretion of RANKL which binds to RANK receptors resulting in the maturation of osteoclasts. Myeloma cell interaction with the BMSCs also releases osteoblast inhibitors such as DKK-1 which in turn suppresses OPG production, a soluble decoy receptor for RANK. This in turn also promotes osteoclastogenesis. Following osteoclast maturation bone resorption ensues resulting in the release of bone matrix derived growth factor such as IL-6 and TGF- β which supports myeloma cell proliferation and survival inside the BM. This establishes a 'vicious' cycle between myeloma cells and osteoclast. RANK= receptor for activation of nuclear factor kappa B, RANKL= receptor for activation of nuclear factor kappa B ligand, DKK-1=Dickkops-1, VLA-1=Very late antigen-1, LFA= leukocyte function associated antigen.

Bone derived growth factors

During osteoclastic bone resorption several growth factors and cytokines are released from the bone tissue into the surrounding BM microenvironment. These include factors like IGF, TGF- β , b-FGF and PDGF (Mohan et al 1991). Additionally, there is also release of calcium (Ca^{2+}) and phosphate (PO_4) due to the breakdown of hydroxyapatite crystals, a major component of the bone mineral matrix (Yoneda et al 2005). The role of IGF, TGF- β , b-FGF and PDGF in myeloma cell survival, proliferation and drug resistance has already been discussed above. Following resorption there is abundant release of bone derived factors into the resorption pit under the osteoclast and into the BM. This makes the BM niche a

very fertile environment for cells to grow. Yamaguchi and colleagues (2002) showed that certain myeloma cells express calcium sensing receptors (Ca^{2+}R). These cells showed proliferative effects when stimulated with Ca^{2+} . The copious release of growth factors supports the survival and proliferation of myeloma cells which in turn activates more osteoclasts thereby establishing a ‘vicious cycle’ leading to uninterrupted bone damage and subsequent tumour expansion. Furthermore, anti-resorptive agents such as bisphosphonates (BPs) and human anti-RANKL antibody (Denosumab) have been shown to reduce tumour burden in *in vivo* preclinical models of myeloma and in clinical trials (Rogers et al 2000; Sordillo et al 2003; Vanderkerken et al 2003b; Avilés et al 2007; Morgan et al 2010a; Iqbal et al 2011). However, the mechanisms responsible are not clearly understood yet.

1.3.4 MYELOMA BONE DISEASE

Myeloma bone disease (MBD) is not merely a functional consequence of the disease progression on the BM microenvironment; it is an ongoing process which promotes MM cell survival and tumour growth. Interactions of myeloma cells with BMSCs results in the production of several osteoclast activating factors (OAFs) which include RANKL, macrophage inflammatory protein-1 α (MIP), VEGF, IL-6 and TNF- α (Lacey et al 1998; Fuller et al 2002; Henriksen et al 2003; Heider et al 2004). RANKL is a TNF-related activation-induced cytokine which binds to the RANK receptor on osteoclasts and is involved in the activation and differentiation of precursor osteoclasts into mature and functionally active osteoclasts (Lacey et al 1998). In normal conditions, RANKL is secreted by osteoblasts, BMSCs and BMECs. The extent of osteoclast activation and consequent bone resorption is limited by the production of OPG, a soluble decoy receptor antagonist for RANKL, mainly produced by osteoblasts and BMSCs (Kong et al 1999). However, in MM there is an up-regulation of RANKL expression by both myeloma cells and the BMSCs (Croucher et al 2001; Giuliani et al 2001). Moreover, myeloma cells were shown to inhibit OPG synthesis by osteoblasts and BMSCs both *in vitro* and *in vivo* (Pearse et al 2001). Additionally, Standal and colleagues (2002) showed MM cells, by their transmembrane heparin sulphate proteoglycan syndecan-I, binds, internalises and degrades circulating OPG. Thus in MM, the RANKL/OPG balance is disrupted resulting in enhanced osteoclastic activity and a subsequent increase in osteoclastic bone resorption.

Myeloma cells also produce MIP-1 α that directly acts through the receptors CCR1, CCR5 and CCR9 expressed on osteoclasts. They promote osteoclast maturation and differentiation both independently of RANKL as well as supporting RANKL and IL-6 induced osteoclast activation (Dunford et al 2001). Studies have shown that MIP-1 α mRNA levels from the BM plasma and serum levels of the protein correspond to the severity of the bone disease in myeloma patients (Choi et al 2000; Terpos et al 2003). Furthermore, a neutralising antibody to MIP-1 α and anti-sense blocking showed inhibition of osteoclast activation and reduction of MBD in a murine model of myeloma (Choi et al 2000; Choi et al 2001). VEGF is another angiogenic cytokine produced by myeloma cells, BMSCs and BMECs and it plays a critical role in osteoclast activation, maturation and migration (Henriksen et al 2003; Yang et al

2008). Lee and colleagues (2004) showed IL-3 produced by myeloma cells activates osteoclasts along with RANKL and MIP-1 α and was consistently found elevated in MM patients. Recently, T lymphocytes in the BM plasma of myeloma patients were shown to produce IL-3 and were involved in osteoclastogenesis (Giuliani et al 2006a). A number of other cytokines such as IL-6, TNF- α , IL-1 β were also shown to be regularly elevated in patients with MBD.

1.3.5 MULTIPLE MYELOMA WITH EXTRAMEDULLARY DISEASE (EMD)

EMD is a condition where there is spread of MM from bone to extraskeletal sites such as kidneys, liver, skin and central nervous system during disease progression. Varettoni et al (2010), in a longitudinal study involving 1003 MM patients showed that 7 to 18% of newly diagnosed patients had EMD and 6 to 20% developed the disease later during follow-up. Extramedullary spread occurs either as a result of direct extension from intramedullary tumour to the local soft tissues through disrupted cortical bone or via metastatic haematogenous spread to distant sites. Disruption in the normal homing mechanisms of the myeloma cells to bone has been attributed to the development of EMD. Studies have suggested that decreased expression of adhesion molecules such as CD44, CD56 and VLA-4 and down regulation of chemokine receptors such as CXCR-4 and CXCL-12 to be responsible for the dissemination of tumour cells from the primary site (Blade et al 2012). It has been shown that myeloma patients who develop EMD have been consistently associated with aggressive disease and poorer prognosis (Damaj et al 2004; Ping Wu 2009). Studies have also shown that the extramedullary plasmacytoma varies characteristically from the medullary disease even in the same patient such as p53 deletion which was seen only in the extramedullary clone and remained refractory to conservative treatments that were used for the systemic disease (Lopez-Anglada et al 2010).

1.4 THE USE OF BISPHOSPHONATES IN MYELOMA MANAGEMENT

Approximately 70-80% of myeloma patients develop MBD characterised by development of bone pain, bone fracture and hypercalcaemia. Currently, BPs are used as osteo-protective agents for the symptomatic management of cancer-induced bone disease in conditions such as MM, breast and prostate cancer. BP's improve bone health by reducing tumour cell induced bone damage and cancer-induced hypercalcaemia. BPs are a class of compounds that are synthetic analogues of the inorganic pyrophosphates where the central oxygen atom ($P-O-P$) is replaced by a carbon atom ($P-C-P$) (figure 1.4-1 A and B). The substitution of the central O_2 moiety to the backbone of the naturally occurring inorganic pyrophosphate has made BPs more stable, resistant to degradation, biologically active and water soluble compounds (Green 2005). The $P-C-P$ backbone motif of the BP acts as a bone-hook binding it to the hydroxyapatite of the bone. This affinity of the BPs is because of their intrinsic property to bind divalent cations such as Ca^{2+} . Substitution of the R_1 side chain with a hydroxyl (-OH) or primary amino (-NH₂) group increases its binding affinity to bone as it permits a tridentate conformation (figure 1.4-1 C) which binds with Ca^{2+} ions more effectively than substitutions with chlorine (Cl) or hydrogen (H⁺) ions which allows only a bidentate conformation (van Beek et al 1998; Rogers et al 2000; Reszka et al 2003; Papapoulos 2006). Although the entire molecular structure is essential for the biological potency of these drugs, the structure of the R_2 side chains significantly alters their anti-resorptive potency (van Beek et al 1998; Winter et al 2008).

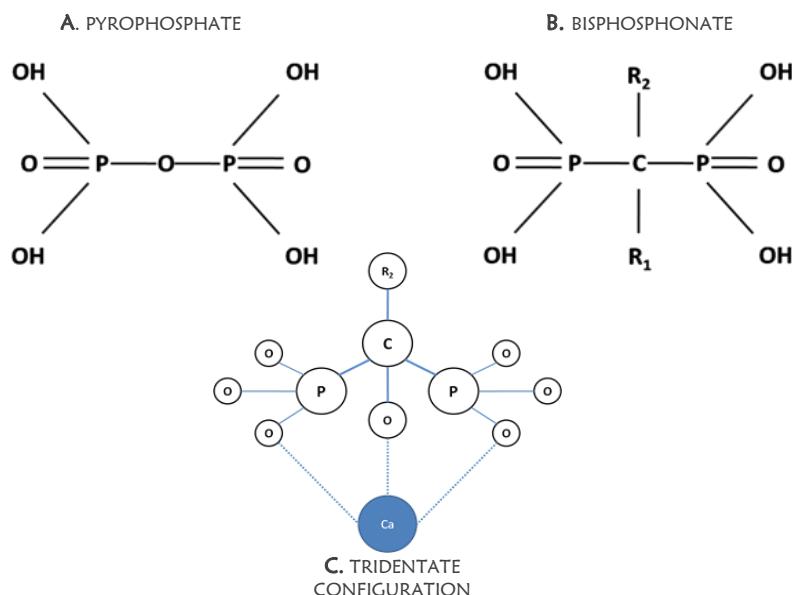


Figure 1.4-1: Tridentate configuration of bone binding by bisphosphonates.

The chemical structure of a pyrophosphate (A), BP (B) and the tridentate configuration of a BP with Ca^{2+} ion (C). The substitution of the OH group at R_1 allows a tight binding with the exposed Ca^{2+} ion at sites of active resorption. The presence of an additional OH group at R_1 contributes to one more covalent bond between the BP and Ca^{2+} in the hydroxyapatite bone matrix.

1.4.1 ZOLEDRONIC ACID (ZA)

ZA (manufactured and marketed by Novartis pharma in the name of Zometa/ Aclasta/ Reclast) is a nitrogen-containing bisphosphonate (NBP) that has been widely used over the past 10 years as an osteotropic agent in the treatment of Paget's disease, osteoporosis and also in malignancy associated osteolysis and hypercalcaemia. ZA is a heterocyclic imidazole ring with two nitrogen atoms at its R₂ moiety and a hydroxyl (–OH) group at its R₁. It is currently a more potent BP commercially available with the highest osteoclast inhibitory effect and the broadest clinical application (Green 2005). It was initially approved for the treatment of bone disease in MM and other solid tumour. Recently, due to increasing evidence of reduction in skeletal related events and anti-tumour effect in phase III MM clinical trials, it is currently under evaluation for considering early integration in the anti-cancer treatment regimens for MM (Morgan et al 2010a).

1.4.2 ANTI-RESORPTIVE MECHANISM OF ZA

ZA is an effective anti-resorptive agent inhibiting osteoclastic bone resorption thereby preventing bone damage. Although all classes of BPs target osteoclasts, their selective activity differs between the group of compounds classified as Non-NBPs (e.g. Clodronate & Etidronate) and the NBPs (e.g. ZA & Risedronate) (Rogers et al 2000). The intrinsic property of BPs to have a high affinity to mineralized bone matrix, favours the rapid relocation of these molecules from the circulation to areas of active bone remodelling, which has rendered them to have a very short plasma half-life and hence low-plasma circulating levels (Sato et al 1991; Masarachia et al 1996; Chen et al 2002; Green 2003). NBPs are internalised into osteoclasts during bone resorption by fluid phase endocytosis (Thompson et al 2006). In agreement, Sato et al (1991) also showed evidence of intracellular accumulation of radio-labelled alendronate (ALN) in various subcellular compartments in rat osteoclasts *in vivo*.

NBP inhibits an enzyme in the mevalonate pathway in the osteoclast and other cells that can actively uptake them (Amin et al 1992; Luckman et al 1998). NBPs inhibits geranyl diphosphate and farnesyl diphosphate synthase (FPPS) which plays a critical role in the conversion of isopentenyl diphosphate (IPP) into farnesyl diphosphate (FPP) of the mevalonate pathway (van Beek et al 1999; Bergstrom et al 2000; Dunford et al 2001) (figure 1.4-2). Inhibition of FPPS results in loss of prenylation of important signalling proteins like Ras, Rho, Rac and hence defective cell signalling, cellular functioning and osteoclast inactivation and apoptosis (Rogers et al 1999; Mönkkönen et al 2007; Russell et al 2008).

Recently, evidence suggests potent NBPs like ZA produce a cytotoxic analogue of ATP known as AppI (triphosphoric acid 1-adenosin- 5'-yl ester 3-(3-methyl-but-3-enyl) ester). AppI in both *in vitro* and *in vivo* conditions can induce osteoclast apoptosis by blocking mitochondrial ATP/ADP translocase (Monkkonen et al 2006; Mönkkönen et al 2007).

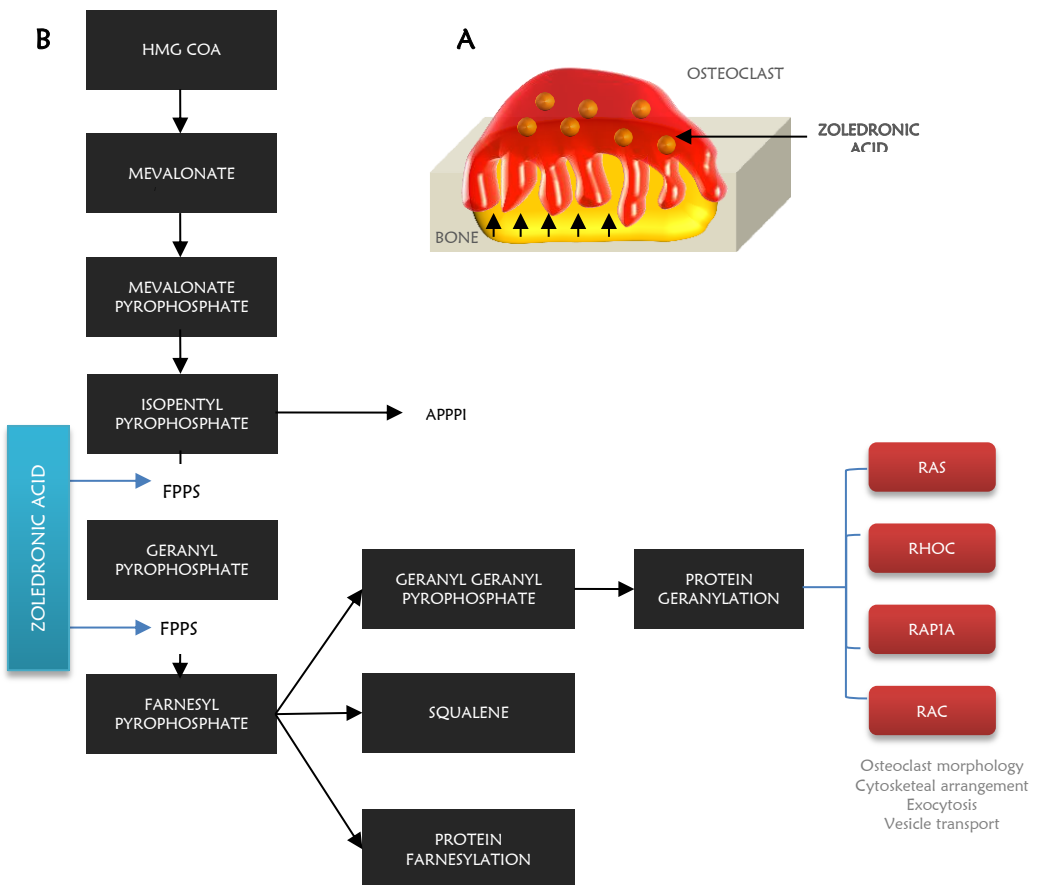


Figure 1.4-2: The inhibition of the mevalonate pathway in osteoclasts by ZA.

ZA binds to the bone and is released into the resorption pit (**A**) as a result of substances released by the osteoclast. The released ZA is internalised by the osteoclast by fluid phase endocytosis. Inside the osteoclast, ZA inhibits the enzyme farnesyl diphosphate synthase (FPPS), an enzyme which plays a key role in the mevalonate pathway (**B**). This in turn inhibits the synthesis of geranyl diphosphate and farnesyl diphosphate which are necessary for protein prenylation and the production of intracellular signaling proteins like Ras, Rac & Rho. Further the accumulation of Isopentyl diphosphate also results in production of Apppl, a cytotoxic analogue of ATP which is toxic to the osteoclast. APPPI= Triphosphoric acid 1-adenosin- 5'-yl ester 3-(3-methyl-but-3-enyl) ester, FPPS= Farnesyl diphosphate synthase.

1.5 THE ANTI-MYELOMA EFFECT OF ZOLEDRONIC ACID

Several preclinical studies have established that BPs as therapeutic agents for the treatment of tumour-induced bone diseases, but emerging evidence suggest that BPs may have a role well beyond being a mere osteolysis inhibitor. In addition to inhibiting tumour-induced osteolysis, BPs were shown to have a remarkable effect on skeletal tumour burden and survival in several preclinical cancer models and clinical trials of bone metastasis (Green 2003; Clezardin 2005; Clezardin et al 2005; Green 2005; Avilés et al 2007; Saad 2008; Morgan et al 2010b).

1.5.1 IN VITRO EVIDENCE OF AN ANTI-MYELOMA EFFECT OF ZA

In vitro evidences suggest that BPs has both cytostatic and apoptotic effect not only on osteoclasts but also on a variety of tumour cells such as MM, breast cancer, prostate cancer, renal cell carcinoma, pancreatic cancer and osteosarcoma (Shipman et al 1997; Shipman et al 1998; Senaratne et al 2000; Lee et al 2001; Kubista et al 2006; Horie et al 2007; Ullén et al 2008). Baulch-Brown and colleagues (2007) showed that ZA had a dose and time-dependent apoptotic effect on NCI-H929, RPMI8226, LP-1, OPM-2 cells and induced cell cycle arrest in the NCI-H929 cell line. Shipman et al (1997) demonstrated that NBPs such as pamidronate (PAM) and incadronate has a dose and time-dependent inhibitory effect on cell proliferation in U226-B1, JJN-3 & HS Sultan myeloma cell lines by inducing cell cycle arrest and apoptotic changes in culture. There was no evidence of anti-tumour effects observed in any cell lines using non-NBPs such as clodronate (CLO). In addition, studies by Tassone et al (2000) and Ural et al (2003) showed *in vitro* synergistic cytoreductive effects on myeloma cell growth when ZA was combined with simvastatin, dexamethasone and thalidomide.

Loss of protein isoprenylation in tumour cells by NBPs has been suggested to be responsible for both the reduction in cell proliferation and induction of apoptosis (Shipman et al 1998). Aparicio and colleagues (1998) demonstrated that ZA has more potent cytoreductive effects compared to PAM in human myeloma cell lines such as RPMI 8226. ZA induced apoptosis on tumour cells was shown by DNA fragmentation and cytoplasmic blebbing. Minodronate, another NBP was reported to exhibit cytoreductive effects on the myeloma cell lines HS Sultan, RPMI8226 and U266 is (Iguchi et al 2003). Recently, it has been demonstrated that ZA had inhibitory effects on the growth of plasma cell lines such as RPMI8226, INA-6, JK-6E, L363 and JK-6L with maximum inhibitory concentration (IC_{50}) ranging from 23-204 μ M. The inhibitory effect was shown to be due to induction of apoptosis using annexin-V and actinomycin D apoptotic assay. No evidence of cytotoxic effects was observed in peripheral blood mononuclear cell (PBMC) even at a concentration as high as 300 μ M (Guenther et al 2010). Despite its direct apoptotic effects, NBPs also have an indirect inhibitory effect on myeloma cells by inhibiting IL-6 synthesis by the BMSCs and osteoblasts. Kawano et al (1988) and Catlett-Falcone et al (1999) showed that IL-6 produced by BMSC and osteoblasts plays a very important role in the development of myeloma in the BM microenvironment. However, the mechanisms of apoptotic

induction by NBPs on myeloma cells were independent of IL-6 production, as exogenous IL-6 did not abrogate the apoptotic effects of ZA or PAM (Aparicio et al 1998; Derenne et al 1999).

1.5.2 PRE-CLINICAL EVIDENCE OF AN ANTI-MYELOMA EFFECT OF ZA

Yaccoby and colleagues (2002) demonstrated that ZA or PAM treatment resulted in the reduction of tumour burden in human bones implanted in SCID-hu mice (severe combined immune-deficient mice implanted with human bone) when compared with untreated controls. The reduction in tumour burden was shown as a reduction in serum levels of human-paraprotein (hlg). However, no effect was seen either with PAM or ZA when the tumour was induced by injecting myeloma cells from patients with extramedullary disease. This shows that the extramedullary tumour growth in myeloma were insensitive to the inhibitory effects of BPs which suggests that the anti-tumour effect mediated by ZA was indirectly through modification of the BM (Yaccoby et al 2002). In the 5T2MM murine model of myeloma, ZA (120 µg/kg) treatment of established tumours resulted in a reduction of tumour-induced osteolytic lesions. In addition, ZA treated mice exhibited reduced tumour area, reduction in micro-vessel density in areas of tumour development in bone, reduction in serum paraprotein levels and prolongation of disease-free survival when compared to untreated controls (Croucher et al 2003b). In another preclinical study, ZA treatment was shown to prolong survival in SCID mice injected with INA-6.Tu1 human myeloma cells. Here, ZA treatment was shown to induce apoptosis in extraskeletal sites. Presence of unprenylated forms of Rap1A in tumour homogenates suggests a direct inhibitory effect on myeloma cells *in vivo* via inhibition of mevalonate pathway (Guenther et al 2010). In another study, ZA treatment in the 5TGM1 murine model of myeloma showed significant reduction in tumour burden as assessed by changes in serum paraprotein level (Dairaghi et al 2012).

1.5.3 EVIDENCE OF AN ANTI-MYELOMA EFFECT OF ZA IN CLINICAL TRAILS

A number of clinical trials have shown ZA treatment to exert an anti-tumour effect not only in MM but also in breast cancer, prostate cancer and renal cell carcinoma. The first clinical evidence of anti-myeloma effects in BPs was demonstrated by Berenson et al (1998) who showed improvement in OS (14 vs. 21 months, $P=0.041$) in 2 out of 198 stage III myeloma patients who received intravenous PAM with anti-myeloma chemotherapy when compared with placebo. Similarly, McCloskey et al (1998), in a double-blind placebo controlled trial in patients without skeletal fractures at the time of treatment showed a significant improvement in survival using oral CLO with standard chemotherapy (59 vs. 37 months; $P=0.006$). Avilés et al (2007) showed ZA treatment with standard chemotherapy (cyclophosphamide, vincristine, melphalan, and prednisone) improved the event-free survival (EFS) and OS in advanced myeloma patients up to 80% compared to 52% and 48% respectively in chemotherapy alone treated control group. Further, ZA treatment along with standard chemotherapy for metastatic prostate cancer showed more than 50% reduction in prostate specific antigen (PSA), a diagnostic marker for prostate cancer progression levels suggesting a possible anti-tumour effect (Dabaja et al 2004; Vordos et al 2004). Monthly doses of ZA prolonged bone metastasis-free survival in

patients with advanced metastatic solid tumours with no evidence of bone metastases at the time of treatment (Mystakidou et al 2005). Moreover, ZA combination with other chemotherapeutic agents in early breast cancer treatment also showed improvement in the disease-free and OS by 32% (Gnant et al 2010). In a recently conducted phase III clinical trial (myeloma IX study) involving 1960 patients, addition of ZA treatment to standard anti-myeloma chemotherapy showed a 16% increase in the OS and a 12% increase in the progression-free survival (PFS) when compared to patients treated with oral CLO (Morgan et al 2010a). More recently, in a single-centered double blind randomized placebo-controlled study involving 308 previously untreated symptomatic myeloma patients using intravenous ZA along with chemotherapy (dexamethasone, all- trans- retinoic acid, and interferon alpha 2b) followed by ASCT resulted in a significant prolongation of 10-year PFS (60.4 vs. 38.4 months; $P<0.001$) and 10-year OS (67 vs. 48 months; $P<0.001$) when compared with placebo-treated control groups (Avilés et al 2013). Furthermore, in a network meta-analysis including 6692 patients from 20 randomized clinical trials ZA treatment showed improved OS when compared with etidronate or placebo (Mhaskar et al 2012). In contrast to these reports, McCloskey et al (1998) showed no improvement in OS in patients receiving oral CLO along chemotherapy when compared with placebo treated patients. Similarly, Mutso et al (2008) showed intravenous ZA treatment (4mg, monthly) administered for a year in asymptomatic patients did not delay the progression to symptomatic disease when compared with untreated control groups over a median follow-up for 64.7 person-months (67 vs. 59 months; $P=0.8312$).

1.5.4 THE MECHANISMS OF AN ANTI-MYELOMA EFFECT BY ZA

There is clear evidence that ZA either independently or in combination with other chemotherapeutic agents, in addition to its anti-resorptive property, also exhibits anti-tumour activity in MM and in other solid tumour with bone involvement. ZA exhibits their anti-myeloma effect in several possible ways (figure 1.5-1).

Mechanisms responsible for the inhibitory effect of ZA on myeloma cell

Several *in vitro* studies have shown that ZA and certain NBPs have a cytostatic and pro-apoptotic effect on primary human myeloma cells and various myeloma cell lines by inhibiting proliferation and inducing apoptosis (Croucher et al 2003a). ZA was shown to achieve maximum inhibitory effect on myeloma cell lines *in vitro* between 10 to 100 μ M (Shipman et al 1997; Aparicio et al 1998; Derenne et al 1999; Croucher et al 2003a; Baulch-Brown et al 2007). Accumulating evidence suggests that NBPs induce inhibitory and apoptotic effects in tumour cell lines by inhibiting the mevalonate pathway similar to the effect on osteoclasts (Diel 2000). Loss of protein prenylation of small GTPases such as Ras, Rap1A and Rho results in defective downstream signalling which causes the apoptotic effects in tumour cells. The administrations of farnesol and geranylgeraniol have been shown to partially prevent the inhibitory effects of BPs (Shipman et al 1998; Iguchi et al 2003). In a study reported by Benford et al (2001), the NBP induced apoptotic effect on osteoclasts was due to caspase-3 activation which

caused loss of mitochondrial membrane potential. Down-regulation of anti-apoptotic proteins of the bcl-2 family of apoptotic genes (*Bcl-xL*, *Bcl-W*) has been attributed to mitochondrial release of cytochrome c which activates caspase 3 (Senaratne et al 2002). Studies by Senaratne et al (2002) demonstrated that NBPs down regulate *bcl-2* induced apoptosis in breast cancer cell lines. Similar results were produced by Aparicio et al (1998) when forced *bcl-2* expression protected IM-9 cells from the ZA induced apoptotic effects but not the cytostatic effect. Interestingly, inhibiting the mevalonate pathway using a HMG CoA reductase inhibitor (fluvastatin) did not affect the Bcl-2 family protein; instead it inhibited anti-apoptotic Mcl-1 and phosphor-Rb (Baulch-Brown et al 2007). However, the *in vivo* BM microenvironment is far more complicated with complex cellular interactions and cell signalling. Moreover, the concentration at which the cytoreductive effects of BPs described in the *in vitro* settings are much higher to the peak plasma concentration of the drug. BPs owing to their high bone binding affinity rapidly translocate from the plasma and concentrates into areas of active bone resorption. ALN, another NBP has been shown to reach a local concentration in the range of 0.1-1 mM. Although, the local concentration of ZA at the osteoclast-bone interface was shown to be well above the anti-tumour threshold, it still remains unclear whether it would reach the myeloma tumour cells in the BM (Sato et al 1991; Clezardin 2005).

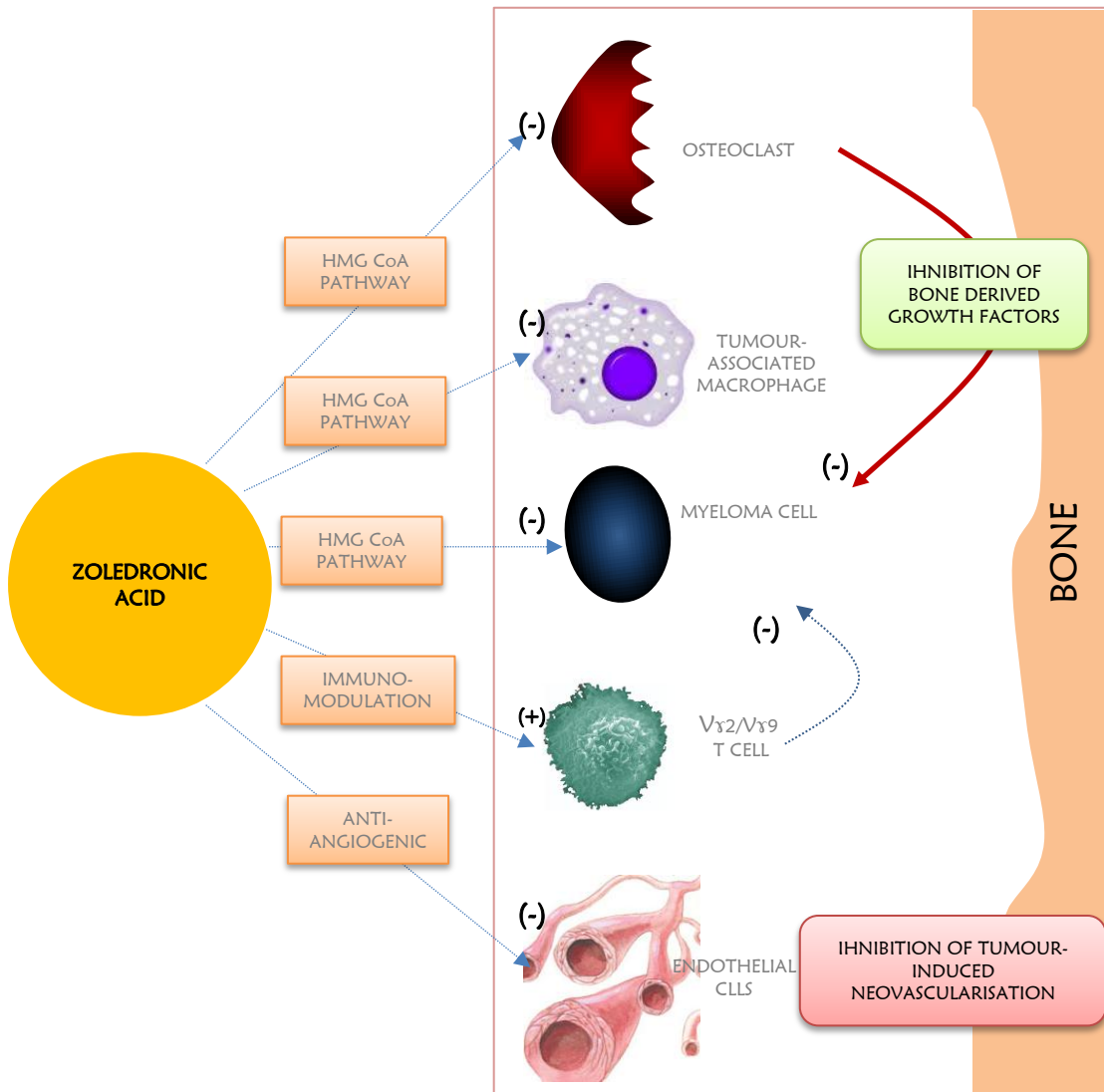


Figure 1.5-1: Possible anti-tumour mechanisms of ZA in MM.

Schematic representation of different possible mechanisms by which ZA mediates an anti-tumour effect in MM. As HMG CoA inhibitor ZA can directly inhibit cell proliferation and induce apoptosis in osteoclasts as well as myeloma cells. Inhibition of osteoclastic activity suppresses the release of bone derived growth factor which may in turn affect myeloma cell survival. Myeloma cell also inhibits tumour associated macrophages which were shown to support and promote tumour growth. ZA treatment improves the antigen recognition of the tumour cells to the V γ 2/V γ 9 T cells thereby causing cancer cell death. ZA also inhibits tumour induced neovasculogenesis.

The indirect anti-myeloma effect of ZA by inhibition of osteoclastic bone resorption

The anti-tumour effects of BPs on most cancer-induced bone metastases suggests that the anti-tumour effect observed may be due to osteoclast inactivation and subsequent suppression of bone resorption. Bone is a complex environment rich in various growth factors including IGF, TGF- β , PDGF, b-FGF, IL-6 and bone morphogenetic protein (BMP) which makes it a fertile environment (niche) for tumour cells to survive and colonise. Following cancer-induced osteoclastic bone resorption, these growth factors are released in the BM microenvironment which will facilitate tumour cell survival and growth. The

tumour cells in turn stimulates the production of factors such as RANKL which promotes osteoclastogenesis and thereby bone resorption, establishing a ‘vicious cycle’ between the tumour cells and the cellular components of the bone (Yoneda et al 2005). BPs are potent inhibitors of bone resorption and they inhibit the release of these factors which facilitates tumour cell survival thereby reducing tumour cell colonisation and eventually skeletal tumour burden. Specific osteoclastogenesis inhibitors such as Fc.OPG and recombinant RANK-Fc were also shown to exhibit anti-tumour effects in bone similar to the BPs (Sordillo et al 2003; Iqbal et al 2011). This suggests that the anti-tumour effect seen with ZA may be an indirect effect mediated by inhibition of osteoclastic bone resorption (Croucher et al 2003b; Vanderkerken et al 2003b).

The anti-angiogenic effect of ZA

ZA has been shown to inhibit angiogenesis in both *in vitro* and *in vivo* models. Wood and colleagues (2002) demonstrated that ZA inhibited foetal calf serum (FCS) and bFGF induced HUVEC proliferation in a dose-dependent fashion at a concentration of 4-5 µM. It also induces cell cycle arrest and prevents HUVEC cell adhesion and migration at concentrations >30 µM. ZA also dose-dependently inhibited capillary formation in the chorio-allantoic membrane at a concentration between 10⁻⁴ to 10⁻³ M. In addition, ZA was also shown to inhibit angiogenesis induced by subcutaneous implants impregnated with bFGF in murine models. Revascularisation of castrated rat prostate was inhibited by NBPs when vascularisation was promoted using testosterone (Fournier et al 2002). ZA was shown to reduce microvessel density in the tibiae and femora developing tumours in 5T2 models of myeloma (Croucher et al 2003b). Similar results were demonstrated with Neridronate, another NBP on HUVEC cell proliferation, matrigel assay and CAM assays (Ribatti et al 2007). There is also evidence suggesting BPs reduce serum concentration of VEGF in cancer patients, ZA induced prolonged inhibition of VEGF (up to 21 days), whereas the effect was observed only for 7 days in PAM (Santini et al 2002; Santini et al 2003). Recently, ZA has been shown to induce apoptosis in endothelial progenitor cells by altering the expression of VEGFR2 and VE cadherin. Inhibitory effect of ZA were almost rescued by the addition of GGOH suggesting that inhibition of protein prenylation was the main mechanism responsible for these effects (Yamada et al 2009).

The immunomodulatory effect of ZA

In addition to direct and indirect anti-tumour effects, BPs exhibits immunomodulatory effects (Kunzmann et al 2000; Das et al 2001; Mariani et al 2005). NBPs cause expansion of $\gamma\delta$ T cells ($\gamma\delta\text{V}\delta 2$ T cells) in PBMC cultures which is dependent on IL-2 and also causes dose-dependent inhibition of plasma cell proliferation in MM patient BM mononuclear cells (BMMC) ($\gamma\delta^+$) cultures, whereas no effects were observed in $\gamma\delta^-$ BMMC cultures (Kunzmann et al 2000). NBPs owing to their structural similarities with prenyl phosphate metabolites such as isopentyl pyrophosphate and geranyl pyrophosphate can bind to the tumour cell surface, acting as a $\gamma\delta$ T cell antigen leading to activation and proliferation of $\gamma\delta\text{V}\delta 2$ T cells through $\gamma\delta$ TCR mediated signalling (Bukowski et al 1998;

Kunzmann et al 2000; Mariani et al 2005). Mature $\gamma\delta$ T cells were shown to induce tumour lysis by cell mediated cytotoxicity in a variety of tumour cells by the secretion of cytokines especially IFN- γ (Fisch et al 1990; Haas et al 1993; Kunzmann et al 2000). No evidence of an immune response was observed with non-NBP like CLO or etidronate. Treatment of cancer patients with bone metastases with ZA also has showed evidence of an increase in the percentage of effector $\gamma\delta$ T cells which produced IFN- γ (Dieli et al 2003).

The effect of ZA on tumour associated macrophages

Studies have shown that tumour associated macrophages (TAMs) play a critical role in the tumour progression and metastases. Macrophages are derived from monocytes and play an important role in the immune system. Based on cell polarisation and functional heterogeneity, macrophages are classified into the M1 (classically activated) which are immunostimulatory (defend the host organism) and the M2 (alternately activated) which are immunosuppressive (Berardi et al 2013). TAMs, which include MM associated macrophages possess pro-tumorigenic property by producing IL-6, IL-10 and VEGF which were shown support and promote myeloma cell survival and proliferation (Kim et al 2012). Scavelli et al (2008) showed that macrophages from myeloma patients promote tumour vasculogenesis and produce capillary-like network (vasculogenic mimicry) upon interaction with VEGF and FGF-2 released by the myeloma cells. Moreover, TAMs were also shown to contribute to myeloma development by immunosuppressive mechanism and chemoresistance to the tumour cells (Berardi et al 2013). Studies have shown that N-BPs such as ZA inhibit proliferation and induce apoptosis in macrophages by inhibiting the mevalonate pathway (Moreau et al 2007). Furthermore, Mönkkönen et al (2006) showed N-BPs in addition to inhibiting FPP synthase also produces cytotoxic AppI analogue which induces macrophage apoptosis. In addition, Coscia et al (Coscia et al 2010) showed that ZA also has the ability to repolarise M2 phenotype TAMs to M1 types which are tumouricidal in *in vivo* ZA treated macrophages.

The effect of ZA on tumour cell adhesion and invasion

BPs in addition to their cytoreductive properties also inhibits adhesion of tumour cells to bone matrices. BP mediated inhibition of adhesion on both mineralised and unmineralised bone matrices was demonstrated in breast and prostate cancer cells (van der Pluijm et al 1996; Boissier et al 1997; Magnetto et al 1999). A dose-dependent increase in inhibition of adhesion was observed at a concentration ranging from 10^{-6} to 10^{-4} M in ibandronate (IBN), ALN and PAM in order of potency which is parallel to their osteoclastic resorptive potency. Little or no effect was observed with non-NBPs such as CLO or etidronate (van der Pluijm et al 1996). The mechanism underlying this effect is not clearly understood. The interference of NBPs with membrane bound adhesion molecules may be a reason for this effect. Increasing evidence suggests that BP mediated inhibition of geranylgeranylation could inhibit integrin activation (Coxon et al 2004; Clezardin et al 2005).

BP treatment was also shown to inhibit tumour cell invasion *in vitro* (Magnetto et al 1999; Boissier et al 2000; Virtanen et al 2002; Denoyelle et al 2003). Tumour invasion is a complex process which involves digestion of the basement membrane followed by cell migration (Magnetto et al 1999). NBPs were shown to inhibit tumour cell invasion at a concentration as low as 10^{-12} M (Boissier et al 2000; Virtanen et al 2002). ZA at a concentration of 0.1 μ M and ALN and CLO at a concentration of 10 μ M were shown to inhibit tumour cell migration. Inhibition of the mevalonate pathway especially geranylgeranylation has been attributed to be responsible for this inhibitory effect as this was rescued by addition of GGOH and not by FOH. Inactivation of the small GTPase RhoA (protein prenylation) and inhibition of SDF-1/CXCR-4 prevented tumour cell migration. No evidence of a reduction in matrix metalloproteinase (MMP) -2 and MMP-9 was shown at the indicated concentrations (Virtanen et al 2002; Denoyelle et al 2003). However, ZA at 100 μ M was shown to inhibit both MMP-2,-9 and -12 activity in MDA-MB-231 breast cancer cell line. The mechanism of MMP inactivation appears to be chelation of divalent cations necessary for MMP activation as the inhibitory activity was completely rescued by exogenous zinc addition (Boissier et al 2000). Interestingly, CLO at 0.1 μ M inhibited tumour cell invasion which is not protected by GGOH or FOH suggesting that it acts through a completely unknown mechanism which warrants investigation (Boissier et al 2000).

1.6 AIMS AND OBJECTIVES

Myeloma cell development in bone depends on the bone microenvironment for colonisation and survival. Evidence that ZA delays the incidence of MBD and EFS in myeloma patients suggests that it may interfere with early cell colonisation events. Blocking the release of bone derived growth factors by inhibiting osteoclastic resorption may therefore alter the BM niche to be unfavourable for the colonisation and survival of myeloma cells. Based on these observations, I hypothesised that 'blocking bone resorption with ZA will prevent the colonisation of myeloma cells and stop the initiation of growing lesions or colonies from myeloma cells that resides in bone thereby preventing development of overt myeloma'.

The main aims were:

1. To determine whether blocking bone resorption with ZA inhibits the initial colonisation of bone by myeloma cells.
2. To determine whether blocking bone resorption with ZA prevents the development of overt myeloma colonies.
3. To determine whether blocking bone resorption with ZA delays the onset of morbidity (hind limb paralysis or sickness).

The objectives were:

1. To determine the time taken by ZA to effectively suppress osteoclastic bone resorption in C57BL/KaLwRij mice.
2. To establish the different developmental stages of myeloma using the 5TGM1 murine model of myeloma.
3. To determine the effect of ZA treatment on the early stages of myeloma development in bone.
4. To determine the effect of ZA treatment on the late stages of myeloma development in bone and the effect of treatment on disease-free survival.

CHAPTER 2 MATERIALS & METHODS

2.1 MATERIALS

2.1.1 ZOLEDRONIC ACID (ZA)

CAS number: [118072-93-8](#)

Zoledronic Acid or Zoledronate (ZA) [1-hydroxy-2-(1H-imidazol-1-yl) ethane-1,1-diyl] bisphosphonic acid was supplied as a disodium hydrate salt (4.5 H₂O) by Novartis Pharma, Basel, Switzerland.

2.1.2 THE 5TGM1 MURINE MYELOMA CELL LINE

The 5TGM1 murine myeloma cell line stably transfected to express eGFP (hereafter referred as 5TGM1-eGFP) was a kind gift from Dr Claire Edwards (University of Oxford, United Kingdom). The 5TGM1 myeloma cells were derived from repeated *in vivo* passaging of 5T33MM murine myeloma tumour-bearing mice cultured in Iscove's Modified Dulbecco's Media (IMDM) with 10% FCS and 10% murine stromal cell-conditioned media (Garrett et al 1997).

2.1.3 C57BL/KaLwRij MICE

C57BL/KaLwRij mice were purchased from Harlan, Harlan laboratories, UK and St. James's Biomedical Services, St. James University Hospital, Leeds, UK and was housed in the University of Sheffield Biological Services located in Royal Hallamshire Hospital, Sheffield, UK. *In vivo* work was approved by UK Home Office under the project licence PPL No: 40/2901 held by Prof. Peter Croucher and PPL No: 40/3462 held by Dr Colby L Eaton, University of Sheffield, UK.

The C57BL/KaLwRij strain was developed in 1921 by Little from a brother and sister pair (57 x 52) of Miss Abby Lathrop's stock. In 1947, they were transferred from Strong, Cold Spring Harbor, New York, to Kaplan, Stanford, California, USA, to Law, National Cancer Institute, Bethesda, MD, USA. In 1965, they were transferred to the Radiobiological Institute TNO, Rijswijk, the Netherlands and transferred to Harlan Laboratories in 1994 through the acquisition of ITRI-TNO, Rijswijk – Harlan Laboratories. The C57BL/KaLwRij strains of mice are the most widely used strain for studies on human idiopathic paraproteinemia and MM. The 5TGM1 murine myeloma model is a variant of the 5TMM series of spontaneously developing murine model of myeloma in aged C57BL/KaLwRij mice in which rapidly proliferating, non-adherent 5T33 cells from BM aspirates of 5T33 tumour-bearing mice were repeatedly cultured in Iscove's Modified Dulbecco's Media (IMDM) with 10% FCS and 10% murine stromal cell-conditioned media (Radl et al 1978; Garrett et al 1997).

2.2 GENERAL METHODS

2.2.1 CELL CULTURE

Cells were passaged in RPMI 1640 media with Glutamax (GIBCO-Invitrogen 1870-010) supplemented with 10% foetal calf serum (FCS), 1% Penicillin-streptomycin (Pen-strep) (100 units/ml of penicillin and 100 µg/ml of streptomycin), 1 mM sodium pyruvate and 100 mM non-essential amino acid (NEAA). The cells were incubated in a 5% CO₂ incubator at 37°C with 95% humidity and passaged every 3-4 day in T75 flasks under sterile conditions in a cell culture hood. Hereafter, the cell culture media with the fore mentioned additives will be referred to as ‘complete media’.

2.2.2 CRYOPRESERVATION AND RESUSCITATION OF CELL LINES

All cell lines were frozen in liquid nitrogen (N₂) for long term storage in cryo-vials. Cells were pelleted by centrifuging at RCF 1509.3 X g for 5 min and suspended in the freezing medium (Foetal calf serum (FCS) + 10% DMSO) at the rate of 2 X 10⁶ cells per ml. The cell suspensions were then transferred to cryo-vials and frozen at the rate of -1°C/min using Nalgene 5100-0001 PC/HDPE Mr. Frosty 1 Degree C left overnight in -80°C freezer. The cryo-vials were transferred to liquid N₂ dewars for long-term storage.

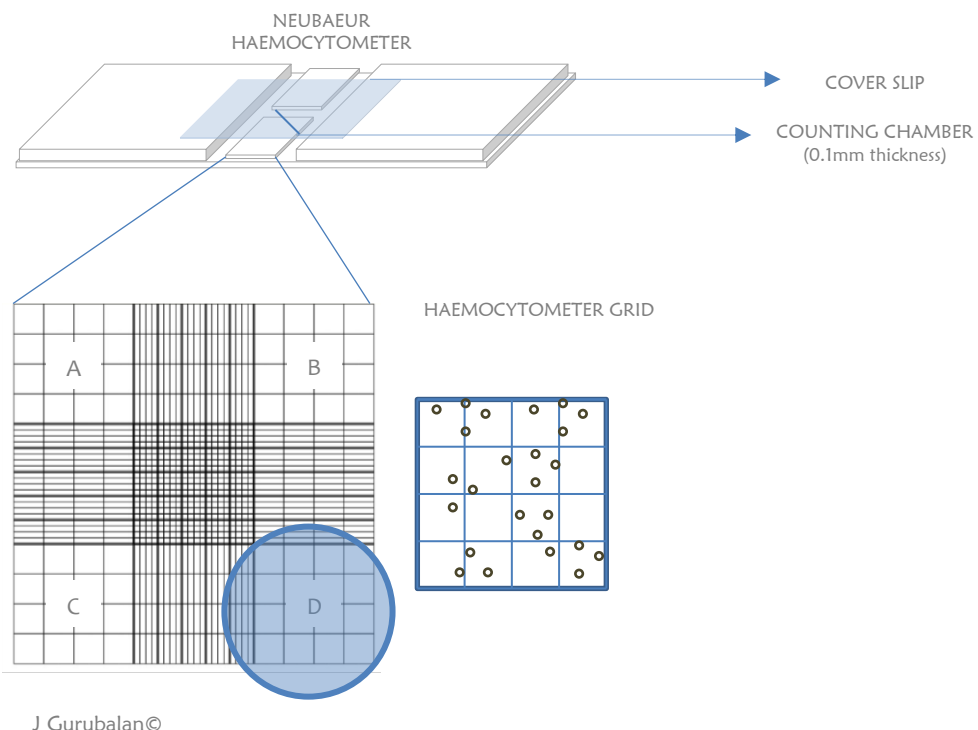
Cell lines preserved in liquid N₂ were thawed rapidly using a 37°C water bath. The cells along with the freezing medium were mixed gently in 19 ml of pre-warmed complete media. The contents were centrifuged at RCF 1509.3 X g for 5 min to obtain cell pellets. Cell pellets were then washed twice in 10 ml of complete media and resuspended in complete media in a sterile flask.

2.2.3 CELL COUNTING USING A HAEMOCYTOMETER

Cell counting was done using a Neubauer haemocytometer. Cells were stained with 0.4% trypan blue (TP) dye (1:1 ratio). 10 µl of a single cell suspension was mixed with 10 µl of TP and loaded in to the capillary space between the cover slip and the counting chamber of the haemocytometer (figure 2.2-1). Using an inverted light microscope the number of cells in the four corner squares was counted. Cells inside the grid and cells touching the bottom and left lines of each square were counted normally, while cells touching the upper and right lines of the square were not counted.

The volume held under a single corner square is 0.1 mm³ (0.0001 ml), so the number of cells (n) in a single square is the number of cells in 10⁻⁴ ml. The number of cells per ml can be calculated using the formula

$$\text{Average no. of cell per ml} = \text{Average cell count (n/4)} \times \text{Dilution factor (D.F)} \times 10^4$$



J Gurubalan©

Figure 2.2-1: Cell counting using a Neubaeur haemocytometer.

A Neubaeur haemocytometer has a laser etched grid on the slide inside a capillary chamber and is used to measure cell density. The numbers of cells in the four corner squares (A, B, C & D) were counted by visualising under a light microscope and the average cell number per ml was measured using the formula **average cell count (n/4) X dilution factor (D.F) X 10⁴**.

2.2.4 DID LABELLING OF 5TMM CELLS

5TGM1-eGFP murine myeloma cells were labelled with 1,1'-dioctadecyl-3,3,3',3'-tetramethylindodicarbocyanine, 4-chlorobenzenesulfonate salt (DID dye) for identification of cells by flow cytometry and multiphoton microscopy. DID is a lipophilic carbocyanine dye that inserts into the phospholipid bilayer of the cell membrane (figure 2.2-2).

Vybrant® DiD Cell-Labelling Solution (Catalogue No. V-22887; *Life Technologies*) was used for labelling 5TGM1-eGFP murine myeloma cells. The amount of myeloma cells to be labelled was suspended in RPMI 1640 with Glutamax (no additives) at concentration of 1×10^6 cells per ml of media. DID vybrant labelling solution was added to the cell at the rate of 10 µl per 1×10^6 cells per ml of serum free media and mixed gently by pipetting (addition of DID dye should be done in dark as light exposure will result in photo bleaching) and incubated for 30 min in a 5% CO₂ incubator. After incubation, FCS (10% of the volume) was added to the mixture and centrifuged at RCF 1509.3 X g for 5 min at RT. Addition of FCS prevented the cell pellet to be lost during centrifugation. Cell pellets were then washed twice using complete media and resuspended in the required volume of sterile PBS (2×10^6 cells in 100 µl of PBS per mouse).

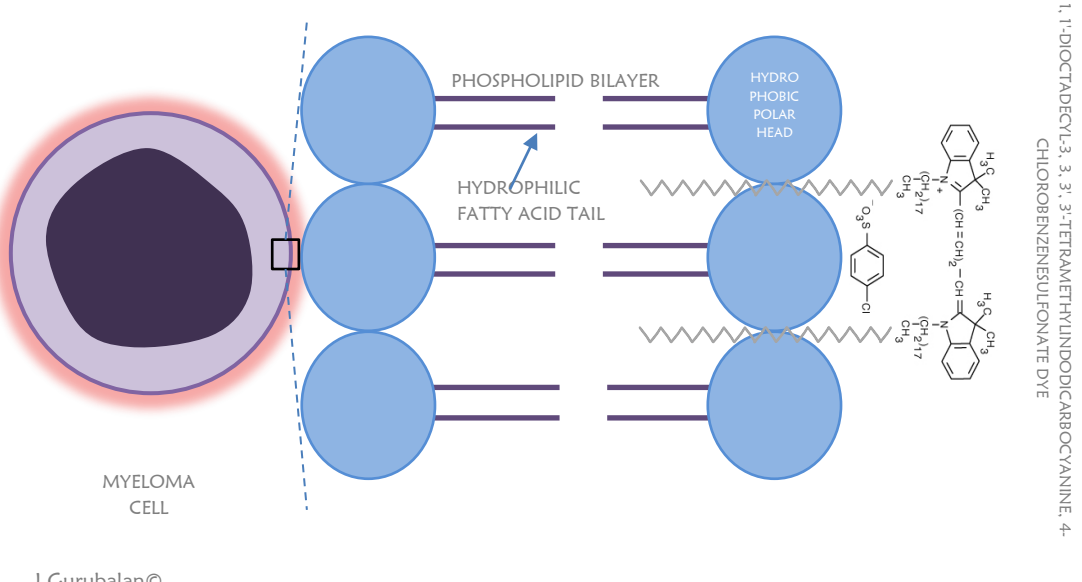


Figure 2.2-2: DID dye labelling cell membrane.

DID belongs to the class of amphiphilic carbocyanine dyes with charged fluorescent head groups and long lipophilic aliphatic tail groups that conveniently inserts into the phospho-lipid bilayer of the cell membrane. A study using fluorescent polarization microscopy has shown that DID dye inserts into the cell membrane using their long lipophilic aliphatic tail chains which anchors into the membrane perpendicularly with the fluorescent heads lying parallel on the cell surface membrane (Axelrod 1979).

2.2.5 DETECTION OF FLUORESCENTLY LABELLED 5TGM1 MURINE MYELOMA CELLS (*IN VITRO*) USING FLOW CYTOMETRY

The proportion of eGFP⁺ and DID⁺ labelled myeloma cells were determined by flow cytometry in order to achieve maximum labelling of the cells prior to injection into the mice. Flow cytometry analysis was done using FACS Calibur flow cytometer (Becton Dickinson, Oxford, UK) with CellQuest software. FACS Calibur is a dual-laser (488 nm - blue laser; 635 nm - red-diode laser) multi-parameter system designed for multi-colour analysis. 1×10^6 cells were washed twice in PBS by centrifuging at RCF 1509.3 X g for 5 min at RT and resuspended in 1 ml of PBS into FACS tubes. Samples were then run through the flow cytometry for the detection of eGFP⁺ or DID⁺ labelled cells for up to 1×10^6 cells. Unlabelled cells were used as negative control for setting up the flow cytometer. 488 nm laser was used to detect eGFP⁺ signals (em: 507-510 nm) in the FL1 channel and 635 nm laser was used to detect DID⁺ (em: 675-710 nm) in the FL4 channel (figure 2.2-3).

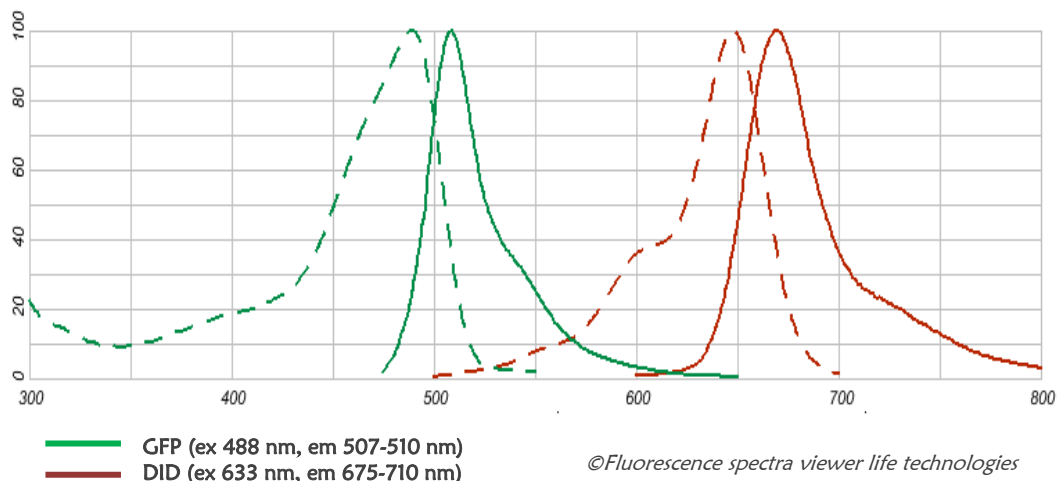


Figure 2.2-3: eGFP and DID excitation and emission spectra.

2.2.6 DETECTION OF FLUORESCENTLY LABELLED 5TGM1 MURINE MYELOMA CELLS IN BONE MARROW (EX VIVO) USING FLOW CYTOMETRY

In order to quantitate the percentage of 5TGM1-eGFP-DID cells in the BM using flow cytometry, the BM cells were flushed out in a 1 ml eppendorf with 500 µl of 1 X PBS using an insulin syringe. BM cells were centrifuged at RCF 1509.3 X g for 3-4 min at RT and the supernatant removed. The BM cells were suspended and incubated in 1 X H-lyse buffer (Whole blood erythrocyte kit, Catalogue No: WL1000 R&D systems) for 10 min at RT until red blood cell lysis was complete. When red blood cell lysis was complete, the supernatant is removed by centrifuging at RCF 1509.3 X g RT for 3-4 min. The cell pellets were then washed twice in 1 ml of 1 X wash buffer (Whole blood erythrocyte kit, Catalogue No: WL1000 R&D systems) by wash centrifuging. Once the cells were washed they were resuspended in 100 µl of 1 X PBS and samples were run through flow cytometer (FACS Calibur, Becton Dickinson, Oxford UK) for up to 10^5 cells for the detection DID⁺, eGFP⁺ or dual labelled 5TGM1-eGFP⁺-DID⁺ cells in the BM. BM cells from naïve tumour-free C57BL/KaLwRij were used as negative control for setting up the flow cytometer. 488 nm laser was used to detect eGFP⁺ signals (em: 507-510 nm) in the FL1 channel and 635 nm laser was used to detect DID⁺ (em: 675-710 nm) in the FL4 channel.

2.2.7 SORTING OF 5TGM1-eGFP-DID LABELLED CELLS

Enrichment of 5TGM1-eGFP murine myeloma cell population in culture was achieved by fluorescent activated cell sorting (FACS) using FACS Aria cell sorter (Becton Dickson Biosciences). Cells were sorted for eGFP⁺ population using 488 nm blue laser into 1 ml of complete media. These cells were then washed twice in PBS or complete media and resuspended in complete media in T75 flask and incubated at 5% CO₂ incubator at 37°C.

2.2.8 INJECTION OF 5TGM1 CELLS INTO MICE UNDER LOCAL ANAESTHESIA

5TGM1-eGFP-DID murine myeloma cells were injected via the lateral tail vein using 1 ml insulin syringe. For the purpose of intravenous injection, the tail was anesthetized by topical application of a local anaesthetic agent. EMLA cream 5% (active ingredient, lidocaine & prilocaine) was applied throughout the tail 60 min prior to the injections. 5TGM1-eGFP murine myeloma cells were labelled with DID dye prior to injection (section 2.2.4). Mice were placed in a 37 °C incubator for approximately 5-10 min in order to dilate the vein. Mice were then restrained using a bench top restrainer and 2 X 10⁶ 5TGM1-eGFP-DID cells suspended in 0.1 ml of sterile PBS were injected slowly through the tail vein.

2.2.9 BLOOD COLLECTION VIA CARDIAC PUNCTURE WHILE MICE ARE UNDER GENERAL ANAESTHESIA

For the purpose of cardiac puncture to obtain blood samples for serum extraction, the mice were sedated using intra-peritoneal injection of sodium pentothal (approx. 0.05-0.1 ml) using insulin syringes. Pinch reflex was practised to assess the depth of anaesthesia before commencing the procedure.

Cardiac blood collection was done using 1 ml syringe with a 27 gauge needle after anaesthetizing the mice using 0.5 ml/kg of pentobarbitone. Blood was withdrawn from the left ventricle by gently inserting the needle perpendicular to the chest wall through the left lateral chest wall for about 5-10 mm. The plunger was withdrawn gently to allow blood to fill the syringe. The blood was then transferred to 1.5 ml eppendorf tube and was allowed to clot at RT for about 60 min and stored at 4°C or ice until processing. Following cardiac bleeding, the mice were euthanized humanely.

2.2.10 SERUM COLLECTION & SAMPLE STORAGE

After blood collection the mice were sacrificed by cervical dislocation. Femora and tibiae were stripped of soft tissues and stored appropriately. Storage conditions for the different samples are discussed in detail in the appropriate chapters.

Serum was obtained from blood samples by centrifuging the blood samples in an eppendorf at RCF 1509.3 X g for 10 min at 4°C so that the blood clots and settles at the bottom and serum on the top. The serum was carefully removed without disturbing the blood clot and stored appropriate aliquots at -80°C.

2.2.11 ADMINISTRATION OF ZOLEDRONIC ACID TO MICE

500 µg/ml stock solution of ZA was prepared in PBS and stored in -20°C. Prior to injection, a working concentration of ZA (125µg/kg) was prepared by dissolving 1 ml of stock solution in 19 ml of sterile

PBS. The ZA solution was filter sterilised using a 0.2 µm pore filter and 0.1 ml was injected subcutaneously into the scruff over the neck of the mouse.

2.2.12 MICRO-COMPUTED TOMOGRAPHY

Micro-computed tomography (MicroCT) was performed using SkyScan 1172 Desktop X-ray tomographer manufactured by SkyScan N.V. Aartselaar, Belgium. This equipment is a modified hospital CAT scan where high resolution cross-section and 3D virtual models can be produced of objects non-destructively. The pixel size of the cross-section images are in micro meter range, hence the high resolution. The system allows quantitative and 3D morphometric analysis of the bone samples.

Micro CT works on the simple principle of x-ray projection, where multiple angular x-ray projection of a 3D object is performed using a cone beam micro focus x-ray source. A planar (2D) x-ray detector is used to capture magnified projection images which are fed to a computer to build 3D virtual cross-section images of the whole object (figure 2.2-4). Complete quantitative analysis on the morphology of the trabecular and cortical component of the long bones were done using a medium sized 2000 X 1048 pixel camera and an x-ray source powered by 50 kV and 200 µA electric current. A 0.5 mm aluminium filter was used to filter out the low energy radiations. The proximal end of tibia was scanned at 4.3 µm pixels for every 0.7° rotation of 180°.

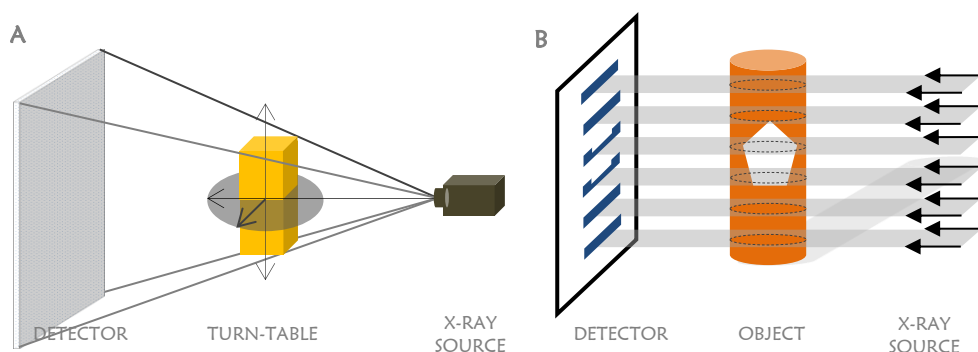


Figure 2.2-4: Principle of micro-computed tomography imaging.

Micro-computed tomography imaging is based on collection of magnified 2D image projection of the 3D object from a micro focus X-ray source. The micro focus source produces a cone X-ray beam which illuminates the object area. The object is placed on a rotatory turntable and planar projection images at multiple angles are collected by the detectors (**A**). As a cone beam x-ray sources are not able to produce parallel beam geometry, tomographic reconstruction is done by reordering the shadow information. A ‘Feldkamp 3D cone beam reconstruction algorithm’ is used to reconstruct the slices to form virtual 3D models of the object scanned (**B**).

The scanned images were reconstructed using NRecon software ver. 1.6.1.1 within a dynamic range of 0 to 0.16 and a ring artefact reduction factor of 1 %. Reconstructed images were then analysed using CTAn ver. 1.9.1.1. Analysis was done on the cross-sectional images of the tibiae at a fixed distance 1.2 mm from the growth plate (reference point). The proximal break in the growth plate was used as a standard reference point for both cortical and trabecular analysis. The analysis was done on a fixed

region extending for 1 mm (figure 2.2-5 A). For trabecular analysis, the trabecular bone was carefully traced on all cross-sectional images of the tibia, not to include cortical bone for the entire region of interest (ROI). Similarly, cortical bone was also analysed. Figure 2.2-5 B shows the trabecular and cortical bone traced out in the cross-section of tibia. Analysis was done in batches using Batch Manager (BatMan) software and the following parameters were measured: trabecular bone volume (% BV/TV), trabecular thickness (Tb. Th), trabecular number (Tb. N), trabecular pattern factor (Tb. Pf), structural model index (SMI) and cortical bone volume (Ct.V). For trabecular analysis the binarised images were thresholded between 80 and 255 and for cortical bones between 90 and 255.

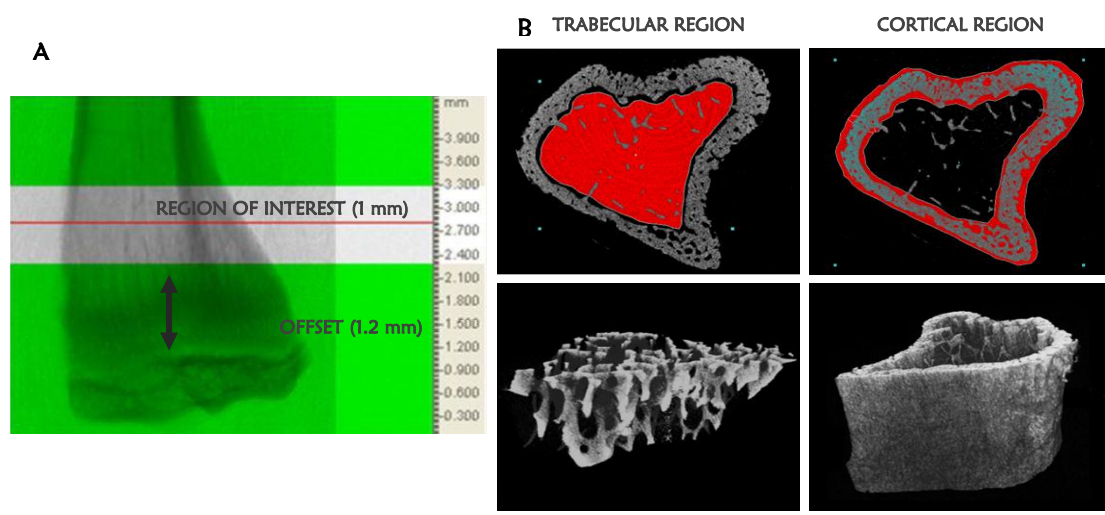


Figure 2.2-5: MicroCT image analysis and quantification.

A longitudinal cross-section of the proximal tibial metaphysis, offset (arrow) 1.2 mm from the distal end of the growth plate, 1 mm ROI for the analysis of cortical and trabecular bone (A). Cortical and trabecular bone were analysed by tracing out boundaries (red) in the ROI and the amount of bone (Ct. V & % BV/TV) and structural parameters were analyzed using CTAn software (B).

2.2.13 CD138 IMMUNOHISTOCHEMISTRY (IHC)

CD138 is a 30 kDa trans-membrane heparan sulphate proteoglycan expressed by normal plasma cells and malignant myeloma cells. CD138 immunohistochemistry (IHC) is a ‘sandwich’ or ‘bridge’ IHC where biotinylated secondary antibody is used for antigen amplification and uses biotin-streptavidin system (antibody-enzyme complex) for antigen detection (figure 2.2-6). CD138 IHC was done using purified rat anti-mouse CD138 (BD Pharmingen Catalogue No. 553712). Slides were incubated at 37°C overnight prior to the day of staining. Slides were dewaxed and rehydrated by dipping them sequentially in xylene 99%, 95% and 70% ethanol 4 min in each followed by water and 1 X PBS. Slides were then incubated with pre-warmed trypsin (A.Menarini Diagnostics MP-955K25) for 10 min at RT for antigen retrieval to break the protein bonds due to formalin fixation and paraffin embedding. After incubation, the slides were washed in 1 X PBS for 5 min. To prevent non-specific binding the tissue samples were incubated in 10% FCS and 10% normal goat serum (Vector Laboratories Catalogue

No.S-1000) for 60 min at RT. Serum block was tapped off and the tissues were incubated in 1:100 purified rat anti-mouse CD138 antibody for 60 min at RT. As Streptavidin-horseradish peroxidase conjugate (SA-HRP) was used for antibody-enzyme detection complex, endogenous peroxide blocking was done by incubating the tissues with 3% H₂O₂ for 30 min at RT. The samples were then washed in PBS and re-incubated in 1:300 dilution of biotinylated goat anti-rat IgG F(ab)₂ for 30 min at RT. After washing in 1 X PBS, the slides were incubated in SA-HRP conjugate for 30 min at RT for the formation of antibody-enzyme detection complex. Slides were then washed in PBS and developed with 3, 3'-diaminobenzidine tetrahydrochloride (DAB) substrate chromogen system (Vector kit SK-4105). After chromogen developing, slides were washed in PBS to remove excess DAB and counter stained with Gills II Haematoxylin (for 20 sec) followed by washing in running tap water for 2-3 min. Slides were then dehydrated and coverslipped using DPX mountant (*Sigma-Aldrich*, Catalogue No. 44581).

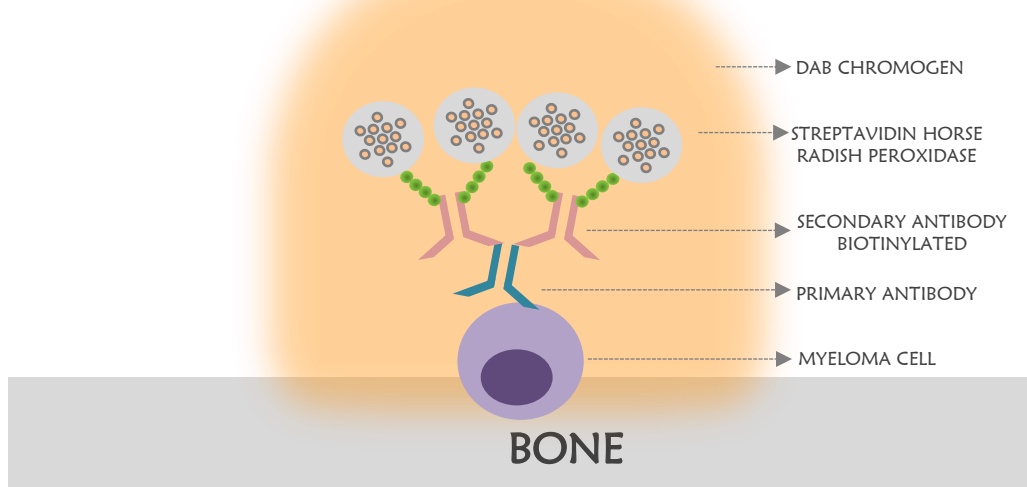


Figure 2.2-6: Principles of ‘sandwich’ or ‘bridge’ immunohistochemical staining of CD138.

CD138 IHC is based on sandwich or bridge immunoassay which depends on biotin binding to avidin. Here, rat anti-mouse CD138 antibody was used as primary antibody to bind to the CD138 expressed by the plasma cells. Biotinylated goat anti-rat IgG F(ab)₂ was used as secondary antibody which binds to the primary antibody. Horse-radish peroxidase (enzyme) conjugated to streptavidin was added which binds to the ‘multiple binding sites’ on the biotin. The main advantage of using a biotin-streptavidin system for antibody-enzyme detection is the potential for amplification due to multiple binding sites for the conjugated streptavidin (antibody-enzyme complex). Finally addition of chromogen results in oxidation of DAB in the presence of horse-radish peroxidase resulting in brown pigments which are firmly deposited around peroxidase on cell membranes or tissues.

2.2.14 SCORING SYSTEM FOR THE QUANTIFICATION OF CD138 POSITIVE CELLS

In tibial biopsies, scoring of CD138⁺ plasma cell was based on the microscopic evaluation of CD138 IHC stained slides using a ScanScope CS digital slide scanner, *Aperio Technologies®* and quantitation was done using Aperio ImageScope software Ver 11.1.2.760, *Aperio Technologies®*. CD138⁺ cells were

identified as brown (DAB) staining around the plasma membrane surrounded by a haematoxylin (blue/purple) stained nucleus. Both individual number of CD138⁺ cells and colony area (mm²) of CD138⁺ colonies were quantified (figure 2.2-7). CD138 IHC was performed on both tumour-free naïve control and tumour-bearing animal to investigate the levels of CD138⁺ cells in the BM.

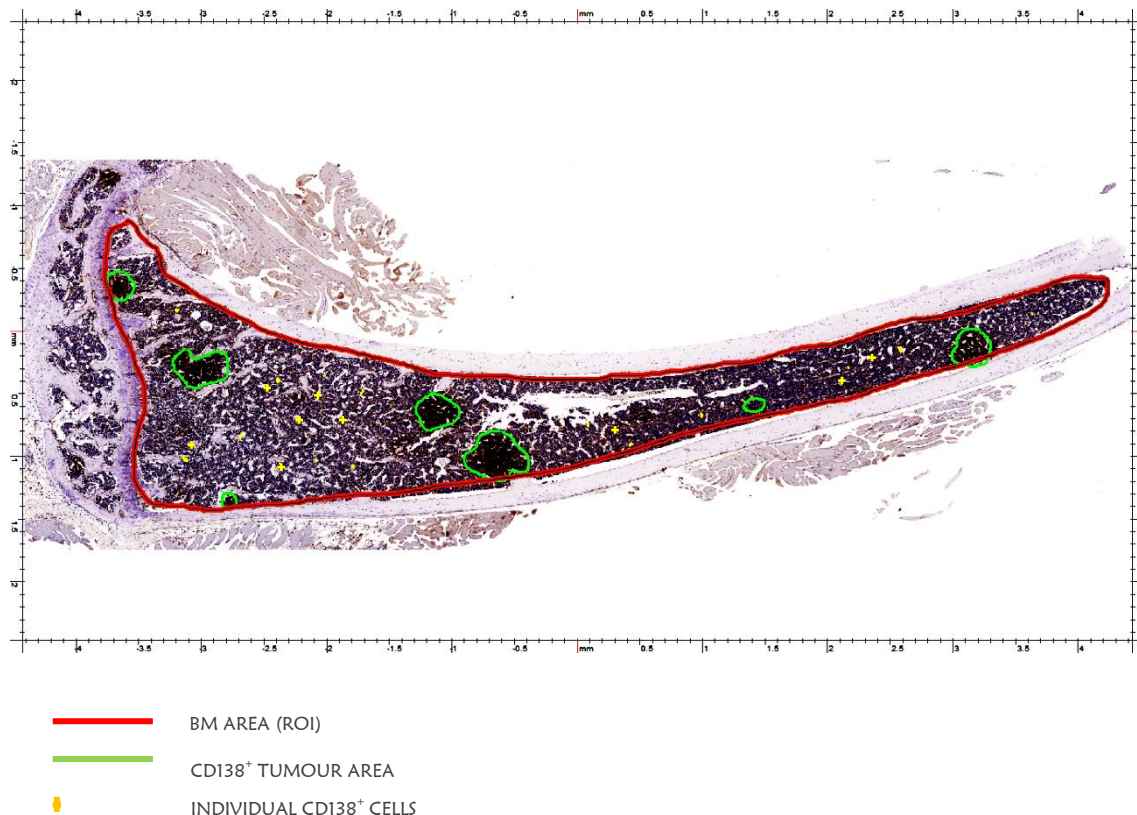


Figure 2.2-7: Scoring system for CD138 IHC.

CD138 IHC stained slides were scanned using an Aperio Slide scanner and the images were loaded on the ScanScope software. Single CD138⁺ cells, CD138⁺ colonies were visually identified and manually traced using ScanScope software. Results were exported as excel files for analysis.

2.2.15 HISTOLOGY

DECALCIFICATION

After MicroCT analysis, bones were decalcified for histomorphometric analysis. Decalcification was done using ethylenediamine tetra acetic acid (EDTA, Fischer Scientific) at RT for a period of 4 weeks. The bones were decalcified in volumes of EDTA approximately 20 times the volume of the bones with the solution changed once a week. Once decalcified, the bone tissues were loaded onto labelled tissue cassettes and washed in running tap water for 60 min.

PROCESSING AND WAX EMBEDDING

Tissue processing was done using a Leica TP1020 automated carousel tissue processor, *Leica Biosystems*. The bones were dehydrated using gradients of alcohol and infiltrated with paraffin wax (Surgipath). Processed tissues were then embedded in paraffin wax using metal moulds where the tibiae samples were placed diagonally with the crest facing down, and then warm melted paraffin was added to the moulds and was allowed to cool.

SECTION CUTTING AND STAINING

Wax embedded tissue blocks were cut using Leica RM2135 rotary microtome which was set to cut sections at a thickness of 3 μ m. The wax moulds were slowly trimmed until the BM was exposed. Chattering was prevented by pre-cooling the exposed tissue surface on ice. Two 3 μ m serial sections were cut and floated onto a water bath maintained at 45°C, these were mounted on Superfrost Plus slide labelled appropriately and then dried overnight in a 37°C incubator. The slides were stored at 4°C until required.

2.2.16 HAEMATOXYLIN & EOSIN STAINING

Slides were dewaxed and hydrated by sequentially dipping into xylene 99%, 95% and 70% ethanol followed by washing in running tap water for 5 min. The slides were then dipped in Gills II Haematoxylin (VWR code: 1.05175.0500) for 90 sec and washed again in running tap water for 5 min. Eosin staining was done by dipping the slides in 1% aqueous solution of eosin containing 1% calcium carbonate for 5 min and washed in running tap water for 2-3 min. The slides were then dehydrated by sequential dipping in 70%, 95% and 99% ethanol followed by Xylene for 3 min and coverslipped (VWR codes 36029/36125) with DPX mountant (*Sigma-Aldrich*, Catalogue No. 44581).

2.2.17 TRAP STAINING

Before staining the slides were dewaxed and dried. The slides were submerged in 2 containers of xylene for 5 min in each to remove the paraffin. After dewaxing, they were dipped consecutively in two jars containing 99% and one jar each containing 95% and 70% industrial methylated spirit (IMS) for 5 min in each for removing the xylene. The slides were then cleared of IMS and rehydrated by rinsing them in tap water.

A standard Naphthol AS-BI phosphate post-coupling method was used for TRAP staining using hexazonium pararosaniline. To prepare 1.2% acetic acid solution 6 ml of absolute acetic acid (Analar Chemicals) was dissolved in 494 ml of distilled water. Acetate buffer (0.2M) was made by dissolving sodium acetate trihydrate salt (*Sigma S-9513*) in 200 ml of distilled water and the pH was corrected to 5.2 by adding 50 ml of 1.2% acetic acid. Sodium tartrate (4.6 gm *Sigma S-4797*) was added to produce

acetate tartrate buffer and warmed to 37°C for 2-4 hrs. The dewaxed slides were incubated in the warm buffer for 5 min at RT.

Solution A was prepared by dissolving 0.02 g of Naphthol AS-BI phosphate (Sigma N-2250) in 1 ml of dimethyl formamide and the resultant solution mixed with 50 ml of acetate tartrate buffer. The slides were then incubated in solution A for 30 min at RT.

4% sodium nitrate solution was prepared by adding 80 mg of sodium nitrate (Sigma S-2252) in 2 ml of distilled water. 2 ml of pararosaniline (Sigma P-3750) was added to this 4% sodium nitrate solution to form hexazonium pararosaniline. Solution B was prepared by adding 2.5 ml of hexazonium pararosaniline/sodium nitrate to 50 ml of pre-warmed acetate tartrate buffer. Solution B had to be prepared fresh and the slides were incubated for 15 min in solution B at RT. The slides were then rinsed and counterstained with Gills II (VW code 1.05175.0500) haematoxylin for 20 sec. The slides were then washed using IMS and dehydrated by xylene and then coverslipped over 2-3 drops of DPX mountant.

2.2.18 SCORING SYSTEM FOR THE QUANTIFICATION OF OSTEOCLASTS & OSTEOBLASTS

A Leica LEITZ DMRB upright microscope connected to a Sony colour video camera and Osteomeasure software (Osteometrics Inc., USA Ver 4.10) was used to quantify the H&E and TRACP stained slides. Cells were analysed at 10X magnification. Bone static histomorphometry was performed in accordance with the guidelines established by ABSMR Histomorphometry Nomenclature Committee (Parfitt et al 1987). TRAP stained slides were used to quantify osteoclasts (Oc) and H&E stained slides were used to quantify osteoblasts (Ob). Trabecular analysis was made on a field size of 0.5625 mm² and 0.5 mm from the proximal margin (resting zone) of the growth plate. Histomorphometric assessment on the cortico-endosteal side was determined on 1.5 mm on each endosteal side 0.5 mm from the growth plate (figure 2.2-8).

The following static variables were measured: total number of Oc per unit area of trabecular bone (i.e., osteoclast index, 1/mm²) and total number of Ob per unit area of trabecular bone (i.e., osteoblast index, 1/mm²) were measured on the trabecular region; total number of Oc and Ob per mm of cortico-endosteal (endocortical) bone surface (1/mm) were measured on the endocortical region. Oc and Ob were identified based on their distinctive morphological features in TRAP and H&E staining respectively. TRAP⁺ cell on the bone surfaces was identified as Oc while Ob was identified by their cuboidal shape and eosin stain with eccentrically placed haematoxylin stained nucleus.

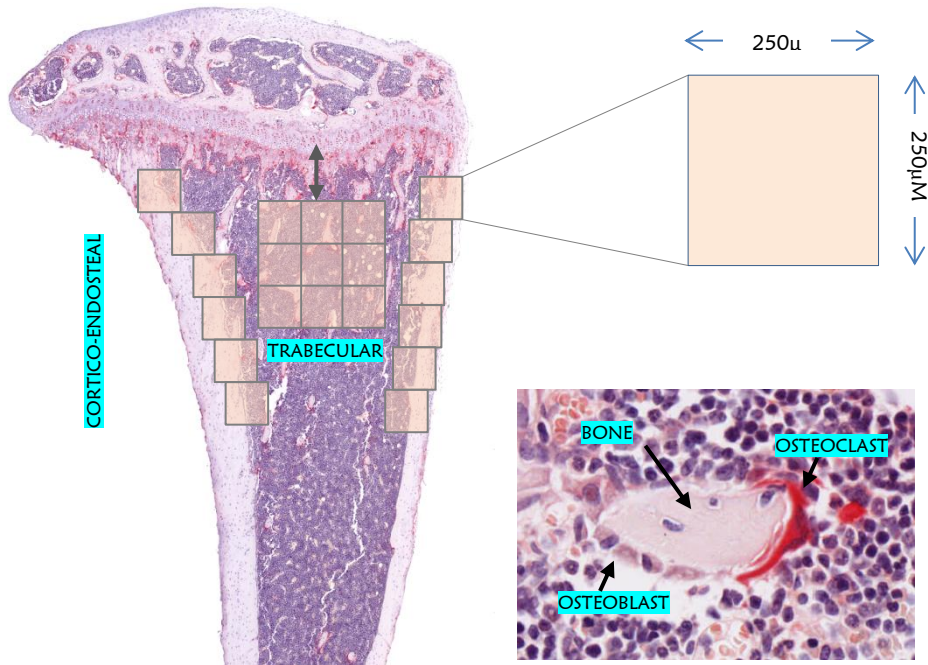


Figure 2.2-8: Scoring of Ocs and Obs in TRAP and H&E stained slides

Osteomeasure software was used to quantify the number of osteoclasts and osteoblasts in the BM. Analysis was done in the proximal tibial metaphysis 0.5 mm below the growth plate using a 10X objective. For trabecular region, a 3 X grid tile fashion each measuring 250 X 250 μm was used. For the endocortical analysis, 6 tiles were traced along the endocortical surface on both sides.

2.2.19 QUANTIFICATION OF OSTEOLYTIC BONE LESIONS

Computerised image analysis (CIA) system using 'Image J' software (NIH) was developed by Ms Holly Evans Research Technician, Mellanby Centre for Bone Research, Sheffield to quantify defects on cortical bone surfaces from 3D models built in *ex-vivo* microCT imaging as an index of osteolytic bone lesion. This technology allowed a cost effective method for the measurement of quantifiable lesion on bone surfaces using in-house microCT images and open source 'Image J' software. 3D models of proximal tibial metaphysis were built from microCT images using CTAn software. Prior to 3D model making the microCT images were resized smaller 3X (smaller image size allowed better processing of the images on the software) and ROI was drawn to include the cortical bone and exclude the trabecular bone. 3D images were then loaded onto CTVol software, SkyScan N.V. Aartselaar, Belgium and cross-sectional cut planes showing the posterior and lateral side were saved as bit map images.

Using ImageJ software the BMP files were converted to 8-bit images for processing. Images were then thresholded using a binary cut-off to highlight the bone. Figure 2.2-9 A & B show raw and processed image showing proximal tibial metaphysis (posterior side) respectively. Following image conversion (8 bit, grayscale, black and white image) and binary thresholding the black background is converted to red colour showing defects on the surface of cortical bone. Using 'analyse particle' module, defects of

all shapes and sizes (circularity between 0.0-1.0) were quantitated on the cortical bone surfaces (ImageJ basics Ver 1.38).

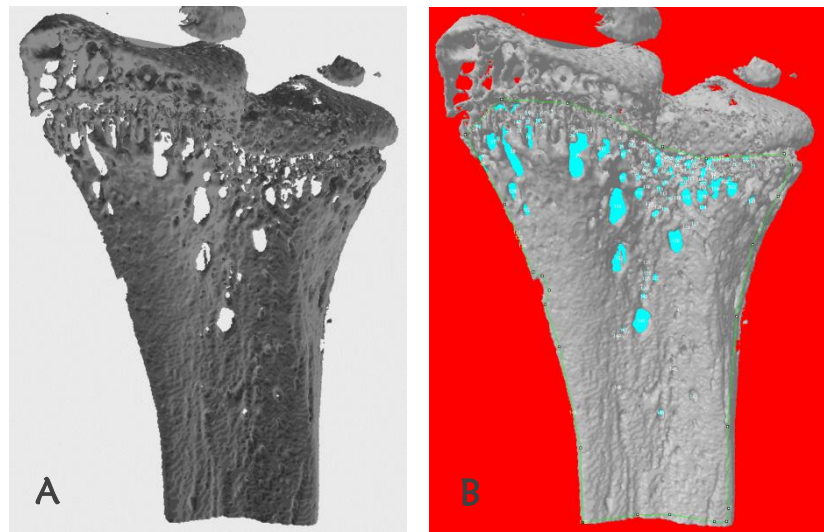


Figure 2.2-9: Quantification of cortical defects using Image J software.

(A) An example raw image of the proximal tibial metaphysis (longitudinal cut-section) showing multiple defects on the surface of the cortical bone. (B) 8-bit grayscale processed image of the same section with background in red, bone in grayscale and cortical defects in blue.

2.2.20 ENZYME LINKED IMMUNOSORBENT ASSAY (ELISA) – SERUM BONE MARKERS

ELISA assay was performed on serum for quantitating serum levels of bone turnover markers. Tartrate resistant acid phosphatase 5b (TRACP5b) was done for osteoclastic bone resorption and Pro-collagen 1 N-terminal propeptide (P1NP) was done for osteoblastic bone formation.

TRACP5B ELISA

Mouse TRACP5b AssayTM (Catalogue no. SB-TR103, Immunodiagnosticssystem, UK Ltd) was used to determine the serum levels of the enzyme TRACP5b expressed by bone resorbing osteoclasts. Mouse TRACP5b is a solid-phase immunofixed enzyme activity assay in which polyclonal anti-TRACP5b capture antibody is bound to anti-rabbit IgG coated microtitre plate (solid phase) upon which antigen (TRACP5b) from the serum is bound thereby forming a sandwich of antibody-antibody-antigen. As TRACP5b is a phosphatase, a chromogenic substrate para-nitrophenyl phosphate (pNPP) is used to produce a soluble yellow colour product para-nitrophenol whose absorbance can be read using a spectrophotometer (figure 2.2-10).

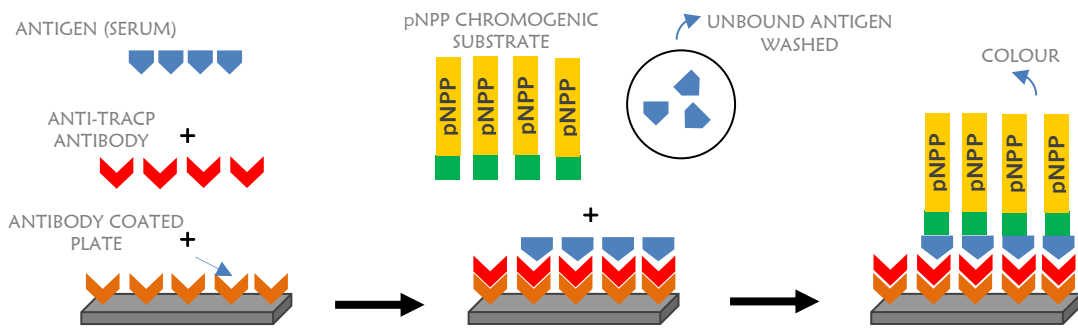


Figure 2.2-10: Principles of the TRACP5b immunoassay.

TRACP5b immunoassay is a 'sandwich' type ELISA where polyclonal anti-TRACP5b capture antibody (red) is attached to anti-rabbit IgG solid phase support (orange antibody in the microtitre plate). Addition of serum sample (TRACP5b) results in binding of the antigen (TRACP5b) with the polyclonal anti-TRAP5b capture antibody. Para-nitrophenyl phosphate (pNPP) is a chromogenic substrate for phosphatases which on addition to phosphatases will yield para-nitrophenol which is yellow in colour and absorbance can be measured using a spectrophotometer with 405 nm light.

The assay was performed according to the manufacturer's protocol. 100 µl of reconstituted polyclonal anti-TRACP5b antibody was added to appropriate wells in an anti-rabbit IgG coated microtitre plate and incubated for 1 hr at RT on a shaker (950 RPM). The plate was manually washed 3 times using a wash buffer to remove excess unbound antibody. 100 µl of calibrators and controls were added to appropriate wells, 75 µl of 0.9% NaCl followed by 25 µl of each sample were added in duplicates. 25 µl of releasing reagent was then added to all wells and incubated for 1 hr at RT on a shaker. The release reagent was added to dissociate the TRACP5b from the binding proteins. The plates were washed 3 times in wash buffer and 100µl of freshly prepared p-nitrophenyl phosphate (pNPP), a colorimetric, soluble substrate for protein, acid or alkaline phosphatase was added. The plates were then incubated for 2 hr at 37° C. 25 µl of NaOH was used to stop the reaction and the plate was read at 405 nm using a SpectraMax M5[®] automated plate reader (*Molecular Devices*).

MURINE P1NP ENZYME IMMUNOASSAY

Pro-Collagen Type 1 N-terminal propeptide (P1NP) is a major component required for the synthesis of bone matrix. During the process of active bone formation and collagen synthesis, propeptides are secreted into the circulation from the pro-collagen molecule from the 'C' (carboxy) and 'N' (amino) terminal. Therefore, quantification of serum levels of P1NP reflects the bone formation rates. Rat/Mouse P1NP EIA (Immunodiagnostic system, Catalogue No: AC-33F1) a competitive enzyme immunoassay was used for the quantification of N terminal propeptides in the serum (figure 2.2-11).

The P1NP assay was performed according to the manufacturer's protocol. 50 µl of calibrators, controls and 5 µl of each sample were added in duplicate to the polyclonal rabbit anti-mouse P1NP antibody coated microtitre plate. 45 µl of sample diluents was added to each well containing sample. 50 µl of P1NP labelled with biotin (Antigen Molecule) was added to all the wells (including calibrators and

controls) and the plate was incubated on a shaker for 60 min at RT. The plates were washed 3 times in 250 µl of wash buffer. 150 µl of horseradish peroxidase enzyme labelled with avidin (this binds with the biotin) was then added to all wells and incubated for 30 min at RT. The plates were washed and 150 µl of chromogenic TMB substrate was added to all wells and incubated for 30 min. Finally 50 µl of HCl (Stop Solution) was used to stop the reaction. The plate was read at 450 nm with a reference range Of 650 nm using SpectraMax M5^e automated plate reader (*Molecular Devices*).

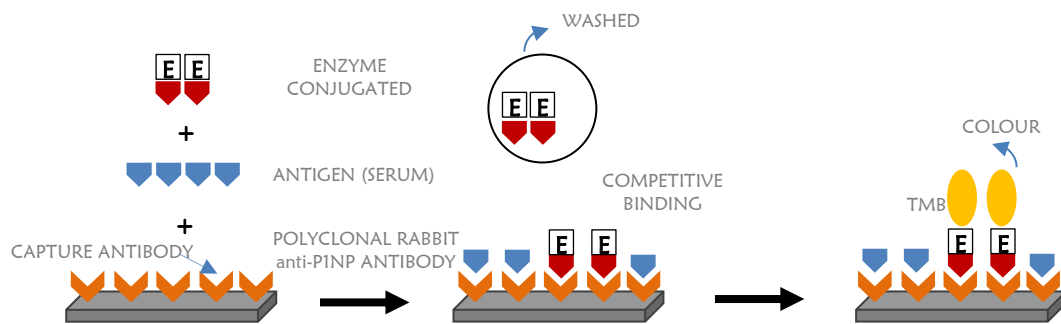


Figure 2.2-11: Principles of P1NP competitive immunoassay.

Competitive enzyme immunoassay works on the principle of competitive binding of the analyte (antigen in the sample to be tested) or the enzyme conjugated antigen (bound enzyme reacts with the substrate) to the available antibody sites in the antibody coated plate/well. After the binding, the plates/well is washed to remove excess unbound analyte or antigen molecule. Substrate is added which can bind to enzyme component of the antigen molecule yielding colour. The more analyte is present in the sample the less will be the available sites for the enzyme conjugate antigen molecule to bind yielding less colour or vice versa.

2.2.21 OPTIMAL CUTTING TEMPERATURE (OCT) EMBEDDING AND CRYOSTAT SECTIONING

OCT embedding of the bone samples was done for longitudinal sectioning of the bone. Embedding of the bone samples was done using a Hexane - methanol freezing bath which was set 20 min prior to the embedding. Bones were placed in plastic moulds with the ventral side of the bone facing downwards. The moulds were filled with OCT; placed on a brass chuck until the OCT froze and stored at -80°C until processing (figure 2.2-12).

Moulds were attached to a pre-cooled metal chuck (-20°C) using OCT. Metal chucks along with OCT embedded bone was mounted on the Cryostat 5030 (Bright Instrument Company, UK) and cut 4-10 µm sections until the BM was exposed over the entire length of the bone (usually 900 µm depth from the surface of the bone). The cut samples were covered in clean foil to prevent contamination of the exposed surface with dirt and to prevent bleaching of the fluorophore and stored at -80° C until processed.

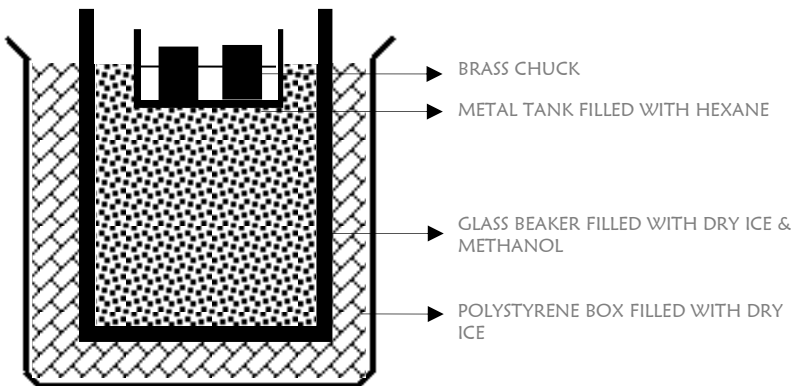


Figure 2.2-12: Design of Hexane-methanol freezing bath

2.2.22 MULTIPHOTON MICROSCOPY

A Zeiss LSM 510 META inverted microscope (Carl Zeiss), equipped with Chameleon™ Compact OPO-Vis (Coherent®) Ti: Sapphire laser for multiphoton imaging was used for scanning the exposed BM of long bones. Multiphoton laser was used to excite the fluorescently labelled myeloma cells present in the BM. The ‘chameleon’ laser module was tuned to deliver mode-locked pulsed near infrared (NIR) laser. Bone samples were cleared of the residual OCT by wash dissolving in 1 X PBS and the flat cut exposed surface was placed onto a 0.35 mm glass bottom petri dish (MatTek Corporation, USA). The sample in the petri dish was covered with PBS to prevent the BM from drying out during the prolonged scanning procedure. The longitudinal cut surface was focused using a 20X dry piece Plan-Apochromat objective lens and a low resolution (128 X 128 pixel size) pilot image was taken to orientate the bone.

AIM® software (Zeiss) was used to configure the microscope to excite the sample using NIR laser and capture the emitted light using separate channels and band pass filters for DID dye and eGFP from fluorescently labelled myeloma cell and second harmonic generation (SHG) from bone. An initial pilot scan was done to determine the location of the bone and the ROI was set appropriately. Proximal metaphysis including the growth plate and epiphysis was chosen as the ROI. Entire ROI is covered as multiple grids (usually 5 X 6 tile scan) and scanned to a depth of 150 μm inside the bone.

Principle of multiphoton microscopy imaging system is described in detail in figure 2.2-13. Long bones (R. Tibia) of 5TGM1-eGFP-DID labelled tumour-bearing mice were scanned using Zeiss LSM 510 META inverted microscope (Carl Zeiss), equipped with Chameleon™ Compact OPO-Vis (Coherent®) laser module for 820 nm multiphoton laser excitation. Bones from tumour-free untreated mice served as negative control. Prior imaging, bone samples were cleared off the residual OCT by wash dissolving it in 1 X PBS and the flat cut surface was placed onto a 35 mm glass bottom petri dish (MatTek Corporation, USA). The petri dish was covered with PBS to prevent the BM from drying out during the 5 hr scanning process. Longitudinal cut surface was focused using a 20X dry piece Plan-Apochromat objective lens and a low resolution (128 X 128 pixel size) pilot image in a 5 X 6 grid fashion which included the upper 1/3 of the proximal tibia was taken. Each grid measured 450 X 450 μm^2 .

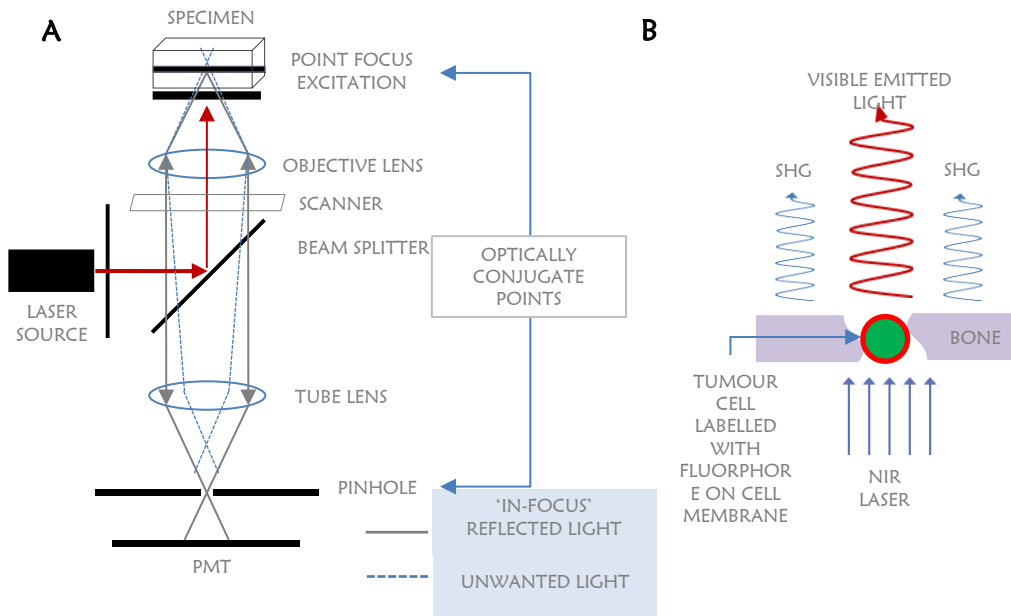


Figure 2.2-13: Principles of multiphoton microscopy and fluorescence imaging.

Multiphoton microscopy is a modified laser scanning method in which there is localised, non-linear excitation of a fluorophore using a pulsed longer wavelength laser causing two-photon or multiphoton excitation. Here two photons of lesser energy are used to produce an excitation (normally excited by a single higher energy photon) by simultaneously interacting with a molecule in approximately less than 10-16s at a point focus. Here the excitation is due to intensity squared dependence (non-linear, quadratic dependence) of the photons which is greater at the point of focus which produces higher fluorescence and greater resolution (Zipfel et al 2003). **(A)** The working principle of a Zeiss META 510 inverted confocal microscope equipped with a Chameleon ‘Coherent’ multiphoton laser module. Here, longer wavelength 740-1140 nm (NIR, invisible) laser passes through a dichroic beam splitter, which deflects the laser light onto the specimen and allows the fluorescent emission to pass through. The emitted light is then projected onto a pinhole diaphragm by the objective and tube lens. The focus of the objective lens (excitation light into the specimen) and the tube lens (emission light onto the pinhole diaphragm) are set at “optically conjugate points” (confocal imaging principle). Appropriate emission band-pass filters are used to select the bandwidth and the signals are then sent to the photomultiplier tubes (PMT) for acquisition and image reconstruction. **(B)** The principle of fluorescence emission and SHG in BM when excited by multiphoton laser. The fluorophore present inside the tumour absorbs the photons from the multiphoton laser and gets excited to a higher energy state. Due to constant colliding of particles at the higher energy levels, the excited molecule slowly loses energy and decays back to the ground level. During this process it emits a photon of higher energy and lesser wavelength according to the fluorophore used. Collagen present in the bone is a non-centrosymmetric material which has the property of SHG when excited with a multiphoton laser. Here, the collagen combines the photons from the multiphoton laser and forms new photons with twice their energy and hence half their wavelengths. As the multiphoton laser used has a wavelength of 820 nm, the SHG generated has a wavelength of 410 nm which falls in the blue/violet range of the visible light (Deniset-Besseau et al 2010).

Scanning was done in multi-track mode. For the first track, 820 nm laser (20% AOTF) was used to excite the bone samples in order to visualise DID and eGFP signals using band pass filters 650-710 nm and 500-550 nm respectively, whereas bone was visualised in a second track as second harmonic generation (SHG) using band pass filter 390-465 nm. Other settings like detector gain (DG) and amplifier offset (AF) were adjusted in each scan to prevent photo-saturation of the photomultipliers (PMTs) and remove the background noise level. Each grid was scanned at 12 bit, frame by frame with a maximum scan speed of 1.92 μ s to a depth of a 150 μ m with 3 μ m between each section at a resolution

of 256 X 256 pixel size) and the resultant image stacks were stitched to produce a three-dimensional image of the bone using the multi-time series protocol.

2.2.23 SPECTRAL FINGERPRINTING

Spectral fingerprinting was done to confirm the emitted signals were correct for the measured fluorophore. A detailed explanation on the principle of spectral fingerprinting is given the figure 2.2-14 below. Spectral analysis was done on some parts of the samples to verify the emission pattern of DID, eGFP and the SHG signals emitted from the bone.

In order to authenticate the fluorescent signals emitted by 5TGM1-eGFP murine myeloma cells, both in *in vitro* cell aliquot and in the BM, tissue sections were imaged in lambda mode using Zeiss LSM510 META microscope. Lambda scans were performed using 820 nm NIR laser at 20% AOTF in a 10.7 nm step size to collect emission signals ranging between 361.8 – 704.2 nm (eGFP e_{\max} 507-510 nm, DID e_{\max} 675-710 nm and SHG e_{\max} 420 nm). Both 2D and 3D stack (40 μm depth for *in vitro* cell aliquot and 150 μm depth for BM) scans were performed using 20 X Plan-Apochromat objectives using a frame size 256 X 256 pixels on tissue sections with an interval of 3 μm between sections for the whole stack.

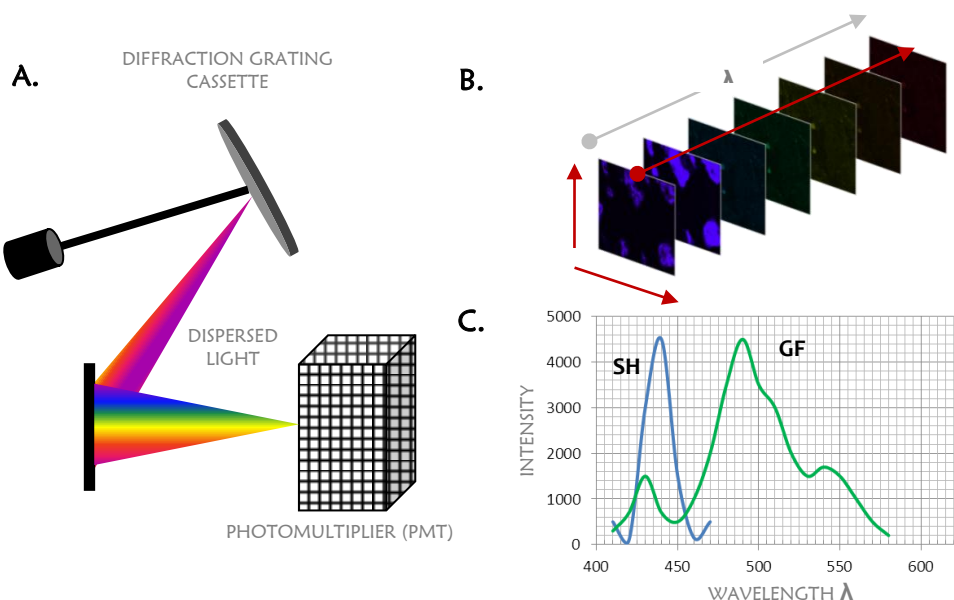


Figure 2.2-14: Principles of spectral fingerprinting.

Spectral or Lambda (λ) Imaging is a technique used to visually separate the emitted light into its component wavelengths by optical grating. **(A)** Emitted light from the specimen is separated into its component wavelength using a prism or a diffraction grating cassette. In the Zeiss LSM510 Meta system every 10.7 nm of wavelength from the emitted light is sent to a separate PMT and signals separated into their component wavelengths. This is then compared with the spectra of the individual dye. The spectral profile (spectral fingerprint) of the dye was defined using the eGFP labelled cells (*in vitro*) and control samples for the spectra and auto-fluorescence due to co-existing conditions inside the specimen. **(B)** A spectral image is a 3D dataset collection of the images from the same location in the specimen measured at different wavelength. **(C)** Spectral profile of SHG and eGFP plotted over the wavelength when excited with 820 nm NIR laser. SHG peaks with a maximum intensity (e_{\max}) 410 nm and eGFP at 507 nm.

2.2.24 THREE-DIMENSIONAL IMAGE PROCESSING, VISUALISATION & QUANTITATIVE ANALYSIS USING VOLOCITY SOFTWARE

Volocity® 3D Image Analysis Software (PerkinElmer, USA) was used for image processing from raw multiphoton microscopy data for 3D visualization and quantitative analysis. Volumetric reconstruction and quantitative analysis was done by thresholding different signals such as eGFP, DID and SHG. Negative controls (tumour-free bone samples) were scanned to identify the maximum fluorescence free signal intensity for different channels and thresholded accordingly. Baseline background fluorescence signal intensity from all channels (DID, eGFP and SHG) was determined from quantitatively analysing tumour-free naïve bone samples. Baseline values were used to threshold the different fluorescent channels in order to identify DID, eGFP and bone (SHG) signals from the raw data for image visualization within the 3D volume of interest (VOI) (figure 2.2-15). VOI was selected by free hand drawing tool drawn to include the BM space in the proximal tibial metaphysis below the growth plate. For quantitative measurement, these thresholded signal intensities from different channels were further ‘size thresholded’. A ‘distance measurement’ protocol was also used to automatically compute the minimum distance between the edges of DID⁺ cell to the edge of the nearest bone (SHG). Results were exported as Microsoft Excel® files for quantitative analysis.

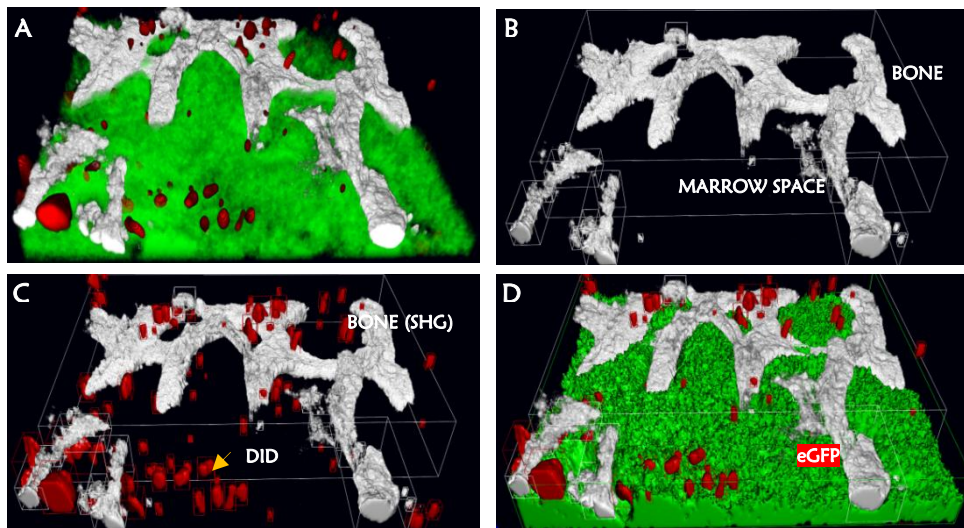


Figure 2.2-15: Volocity image processing for quantitation and analysis.

(A) 3-D raw image acquired from Zeiss LSM 510 META microscope. Image shows signals from all three channels i.e., bone (white/gray) seen in SHG, DID (red) and eGFP (green) fluorescence as visualised from the MP. (B) Bone selection using volocity protocol in 3D. Bone selection protocol identifies SHG signals. (C) DID object signal superimposed on the SHG (bone) signals. (D) Processed eGFP signals superimposed on DID and bone signals.

2.2.25 STATISTICAL ANALYSIS

Statistical analysis was done using Microsoft Excel Professional 2010 and Prism GraphPad Ver 6.0 to plot graphs and the graphs were expressed as mean \pm SEM unless stated otherwise. For simple comparison between two independent populations a ‘non-parametric’ test with Mann Whitney-Wilcoxon test was used where a P value less than 0.05 was statistically significant (Confidence interval > 95%). To determine the effect of ZA treatment on the event-free survival ‘Kaplan-Meir Survival Analysis’ from GraphPad software was used.

CHAPTER 3 MODULATION OF THE MURINE BONE MICROENVIRONMENT BY ZOLEDRONIC ACID

3.1 INTRODUCTION

The role of BPs as inhibitors of osteoclastic bone resorption has been well established. Currently BPs, especially ZA, are the drugs of choice for the treatment of several osteolytic bone diseases including MBD and it has been identified as the most potent BP to-date. Recently, studies have shown that ZA, in addition to its anti-resorptive effects, also shows evidence of an anti-tumour effect in MM both in preclinical models and clinical trials (Croucher et al 2003b; Avilés et al 2007; Morgan et al 2010a; Avilés et al 2013). However, the preclinical evidence that supports the anti-tumour effect of ZA has focused on the late stages of the disease (Yaccoby et al 2002; Croucher et al 2003b). Although BPs like ZA and CLO showed evidence of delayed tumour incidence and prolonged survival, both in animal and human trials, no studies have so far focused on the effect of ZA induced inhibition of bone resorption on the homing and colonisation of myeloma cells in the BM.

Over the last few years, a large body of work has been done to understand the interaction between the myeloma cell and the host BM milieu which might be responsible for the selective migration and development of myeloma cells in bone, at least during the early stages of disease development. Although myeloma cells were shown to interact positively with different cells of the BM milieu, the functional interplay between myeloma cell and osteoclast is alleged to result in a vicious cycle between bone destruction, release of bone derived growth factors, tumour angiogenesis and myeloma expansion (Hobbs 1969; Libouban et al 2003; Oyajobi et al 2007). Under these circumstances, it has been argued that the anti-myeloma effect exerted by BPs is a result of breaking the chain of propagation where inactive osteoclast and the subsequent inhibition of bone resorption will make the BM milieu a less conducive environment for the myeloma cell (Abe et al 2004).

In order to investigate the effect of ZA induced inhibition of bone resorption on the different developmental stages of MM in bone: from homing and colonisation of the tumour cell to the development of overt myeloma colonies, it was essential to achieve adequate suppression of the bone resorption using ZA prior to tumour cell injection and maintain this condition throughout the experimental time points in the *in vivo* myeloma models. In studies so far, the effect of BPs on myeloma development was studied where the treatment with ZA or any other BP was either initiated along with the tumour cell inoculation or after established disease and not prior to tumour cell inoculation (Dallas et al 1999; Croucher et al 2003b; Guenther et al 2010). So far no study has optimised the dosage and duration of ZA treatment to effectively suppress osteoclastic bone resorption in murine models of myeloma. In this chapter, the dosage frequency effect of a subcutaneously administrated, clinically equivalent, dose of ZA was tested in C57BL/KaLwRij mice (5T series of transplantable syngeneic murine myeloma model) for a better understanding of the effect over time in order to determine the time taken for the onset of response and the suppression of bone resorption. The results from this experiment will be used in designing future experiments to achieve adequate ZA induced suppression of bone resorption prior to tumour cell inoculation and study the effect of these on myeloma development.

3.2 AIMS & OBJECTIVES

The aim of this chapter was to adequately and continuously suppress osteoclast induced bone resorption, over a period of time, using a clinically equivalent dose of ZA in C57BL/KaLwRij mice.

Hypothesis: Short-term treatment of ZA (125 µg/kg X2) will be as effective as continuous treatment in maintaining suppression of osteoclastic bone resorption in C57BL/KaLwRij mice.

To test this hypothesis, the effect of short-term treatment, ZA (125 µg/kg two doses in one week subcutaneously), was compared with a continuous treatment strategy (125 µg/kg twice a week, repeated every week).

The objectives were:-

1. To determine the time taken for the onset of ZA induced suppression of osteoclastic bone resorption.
2. To determine whether short-term or continuous ZA treatment was required to maintain the inhibition of osteoclastic bone resorption over time.

3.3 MATERIALS & METHODS

Detailed information on individual techniques performed are given in [Chapter 2: General Materials and Methods.](#)

3.3.1 IN VIVO EXPERIMENT

All animal work and experimental conditions were in accordance with the local guidelines and with the UK HOME OFFICE approval under the project licence number PPL No: 40/2901 held by Prof. Peter Croucher and PPL No: 40/3462 held by Dr. Colby L Eaton, University of Sheffield, UK.

3.3.2 EXPERIMENTAL DESIGN

For the short-term and continuous treatment regimen, age and sex matched 6-11 week old C57BL/KaLwRij mice were purchased from Harlan Animal Research Laboratory and housed in the University of Sheffield, Biological Services. For the short-term treatment regimen, mice (n=30) were injected with either ZA 125 µg/kg two doses three days apart or PBS subcutaneously. ZA treated (n=5) and PBS (control) (n=5) treated animal were sacrificed after 7, 14 and 21 days. A schematic description of the study design is given in figure 3.3-1 experiment I. All animals were starved 6 hr prior to the sacrifice in order to eliminate the circadian variation in the serum bone biomarkers. Mice were anaesthetized using 50-100 µl of pentobarbitone (intra-peritoneal injection) and blood samples were collected by cardiac puncture using 28G insulin syringe. All animals were culled by cervical dislocation and tissues harvested. Right tibiae from all mice were excised free of soft tissues and were stored in 10% buffered formalin for microCT analysis and histology. Serum was collected from the blood by centrifugation and was stored in -80°C for ELISA analysis.

For the continuous treatment regimen, mice (n=32) were injected with either ZA 125 µg/kg two doses three days apart or PBS every week for 4 weeks. Animals (n=4, each group) were periodically sacrificed from both ZA treated and PBS treated control groups after 10, 17, 21 and 28 days. A schematic description of the study design is given in figure 3.3-1 experiment II. All animals were starved 6 hr prior to the sacrifice in order to eliminate the circadian variation in the serum bone biomarkers. Animals were anaesthetized using 50-100 µl of pentobarbitone (intra-peritoneal injection) and blood samples were collected by cardiac puncture. Afterwards, the animals were culled by cervical dislocation and tissues harvested. Left tibiae from all animals were excised free of soft tissues and were stored in 4% paraformaldehyde (PFA) for microCT analysis and histology. Serum was collected from the blood by centrifugation and was stored in -80°C for ELISA analysis.

EXPERIMENT I: SHORT-TERM TREATMENT



EXPERIMENT II: CONTINUOUS TREATMENT

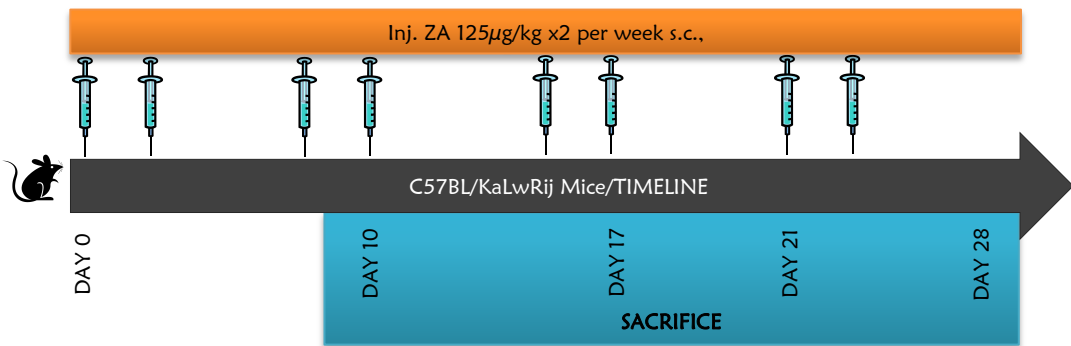


Figure 3.3-1: Experimental design to study the effect of short-term and continuous ZA treatment.

For the short-term treatment study (Expt I), mice were injected with 125 μ g/kg ZA or PBS subcutaneously on 'day 0' and 'day 3' and sacrificed after 7, 14 and 21 days following the first injection. For the continuous treatment study (Expt II), mice were injected with 125 μ g/kg ZA or PBS on 'day 0' and 'day 3' and the treatment was repeated every week. Animals were sacrificed after day 10, 17, 21 and 28.

3.4 RESULTS

3.4.1 CONTINUOUS TREATMENT WITH ZA IS MORE EFFECTIVE AT INHIBITING OSTEOCLASTS AND OSTEOBLASTS THAN SHORT-TERM TREATMENT

The number of osteoclasts (Oc) and osteoblasts (Ob) were counted in the proximal tibial metaphyseal region on sections stained with TRAP and H&E respectively. According to ASBMR, variables between subjects can be compared only when standardised to a common referent (Parfitt et al 1987). As ZA is a potent bone anti-catabolic agent, a reduction in Oc number or activity following treatment is accompanied by an increase in bone volume. If the variables are expressed in terms of number per mm of bone in the trabecular region, it will result in an opposite interpretation as ZA treatment is accompanied by reduction in Oc number and increase in bone area and perimeter (dependent referent). In order to eliminate the measurement bias, for trabecular analysis, the results are expressed in terms of osteoclast and osteoblast index (i.e. the number of Oc or Ob per unit tissue area). For endocortical histomorphometric analysis, the results are expressed as Oc or Ob per mm of the endocortical bone, as endocortical bone perimeter is an independent referent.

After 7 days post short-term ZA treatment, thickening of the growth-plate metaphyseal junction at the ‘zone of provisional calcification’ where transition from cartilage to bone occurs with distortion in the trabecular architecture was observed. Interestingly, after 14 and 21 days post-treatment, although there was a continual expansion of the zone of provisional calcification with minimal inter-trabecular spaces in the metaphyseal end and increased inter-trabecular space at the growth plate end, we also observed a progressive replacement of the upper region of this zone of calcified cartilage by normal BM separating it from the growth plate structures (figure 3.4-1). However, following a continuous ZA dosage regimen, only a moderate thickening of the zone of provisional calcification into the metaphysis of the tibia even after 28 days from the start of the treatment regimen was seen (figure 3.4-2).

Following short-term ZA treatment strategy, quantitative static histomorphometry showed a significant reduction in Oc number in the trabecular region only after 7 days but an exponential increase after 14 (~90%; P<0.01) and 21 days (~147%; P<0.01) post-treatment (figure 3.4-3 A). Comparison with PBS treated control mice showed that the high numbers of Oc in the ZA treated groups were seen on the surface of calcified cartilage that fills the tibial metaphysis. However, in the control mice, cartilage was promptly removed by osteoclastic resorption to form cancellous trabecular bone. Endocortical analysis, due to large variation, showed no clear evidence of changes in Oc number following short-term treatment strategy (figure 3.4-3 C).

Quantitative analysis following continuous dosage with ZA showed significant increase in Oc number in the trabecular region at day 17 when compared with PBS treated control mice. However, no differences was observed at other time-points (figure 3.4-3 B). In the endocortical region, a significant

reduction in Oc number was seen after 28 days (figure 3.4-3 D). But, unlike the short-term regimen, there was no evidence of the thick band of calcified cartilage in the metaphysis following continuous treatment. However, a slight progressive thickening of the zone of the provisional calcification was observed in mice treated with ZA after all-time points. As the effect of ZA on cartilage resorption and growth plate modification was beyond the scope of this experiment, they were not investigated any further.

In order to elucidate the effect of ZA treatment on bone formation, the numbers of Ob were quantitated. For trabecular analysis Ob index and for endocortical region the number of Ob per mm of endocortical bone was assessed. Short-term treatment regimen showed a temporary inhibition of Ob number in the trabecular region after 7 days when compared with PBS treated control groups; however, the Ob numbers resumed to control levels after 14 and 21 days post-treatment (figure 3.4-3 E). In the continuous treatment study, there was a persistent reduction in Ob number in the trabecular region after all time-points when compared with PBS treated control groups (figure 3.4-3 F). In accordance, the endocortical analysis also showed significant reduction in number of Ob per mm of endocortical bone in both short-term and continuous dosage regimens when compared with PBS treated control groups at all-time points (figure 3.4-3 G and H).

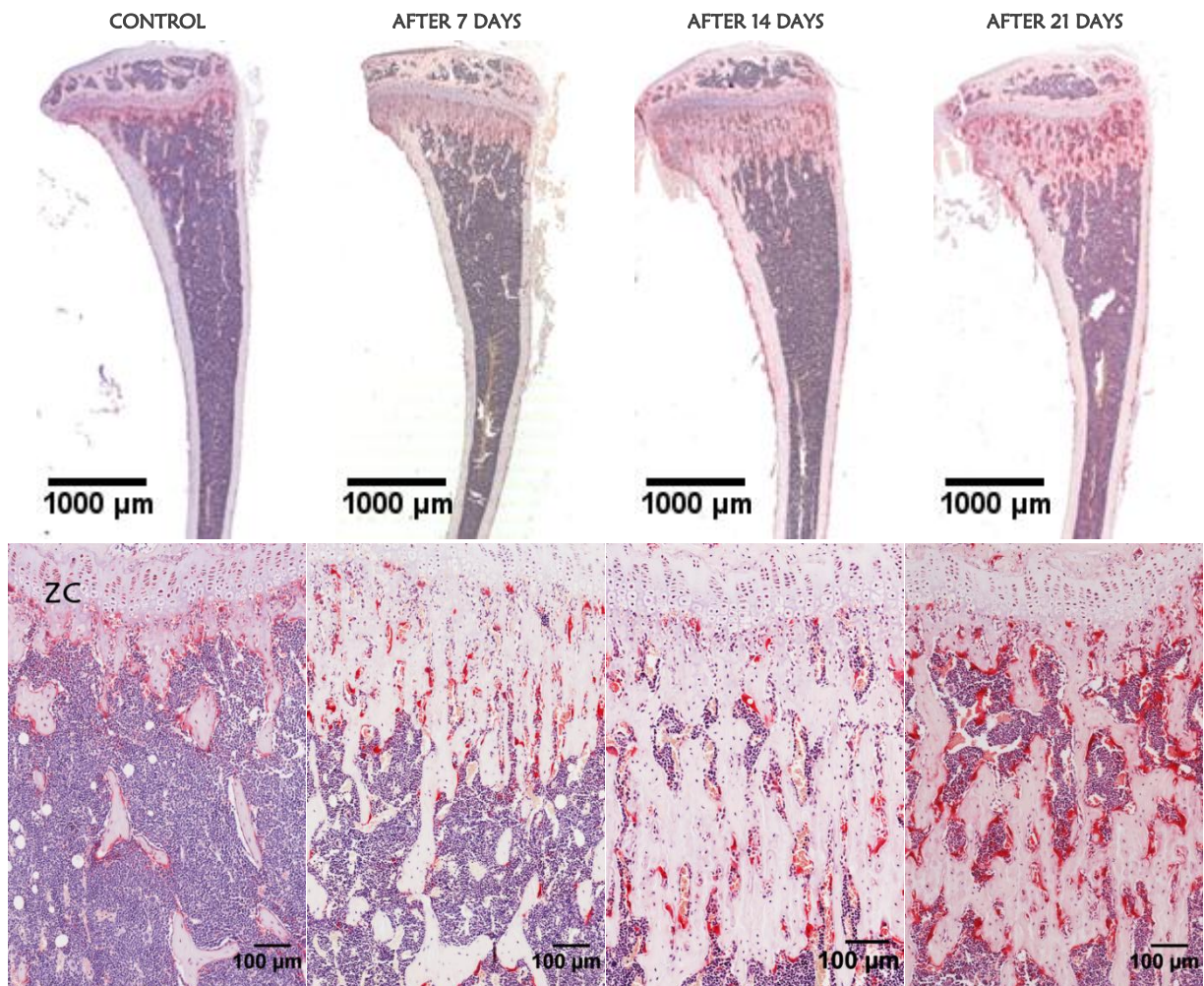


Figure 3.4-1: The effect of short-term ZA treatment on bone in C57BL/KalwRij mice.

The top panel shows representative images of TRAP stained sections of tibiae following short term ZA treatment after 7, 14 and 21 days post-treatment respectively. Bottom panel shows magnified proximal tibial metaphyseal region including the growth plate cartilage. In control PBS treated mice, the metaphyseal region showed normal trabecular architecture with widely interspersed trabecular bone. Following a short-term treatment strategy, progressive thickening of the zone of provisional calcification (ZC) extending into the metaphyseal region with distorted trabecular architecture was observed which was rich in osteoclasts with minimal inter-trabecular spaces between them. Interestingly, after 14 and 21 days, a separation between the trabecular bone and the growth plate cartilage was seen probably due to resumption of osteoclastic bone resorption.

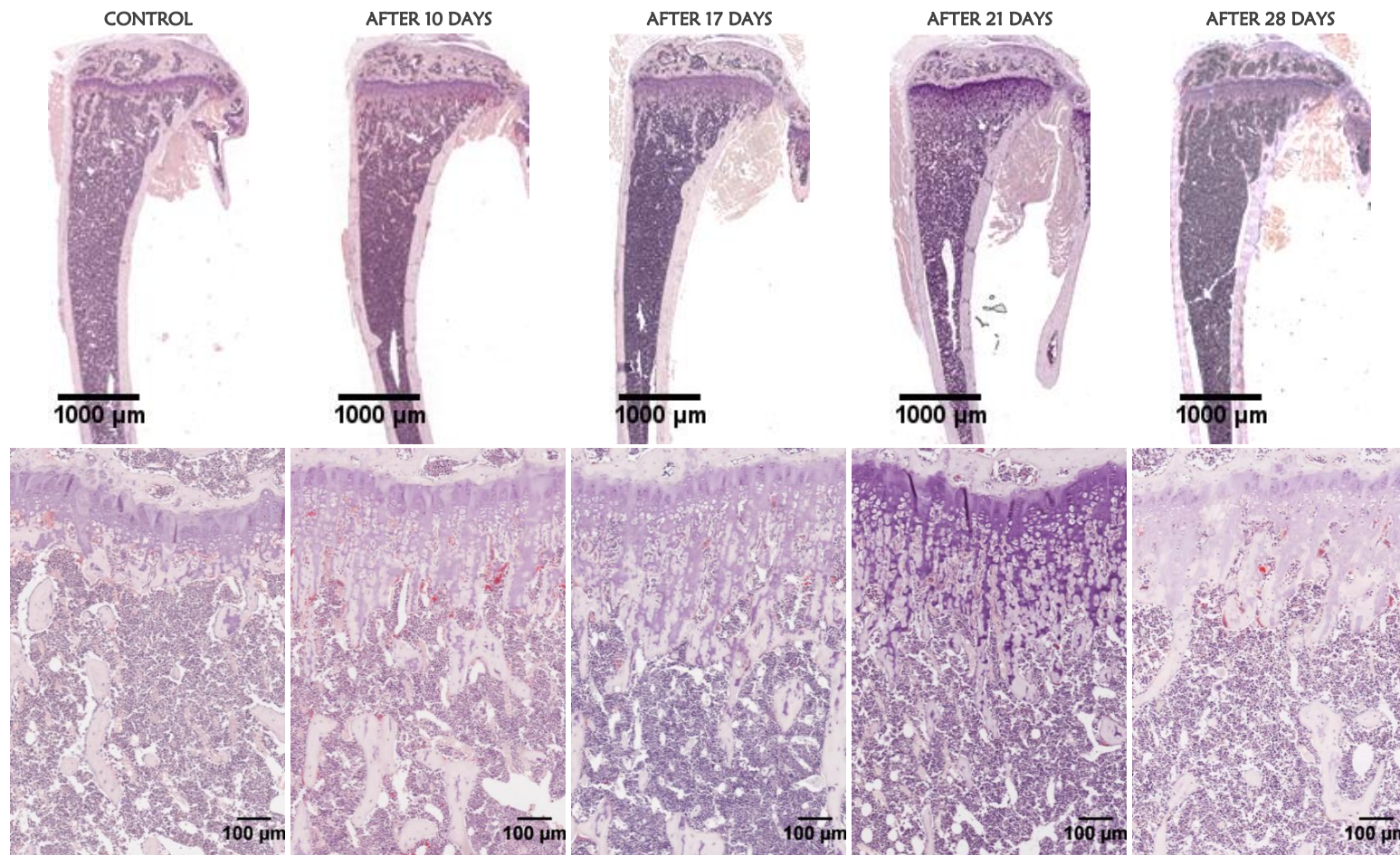
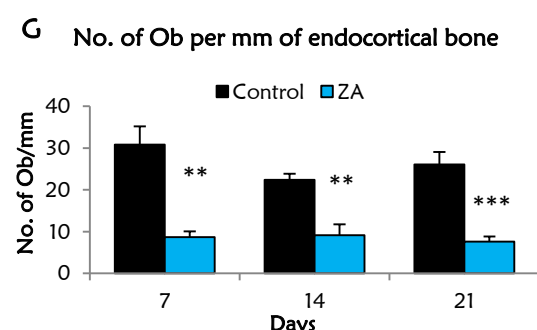
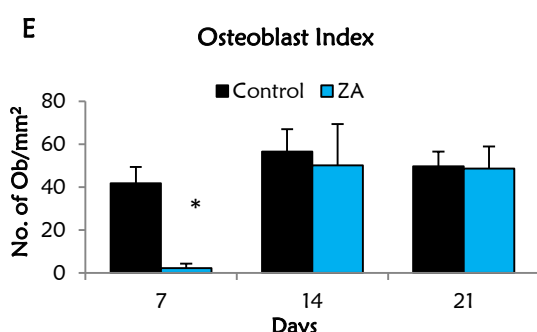
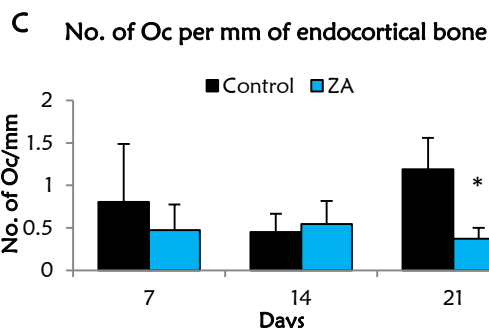
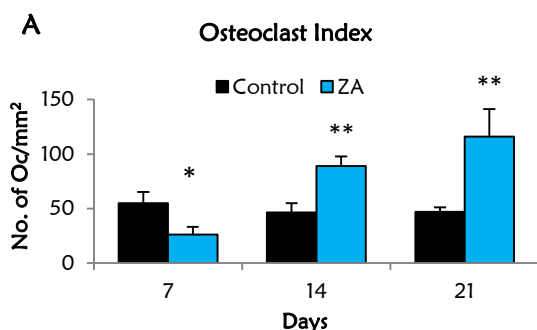


Figure 3.4-2: The effect of continuous ZA treatment on bone in C57BL/KalwRij mice.

The top panel shows representative TRAP stained sections of tibiae from PBS treated mice (control) and following long term ZA treatment after 10, 17, 21 and 28 days. Bottom panel shows magnified proximal tibial metaphysis including the growth plate cartilage after 10, 17, 21 and 28 days. Following continuous ZA treatment only a minimal thickening of the zone of provisional calcification was seen. At this point, it is interesting to note that, unlike the short-term treatment regimen, in this region reduced osteoclast numbers were seen.

SHORT-TERM ZA TREATMENT



CONTINUOUS ZA TREATMENT

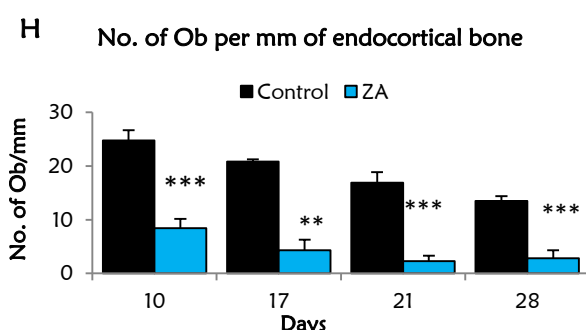
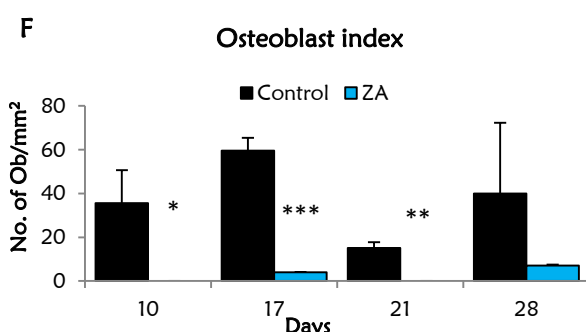
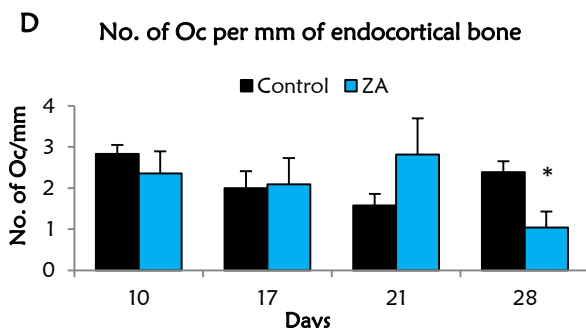
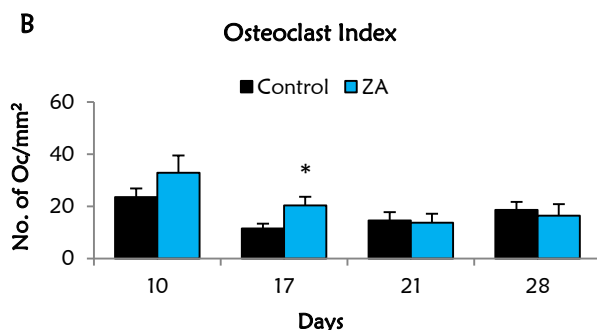


Figure 3.4-3: The effect of short-term and continuous ZA treatment on the number of trabecular and cortical osteoclasts and osteoblasts.

Changes in Oc index (A) and Oc number per mm of endocortical bone (C) following short-term ZA treatment. Changes in Oc index (B) and Oc number per mm of endocortical bone (D) following continuous ZA treatment. Changes in Ob index (E) and Ob number per mm of endocortical bone (G) following short-term ZA treatment. Changes in Ob index (F) and Ob number per mm of endocortical bone (H) following continuous ZA treatment. Mann-Whitney's non-parametric two-tailed test was performed to determine significant differences between the control and ZA treated groups for each time point. For short-term ZA treatment n=5 for all time points and for the continuous ZA treatment n=4 for all time points. *P<0.05, **P<0.01, ***P<0.001.

3.4.2 BOTH SHORT-TERM AND CONTINUOUS ZA TREATMENT REDUCED SERUM LEVELS OF BONE RESORPTION (TRACP5b) AND BONE FORMATION (P1NP) MARKERS

ELISA analysis was performed to determine the serum levels of TRACP5b and P1NP following short-term and continuous ZA treatment. Both short-term and continuous ZA treatment regimens showed significant reduction in serum levels of TRACP5b and P1NP after all time points (figure 3.4-4 A, B, C and D). At this point, it is interesting to note that following the short term dosage regimen, quantitative static histomorphometry showed a gross increase in osteoclast numbers after 14 and 21 days despite persistent reduction in serum TRACP5b levels following treatment. Interestingly, the elevated osteoclast numbers were also accompanied by grossly unresorbed trabecular bone in the tibial metaphysis which implies that following short-term ZA treatment, there is only a temporary cessation in the osteoclastic activity (both in terms of number and activity) which is followed by resumption of resorption recruiting new Oc which might be functionally less active explaining the reduced serum TRACP5b levels.

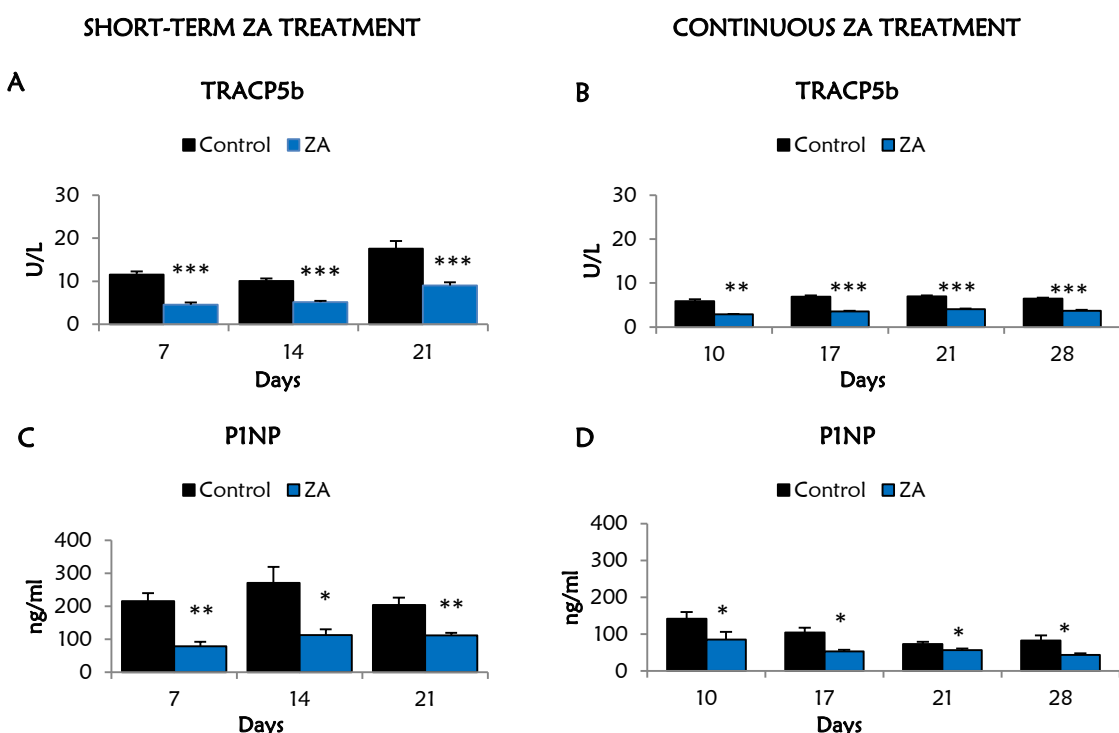


Figure 3.4-4: Changes in serum levels of TRACP5b and P1NP following short-term and continuous ZA treatment.

Changes in serum levels of TRACP5b (A) and P1NP (C) following short-term ZA treatment. Changes in serum levels of TRACP5b (B) and P1NP (D) following continuous ZA treatment assessed by ELISA analysis. For short-term ZA treatment n=5 for all time points and for the continuous ZA treatment n=4 for all time points Mann-Whitney's non-parametric two-tailed test was performed to determine significant differences between the control and ZA treated groups for each time point. *P<0.05, **P<0.01, ***P<0.001.

3.4.3 CONTINUOUS ZA TREATMENT IS MORE EFFECTIVE IN PRESERVING BONE THAN SHORT-TERM TREATMENT

As described in [Chapter 2: General Materials & Methods](#), microCT was performed on the proximal tibial metaphysis to determine the structural changes following ZA treatment. Parameters such as trabecular bone volume (% BV/TV), cortical bone volume (Ct. V), trabecular number (Tb. N), trabecular thickness (Tb. Th), trabecular pattern factor (Tb. pf), structural modal index (SMI) were analysed. Analysis was done on a region 1 mm in length of the proximal tibial metaphysis region at a distance of 1.2 mm from the proximal epiphysis growth-plate junction (figure 2.2-5).

Figure 3.4-5 shows longitudinal cross-sectional microCT images of tibiae treated with short-term ZA or PBS after 7, 14 and 21 days. Thickening of the growth plate was seen after 7 days post short-term ZA treatment; however after 14 and 21 days post ZA treatment, there was a thick band of calcified trabeculae with distorted architecture seen below the growth plate. At this point, it is interesting to note that there is widening of partially mineralised region between the calcified zone of the growth plate and the trabeculae below.

Quantitative analysis showed a significant increase in both % BV/TV, Ct. V and Tb. N after 7, 14 and 21 days whereas a reduction in Tb. Th, Tb. Pf and SMI were seen (figure 3.4-7 A, B, C D, E and F). Following short-term ZA administration a 2 fold, 3 fold and 5 fold increase in % BV/TV after 7, 14 and 21 days respectively was seen with a concomitant increase in Tb. N in the metaphysis. Tb. Pf is quantitative parameter describing the trabecular inter-connectivity, while SMI describes the plate-rod characteristics of the trabeculae. Reduction in Tb. Pf and SMI following short-term ZA treatment showed that the highly interconnected trabecular architecture seen after 14 is a result of delayed osteoclastic resorption of the expanding growth-plate structures. At this point, it is interesting to note that the Tb. Pf and SMI values are negative after 14 and 21 days which describe the complexities of the calcified structure with multiple enclosed cavities within them.

Following continuous ZA treatment, a significant increase in % BV/TV, Ct. V and Tb. N and a reduction in Tb. Pf and SMI was seen. No clear evidence of changes in Tb. Th was observed following continuous ZA treatment (figure 3.4-7 G, H, I J, K and L). Unlike the short-term treatment regimen, in continuous ZA treatment experiment there was no dramatic increase in the % BV/TV and Tb. N. Furthermore, there was no thick band of distorted trabeculae or calcified cartilage structures in the proximal tibial metaphysis as seen in the metaphysis of the short-term regimen. Morphologically, following continuous ZA regimen, the proximal tibial metaphysis showed architecturally similar trabecular structures when compared with control animals (figure 3.4-6).

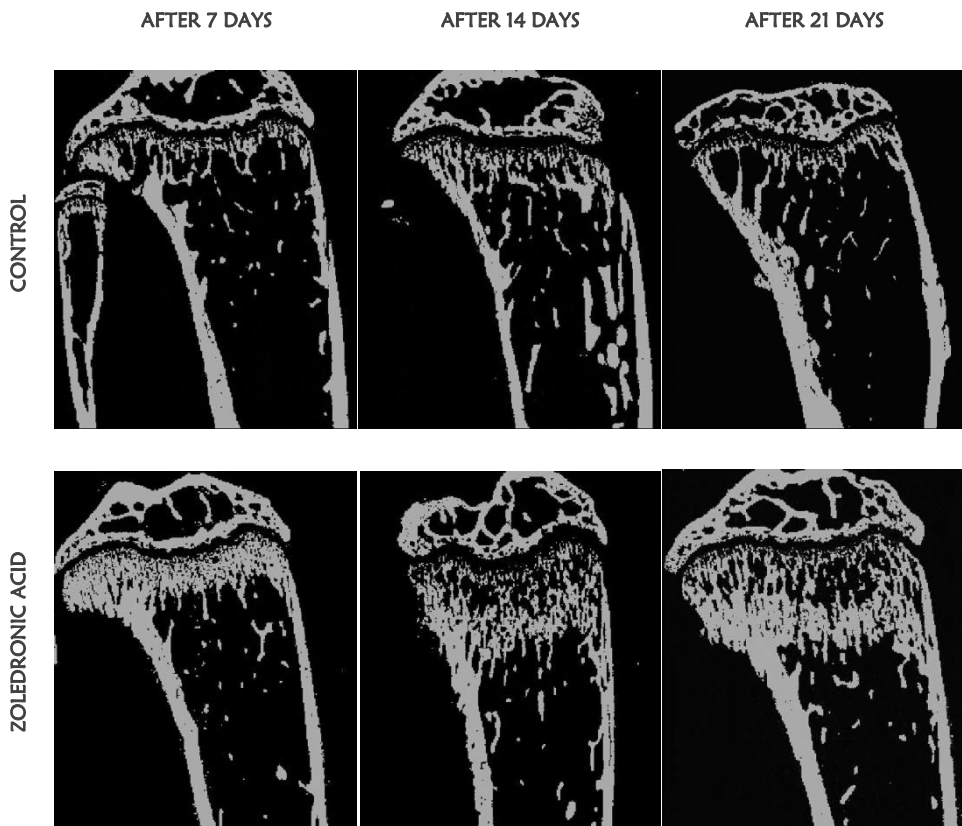


Figure 3.4-5: The microCT changes in tibia following short-term ZA treatment.

Representative longitudinal microCT cross-sections of tibiae showing the proximal tibial metaphysis of control and short term ZA treated animals after 7, 14 and 21 days respectively. Generalized thickening of cortical and trabecular bone was observed with the ZA treated mice when compared with PBS treated control animals. Following short term ZA treatment, we observed progressive thickening of the trabecular bone below the growth plate. Growth plate is the radiolucent (black) region which lies between the epiphysis and the trabecular bone below. After 14 and 21 days post-treatment, we also observed progressive widening between the trabecular bone and the calcified end of the growth plate structures. The trabecular bone which filled the metaphyseal region was distorted with highly interconnected trabecular bone in the short term ZA treated mice. In the control mice, this region was promptly resorbed by normal bone remodelling resulting in organized trabecular structures with normal trabecular architecture. Although the preservation of the trabecular bone in the short term ZA treatment indicated inhibition of bone resorption, the progressive widening of the space between the trabecular bone and the growth plate and the continued expansion of the trabecular bone into the metaphysis suggest only a temporary inhibition of osteoclastic bone resorption and osteoblastic bone formation.

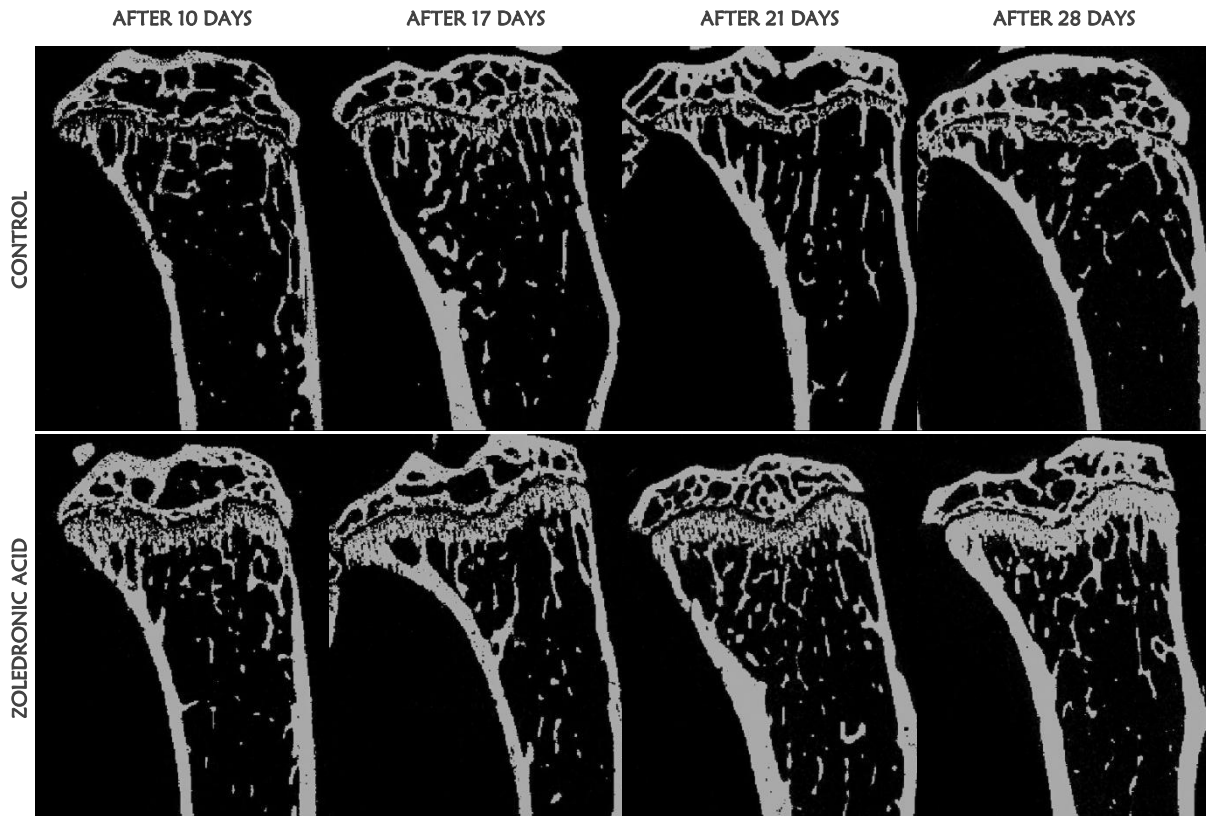
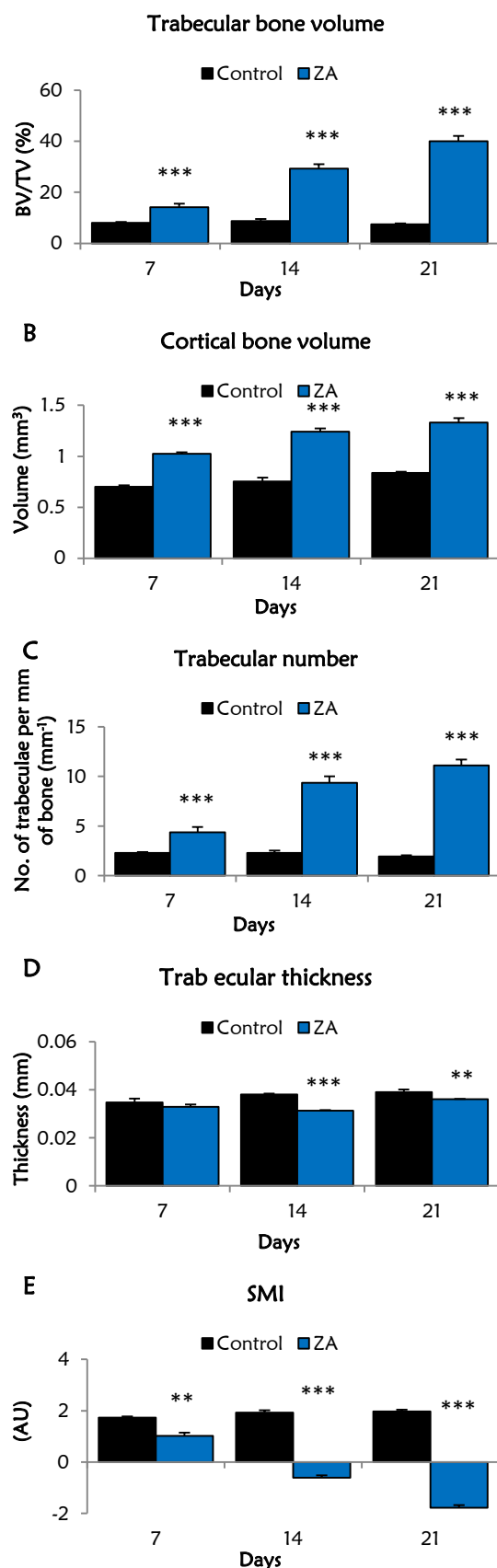


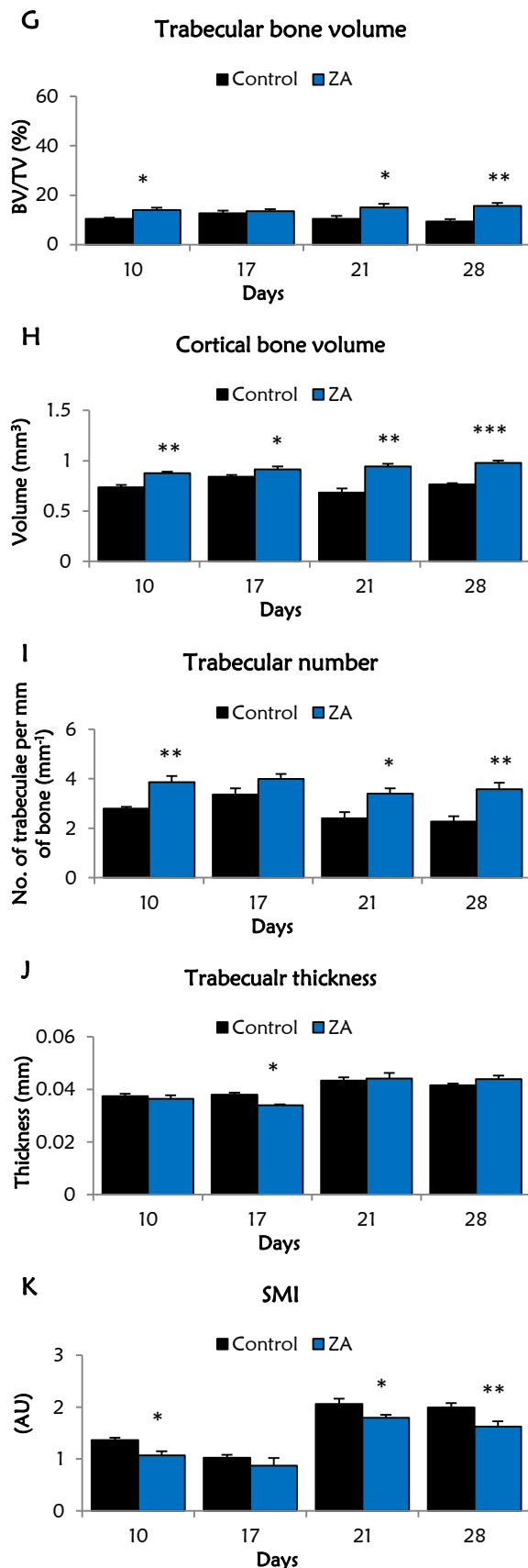
Figure 3.4-6: The microCT changes in tibia following continuous ZA treatment.

Representative longitudinal microCT cross-sections of tibiae showing the proximal tibial metaphysis of control and long term ZA treated animals after 10, 17, 21 and 28 days respectively. Like the short term ZA regimen, the long term ZA dosage also showed generalised thickening of both the cortical and trabecular bone when compared to PBS treated control mice. But unlike the short term dosage, here we observed only a minimal expansion of the calcified end of the growth plate structures. Although the metaphyseal region showed increased and thickened trabecular bone, the normal trabecular architecture was preserved and resembled the control animals. It is important to notice that, quantitative histomorphometry revealed continued osteoclastic and osteoblastic suppression following long term ZA regimen. This suggests that the continued suppression of osteoclastic bone resorption resulted in thickening of the cortical and trabecular bone which might have been removed or remodelled by normal bone remodelling whereas the continuous suppression of the osteoblastic bone formation resulted in the prevention of newly formed trabecular bone structures projecting and expanding into to the metaphyseal region.

SHORT-TERM ZA TREATMENT



CONTINUOUS ZA TREATMENT



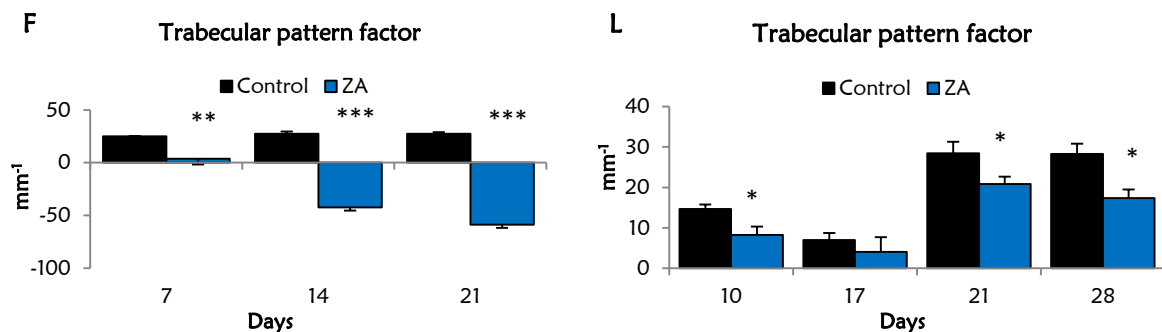


Figure 3.4-7: Quantitative microCT analysis following short-term and continuous ZA treatment.

Graphs show changes in the quantitative microCT parameters in tibia following short and continuous ZA treatment when compared with PBS treated age and sex matched control animals. Quantitative parameter include %BV/TV. Ct. V, Tb. N and Tb. Th, and structural parameters include Tb. Pf and SMI. For short-term ZA treatment n=5 for all time points and for the continuous ZA treatment n=4 for all time points. Non-parametric Mann-Whitney Wilcoxon's test was used to compare the difference between the control and ZA treated groups. *P<0.05, **P<0.01, ***P<0.001.

3.5 DISCUSSION

In this chapter, the effect of short-term and continuous treatment of ZA on bone remodelling was studied in the long bones of young C57BL/KaLwRij mice by histomorphometric evaluation of osteoclast and osteoblast numbers, serum levels of TRACP5b and H&E and microstructural changes in trabecular and cortical bone by microCT. As young naïve C57BL/KaLwRij mice are used to develop the 5TMM murine myeloma model (used in future experiments), which develops MM over a period of 3-6 weeks post tumour cell injection, it was essential to understand the quantitative and structural changes in the bone following ZA treatment. The main aim of this experiment was to determine the frequency of ZA treatment to effectively suppress osteoclastic bone resorption in young C57BL/KaLwRij mice. To the best of our knowledge, this is the first study that compared the effect of short-term and continuous doses of ZA over time in young naïve C57BL/KaLwRij mice.

Bone remodelling is a tightly controlled process between osteoclastic bone resorption and osteoblastic bone formation by which bone is constantly renewed in order to maintain its structural and functional integrity (Raggatt et al 2010). These processes also play an important role during the remodelling of the primary spongiosa which includes the resorption of the calcified cartilage, deposition of new bone and formation of trabecular bone during the longitudinal growth in young animals (Stroh et al 2005). Response to inhibition of osteoclastic bone resorption will be more evident at parts of the bone that are actively remodelled at the time of treatment. In growing animals, the metaphyseal region of the bone is where there is on-going hyperactive modelling and remodelling directed toward resorption of the cartilage septa and bone deposition to form the organised trabecular bone. Therefore, static bone histomorphometry and microCT analysis was confined to analysing the proximal tibial metaphysis.

The data reported in the present study shows both short-term and continuous ZA treatment inhibited osteoclastic bone resorption in young C57BL/KaLwRij mice which resulted in significantly greater bone mass. However, some clear differences have been demonstrated between the two dosage regimens. Short-term dosage of ZA was associated with a transient inhibition of calcified cartilage remodelling in the growth-plate metaphyseal junction. In contrast, following continuous ZA treatment, a continued inhibition of resorption in the zone of provisional calcification was seen. Interestingly, following short-term ZA regimen there was continuous expansion of calcified cartilage structures extending from the zone of provisional calcification into the tibial metaphysis which contributed towards the dramatic increase in the trabecular bone volume when compared with continuous ZA treatment. In young animals, during the longitudinal growth phase, there is continuous remodelling of the calcified cartilage from the metaphyseal end of the growth plate which forms the cancellous trabecular bone (Schenk et al 1973). In the present study, after short-term treatment of ZA, although there was a transient reduction in the osteoclastic bone resorption after 7 days post-treatment, the presence of a widening band of complex calcified trabecular structure in the metaphysis after 14 and 21 days, rich in osteoclasts, suggest resumption of normal cartilage remodelling and/or resorption thus producing calcified cartilage scaffolds, vascular invasions and recruitment of new osteoclasts. Contrastingly, following continuous ZA

treatment, although there was greater cortical and trabecular bone mass, there was no significant variation in the osteoclast numbers when compared to PBS treated control bones. Furthermore, the absence of calcified cartilage structure in the tibial metaphysis suggests an inhibition of growth plate expansion in continuous ZA treatment regimen due to the presence of high levels of intercellular ZA. Similar findings were reported by Schenk et al (1973) where treatment with BPs showed differential effects from inhibition of cartilage resorption to defective bone matrix mineralisation depending on the type of BP and the frequency of administration.

To-date, ZA is a potent anti-resorptive agent with a high bone binding affinity (Green 2005). The inhibitory effect of ZA on osteoclastic bone resorption seems to be mediated by several different mechanisms: inhibition of osteoclast formation, interference with osteoclast function and induction of apoptosis (Coxon et al 2000; Pan et al 2004; Nyangoga et al 2010). In addition to the inhibitory effect on osteoclasts, BPs were also shown to affect osteoblasts and their function. However, the effect of BPs on osteoblasts is quite controversial. BPs were shown to promote (Reinholz et al 2000; Pan et al 2004) and inhibit (Khokher et al 1989; Klein et al 1998) osteoblast formation, activation and mineralisation. Recently, Patntirapong et al (2012) showed in addition to their inhibitory effect on osteoclasts, BPs also inhibited mineralisation and differentiation of MSCs and osteoblasts by direct cytotoxicity. At this point, it is interesting to note that in this experiment short-term ZA treatment was associated with a transient reduction (only after 7 days post-treatment) in osteoblast numbers in the trabecular region whereas normal control numbers were present after 14 and 21 days. However, in the case of continuous dosage regimen, there was a sustained reduction in osteoblast numbers in the metaphyseal region at all-time points. This suggests that the inhibitory effect of ZA on osteoblast is short-lived with the effect being prominent only for a short period following ZA injection and repeated dosage resulted in continuous suppression of osteoblast. Whether this reduction in osteoblast numbers in the metaphyseal region was a consequence of ZA induced direct cytotoxicity on osteoblasts or indirect effect due to inhibition of osteoclastic bone resorption was not clear from this experiments.

Serum levels of bone resorption (TRACP5b) and bone formation (P1NP) markers were quantitated to assess the systemic changes in bone remodelling following ZA treatment. A significant reduction in both TRACP5b and P1NP levels suggested profound inhibition of both osteoclastic and osteoblastic activity after short-term ZA administration. However, it is particularly interesting that the serum TRACP5b levels remained low despite a substantial increase in osteoclast numbers in the trabecular region after 14 and 21 days of short term ZA treatment. TRACP5b is produced by osteoclasts during active osteoclastic bone resorption and serves as an indicator for both osteoclast activity and osteoclast number (Halleen et al 2006). Nordhal et al (1998) showed osteoclasts that are involved in cartilage resorption (also referred as chondroclast) near the growth plate structurally differ in terms of high levels of intrinsic TRACP5b enzyme that is not released into the circulation. Furthermore, P1NP levels which are breakdown products released into circulation during osteoblastic bone formation were profoundly low in the ZA treated groups. This further implies that the trabecular bone mass observed in the

metaphyseal region was not the product of osteoblastic bone formation, but due to the preservation of calcified cartilage structure due to delayed osteoclastic bone resorption.

It is now clear that, ZA treatment used to inhibit osteoclastic bone resorption is also accompanied by substantial inhibition in the osteoblastic bone formation. Importantly, the inhibitory effect of ZA on osteoblasts may be secondary to inhibition of osteoclastic resorption or due to direct cytotoxic effects (Patntirapong et al 2012). However, the mechanisms responsible are not known. Furthermore, data from the present study also showed that ZA treatment is associated with considerable micro-structural alteration of the bone at least in growing animals, whether this will affect tumour progression in models of MM grown in these animals is not known. Most animal models of MM and bone metastases involve young animals; therefore interpretation of ZA effect on osteoclastic bone resorption has to be done with caution and must consider the effects on osteoblasts and bone formation.

To conclude, short-term ZA treatment was associated only with a temporary inhibition of osteoclastic bone resorption and abnormal bone remodelling while a continuous ZA treatment was associated with continuous inhibition of osteoclastic bone resorption. Additionally, short-term ZA treatment was accompanied with a transient inhibition of bone formation and considerable micro-structural alteration of the trabecular bone, while continuous ZA treatment resulted in a continual suppression preserving the normal trabecular architecture in the metaphyseal region. Therefore, a continuous ZA treatment will be more suitable to achieve profound inhibition of osteoclastic bone resorption in experimental animals to study the effect of ZA on myeloma development.

CHAPTER 4 ESTABLISHING THE DEVELOPMENTAL STAGES OF MULTIPLE MYELOMA

4.1 INTRODUCTION

Unlike other haematological cancer, MM is an antibody producing B lymphocyte malignancy characterised by infiltration of myeloma to the BM, profound increase in osteoclastic bone resorption, and development of severe osteolytic bone disease. This is attributed to the selective localisation of myeloma cells to the BM during the main course of the disease progression. Several studies have suggested that the interaction between the myeloma cell and the host BM microenvironment plays an important role in the selective migration and colonisation of myeloma cell to bone (Manier et al 2012). Furthermore, myeloma cell interactions with the BM microenvironment have also been implicated in the contribution of survival advantage and protection to myeloma cells against anti-myeloma chemotherapy (Wei et al 2005; Castells et al 2012).

Recent studies have focused on identifying the functional interactions between the myeloma cells and the cells of the BM microenvironment in an attempt to find newer therapeutic targets (Cheung et al 2001). The concept of ‘metastatic niche’ in which the non-cancerous cells such as BMSC, BMEC and osteoclasts and the liquid milieu in the BM rich in bone-derived growth factors, chemokines and cytokines primes and augments the BM microenvironment for the homing and growth of myeloma cells has led to the possibility that targeting these non-cancerous compartments will offer therapeutic benefits (Manier et al 2012). In particular, the role of osteoclasts (Roodman 2001; Abe et al 2004), which contributes to the ‘vicious cycle’ between osteolytic bone destruction and myeloma expansion and the availability of specific inhibitors of osteoclastic bone resorption such as CLO and ZA have made these cells an attractive target for myeloma management (Galson et al 2013).

In order to study myeloma-osteoclast interactions, to identify key time points in myeloma progression and to study the effect of anti-osteoclast treatment, it is essential to characterise the developmental stages of myeloma and the associated BM alterations. Currently, *in vivo* murine models of myeloma such as SCID-hu model and 5T series are the extensively used to study these complex interactions and to determine the impact of drug treatment. In this study, flow cytometry, CD138 immunohistochemistry and three-dimensional (3D) multiphoton microscopy techniques were used to detect and map the tumour cells in bone and to evaluate the progression of tumour burden from a ‘single’ cell that reached the BM to established ‘colonies’ using the 5TGM1 murine model of myeloma. Furthermore, myeloma bone disease progression was also monitored by histomorphometry, microCT, measuring serum levels on bone turnover markers and computational image analysis methods to assess the changes in osteoclast and osteoblast numbers, microstructural alteration in bone, systemic changes in bone remodelling markers and myeloma induced osteolytic lesions respectively during myeloma progression.

4.2 AIMS & OBJECTIVES

The aim of this chapter was to identify key time points and the temporo-spatial orientation of myeloma cells in bone during the developmental stages of the disease in bone: from a single cell to the development of overt myeloma colonies in bone using the 5TGM1 murine model of myeloma.

Hypothesis: Individual myeloma cells extravasate from the peripheral circulation, home to specific locations in the BM and proliferate to establish overt myeloma colonies.

In order to detect 5TGM1 cells in bone by flow cytometry and multiphoton microscopy, eGFP labelled 5TGM1 cells were used. As eGFP was not adequately expressed until established colony formation the cells were further labelled with 1, 1'-dioctadecyl-3,3',3'- tetramethylindodicarbocyanine 4-chlorobzenesulfonate (DID), a far-red lipophilic fluorescent cell membrane dye in order to visualise the cells during early stages of disease.

The preliminary objectives were:-

1. To optimise the DID labelling of 5TGM1-eGFP murine myeloma cells.
2. To determine the effect of DID labelling on myeloma cell proliferation and of cell proliferation on DID labelling.

The main objectives were:-

1. To identify and quantify the number of 5TGM1 murine myeloma cells that arrive in the bone, the number of cells that proliferate to form colonies and the overall tumour burden in the bone at the end stages of disease.
2. To study the local and systemic effects in bone during the development of myeloma.

4.3 MATERIALS & METHODS

Detailed information on individual techniques performed is given in [Chapter 2: General Materials and Methods.](#)

4.3.1 DETERMINING THE OPTIMAL CONCENTRATION OF VYBRANT DID DYE TO LABEL 5TMM-eGFP MURINE MYELOMA CELL

In order to determine the concentration of DID dye required to stably label eGFP expressing 5TMM murine myeloma cells, 2.5, 5, 10 and 15 $\mu\text{l}/10^6$ cell concentrations of the Vybrant DID dye (Catalogue No. V-22887; *Life Technologies*) was tested to identify the optimal concentration. 5TMM-eGFP murine myeloma cells were washed in PBS and suspended at concentration of 1×10^6 cells per ml of serum free media (RPMI 1640). Vybrant® DiD Cell-Labelling solution was added at concentration 2.5, 5, 10 and 15 $\mu\text{l}/\text{ml}$ and mixed by gentle pipetting. Unlabelled 5TMM-eGFP cells were used as negative control. Cells were incubated in dark at 37°C in 5% CO_2 incubator for 30 min. After incubation, cells were pelleted down by adding foetal calf serum (10% of the volume) and centrifuging at 1500 RPM for 5 min. Cell pellets were then washed with normal complete media and resuspended in 1 ml of PBS ([Refer Materials & Methods Section 2.2.4](#)). Flow cytometry analysis was done to determine the percentage of DID labelled cells. Propidium Iodide (PI) staining method was used to determine cell viability and the percentage of viable DID label and dead cells were computed.

4.3.2 DETERMINING THE EFFECT OF DID LABELLING ON 5TGM1 MURINE MYELOMA CELL GROWTH

5TGM1-eGFP murine myeloma cells were labelled with 10 μl of DID (optimal concentration) or unlabelled. Cell proliferation was measured over time after 0, 1, 3, 5, 7, 9 and 11 days by cell counting and flow cytometry was used to measure DID labelled cell at each time point. Unlabelled 5TGM1-eGFP cells were used as negative controls. [Refer Chapter 2: Materials and Methods](#) for detailed explanations on Neubauer cell counting method, flow cytometry and multiphoton microscopy detection of DID labelled 5TGM1-eGFP cells.

5TGM1-eGFP-DID and unlabelled 5TGM1-eGFP cells were seeded at a concentration of 1×10^5 cells in 10 ml of complete media and incubated at 37°C in a 5% CO_2 incubator in T25 flask (Becton, Dickinson and Company). Four replicates were maintained in separate T25 flasks for both cell types for each day. At days 2, 4, 6, 8 and 10, 5 ml of fresh media was replaced in each flask by gently pipetting out 5 ml of used media. Detailed experimental design is given in figure 4.3-1. For *in vitro* multiphoton microscopy a small aliquot of cells were placed on a glass slide with a 0.1 mm cover-slip on top and scanned using 820 nm laser for the detection of both DID and eGFP signals. Scanning was done on each of the four replicates to a depth of 40 μm and images were analysed using Volocity™ software.

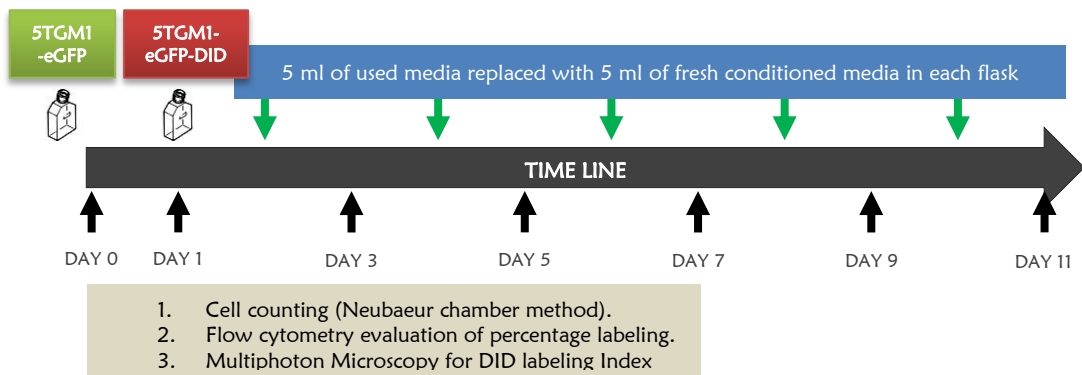


Figure 4.3-1: Experimental design for determining the effect of DID labelling on cell proliferation.

An *in vitro* longitudinal study was performed to investigate the effect of DID labelling on 5TGM1eGFP myeloma cell growth. DID labelled and unlabeled 5TGM1-eGFP cells were seeded at a concentration of 1×10^5 cells in 10 ml normal complete media (RPMI 1640 + additives) in T25 flasks and maintained at 5% CO₂ incubator at 37° C. Four T25 flasks were maintained for each cell type for every time point. 5 ml of fresh media was used to replace used media from every flask on days 2, 4, 6, 8 and 10.

4.3.3 EXPERIMENTAL DESIGN TO CHARACTERISE THE DEVELOPMENTAL STAGES OF MYELOMA IN BONE

All animal work and experimental conditions were in done accordance with the local guidelines and the with the home office approval provided under the project licence number PPL No: 40/3462 held by Dr. Colby L Eaton University of Sheffield, UK.

Age and sex matched 7-11 weeks old C57BL/KaLwRij mice were injected with 2×10^6 5TGM1-eGFP-DID cells (tumour-bearing) or PBS (tumour-free control) via the tail vein. Mice were randomised and sequentially grouped into four time points to study the early (day 3), intermediate (days 10 and 14) and end stage (day 21 +) of the disease. For the end stage, all animals were culled when the first animal show signs of morbidity such as development of hind limb paralysis or sickness. A schematic representation of the study design and the number of animals in each group at each time points is given figure 4.3-2.

All animals were starved 6 hr prior to the sacrifice in order to eliminate the circadian variation in the serum bone biomarkers. Mice were anaesthetised using 0.5 ml/kg of pentobarbitone (intra-peritoneal injection) and blood samples were collected by cardiac puncture. Animals were culled by cervical dislocation while under deep non-recoverable anaesthesia and tissues harvested. The following tissues were harvested and stored appropriately.

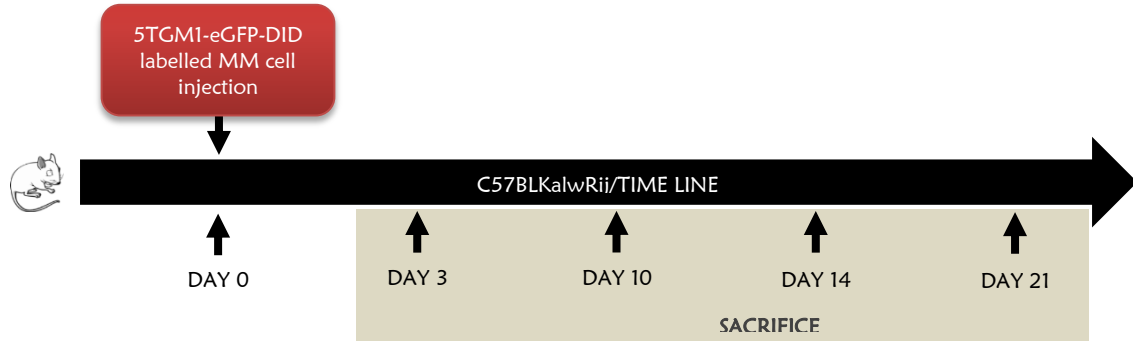


Figure 4.3-2: Experimental Design for longitudinal assessment of myeloma development in the 5TGM1 murine model of myeloma.

Naïve C57BL/KaLwRij mice were injected with either PBS or 2×10^6 5TGM1-eGFP-DID cell via the tail vein and were sacrificed periodically after 3, 10, 14 and 21 days to investigate the different phases of myeloma development in bone over time. After 3, 10 and 14 days post injection time points naïve controls ($n=4$) and 5TGM1-eGFP-DID tumour ($n=8$) and after 21 days naïve controls ($n=4$) and 5TGM1-eGFP-DID tumour-bearing mice ($n=7$) were culled.

4.3.4 STATISTICAL ANALYSIS

Microsoft Office Excel 2010® was used to plot the graphs and values represented as Mean \pm SEM unless stated otherwise. Prism GraphPad Ver 6.0 was used for comparison of parameters between naïve PBS and 5TGM1 tumour-bearing animals between two independent populations a two-tailed ‘non-parametric’ Mann Whitney-Wilcoxon test was used in unpaired tests to compare means with $P < 0.05$ as being statistically significant (Confidence interval $> 95\%$).

4.4 RESULTS

4.4.1 OPTIMISING DID LABELLING OF 5TMM-eGFP MURINE MYELOMA CELLS

In order to detect and visualise the 5TMM myeloma cells in bone as they arrived and started to form colonies they were labelled with DID and eGFP. The preliminary objective was to identify the optimal Vybrant DID dye concentration required for labelling 5TGM1-eGFP cells. Flow cytometry evaluation was used to measure the percentage of cell death and viable DID labelled 5TMM-eGFP cell following the staining procedure.

Results showed that DID labelling at a concentration of $10 \mu\text{l}/10^6$ cells for 30 min, incubated in 5% CO_2 incubator, achieved maximum labelling ($>95\%$) with minimal cell death (figure 4.4-1) while a lesser dosage resulted in reduced labelling and higher dosage resulted in increased cell death following labelling. This dose was used hereafter to label 5TGM1-eGFP myeloma cells.

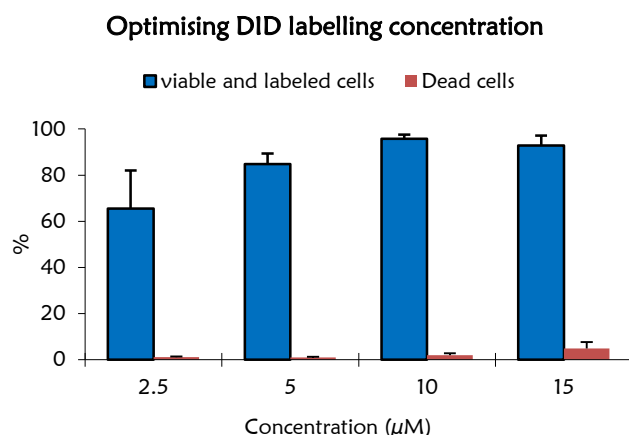


Figure 4.4-1: DID concentration versus 5TGM1-eGFP-DID cell viability.

Concentration of vybrant DID labelling solution versus percentage viable and DID labelled cells and percentage cell death assessed by flow cytometry following 2.5, 5, 10 and 15 μl of vybrant labelling solution ($n=3$).

4.4.2 5TGM1 CELL PROLIFERATION EFFECTS ON DID LABELLING OVER TIME

In order to understand the effect of DID labelling on 5TGM1-eGFP cell proliferation and of cell proliferation on DID labelling a longitudinal study was performed to changes in percentage labelling over time by flow cytometry. Multiphoton microscopy was used to quantitate DID labelling and spectral fingerprinting to authenticate the DID and eGFP signals.

Effect of DID labelling on 5TGM1-eGFP cell proliferation

Results showed that there was no difference between DID labelled 5TGM1-eGFP cells and unlabelled 5TGM1-eGFP cells in their rate of proliferation *in vitro* over a period of 11 days in complete media (figure 4.4-2).

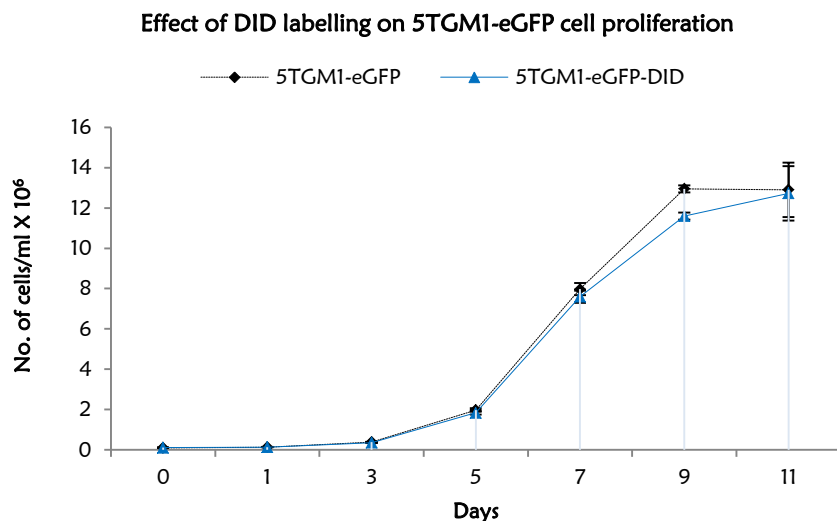


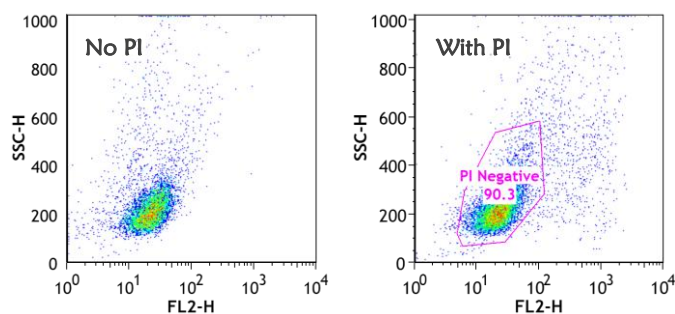
Figure 4.4-2: Effect of DID labelling on the proliferation of 5TGM1-eGFP cells *in vitro*.

The number (in millions) of 5TGM1-eGFP-DID and unlabelled 5TGM1-eGFP cells after day 0, 1, 3, 5, 7, 9 and 11 post DID dye labelling *in vitro* culture (n=4).

The effect of 5TGM1-eGFP cell proliferation on DID labelling

Flow cytometry quantitation of live and viable DID labelled 5TGM1-eGFP cells was done using the FACS Calibur flow cytometer (Becton Dickinson, Oxford UK). A Propidium Iodide (PI) staining method was used for the detection of dead cells. Figure 4.4-3 shows flow cytometry profile for live cell gating using PI staining method. The results showed that the DID labelling was stable and above 90% after day 0 and day 1 post labelling, however DID labelling dropped to 42.5% and 7.2% on day 3 and day 5 respectively and continued to fall (figure 4.4-4 A). Interestingly, the mean fluorescence intensity (MFI) which is flow cytometric measure of the fluorescence intensity of DID labelled cells also followed a similar pattern like the percentage labelling (figure 4.4-4 B) shows typical flow cytometry changes following labelling after 0, 1, 3, 5, 7, 9 and 11 days post DID labelling. A dramatic shift in the DID labelled 5TGM1-eGFP population over the FL-4 axis which suggested that there was not only a reduction of DID labelled cells but also a reduction in the DID labelling at individual cellular levels was also seen.

A. PI staining for detection of viable cell



B. Percentage changes in DID labelling over time

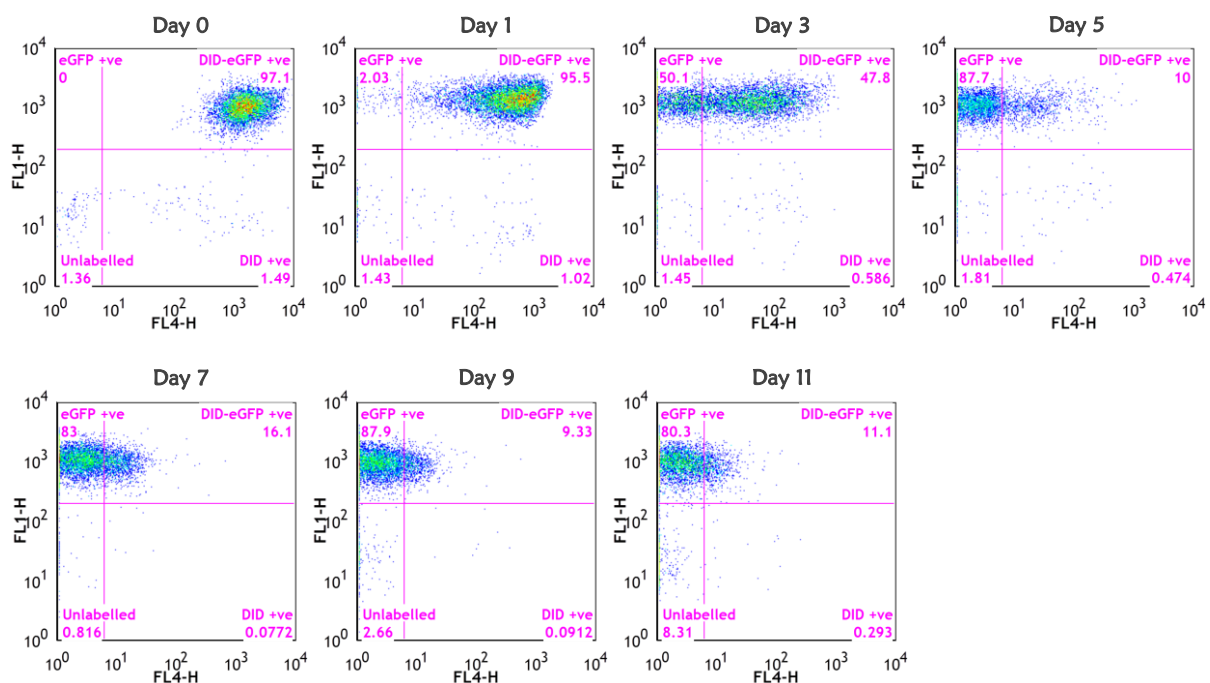


Figure 4.4-3: Flow cytometric analysis of DID labelling of 5TGM1-eGFP cells over time.

(A) Flow cytometry analysis was done to identify viable cell using Propidium iodide staining method with 5TGM1-eGFP-DID cells without PI with side scatter (SSC) on X-axis and FL2 on Y-axis and the shift in the FL2-H channel following PI staining ($n=4$). A polygon gate was used to gate the PI negative viable cell population. **(B)** DID labelling of 5TGM1-eGFP cells was done and monitored for the percentage DID labelled cells longitudinally after day 0, 1, 3, 5, 7, 9 and 11 days using flow cytometry. Figures show serial flow cytometry profiles with FL1-H (eGFP $^{+}$) on the x-axis and FL4- H (DID $^{+}$) on the Y-axis ($n=4$). Percentage DID $^{+}$ cells were analyzed only on the viable population. Figure shows a reduction in the percentage 5TGM1-DID $^{+}$ cell and also a gradual shift (from right to left) in the DID $^{+}$ population along the FL4-H axis suggesting a reduction in the mean fluorescence intensity (MFI) over time.

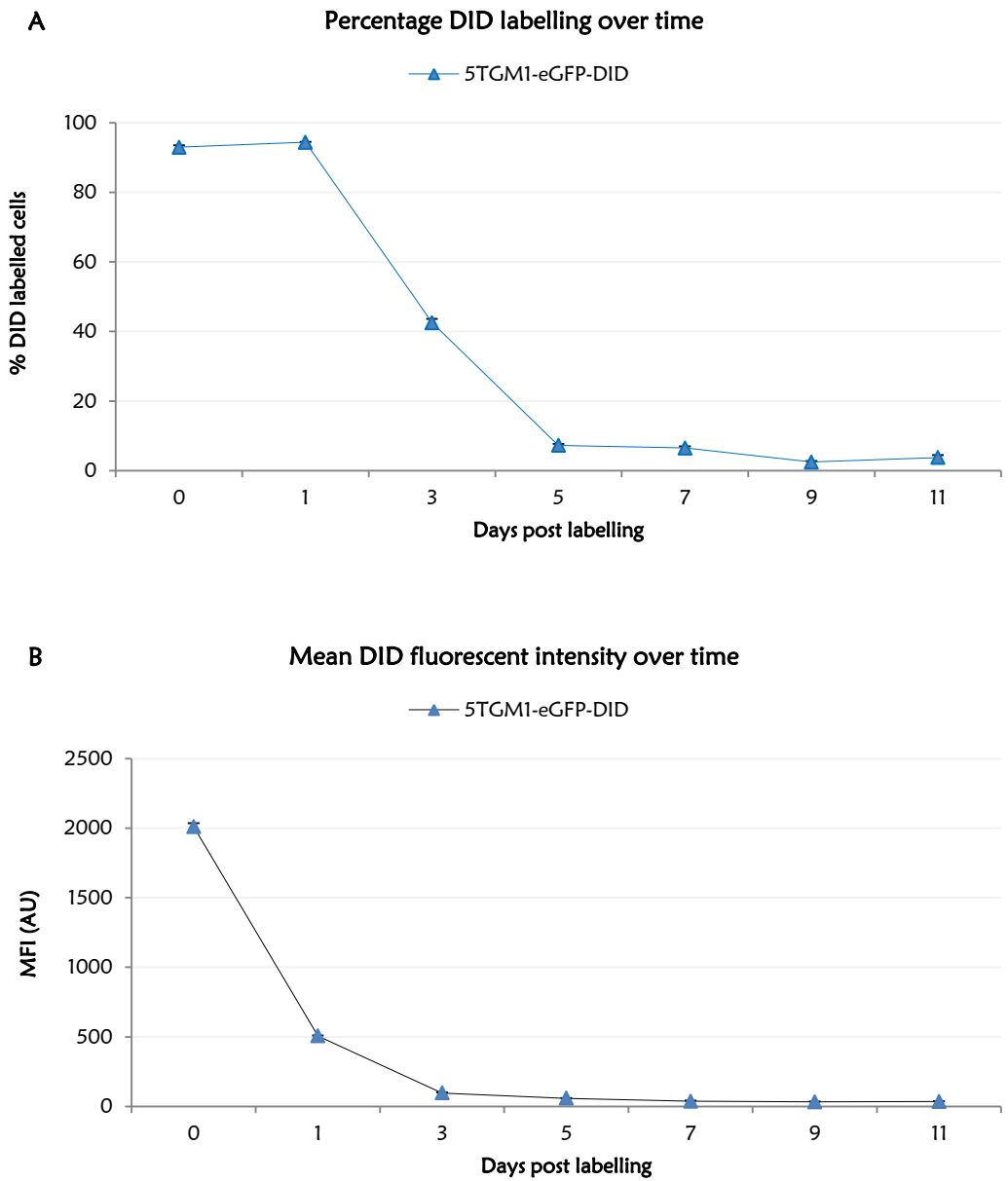


Figure 4.4-4: The effect of proliferation on DID labelled 5TGM1-eGFP cells as assessed by flow cytometry.

(A) *In vitro* changes in the percentage 5TGM1-DID⁺ cells over time (n=4). (B) Changes in mean fluorescent intensity (MFI) of the 5TGM1-DID⁺ population following DID labelling of 5TGM1-eGFP cells (n=4).

Multiphoton spectral confirmation of 5TGM1-eGFP-DID murine myeloma cells *in vitro*

Lambda imaging or spectral fingerprinting was done on *in vitro* 5TGM1-eGFP-DID cells in order to authenticate the emission fluorophore wavelengths. *In vitro* imaging of 5TGM1-eGFP-DID cells on glass slides showed emission signals that peaked at both 507 nm and 675 nm which corresponded to DID and eGFP signals respectively (figure 4.4-5).

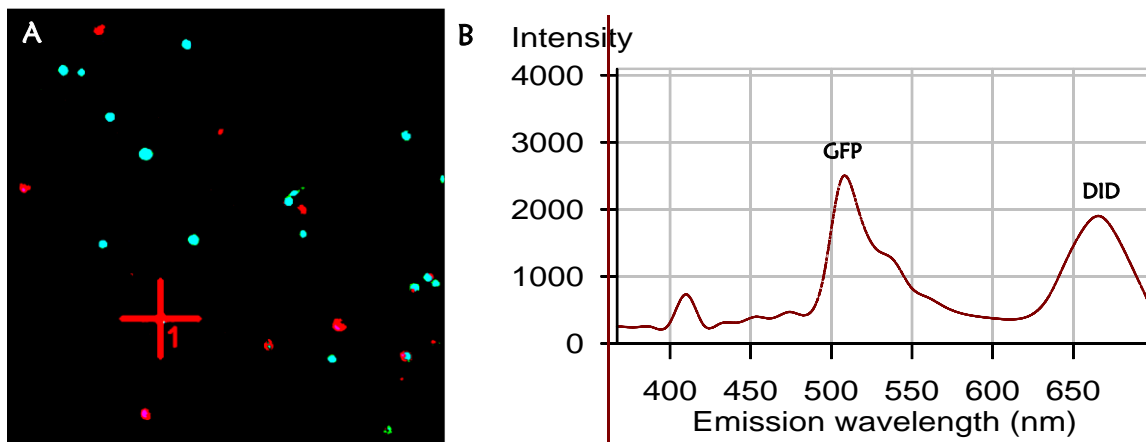
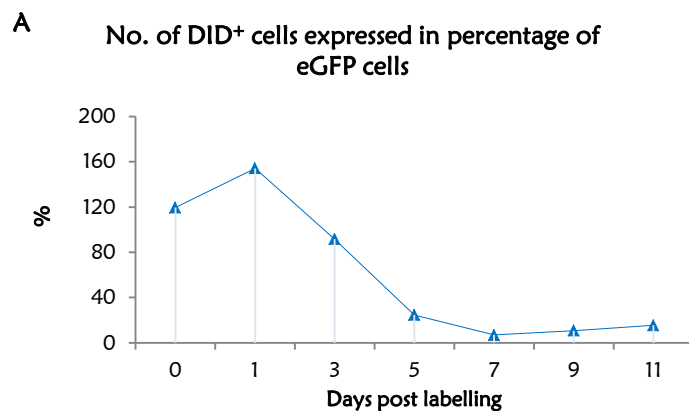


Figure 4.4-5: *In vitro* spectral imaging of 5TGM1-eGFP-DID cell.

(A) Spectral image of 5TGM1-eGFP-DID cells (*in vitro*) scanned using LSM 510 META microscope showing DID⁺ and eGFP⁺ objects. Fig B shows spectral profile with emission peaks of the emitted signals from the 5TGM1-eGFP-DID cells. (B) Wavelength against maximum fluorescence intensity of the emitted light showing emission peaks 507-509 nm and 650-675 nm which corresponds to eGFP and DID spectral profiles suggesting emission of both eGFP and DID signals.

The effect of 5TGM1-eGFP-DID cell proliferation on the distribution of the DID label on the cell membrane

Multiphoton microscopy analysis was done to determine the number of 5TGM1-DID⁺ present in culture over time post-labelling. As the cells were labelled with both DID and eGFP results were expressed as the number of 5TGM1-DID⁺ per cent 5TGM1-eGFP⁺ cells. Results showed that the number of 5TGM1-DID⁺ labelled cells were 120% and 155% compared to the percentage of 5TGM1-eGFP⁺ cells after 0 and 1 days post labelling respectively and drastically dropped down to 24.5% after day 3 and continued to drop to 15.4% on day 11 post labelling (figure 4.4-6 A). This was unexpected, but may just reflect the increased intensity of DID labelling compared to eGFP and the ease of detection of these fluorophores. Figure 4.4-6 B shows multiphoton microscopy images of 5TGM1-eGFP-DID cell aliquot (*in vitro*) over time.



B. *In vitro* multiphoton microscopy of 5TGM1-eGFP-DID cells over time

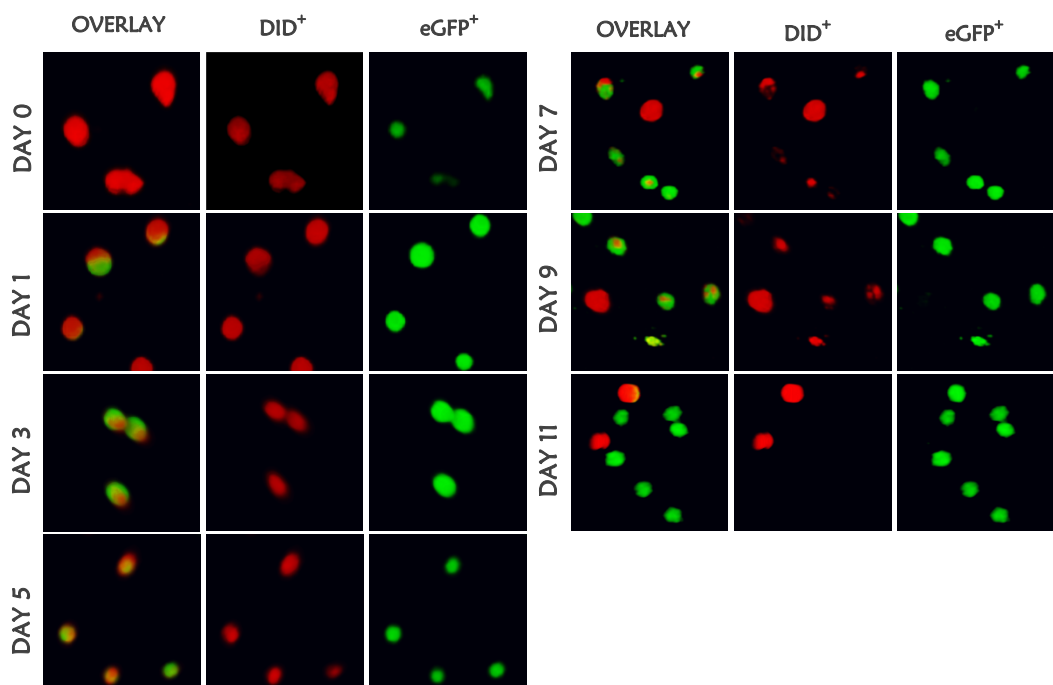


Figure 4.4-6: Effect of 5TGM1-eGFP-DID cell proliferation on DID labelling by multiphoton microscopy.

(A) Changes in the number of 5TGM1-DID⁺ cells expressed as a % of the 5TGM1-eGFP⁺ population (*in vitro* culture system) after 0, 1, 3, 5, 7, 9 and 11 days post DID labelling as detected by multiphoton microscopy (n=4). (B) Representative multiphoton microscopy images of *in vitro* 5TGM1-eGFP-DID over time in DID-eGFP superimposed overlay, DID⁺ (red) and eGFP⁺ channels (green). *In vitro* 5TGM1-eGFP-DID cells were scanned using 820 nm laser using 20X objective in multiphoton microscopy. At day 1, cells were seen to be completely covered with DID label, however there was a gradual reduction in the amount of DID labels distributed on the surface of 5TGM1-eGFP⁺ cells from day 1 to day 11. As DID label is a lipophilic cell membrane dye, cell proliferation resulted in random sharing of DID dye between the daughter cell causing gradual loss of the DID label from the cell membrane of rapidly dividing cell over time. However, even after day 11 there is a small population of 5TGM1-DID⁺ cells suggesting a quiescent pool of 5TGM1 cells which has preserved their DID labelling.

4.4.3 ASSESSMENT OF TUMOUR PROGRESSION IN 5TGM1 MURINE MODEL OF MYELOMA

Flow cytometric evaluation of tumour burden over time

Flow cytometric evaluation of the BM cells was done in order to quantify the number of 5TGM1-eGFP-DID cells present in bone. The process of BM extraction and flow cytometry analysis are described in detail in [Chapter 2.2.6](#). As the 5TGM1 cells were dual labelled (both eGFP and DID), quantitation was done on DID⁺, eGFP⁺ and dual labelled DID⁺ eGFP⁺ cells. BM cells from naïve tumour-free mice served as negative control for gating unlabelled cells. Compensations were not required as there was no cross talk between eGFP (emax 507 nm) and DID (emax 675 nm). Quadrant gating was applied based on the naïve BM cells (negative control from tumour-free mice) to eliminate unlabelled cells and the percentage of eGFP⁺, DID⁺ and eGFP⁺-DID⁺ cells were measured (figure 4.4-7).

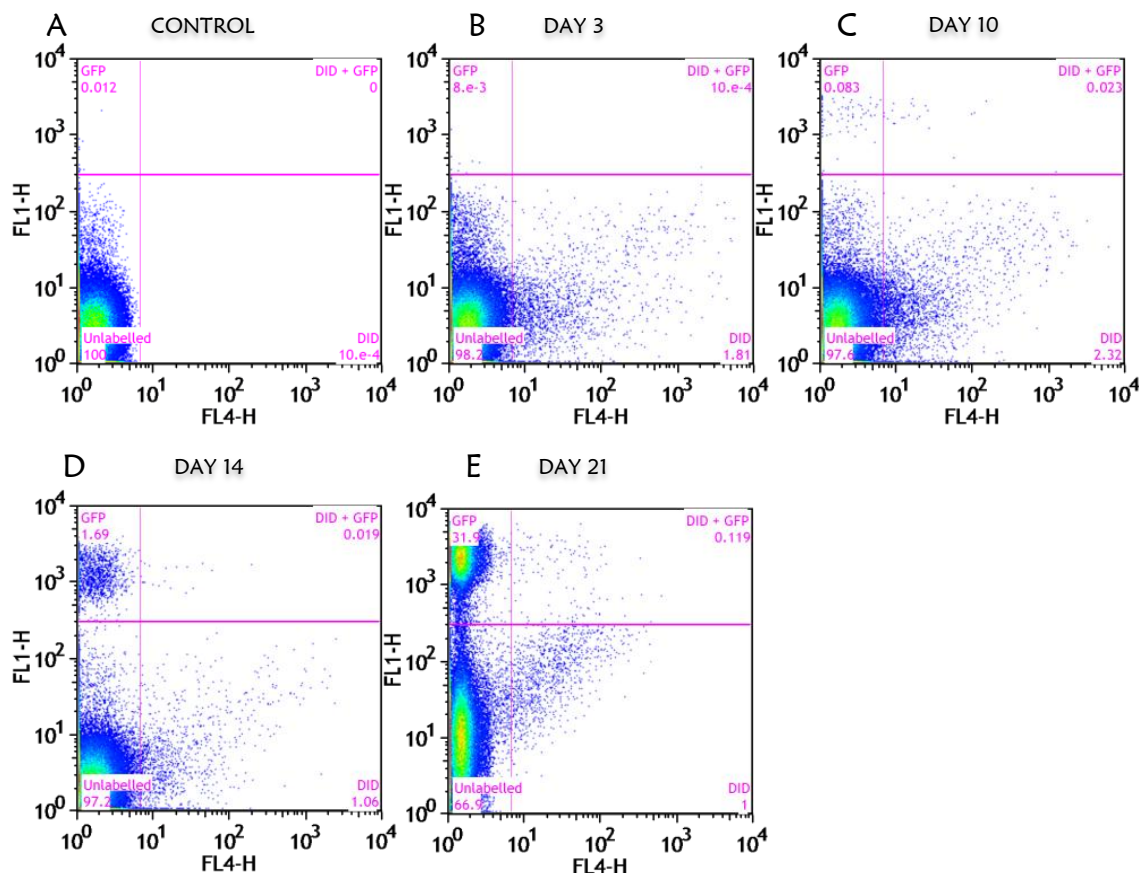


Figure 4.4-7: Flow cytometric profiles of 5TGM1-eGFP-DID tumour cells in the BM over time.

Flow cytometry was done using Becton Dickinson FACS Calibur flow cytometer equipped with Cell quest software and the data was analysed using Flow Jo software. Percentage eGFP⁺, DID⁺ & dual DID-GFP⁺ cells were measured from BM cells over time and expressed as 'Pseudo colour plots'. **(A)** Representative flow cytometry profile of naïve murine BM cell which served as a negative control. **(B-F)** Representative flow cytometry profiles of BM from 5TGM1-eGFP-DID tumour-bearing mice after 3, 10, 14 and 21 days respectively.

Results showed the presence of 5TGM1-DID⁺ cells ($1.64 \pm 0.14\%$) in BM after 3 days post tumour cell injection, whereas there was no evidence of eGFP⁺ or dual labelled 5TGM1-eGFP⁺-DID⁺ population. However, after 10 and 14 days, there was a gradual reduction in the percentage 5TGM1-DID⁺ population ($1.64\% \pm 0.14$ to $0.66 \pm 0.06\%$), while there was a gradual and increasing percentage of 5TGM1-eGFP⁺ cell population evident in the BM ($0.05 \pm 0.01\%$ to $0.86 \pm 0.17\%$). At 21 days post injection, when the mice were sacrificed due to development of either sickness or hind limb paralysis, a $1.35 \pm 0.16\%$ of 5TGM1-DID⁺ cells and a dramatic increase in the 5TGM1-eGFP⁺ tumour population ($29.4 \pm 2.88\%$) was seen. The percentage of dual labelled 5TGM1-eGFP⁺-DID⁺ cell population was noticeably very low at all-time points (figure 4.4-8).

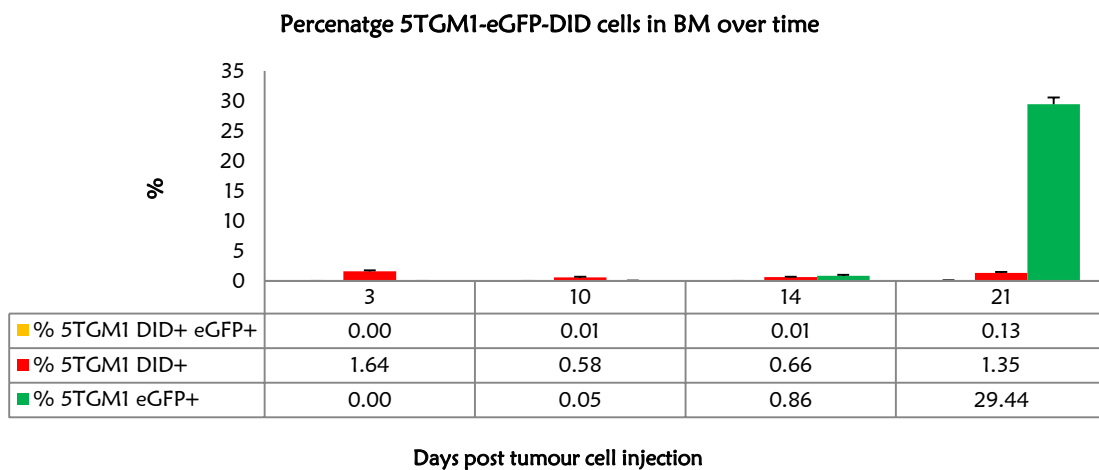


Figure 4.4-8: Quantitative flow cytometry analysis of 5TGM1-eGFP-DID tumour development in bone over time.

Changes in the percentage of DID⁺, eGFP⁺, dual labelled 5TGM1-eGFP⁺-DID⁺ cells in BM after 3, 10, 14 and 21 days post 5TGM1-eGFP-DID tumour cell injection (n=8 for day 3, 10 and 14; n=7 for day 21).

Quantification of CD138 positive plasma cells in BM following 5TGM1 myeloma development

Results showed that CD138⁺ population in naïve tumour-free animals appeared as single cells distributed throughout the BM at all-time points. There was no evidence of CD138⁺ cell colonies in tumour-free naïve control animals. However, in the 5TGM1 tumour-bearing animals, CD138⁺ colonies appeared in the BM as early as 10 days post tumour cell injection. Interestingly, quantitative analysis showed that there was no difference in the number of single CD138⁺ cells between naïve and tumour-bearing animals after 3 and 10 days post tumour cell injection. However, after 10 days post tumour cell injection, in tumour-bearing animals $0.11 \pm 0.03\%$ of the BM space was occupied by CD138⁺ tumour colonies. After 14 days post tumour cell injection, there was an increase in both single cells and CD138⁺ colonies in the tumour-bearing group with almost the entire BM being replaced with CD138⁺ population at 21 days. At this point, the entire BM was densely packed with CD138⁺ cell which made

detection of single CD138⁺ cells highly impracticable and therefore the end point was described as percentage BM space filled with CD138⁺ tumour (figure 4.4-9 & figure 4.4-10).

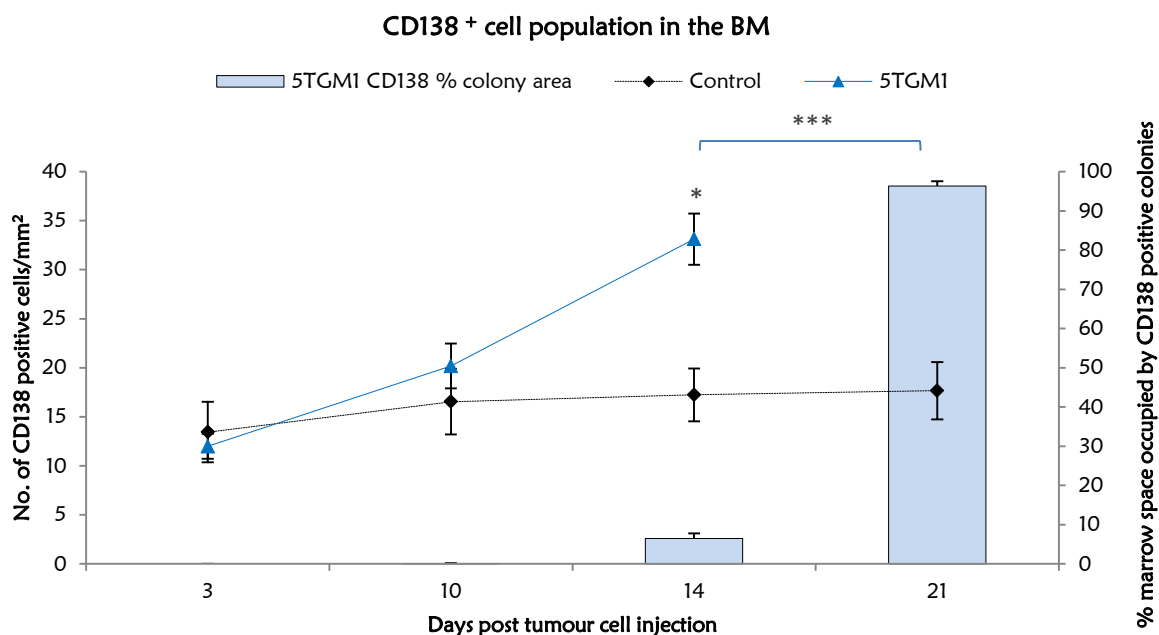


Figure 4.4-9: Changes in CD138 positive cells in the BM over time post injection of 5TGM1 cells.

Double Y-axis graph showing changes in CD138⁺ cell number and percentage BM space occupied by CD138⁺ colonies in naïve and 5TGM1 tumour-bearing animals after 3, 10, 14 and 21 days post tumour cell injection ($n=8$ for day 3, 10 and 14; $n=7$ for day 21). Non-parametric Mann-Whitney Wilcoxon's test was used to compare the difference in single CD138⁺ cell between the control and 5TGM1 tumour-bearing groups. * $P<0.05$, ** $P<0.01$, *** $P<0.001$.

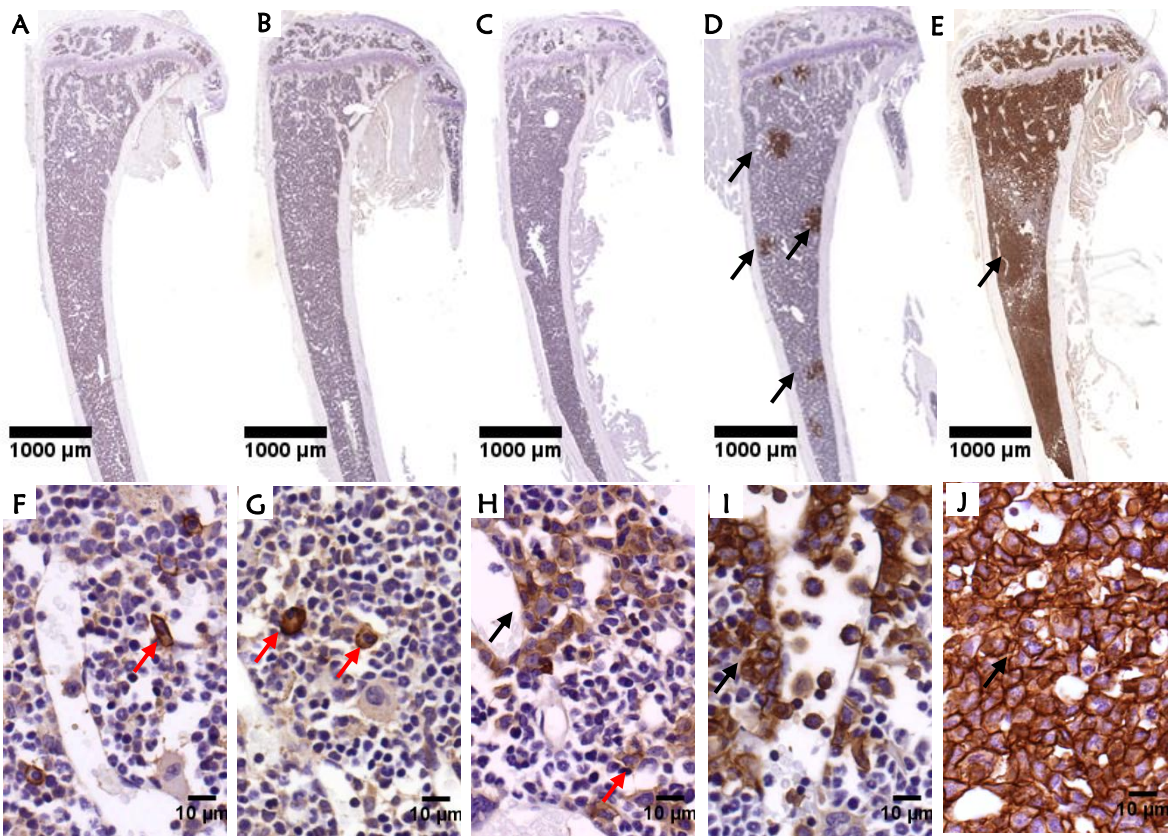


Figure 4.4-10: CD138 immunohistochemistry staining showing the developmental stages of 5TGM1 murine myeloma in bone.

Representative CD138 IHC stained tibial sections of naïve tumour-free (A) and 5TGM1 tumour-bearing mice after 3 (B), 10 (C), 14 (D) and 21 (E) days post tumour cell injection showing CD138⁺ tumour colonies (black arrow). IHC was performed for all time points on naïve and 5TGM1-eGFP-DID tumour-bearing mice to detect the presence of single CD138⁺ plasma/myeloma cells (red arrow) and CD138⁺ tumour colonies (black arrow) in the BM. Magnified images of proximal tibial metaphysis of naïve (F) and 5TGM1 tumour-bearing mice after 3 (G), 10 (H), 14 (I) and 21 (J) days post tumour cell injection shows the development of myeloma from single cell to overt myeloma colonies that fills the entire BM. Strong cell membrane CD138 immune reactivity is observed in both naïve and myeloma tumour-bearing animals.

Three-dimensional quantification of tumour burden in the 5TGM1 murine model of myeloma using multiphoton microscopy

In order to understand the temporal and spatial relationship of 5TGM1-eGFP-DID myeloma development in bone over time, multiphoton microscopy was performed for the detection of 5TGM1-eGFP-DID labelled tumour cell and bone using SHG ([section 2.2.22](#)). In order to confirm and authenticate DID, eGFP and SHG signals, spectral fingerprinting was done on bone samples with established tumour formation. *In vivo* spectral imaging from bone showed emission signals which peaked at 410 nm (blue), 507 nm (green) and 675 nm (red) which corresponded to bone, eGFP and DID wavelengths respectively (figure 4.4-11).

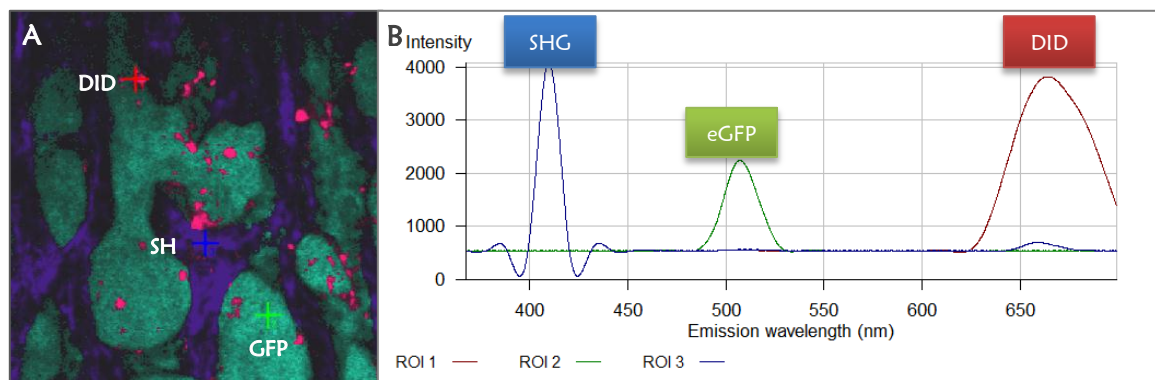


Figure 4.4-11: *In vivo* spectral fingerprinting.

(A) 2D spectral image (256 X 256 pixels) of 5TGM1-eGFP-DID tumour-bearing bone scanned using lambda mode using 820 nm NIR laser. (B) The spectral profiles and emission peaks (e_{max}) of individual wavelengths (λ) emitted from bone, GFP and DID components. Bone emitted at 410 nm which is the second harmonic generation produced when 820 nm NIR laser is split into two individual photons with double the energy and half the wavelength (410 nm). eGFP present inside the cell cytoplasm emitted between 507-510 nm and DID that labels the cell membrane peaked between 675-710 nm.

Results showed that 5TGM1-DID⁺ cells were seen in the BM at all-time points and 5TGM1-eGFP⁺ colonies were seen only from 14 days post tumour cell injection (figure 4.4-12). Therefore quantitative results were expressed as number of 5TGM1-DID⁺ per mm³ of BM and percentage of BM occupied by 5TGM1-eGFP⁺ colonies (volume of 5TGM1-eGFP⁺ colonies/volume of BM). Quantitative analysis showed significant reduction difference in the number of 5TGM1-DID⁺ cells per mm³ of BM after day 10 and day 21 post tumour cell injection when compared with day 3 post tumour cell injection ($P<0.05$; figure 4.4-13 A). 5TGM1-eGFP⁺ tumour colonies appeared in the BM only at day 14 ($1.8 \pm 0.76\%$) with a dramatic increase at day 21 ($47.34 \pm 6.03\%$; figure 4.4-13 B).

In order to study the spatial distribution 5TGM1-DID⁺ cell in the BM over time, minimum distance of all 5TGM1-DID⁺ cell to the nearest bone was measured. This analysis was restricted to 5TGM1-DID⁺ cell and not to 5TGM1-eGFP⁺ tumour colonies, as they were surrounding the trabecular bone and revealed a value '0' for all the 5TGM1-eGFP⁺ colonies. Results showed that the 'minimum distance' of 5TGM1-

DID⁺ cells from the nearest bone were constant and ranged between 42.29 ± 1.58 μm (day 3), 42.75 ± 3.88 μm (day 10) and 42.21 ± 2.55 μm (day 14) followed by a dramatic reduction to 23.53 ± 2.33 μm at day 21 post tumour cell injection (figure 4.4-13 C).

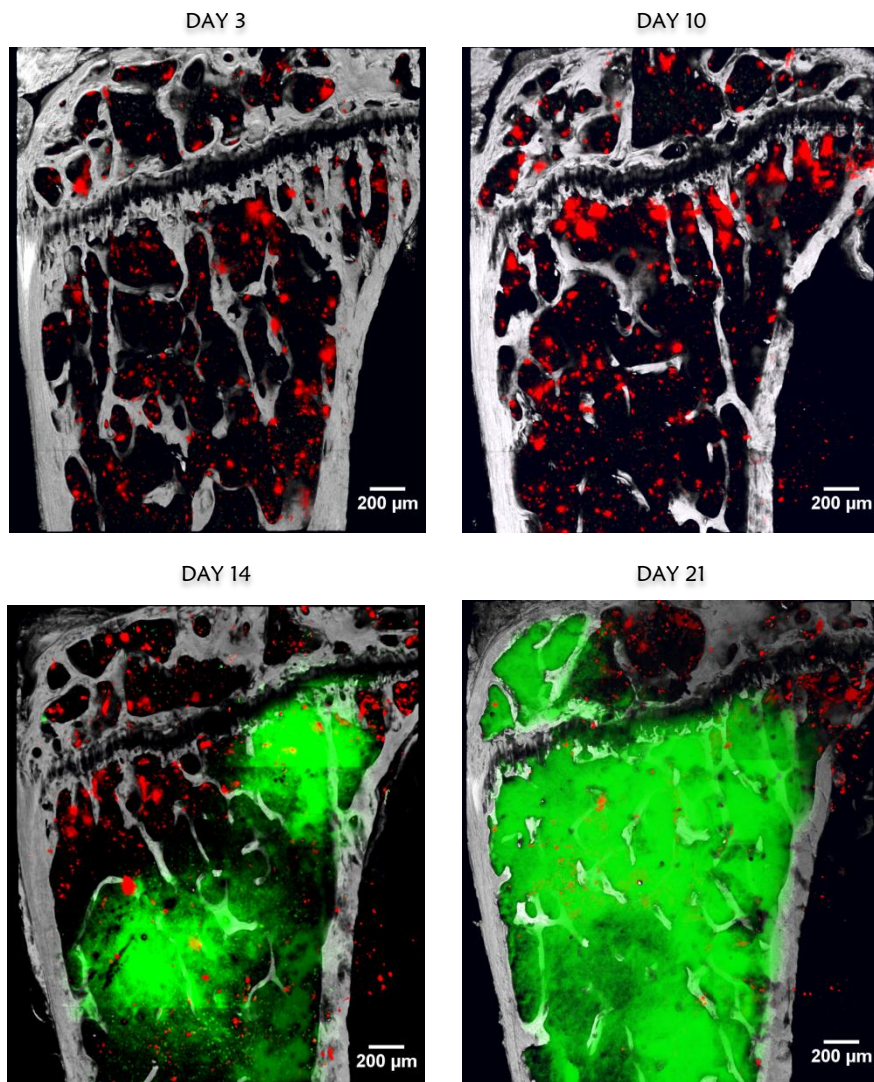


Figure 4.4-12: Multiphoton microscopy images showing the development of 5TGM1-eGFP-DID murine myeloma cells in bone.

Representative examples of 3D cut sections of multiphoton images of tibia following development of myeloma using 5TGM1-eGFP-DID cells after 3, 10, 14 and 21 days post tumour cell injection. Multiphoton microscopy was performed using 820 nm pulsed multiphoton laser in order to visualise bone using second harmonic generation, DID and eGFP signals from the 5TGM1-eGFP-DID cells. Images show the presence of DID labelled 5TGM1 cells (red objects) randomly distributed within the BM. eGFP expressing 5TGM1 myeloma colonies (green) were first observed at day 14 post tumour cell injection which progressively filled the BM at day 21.

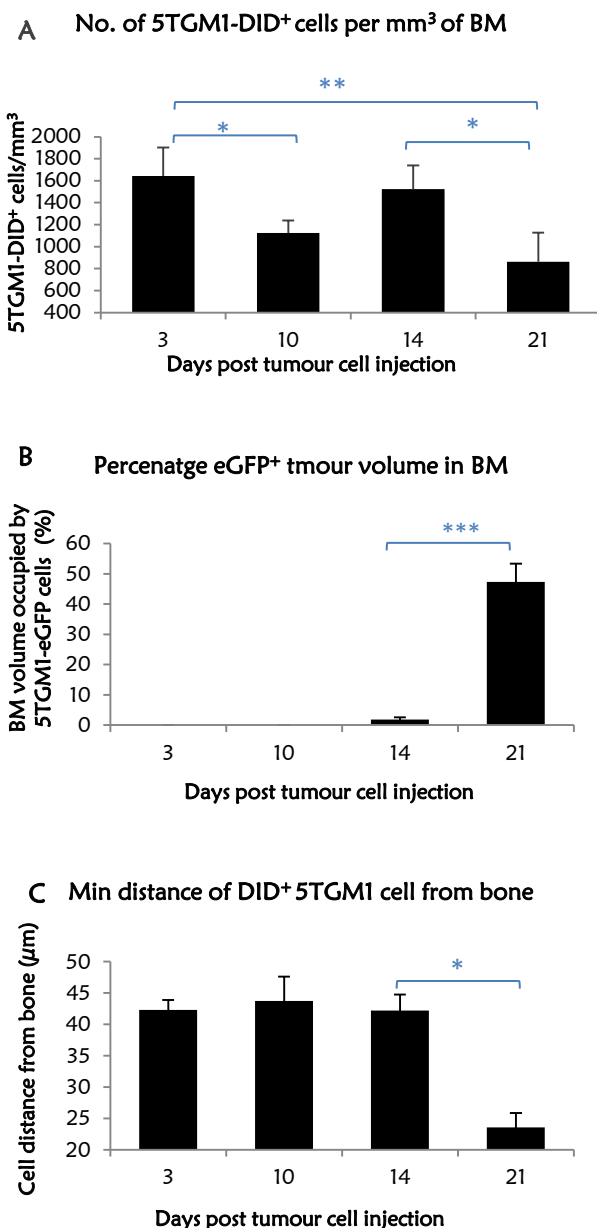


Figure 4.4-13: Quantitative assessment of tumour burden in 5TGM1 murine model of myeloma using multiphoton microscopy.

(A) The number of DID⁺ cells per mm³ of BM, **(B)** percentage BM occupied DID⁺ cell, **(C)** percentage BM space occupied by 5TGM1-eGFP⁺ colonies after 3, 10, 14 and 21 days post tumour cell injection. **(D)** Changes in the average minimum distance of 5TGM1-DID⁺ cell to the nearest bone after 3, 10, 14 and 21 days post tumour cell injection ($n=8$ for day 3, 10 and 14; $n=7$ for day 21). Values represent mean \pm SEM. Mann-Whitney's non-parametric two-tailed test was performed to determine significant differences between time points. * $P<0.05$, ** $P<0.01$, *** $P<0.001$.

4.4.4 THE EFFECT OF MYELOMA DEVELOPMENT ON GROSS MORPHOLOGY

No obvious morphological or clinical signs were observed in 5TGM1-eGFP-DID tumour-bearing mice until the latter stages of disease development when the animals developed unilateral or bilateral hind limb paralysis, generalized signs of morbidity such as hunched-back appearances, lethargy or weight loss. 4 out of 7 5TGM1 tumour-bearing animals developed bilateral hind limb paralysis after 21 days post tumour cell injection. 5TGM1-eGFP-DID myeloma bearing mice lost approximately 10% of body mass when compared with tumour-free control groups and a three-fold increase in the spleen weight and a one-fold increase in the liver weight was observed in the tumour-bearing group by the time they showed signs of morbidity when compared with tumour-free control group (figure 4.4-14).

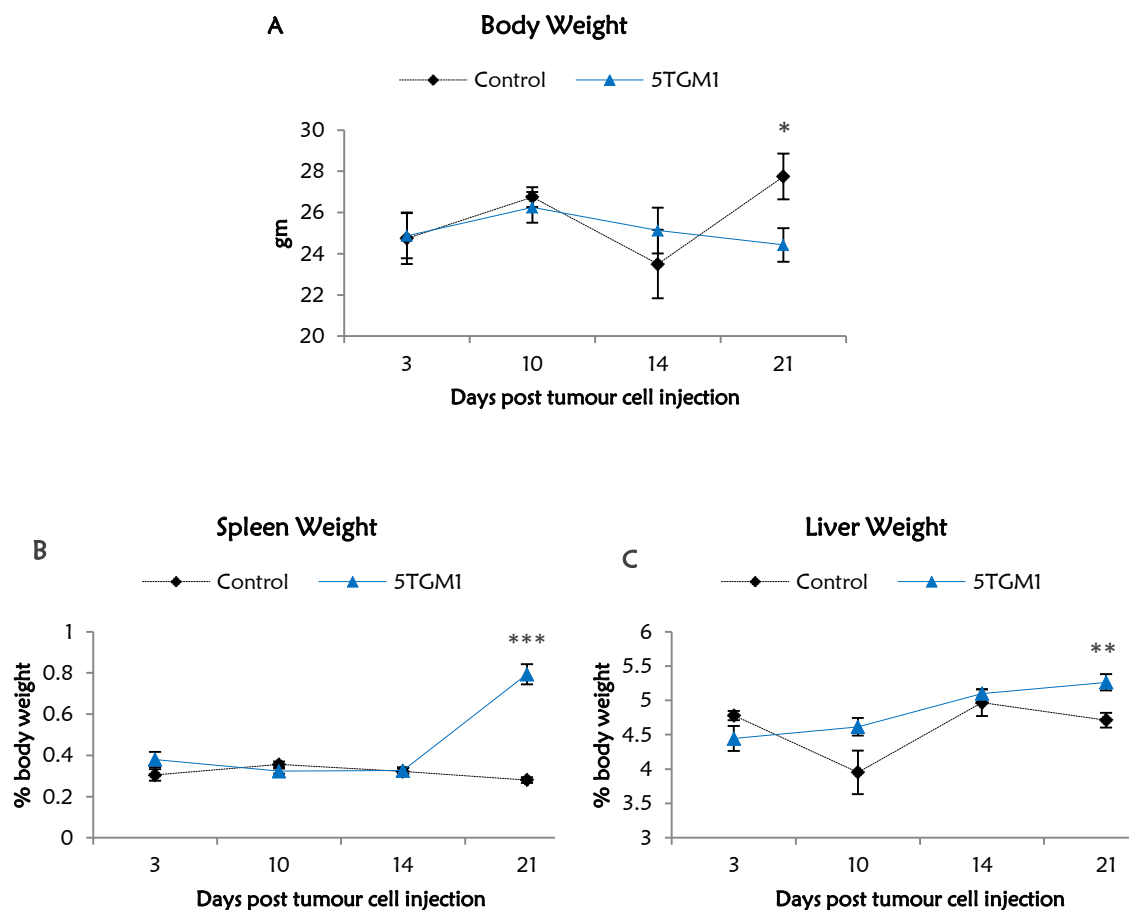


Figure 4.4-14: Effect of 5TGM1 tumour development on gross morphology

Changes in body weight (A), Spleen weight (B) and liver weight (C) following 5TGM1 murine myeloma development when compared with disease-free control animals after 3, 10, 14 and 21 days post 5TGM1-eGFP-DID tumour cell injection (Controls n=4 for all time points; 5TGM1 tumour-bearing groups n=8 for day 3, 10 and 14; n=7 for day 21). Mann-Whitney's non-parametric two-tailed test was performed to determine significant differences between the control and 5TGM1 tumour-bearing groups between each time point. *P<0.05, **P<0.01, ***P<0.001.

4.4.5 THE EFFECT OF MYELOMA DEVELOPMENT ON BONE REMODELLING

Changes in osteoclast and osteoblast numbers during disease progression

In order to understand the effect of myeloma development on the cellular compartments of bone remodelling, a comprehensive quantitative analysis of the osteoclast (Oc) and osteoblast (Ob) distribution in the left tibia by static histomorphometry was performed. Changes in Oc and Ob numbers were analysed both in the endocortical and trabecular regions of the proximal tibial metaphysis. Like the previous chapter, results are expressed as osteoclast and osteoblast index for trabecular region analysis and no. of osteoclast or osteoblast per mm² of endocortical bone for the endocortical region. Results showed no significant change in the osteoclast index but a significant reduction in osteoblast index at day 10 ($P<0.01$) in the trabecular region between the naïve tumour-free (control) group and 5TGM1 myeloma bearing group (figure 4.4-15). However, in the endocortical region, a significant increase in the number of Oc (2.38 ± 0.26 vs. 4.41 ± 0.49 , $P<0.01$) and a significant reduction in the number of Ob only after 14 (16.98 ± 1.9 vs. 11.95 ± 1.67 , $P<0.01$) and 21 days (13.5 ± 0.9 vs. 0.89 ± 0.39 , $P<0.001$) in the 5TGM1 tumour-bearing animals when compared with control mice was observed (figure 4.4-16).

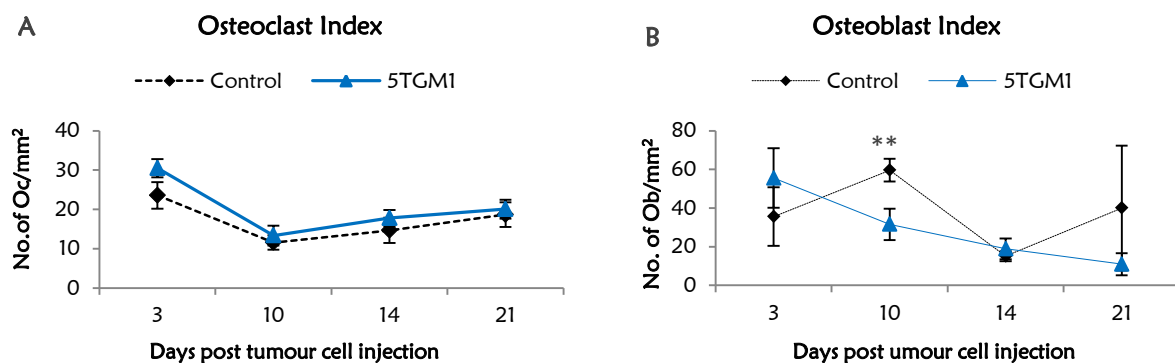


Figure 4.4-15: Trabecular changes in osteoclast and osteoblast numbers following 5TGM1 myeloma development

Changes in osteoclast index (A) and osteoblast index (B) following 5TGM1 tumour cell injection after 3, 10, 14 and 21 days. Age and sex matched tumour-free naïve mice ($n=4$) were used as controls for each time point. The following numbers of mice were used for the 5TGM1 tumour-bearing group for each time point: day 3 $n=8$, day 10 $n=8$, day 14 $n=8$ and day 21 $n=7$. Mann-Whitney's non-parametric two-tailed test was used to determine the statistical significance between controls and tumour-bearing groups. * $P<0.05$, ** $P<0.01$, *** $P<0.001$.

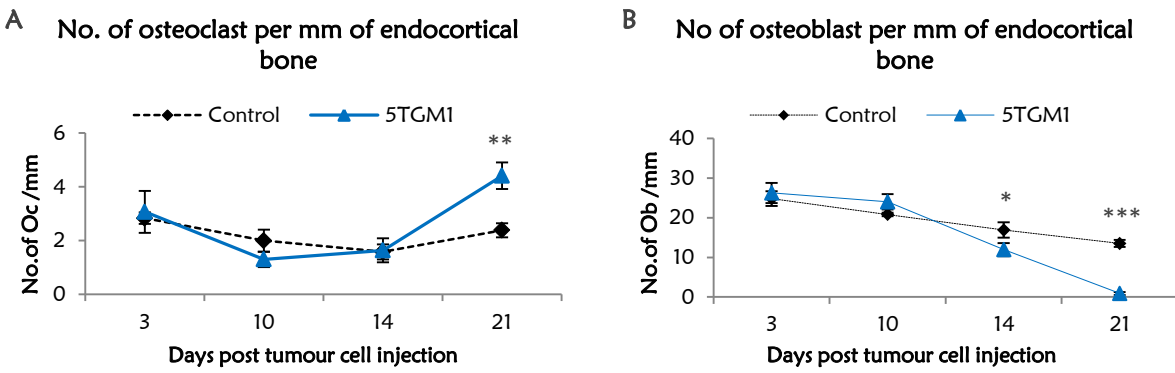


Figure 4.4-16: Endocortical changes in osteoclast and osteoblast number following 5TGM1 myeloma development.

Changes in osteoclast numbers per mm of endocortical bone (**A**) and osteoblast numbers per mm of endocortical bone (**B**) following 5TGM1 tumour cell injection after 3, 10, 14 and 21 days. Age and sex matched tumour-free naïve mice ($n=4$) were used as controls for each time point. The following numbers of mice were used for the 5TGM1 tumour-bearing group for each time point: day 3 $n=8$, day 10 $n=8$, day 14 $n=8$ and day 21 $n=7$. Mann-Whitney's non-parametric two-tailed test was used to determine the statistical significance between controls and tumour-bearing groups. * $P<0.05$, ** $P<0.01$, *** $P<0.001$.

Tumour-induced changes in bone structure and morphology

5TGM1 myeloma associated morphometric changes in long bones (tibia) were studied by micro-computed tomographic analysis of proximal tibial metaphysis. Ct. Vol, % BV/TV, Tb. N and Tb. Th, Tb. Pf and SMI were assessed to study the micro-structural changes in bone following tumour development. Figure 4.4-17 shows representative examples of cross-sectional microCT images of tibia from naïve and 5TGM1 tumour-bearing mice after 3, 10, 14 and 21 days post tumour cell injection. Quantitative microCT analysis showed a significant reduction in Ct. Vol, %BV/TV and Tb. N ($P<0.05$) and significant increase in Tb. Pf and SMI ($P<0.05$) only at 10 day post tumour cell injection when compared with age-matched tumour-free naïve mice. Interestingly, no differences were observed at any other time points (figure 4.4-18).

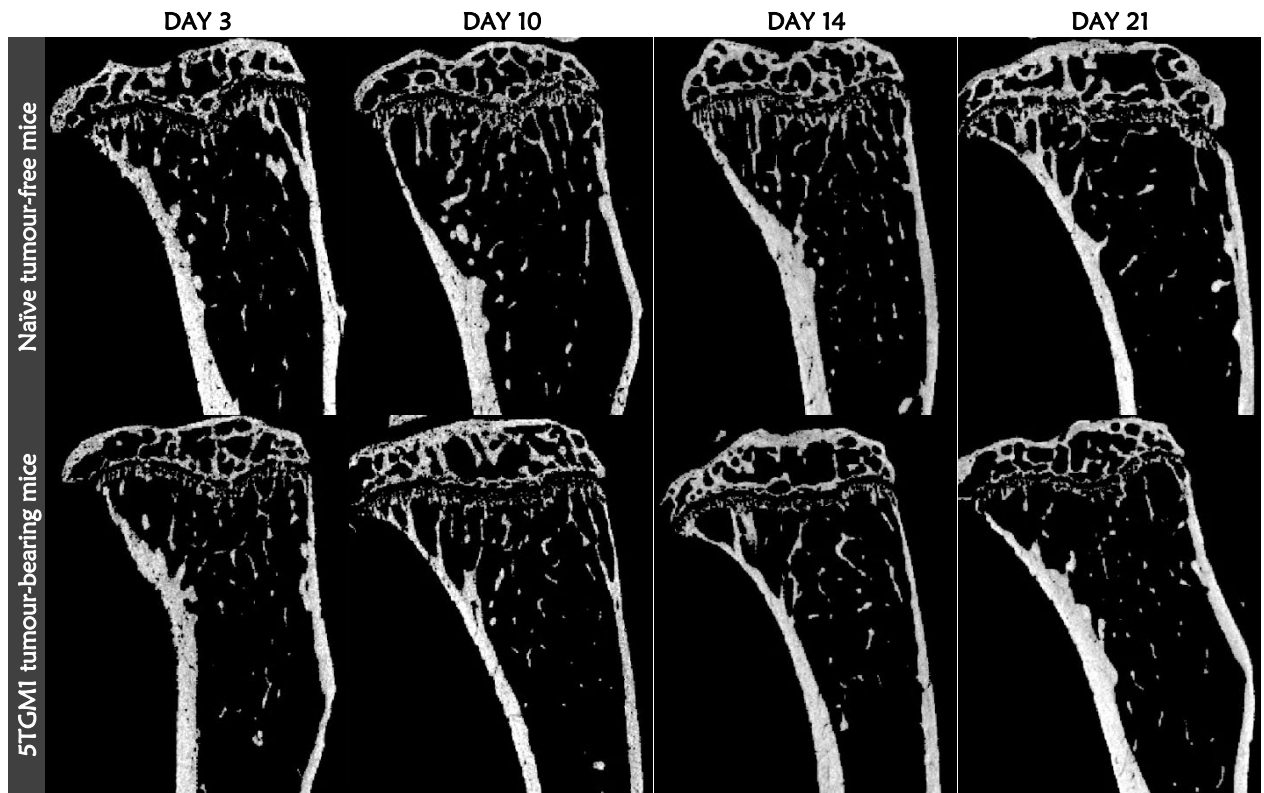


Figure 4.4-17: Structural changes in tibia following 5TGM1 myeloma development over time.

Representative micro-computed tomography cross-sectional images of the L. tibiae showing the proximal tibial metaphysis of both tumour-free control and tumour-bearing 5TGM1 mice after 3, 10, 14 and 21 days post tumour cell injection. No difference in the cortical or trabecular bone was seen between the tumour-free or tumour-bearing mice after all time-points.

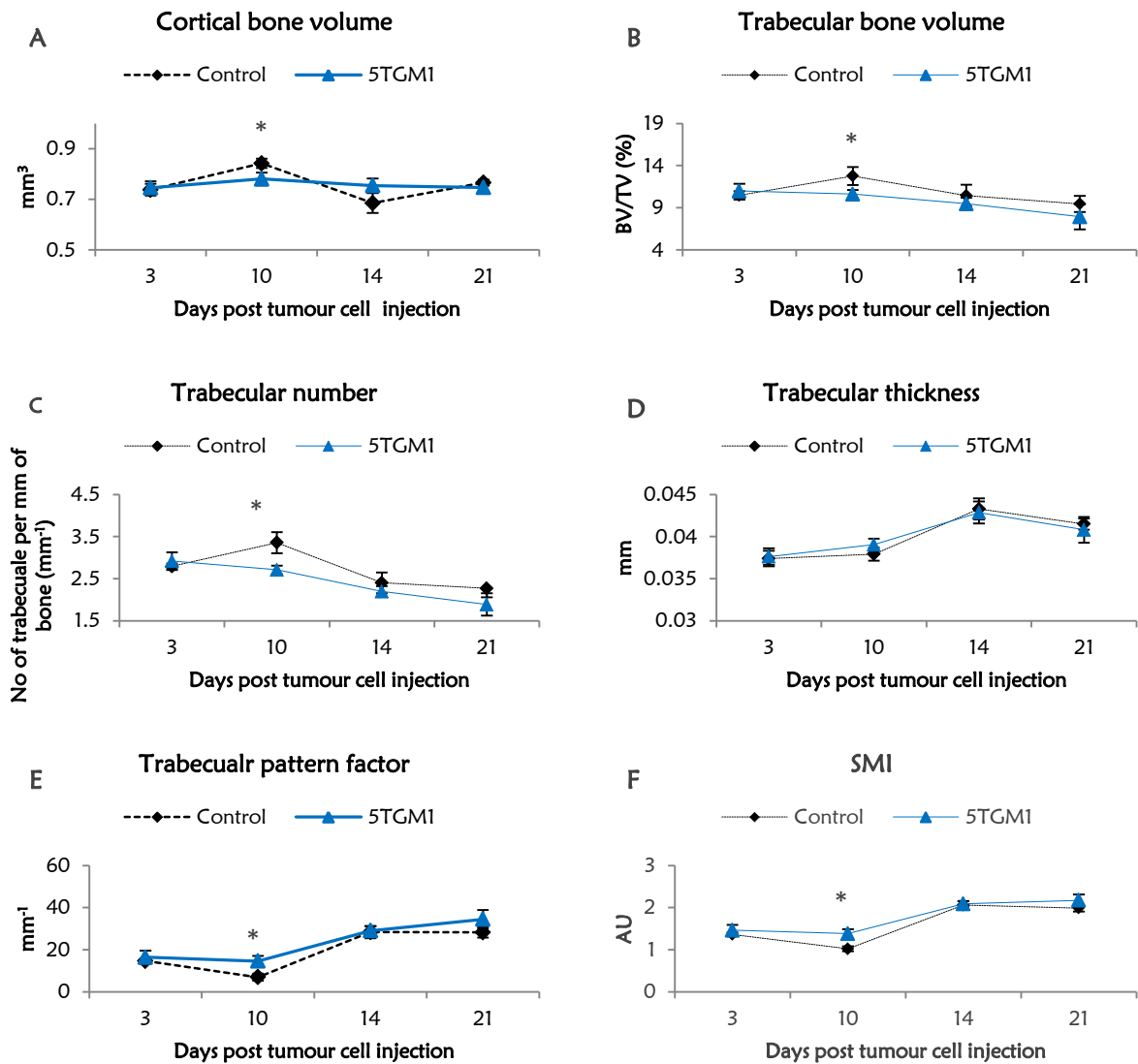


Figure 4.4-18: Quantitative microCT analysis following 5TGM1 murine myeloma development.

Changes in cortical bone volume (A), trabecular bone volume (B), trabecular number (C), trabecular thickness (D), trabecular pattern factor (E) and SMI (F) in the 5TGM1 tumour-bearing mice when compared to tumour-free age matched control animals. Age and sex matched tumour-free naïve mice ($n=4$) were used as controls for each time point. The following numbers of mice were used for the 5TGM1 tumour-bearing group for each time point: day 3 $n=8$, day 10 $n=8$, day 14 $n=8$ and day 21 $n=7$. Non-parametric Mann-Whitney Wilcoxon's test was used to compare the difference between the control and ZA treated groups. * $P<0.05$, ** $P<0.01$, *** $P<0.001$.

Changes in systemic levels of bone turnover markers during disease progression

In order to understand the effect of myeloma development in bone remodelling, systemic levels of bone turnover markers TRACP5b (osteoclastic resorption) and P1NP (osteoblastic formation) were determined by ELISA. Serum levels of TRACP5b showed no significant difference between naïve and 5TGM1 tumour-bearing animals until 14 days post tumour cell injection. However, there was a significant increase in the TRACP5b levels in the tumour-bearing animals at 21 days post tumour cell injection (figure 4.4-19 A). However, serum levels of P1NP showed reduced levels in the 5TGM1 tumour-bearing mice after 3 days ($P<0.05$) and 21 days ($P<0.05$) when compared with naïve tumour-free mice, whereas no difference was observed at 10 and 14 days (figure 4.4-19 B).

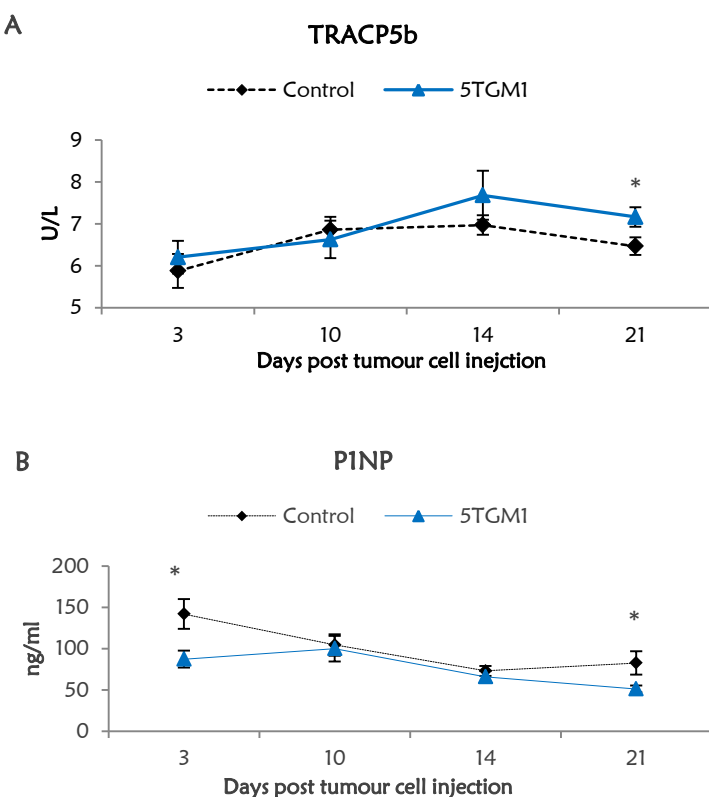


Figure 4.4-19: Changes in systemic bone remodelling markers following 5TGM1 myeloma development.

Changes in serum levels of TRACP5b (A) and P1NP (B) respectively between naïve and 5TGM1 tumour-bearing mice. Age and sex matched tumour-free naïve mice ($n=4$) were used as controls for each time point. The following numbers of mice were used for the 5TGM1 tumour-bearing group for each time point: day 3 $n=8$, day 10 $n=8$, day 14 $n=8$ and day 21 $n=7$. Mann-Whitney's non-parametric one-tailed test was performed to determine significant differences between the control and tumour-bearing groups for each time point. * $P<0.05$, ** $P<0.01$, *** $P<0.001$.

5TGM1 myeloma induces formation of osteolytic bone lesions in the skeleton

Bone lesions were quantified on the posterior and lateral surfaces of the tibia in 2D in both naïve tumour-free and 5TGM1 tumour-bearing mice for all time points ([Materials & Methods section 2.2.19](#)). Figure 4.4-20 shows representative 3D microCT models of proximal tibial metaphysis (posterior surface) of 5TGM1 tumour-bearing mice. Results showed that mice injected with 5TGM1 myeloma cells developed osteolytic bone lesion as early as 10 days post tumour cell injection with a dramatic increase in the percentage bone surface occupied by osteolytic bone lesion observed after 21 days post tumour cell injection ($P<0.05$) (figure 4.4-21 A). A gradual increase in the average size (arbitrary unit) of the observed lesions (cortical holes) in the 5TGM1 tumour-bearing mice when compared with tumour-free control animals was also observed (figure 4.4-21 B; $P<0.05$).

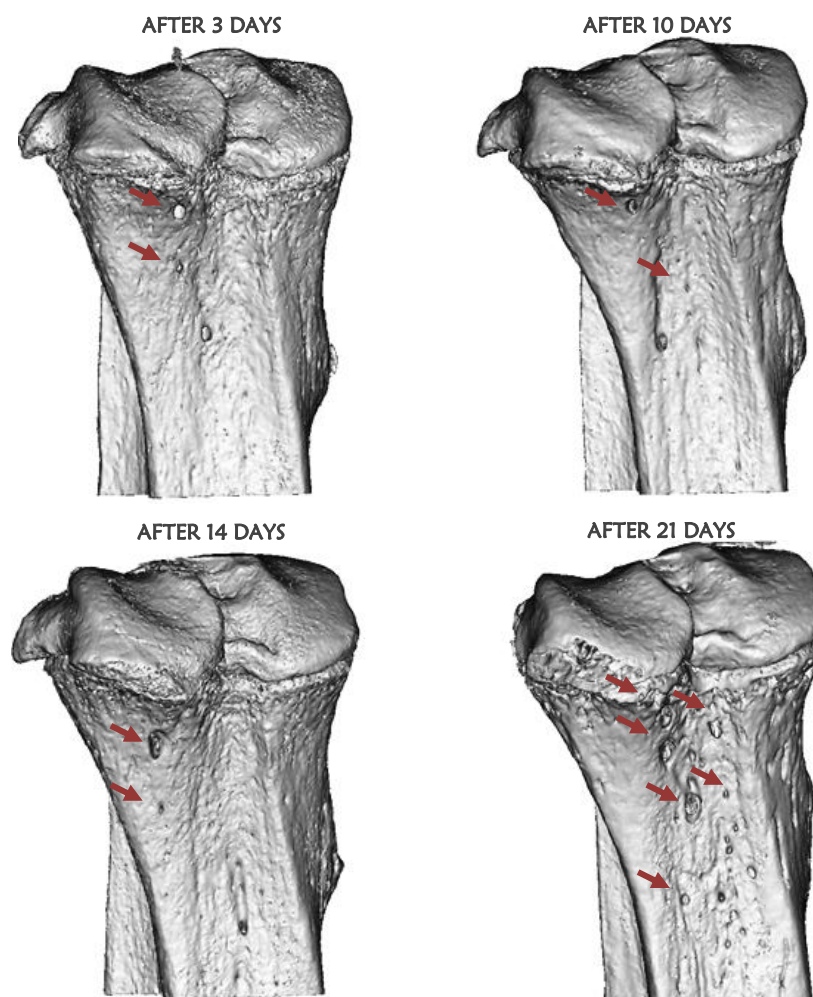


Figure 4.4-20: 5TGM1 myeloma induced development of osteolytic lesions.

Representative 3D models of tibiae showing osteolytic lesion (arrow) in the 5TGM1 tumour-bearing mice after 3, 10, 14 and 21 days post tumour cell injection respectively. Development of osteolytic lesion was observed from 10 days with a dramatic increase in both the percentage bone surface occupied by osteolytic lesions and lesion size at 21 days post injection.

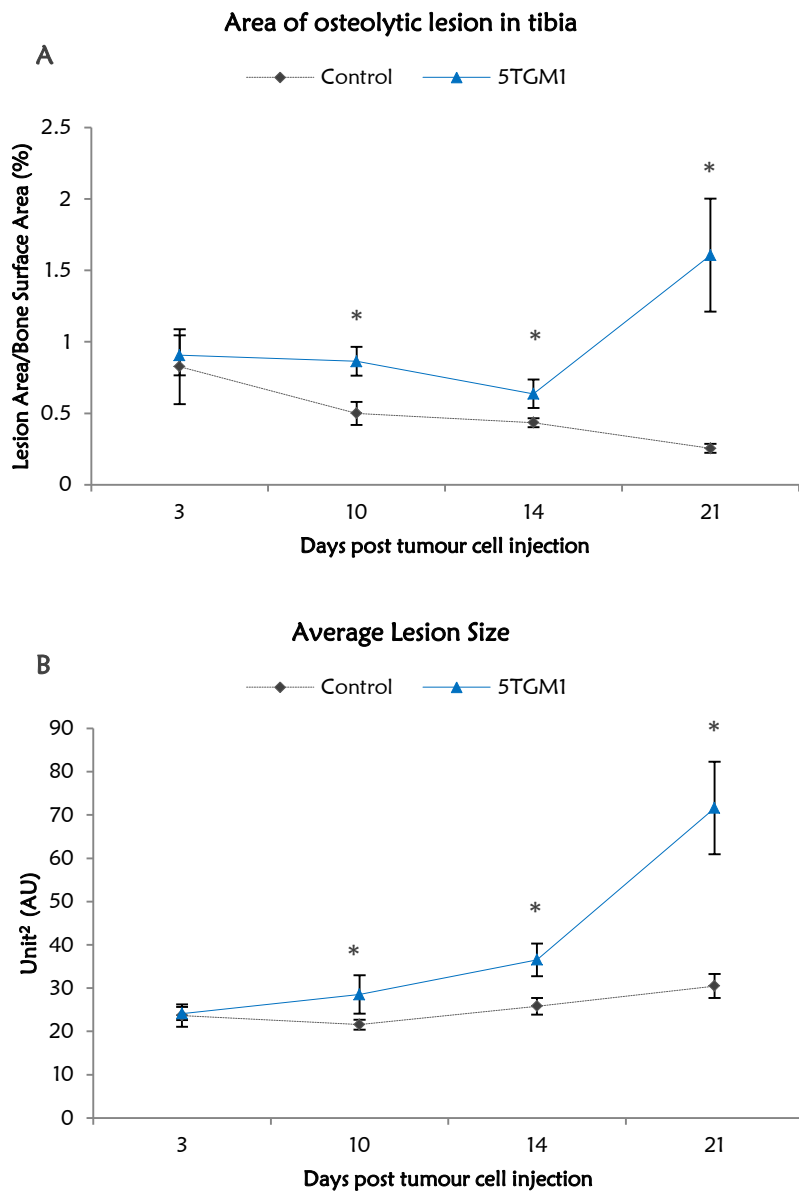


Figure 4.4-21: Quantification of myeloma induced osteolytic bone lesions in the 5TGM1 model over time.

Quantitative image analysis was performed using Image J to quantify the number of lesions (**A**) and average lesion size (**B**) on the posterior and medial cortical surfaces in 3D microCT models of L. tibia. Tumour-free naïve mice were also analysed to determine the base level cortical defects due to normal bone remodelling and vasculature. The following numbers of mice were used for the 5TGM1 tumour-bearing group for each time point: day 3 n=8, day 10 n=8, day 14 n=8 and day 21 n=7. Mann-Whitney's non-parametric two-tailed test was performed to determine significant differences between the control and tumour-bearing groups for each time point. *P<0.05, **P<0.01, ***P<0.001.

4.5 DISCUSSION

Currently, *in vivo* models of myeloma that precisely mimic human disease are needed not only to understand the cellular and molecular events related to the homing of myeloma cells to bone but also to test various anti-cancer treatment strategies. Although the currently available models such as the 5TMM series and the SCID–*hu* model mimic the human disease (Asosingh et al 2000; Tassone et al 2005), the lack of modalities to readily detect tumour cell development during the early stages of disease development in bone has been a limitation for testing newer anti-cancer therapies. In this study, a highly sensitive tumour detection system in bone using three-dimensional multiphoton microscopic imaging, CD138 immunohistochemical staining and flow cytometry in the *in vivo* 5TGM1 murine model of myeloma was developed. The main aim of this chapter was to identify key stages in the development of MM in bone from single cells arriving in the bone to the development of tumour colonies in BM and the accompanied cellular and micro-structural alterations that occur during the concurrent development of osteolytic lesions.

In order to detect 5TGM1 murine myeloma cell in bone using multiphoton microscopy and flow cytometry, 5TGM1-eGFP labelled myeloma cells were used. As eGFP expression by the 5TGM1-eGFP cell could not be detected early on (personal communication with Dr Michelle Anne Lawson, University of Sheffield), the 5TGM1-eGFP cells were further labelled with DID, a far-red lipophilic fluorescent cell membrane dye. Preliminary objectives were focused on determining the effect of DID on 5TGM1-eGFP cell proliferation. From the results, it was clearly shown that DID labelling of 5TGM1-eGFP cells did not affect their proliferation *in vitro*, but DID label was eventually lost during proliferation. At this point, it is important to understand that the 5TGM1 cells were transduced to produce eGFP continuously, whereas DID labels the cell membrane once, at the time labelling. Proliferation of 5TGM1-eGFP-DID cell resulted in non-homogenous distribution of the DID over the cell membrane due to arbitrary sharing of cell membrane between the daughter cells, resulting in progressive loss of DID in cells that are actively proliferating. This posed an important problem as this resulted in underestimation of the actual number 5TGM1-DID⁺ cell as eGFP is not detected *in vivo* during the early stages of tumour development in bone, and assessment of tumour burden during early stages was solely dependent on the number of 5TGM1-DID⁺ cell. Despite gradual loss of DID from the 5TGM1 cell over time, a small number of 5TGM1-DID⁺ cells were seen even after 11 days post labelling suggesting that these cells may be cytokinetically quiescent. Hence this method can be also extended as a surrogate for the identification of non-dividing 5TGM1 cells *in vivo* in bone (Wallace et al 2008).

Data from the current study demonstrated the developmental course of 5TGM1 murine model of myeloma from homing of fluorescently labelled 5TGM1-eGFP-DID myeloma cells from circulation to the establishment of overt colonies in the skeleton. It is well accepted that the 5TGM1 murine model of myeloma mimics the human disease (Asosingh et al 2000; Vanderkerken et al 2003a) with homing of circulating myeloma cells to BM, paraproteinemia, development of osteolytic bone lesion at specific anatomical locations and resulting in typical MM clinical manifestations characterised by hind limb

paralysis. In my experiments, using 2×10^6 5TGM1-eGFP-DID cells injected via the tail vein, myeloma was developed in young C57BL/KaLwRij mice which developed hind limb paralysis approximately 3 weeks following tumour cell injection. Recently, bioluminescence imaging and confocal microscopy are being increasingly used to trace fluorescently tagged tumour cells for monitoring the development of cancer over time and treatment responses (Oyajobi et al 2007; Rozemuller et al 2008; Fryer et al 2013). However, reports from these studies have shown that although eGFP transduction of myeloma cell was successful in tracking the tumour cell, the relatively low expression of eGFP during the early stages of development in the BM has posed a problem for their detection during the early stages of myeloma development. In previous studies, myeloma detection was possible only after established tumour foci using eGFP myeloma cells (Oyajobi et al 2007). Data from the present study confirmed the presence of tumour cells (5TGM1-DID⁺) in bone as early as 3 days post tumour cell injection by flow cytometry, and multiphoton microscopy. Contrastingly, no difference in the number of CD138⁺ cells in BM of the 5TGM1 tumour-bearing mice when compared with tumour-free control groups after 3 days post tumour cell injection, however CD138⁺ colonies appeared in BM from day 10 post tumour cell injections.

Following initial engraftment at day 3, flow cytometry showed a dramatic increase in the percentage 5TGM1-eGFP⁺ cells from day 14 to 21 ($0.86 \pm 0.17\%$ to $29.4 \pm 1.1\%$). This correlated well with the multiphoton microscopy finding which showed an increase in the percentage BM occupied by 5TGM1-eGFP⁺ tumour colonies from day 14 to 21 ($1.8 \pm 0.76\%$ to $47.34 \pm 6.03\%$). CD138 IHC correlated well with the flow cytometry and multiphoton microscopic assessment of tumour burden which demonstrated the presence of CD138⁺ colonies in BM from 10 days but a dramatic increase between 14 and 21 days post tumour cell injection ($6.47 \pm 1.31\%$ to $96.37 \pm 1.18\%$). The main advantage in this model is that flow cytometry and multiphoton microscopy revealed the presence of myeloma cell in BM at early stage (day 3) which was not possible by CD138 IHC. However, CD138 IHC demonstrated the colony formation begins day 10 which was not possible with the other techniques. Although flow cytometry revealed the presence of minimal number of 5TGM1-eGFP⁺ cells in BM from day 10, there was no evidence of single 5TGM1-eGFP⁺ cell or 5TGM1-eGFP⁺ colonies within the BM by multiphoton microscopy. 5TGM1-eGFP⁺ tumour colony formation using multiphoton microscopy could only be demonstrated after day 14 post tumour cell injection. This can be explained by the difference in the techniques involved in these detection systems. In flow cytometry, the BM cells are extracted and processed before subjecting them to analysis. Here single photon laser light are directed to hydrodynamically focussed streamlined liquid which contains the fluorophore labelled myeloma cells and this allows direct unimpeded detection benefits. However, in the multiphoton microscopy system, the multi-photon laser was directed through a thick band of biological BM tissue with heterogeneous refractive index which results in multiple scattering and reduced laser intensity before reaching the focal area (Theer et al 2006; Crosignani et al 2012). Similar results were reported by Oyajobi et al (2007), where eGFP⁺ tumour foci in bone were observed only after 10 days post tumour cell inoculation using bioluminescence imaging. Taken together, the study shows that 3 days post tumour cell injection

myeloma cells could be seen in BM and colony formation begins as early as 10 days post tumour cell injection. Contrary to reports from a previous study by Iriuchishima et al (2012) which showed MM cells engraft adjacent to BM endosteum, no preferential localisation of MM cells was observed and the cells were randomly distributed throughout the BM in the present study.

Although there was a progressive reduction in the 5TGM1-DID⁺ cell over time with a substantial replacement of the entire BM with myeloma colonies, a significant number of 5TGM1-DID⁺ cells ($1.35 \pm 0.16\%$ of the BM cells) were seen even at 21 days post tumour cell injection. From *in vitro* studies, it has already been shown that proliferation of DID labelled 5TGM1-eGFP cells resulted in loss of DID over time. Therefore, the presence of 5TGM1-DID⁺ cells in the BM even after 21 days post tumour cell injection suggests that these 5TGM1-DID⁺ cells may be in a quiescent state. This is particularly important as it shows that not all tumour cells that arrive in bone proliferate to form colonies (Matsui et al 2004). Furthermore, when these quiescent cells are in the presence of other rapidly dividing cells, this suggests that they may represent a MM stem cell or a reserve population that could contribute to the pool of chemo-resistant cells when tumours are subjected to conventional chemotherapy which targets only the rapidly dividing cells (Allan et al 2006). Interestingly, these 5TGM1-DID⁺ cells were located closer to the bone suggesting that specific locations play a role in preserving these cells in quiescent state. Zhang et al (2003) showed that long-term quiescent HSCs are found closer to the trabecular bone surfaces lined especially with spindle-shaped osteoblastic lining cells. This may also indicate that the location and the cellular association may regulate quiescence in these cells.

The present study demonstrates the sequential alteration in the cellular and structural components of the host BM microenvironment during the concurrent course of myeloma development. From the present study, It is clear that the 5TGM1 myeloma induced alterations in the host BM were observed only at the later stages (day 21) of disease development including gross morphological changes such as loss of body weight, liver and splenic infiltration. Analysis of earlier time points (day 3, 10 and 14) revealed no alterations either in the osteoclast numbers or serum TRACP5b levels suggesting that smaller tumour foci do not significantly enhance osteoclastogenesis (Brown 2012). However, increase in osteoclast numbers and serum TRACP5b levels were observed only at later stages (day 21) when the BM was filled with gross tumour colonies. Several studies have shown that myeloma cells promote osteoclastogenesis both *in vitro* and *in vivo* (Roodman 2001). Certain myeloma cell lines have been shown to produce RANKL (Sezer et al 2002; Buckle et al 2012), MIP-1 α (Uneda et al 2003) and MIP-1 β (Abe et al 2002) which induces local activation and osteoclast maturation. Furthermore, myeloma cells via direct cell contact also inhibits stromal cell mediated production of osteoprotogerin (OPG) which in turn promotes osteoclastic bone resorption (Michigami et al 2000). In the present study, significant suppression in serum P1NP levels after 3 and 21 days post 5TGM1 tumour cell injection and a significant reduction in osteoblast numbers after 21 day post tumour cell injection were observed. Several studies have established that MM cell inhibits osteoblastogenesis (Giuliani et al 2006b; Roodman 2011).

Guiliani and colleagues reported that several factors such as Wnt antagonist, Runx2, IL-3 and IL-7 are involved in MM induced suppression of osteoblastogenesis by inhibiting differentiation of MSCs (Giuliani et al 2005; Giuliani et al 2006b). Although the reduction in serum P1NP levels correlated with suppression of osteoblast numbers at 21 days post tumour cell injection, the reason for the transient reduction in serum P1NP levels 3 days post tumour cell injection was not clear (Similar observation was seen by Dr Lawson M A - personal communication). One possible explanation is that, DID dye used to label the 5TGM1 murine myeloma cells may be responsible for the observed effect. However, this is not clear and needs to be investigated further. Furthermore, in the present study, suppression of osteoblasts and activation of osteoclasts following tumour development (day 21) was seen only on the endocortical sites. This suggests a spatial involvement in the disruption of balanced or coupled bone remodelling associated with the tumour growth. Moreover, the relatively smaller tumour foci seen during the early and intermediate time points (day 3, 10 and 14) with no significant alterations in bone remodelling suggests not only a paracrine mechanism but also a spatial dependency associated with myeloma induced changes in bone turnover (Brown 2012; Iriuchishima et al 2012).

It is well known that clinically MM is associated with development of osteolytic bone lesions owing to myeloma-osteoclast interaction aggravating osteoclastogenesis and subsequent osteoclastic bone resorption. Interestingly, in the present study development of osteolytic lesions in the 5TGM1 tumour-bearing mice was seen from day 10 post tumour cell injections despite no significant increase in osteoclast number or serum TRACP5b levels. Results were contrary to reports from breast cancer-induced bone metastasis study where obvious bone remodelling changes were observed prior to the formation of osteolytic bone lesion (Brown 2012). Strikingly, in previous studies changes in reduction in bone volume by microCT were used for measuring osteolytic lesions which may not be sensitive enough to detect cortical defects at early stages: changes in bone volume following micro-structural bone defects might not significantly alter bone volume. Although myeloma development in the 5TGM1 model showed evidence of disrupted bone remodelling only at late stages (day 21) of disease development, cortical defects were seen as early as 10 day post tumour cell injection. This suggests that of myeloma induced bone disease begins even before obvious changes in bone remodelling.

In summary, this is the first study to the best of our knowledge to demonstrate the temporo-spatial relationship of the tumour development in bone in the 5TGM1 murine model of myeloma. Using multiple techniques (flow cytometry, CD138 immunohistochemistry and multiphoton microscopy), myeloma cells were shown to home the BM as early as 3 days post intravenous injection and begin to form colonies 10 days post tumour cell injection. Furthermore, the present study also reports the presence dormant myeloma cells close to bone. Finally, tumour-induced osteolysis was shown to begin at early stages without apparent disruption in bone remodelling.

CHAPTER 5 THE EFFECT OF ZOLEDRONIC ACID TREATMENT ON THE EARLY STAGES OF MYELOMA DEVELOPMENT IN BONE

5.1 INTRODUCTION

ZA has been used in conjunction with standard chemotherapy to prevent bone damage and improve bone health in patients with MM for over 10 years. With emerging evidences from clinical trials and preclinical studies that support additional anti-tumour effects associated with ZA treatment (Croucher et al 2003b; Morgan et al 2010a; Avilés et al 2013) there have been an increasing number of research studies conducted to investigate the mode of action of ZA in this context. Recently, studies have provided evidence that the addition of ZA to standard chemotherapy has improved OS and clinical outcome in early-diagnosed cases of MM (Berenson et al 2006; Avilés et al 2007; Morgan et al 2010c).

Several studies have shown that BPs exert their anti-myeloma potential in various ways. *In vitro* studies have shown ZA have a direct cytotoxic effect on tumour cells inducing apoptosis and inhibiting cell proliferation in several myeloma cell lines (Ural et al 2003; Baulch-Brown et al 2007; Guenther et al 2010). In addition, studies also showed *in vitro* synergistic cytoreductive effects on myeloma cell growth when ZA was combined with simvastatin, dexamethasone and thalidomide (Tassone et al 2000; Ural et al 2003; Schmidmaier et al 2006). Several preclinical studies have also shown that BP treatment was associated with inhibition of tumour burden, osteolytic bone disease and tumour-induced angiogenesis (Croucher et al 2003b; Guenther et al 2010). Moreover studies by Sato et al (2005) and Yuasa et al (2009) have shown ZA treatment also activates V γ 9V δ 2 subset T cells anti-cancer response targeting tumour cells. However, the exact mechanisms that underlie the anti-myeloma effect *in vivo* are not clearly understood. The evolving concept of the myeloma niche and the factors involved in the entry or exit of the tumour cell from the niche are in far the focus of research interest. In particular, osteoclast activity in remodelling bone could disrupt niche structures, releasing tumour cells and initiating the release of tumour promoting factors from bone (Abe et al 2004; Corso et al 2005; Massaia et al 2009).

So far, the anti-myeloma significance of ZA has been related to the end stage myeloma development. No study has focused on interrupting the early events of myeloma cell homing and colonisation in bone. With emerging evidences suggesting that myeloma-osteoclast interdependence ensures myeloma cell survival and growth within the BM, attempting to alter the BM microenvironment with ZA to inhibit osteoclastic resorption prior to myeloma cell arrival in the BM may inhibit the eventual development of growing lesions. In this study, the main aim was to investigate the effect of ZA induced suppression of osteoclastic bone resorption on the early events of homing and colonisation of myeloma cell using the 5TGM1 murine myeloma model. From the previous chapter, it was shown that myeloma-osteoclast interaction begins as early as 10 days post tumour injection, as evidenced by the development of tumour-induced osteolytic bone disease. Therefore, it was hypothesised that blocking bone resorption using ZA will inhibit early tumour cell colonisation and growth in the 5TGM1 murine model of myeloma.

5.2 AIMS & OBJECTIVES

The aims of this chapter were to test whether treatment with ZA initiated prior or after the tumour cell injection will affect the early stages of tumour cell homing and colonisation.

Hypotheses: ZA treatment initiated prior to tumour cell injection will inhibit the colonisation of myeloma cell in bone in the 5TGM1 murine model of myeloma.

The objectives were:-

1. To determine whether treatment of mice with ZA pre or post tumour cell injection significantly inhibits osteoclastic bone resorption.
2. To determine whether ZA treatment initiated pre or post tumour cell injection will prevent the development of MBD.
3. To determine whether ZA treatment initiated pre or post tumour cell injection will inhibit the myeloma cell colonising the bone during the early stages of myeloma development.

5.3 MATERIALS & METHODS

Detailed information on individual techniques performed is given in [Chapter 2: Materials and Methods.](#)

5.3.1 EXPERIMENTAL DESIGN TO STUDY THE EFFECT OF ZA TREATMENT INITIATED PRIOR TO TUMOUR CELL INJECTION ON THE EARLY STAGES OF MYELOMA DEVELOPMENT (PRE-TREATMENT EXPERIMENT)

All animal work and experimental conditions were done in accordance with the local guidelines and with the home office approval under the project licence number PPL No: 40/3462 held by Dr. Colby L Eaton University of Sheffield, UK.

9-12 week old C57BL/KaLwRij mice were randomised, age matched and grouped as shown in figure 5.3-1. All mice were treated with either PBS (n=12) or ZA (n=12) (125 µg/kg subcutaneously twice-weekly) throughout the experiment. 7 days after the initiation of ZA or PBS treatment, animals in groups 3 and 4 were injected with 2×10^6 5TGM1-eGFP-DID labelled cells via the tail vein. All the animals were regularly monitored for signs of illness or the development of hind limb paralysis. In order to study the effect of ZA treatment on the early stages of disease, the mice were sacrificed after 10 days post tumour cell injection. Naïve C57BL/KaLwRij mice treated with PBS (n=4) or ZA (n=4) were used as tumour-free controls. A schematic representation of the study design is given below

All animals were starved 6 hr prior to the sacrifice in order to eliminate the circadian variation in the serum bone biomarkers. Mice were anaesthetised using 0.5 ml/kg of pentobarbitone (intra-peritoneal injection) and blood samples were collected using cardiac puncture.

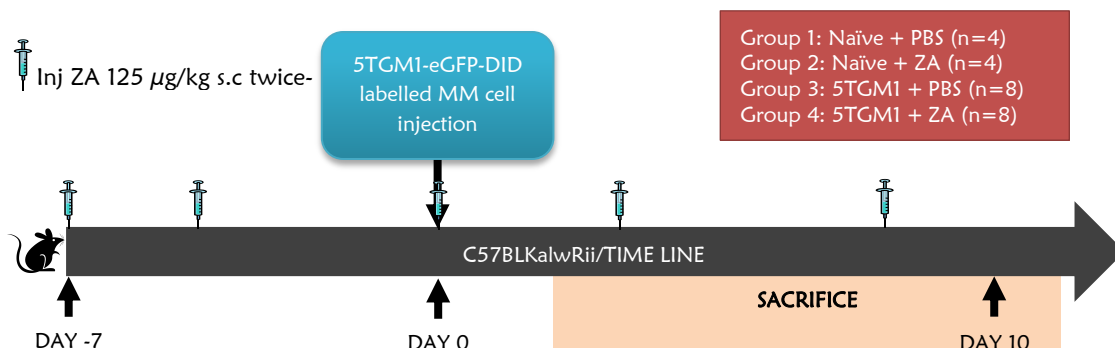


Figure 5.3-1: Experimental design to study the effect of ZA treatment initiated prior to tumour cell injection on the early stages of myeloma.

Mice were age matched, randomised and grouped into those receiving ZA or PBS treatment. ZA treatment was initiated 7 days prior to tumour cell injection. Mice were injected with 125 µg/kg ZA (n=8) or sterile PBS (n=8) subcutaneously twice a week (three days apart) and repeated till the day of sacrifice. Mice were injected with 2×10^6 5TGM1-eGFP-DID cells via the tail vein on Day 0 and sacrificed after 10 days post tumour cell injection. Naïve tumour-free mice injected with PBS (n=4) or ZA (n=4) served as tumour-free controls for each group.

5.3.2 EXPERIMENTAL DESIGN TO STUDY THE EFFECT OF ZA INITIATED AFTER TUMOUR CELL INJECTION ON THE EARLY STAGES OF MYELOMA DEVELOPMENT (POST-TREATMENT EXPERIMENT)

6-9 week old female C57BL/KaLwRij mice were randomised, age matched and grouped as shown in figure 5.3-2. Mice were randomised, age matched and sequentially grouped to receive either PBS ($n=12$) or ZA ($n=13$). 3 days prior to ZA or PBS treatment, group 3 and 4 were injected with 2×10^6 5TGM1-eGFP-DID labelled cells via the tail vein. Animals were injected with either ZA 125 $\mu\text{g}/\text{kg}$ two doses three days apart or PBS every week. Mice were sacrificed after 10 days post tumour cell injection. Naïve C57BL/KaLwRij mice treated with PBS ($n=4$) or ZA ($n=5$) were used as tumour-free controls. On the day of the sacrifice, all animals were starved 6 hr prior to the sacrifice in order to eliminate the circadian variation in the serum bone biomarkers.

Mice were anaesthetised using 0.5 ml/kg of pentobarbitone (intra-peritoneal injection) and blood samples were collected using cardiac puncture. Animals were culled by cervical dislocation while under deep non-recoverable anaesthesia and tissues harvested.

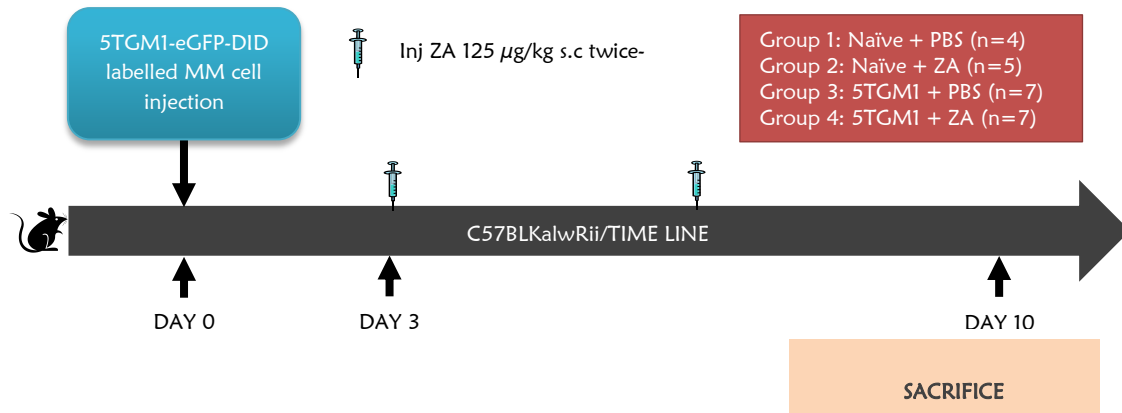


Figure 5.3-2: Experimental design to study the effect of ZA treatment initiated after the tumour cell injection on the early stages of myeloma.

Mice were age matched, randomised and grouped into those receiving ZA or PBS treatment. ZA treatment was initiated 3 days after tumour cell injection. Mice were injected with 125 $\mu\text{g}/\text{kg}$ ZA ($n=7$) or sterile PBS ($n=7$) subcutaneously twice a week (three days apart) and repeated till the day of sacrifice. Mice were injected with 2×10^6 5TGM1-eGFP-DID cells via the tail vein on Day 0 and sacrificed after 10 days post tumour cell injection. Naïve tumour-free mice injected with PBS ($n=4$) or ZA ($n=5$) served as tumour-free controls for each group.

5.4 RESULTS

5.4.1 ZA TREATMENT EITHER PRE OR POST INJECTION OF 5TGM1 MURINE MYELOMA CELLS SIGNIFICANTLY SUPPRESSED BOTH OSTEOCLASTS AND OSTEOBLASTS IN THE 5TGM1 MURINE MODEL OF MYELOMA DURING THE EARLY STAGES OF MYELOMA DEVELOPMENT

The effect of ZA treatment on osteoclast numbers assessed 10 days after injection of 5TGM1 murine myeloma cell

Static histomorphometry was performed to assess the changes in Oc numbers following ZA treatment. Following the ZA pre-treatment strategy, no significant difference in Oc index ($1/\text{mm}^2$) between PBS and ZA treated 5TGM1 tumour-bearing mice was observed. However, a significant increase in the Oc number was seen in the tumour-free group treated with ZA when compared to tumour-free PBS treated controls ($P<0.05$) (figure 5.4-1 A). Moreover, a significant increase ($P<0.05$) in the no. of Oc per mm of endocortical bone surface ($1/\text{mm}$) following ZA treatment in the 5TGM1 tumour-bearing group when compared with PBS treated 5TGM1 tumour-bearing group was seen. However, no difference in the number of Oc per mm of endocortical bone surface was observed between tumour-free naïve mice treated with PBS or ZA (figure 5.4-1 C).

Following the ZA post-treatment experiment, a significant reduction was seen in Oc index in the ZA treated 5TGM1 tumour-bearing group when compared with PBS treated 5TGM1 tumour-bearing mice ($P<0.05$). However, no difference was seen between ZA or PBS treated tumour-free naïve group (figure 5.4-1 B). No difference in the number of Oc per mm of endocortical bone between ZA and PBS treated 5TGM1 tumour-bearing or tumour-free naïve control groups was observed (figure 5.4-1 D).

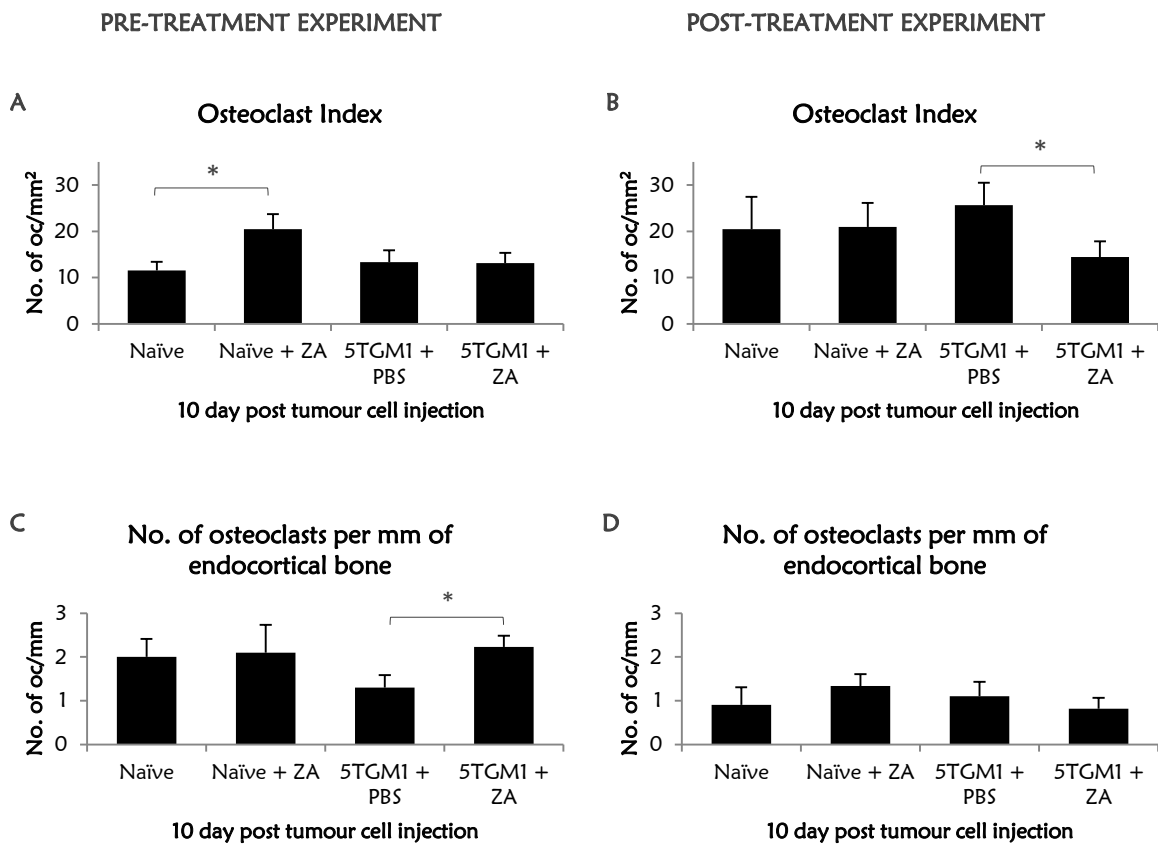


Figure 5.4-1: The effect of ZA treatment on Oc numbers in the 5TGM1 murine model of myeloma 10 days post tumour cell injection.

Changes in Oc index (A) and number of Oc per mm of endocortical bone (C) in 5TGM1 tumour-bearing mice pre-treated for 7 days with ZA (n=8) or PBS (n=8) assessed 10 days post tumour cell injection. Tumour-free mice injected with either PBS (n=4) or ZA (n=4) served as controls. Changes in Oc index (B) and number of Oc per mm of endocortical bone (D) in 5TGM1 tumour-bearing mice post-treated with ZA (n=7) or PBS (n=7) 3 days after tumour injection, assessed 10 days post tumour cell injection. Tumour-free mice injected with either PBS (n=4) or ZA (n=5) served as controls. Comparison was done between PBS or ZA treated groups in both naïve tumour-free and 5TGM1 tumour-bearing groups using a one-tailed ‘non-parametric’ Mann Whitney-Wilcoxon test with P<0.05 as statistically significant. *P<0.05, **P<0.01, ***P<0.001.

The effect of ZA treatment on osteoblast numbers assessed 10 days after injection of 5TGM1 murine myeloma cells

Ob Index (1/mm²) was determined for trabecular region analysis and the number of Ob per mm of endocortical bone surface (1/mm) for endocortical region analysis. Results showed that following pre-treatment with ZA, there was a significant reduction in both Ob index (P<0.01) and number of Ob per mm of endocortical bone (P<0.001) in mice when compared with PBS treated groups in both 5TGM1 tumour-bearing group 10 day post tumour cell injection. A significant reduction in both Ob index (P<0.001) and number of Ob per mm of endocortical bone (P<0.01) in tumour-free mice pre-treated with ZA when compared with PBS treated tumour-free naïve mice was observed (figure 5.4-2 A & C).

Following ZA post-treatment, a significant reduction was observed in both Ob index ($P<0.01$) and number of Ob per mm of endocortical bone ($P<0.01$) in 5TGM1 tumour-bearing mice treated with ZA when compared with PBS treated 5TGM1 tumour-bearing mice 10 day post tumour cell injection. However, when comparing the effect of ZA post-treatment in the tumour-free mice, a significant reduction only in the number of Ob per mm of endocortical bone ($P<0.01$) in the ZA treated group when compared with PBS treated groups was observed. No significant difference was observed in the Ob index between ZA or PBS treated naïve tumour-free mice (figure 5.4-2 B & C).

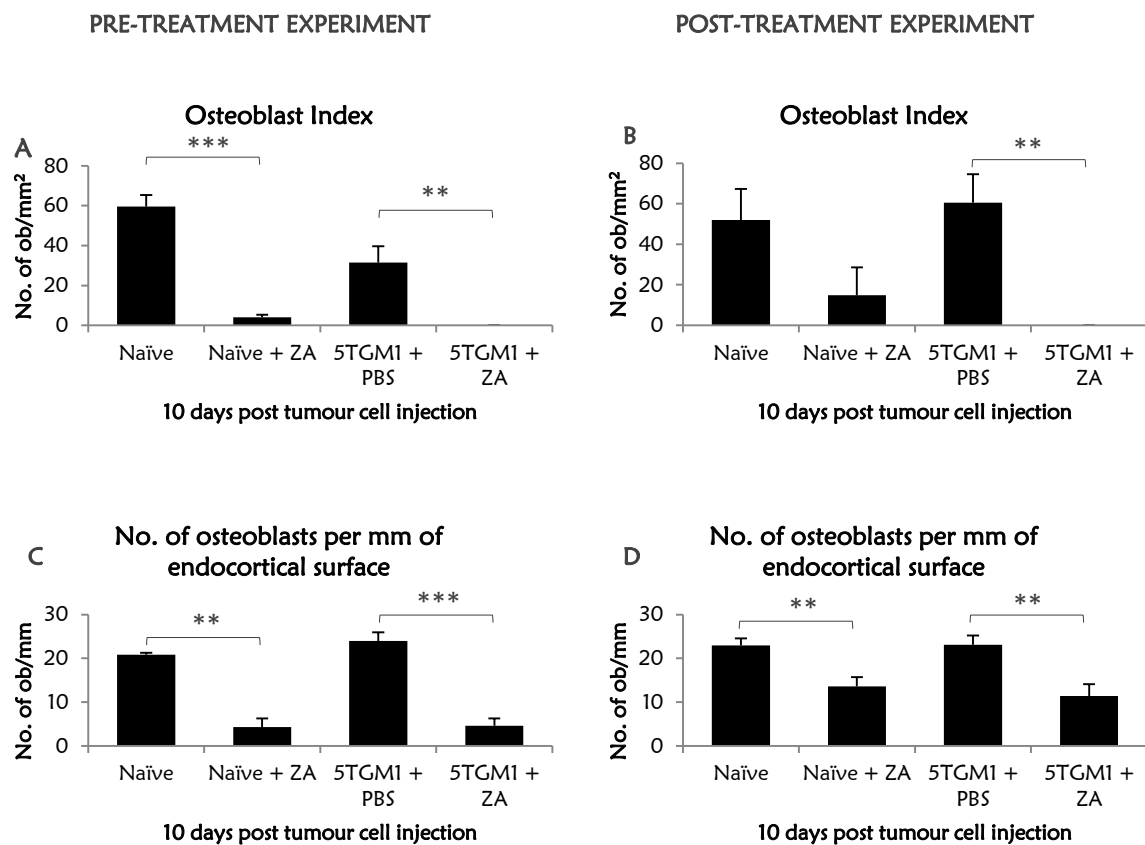


Figure 5.4-2: The effect of ZA treatment on Ob numbers in 5TGM1 murine model of myeloma 10 days post tumour cell injection.

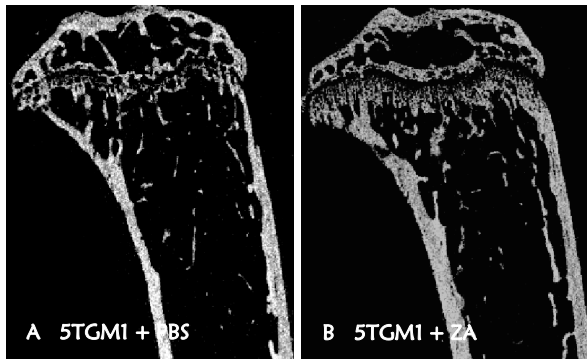
Changes in Ob index (A) and number of Ob per mm of endocortical bone (C) in 5TGM1 tumour-bearing mice pre-treated for 7 days with ZA ($n=8$) or PBS ($n=8$) assessed 10 days post tumour cell injection. Tumour-free mice injected with either PBS ($n=4$) or ZA ($n=4$) served as controls. Changes in Ob index (B) and number of Ob per mm of endocortical bone (D) in 5TGM1 tumour-bearing mice post-treated with ZA ($n=7$) or PBS ($n=7$) 3 days after tumour injection, assessed 10 days post tumour cell injection. Tumour-free mice injected with either PBS ($n=4$) or ZA ($n=5$) served as controls. Comparison was done between PBS or ZA treated groups in both naïve tumour-free and 5TGM1 tumour-bearing groups using a one-tailed ‘non-parametric’ Mann Whitney-Wilcoxon test with $P<0.05$ as statistically significant. * $P<0.05$, ** $P<0.01$, *** $P<0.001$.

Treatment with ZA either pre or post injection of 5TGM1 murine myeloma cells preserved both trabecular and cortical bone volume in 5TGM1 model assessed 10 days post tumour cell injection

Representative microCT images of tibia of 5TGM1 tumour-bearing mice after pre-treatment with PBS or ZA are shown in figure 5.4-3 A & B. Results showed that ZA treatment was initiated prior to 5TGM1 tumour cell injection cells (pre-treatment experiment) there was a significant increase in Ct. V in both 5TGM1 tumour-bearing group ($P<0.001$) and tumour-free naïve control ($P<0.01$) group when compared with PBS treated 5TGM1 tumour-bearing and PBS treated-free control groups. A significant increase in % BV/TV ($P<0.001$) following ZA treatment in the 5TGM1 tumour-bearing animals when compared with PBS treated 5TGM1 mice was also observed (figure 5.4-3 E & G).

Similarly, in mice where ZA treatment was initiated after the 5TGM1 tumour cell injection (post-treatment experiment), a significant increase in Ct. V ($P<0.01$) and % BV/TV ($P<0.01$) was observed when compared with PBS treated 5TGM1 tumour-bearing mice (figure 5.4-3 F and H). Representative micro CT images of tibia of 5TGM1 tumour-bearing mice after post-treatment with ZA or PBS are shown in figure 5.4-3 C and D.

PRE-TREATMENT EXPERIMENT



POST-TREATMENT EXPERIMENT

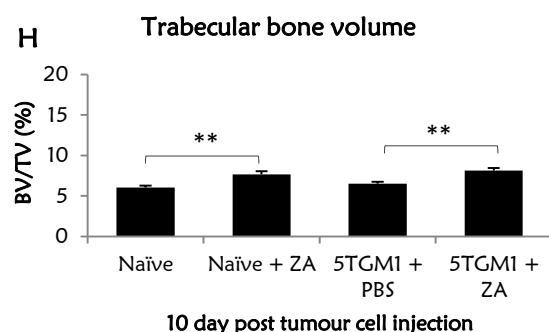
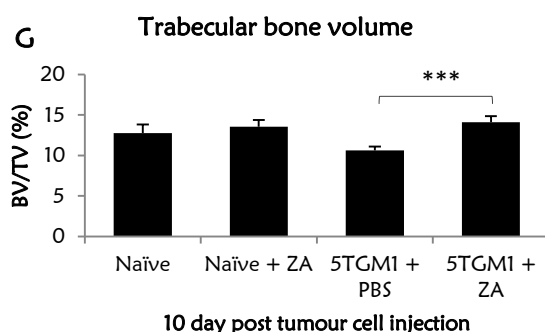
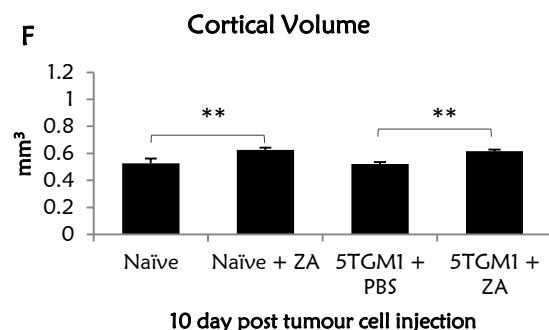
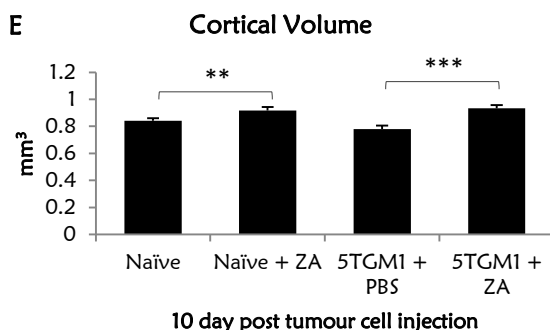
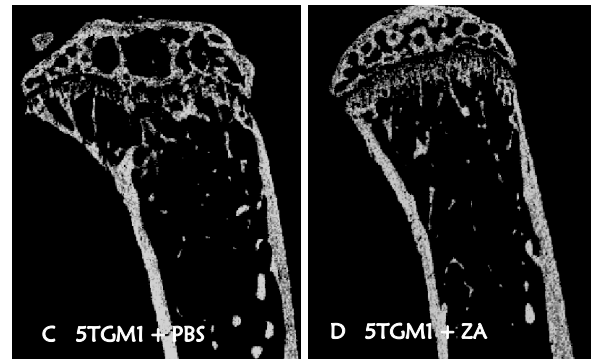


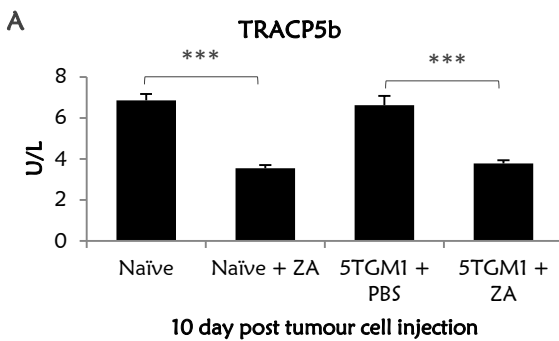
Figure 5.4-3: MicroCT changes following ZA (pre or post) treatment in the 5TGM1 murine model of myeloma assessed 10 days post tumour cell injection.

Representative micro CT longitudinal cross-section images of tibia from 5TGM1 tumour-bearing mice 10 day post tumour cell injection following pre (A, B) and post-treatment (C, D) with ZA or PBS respectively. Changes in Ct. V (E) and % BV/TV (G) in 5TGM1 tumour-bearing mice treatment initiated 7 days prior to tumour cell injection with ZA (n=8) or PBS (n=8) assessed 10 days post tumour cell injection. Tumour-free mice injected with either PBS (n=4) or ZA (n=4) served as controls. Changes in Ct. V (F) and % BV/TV (H) following post ZA treatment where treatment was initiated 3 days after tumour cell injection with ZA (n=7) or PBS (n=7). Tumour-free mice injected with either PBS (n=4) or ZA (n=5) served as controls. Comparison was done between PBS or ZA treated groups in both naïve tumour-free and 5TGM1 tumour-bearing groups using a one-tailed ‘non-parametric’ Mann Whitney-Wilcoxon test with P<0.05 as statistically significant. *P<0.05, **P<0.01, ***P<0.001.

The effect of ZA treatment on serum bone turnover markers assessed 10 days post injection of 5TGM1 murine myeloma cells.

In this study, the serum levels of TRACP5b and P1NP in both ZA and PBS treated 5TGM1 tumour-bearing mice (after 10 days post tumour cell injection) were measured in order to understand the early effects of ZA treatment in the 5TGM1 model. Results showed that ZA treatment (pre or post-treatment experiments) was associated with a significant reduction ($P<0.001$) in serum levels of TRACP5b in both the 5TGM1 tumour-bearing and tumour-free age-matched control mice (figure 5.4-4 A and B). Regarding the serum levels of P1NP in the pre-treatment experiment, no significant reduction in the ZA treated 5TGM1 tumour-bearing mice was seen when compared with PBS treated 5TGM1 tumour-bearing control groups. Interestingly, a significant reduction ($P<0.001$) in P1NP levels were observed in the ZA treated groups when compared to PBS treated age-matched tumour-free control mice (figure 5.4-4 C). However, a significant reduction in serum P1NP levels were observed following ZA treatment (post-treatment experiment) in both 5TGM1 tumour-bearing and age-matched tumour-free control groups when compared with their respective controls ($P<0.001$) (figure 5.4-4 D).

PRE-TREATMENT EXPERIMENT



POST-TREATMENT EXPERIMENT

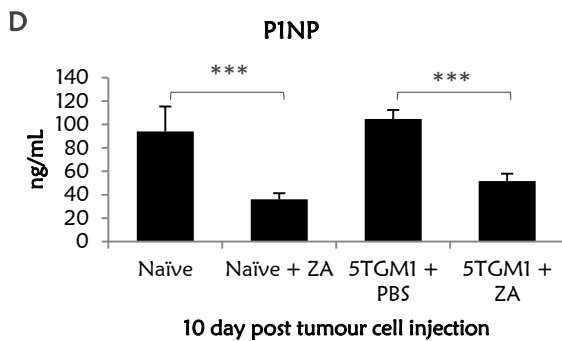
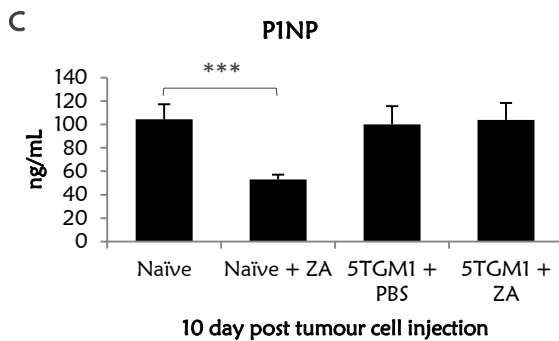
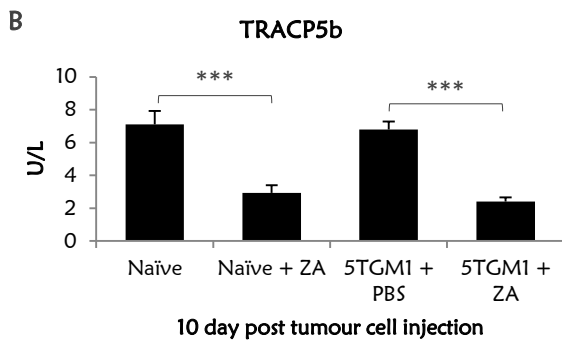


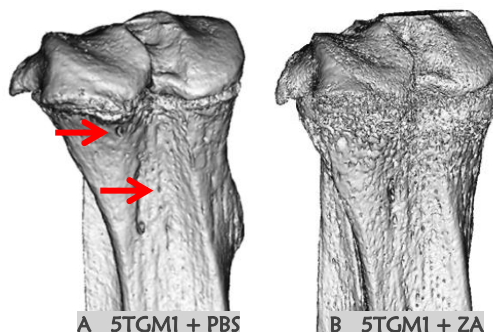
Figure 5.4-4: The effect of ZA treatment on serum TRACP5b and P1NP levels in the 5TGM1 murine model of myeloma 10 days post tumour cell injection.

Changes in serum levels of TRACP5b (**A**) and P1NP (**C**) respectively in 5TGM1 tumour-bearing mice pre-treated with ZA (n=8) or PBS (n=8) assessed 10 days post tumour cell injection. Age matched naïve tumour-free C57BL/KaLwRij mice injected with either PBS (n=4) or ZA (n=4). Changes in serum levels of TRACP5b (**B**) and P1NP (**D**) respectively in 5TGM1 tumour-bearing mice post-treated with ZA (n=7) or PBS (n=7) assessed 10 days post tumour cell injection. Age matched naïve tumour-free C57BL/KaLwRij mice injected with either PBS (n=4) or ZA (n=5). Comparison was done between PBS or ZA treated groups in both naïve tumour-free and 5TGM1 tumour-bearing groups using a one-tailed ‘non-parametric’ Mann Whitney-Wilcoxon test with P<0.05 as statistically significant. *P<0.05, **P<0.01, ***P<0.001.

ZA prevents formation of early osteolytic bone lesions induced by myeloma cell growth, assessed 10 days post tumour cell injection

In order to investigate whether ZA treatment would inhibit the development of osteolytic lesions induced by 5TGM1 myeloma cells in the BM at early time points, the percentage cortical bone surface area (posterior and medial) with cortical defects and number of osteolytic lesions were quantified in both the pre and post-treatment experiments. In the pre-treatment experiment, a significant increase in the percentage of bone surface occupied by lesion ($P<0.01$) and average number of lesions ($P<0.05$) was observed in the 5TGM1 tumour-bearing mice when compared to tumour-free naïve control mice (figure 5.4-5 E and G). With ZA pre-treatment, a significant 74.41% ($P<0.001$) reduction in both percentage lesion area in bone and 53.93% reduction ($P<0.01$) in the average number of lesions was observed when compared to PBS treated 5TGM1 tumour-bearing mice. Interestingly, there was also a significant reduction in the percentage lesion area ($P<0.05$) and average lesion numbers ($P<0.05$) in the ZA treated tumour-free mice when compared with PBS treated tumour-free group. In contrast, in the ZA post-treatment experiment, no significant difference in the percentage lesion area or average lesion numbers was seen in the 5TGM1 tumour-bearing group when compared to tumour-free control group. However, a 69.5% significant reduction ($P<0.001$) was observed in the percentage lesion area and 72.2% reduction in average lesion numbers ($P<0.001$) in the ZA treated 5TGM1 tumour-bearing animals when compared with PBS treated 5TGM1 group (figure 5.4-5 G and H). Representative images showing the posterior surface of the tibia with cortical defects from 5TGM1 tumour-bearing mice with or without ZA pre or post-treatment are shown in figure 5.4-5 A, B, C and D respectively.

PRE-TREATMENT EXPERIMENT



POST-TREATMENT EXPERIMENT

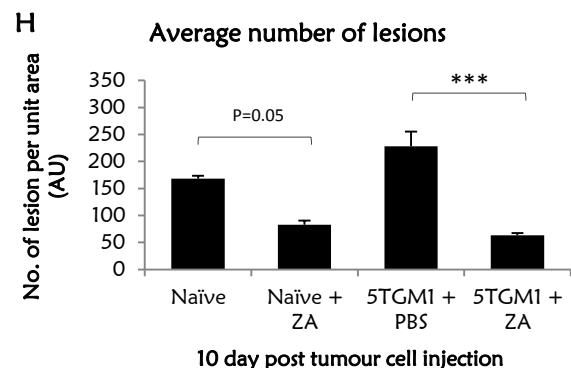
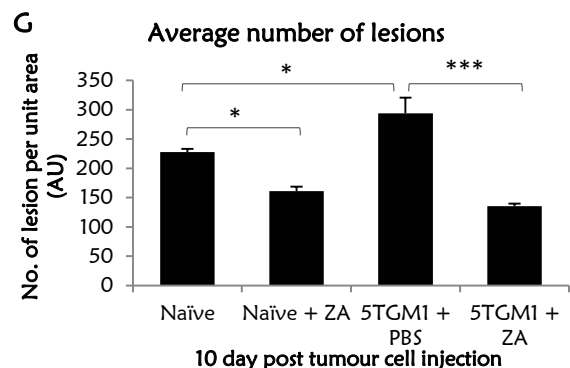
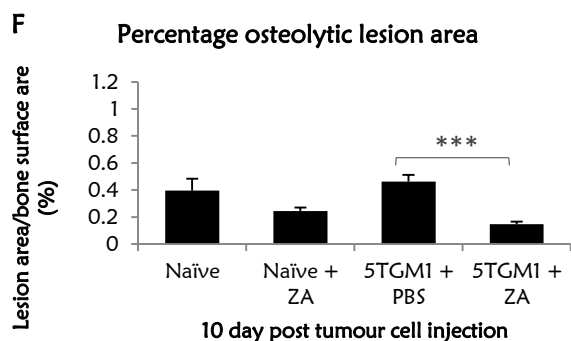
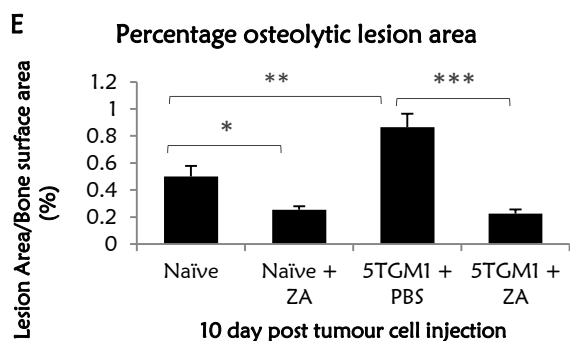
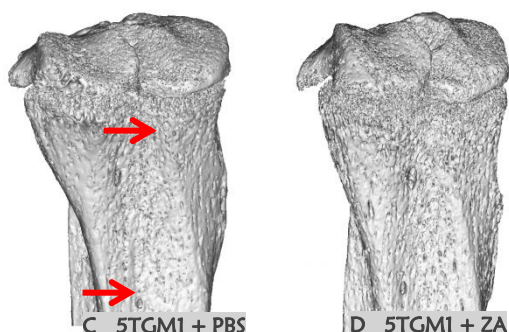


Figure 5.4-5: The effect of ZA treatment on the onset of tumour-induced osteolysis in the 5TGM1 murine model of myeloma.

Representative 3D models of proximal tibial metaphysis of 5TGM1 tumour-bearing mice following PBS or ZA treatment assessed 10 days post tumour cell injection showing osteolytic bone lesion (A), (B), (C) and (D). Osteolytic lesions (cortical defects) are shown in red arrows in the PBS treated 5TGM1 tumour-bearing mice. Changes in percentage osteolytic lesion (E) and average number of lesions (G) in the 5TGM1 tumour-bearing mice pre-treated with ZA ($n=8$) or PBS ($n=8$) assessed 10 days post tumour cell injection. Age matched naïve tumour-free C57BL/KaLwRij mice injected with either PBS ($n=4$) or ZA ($n=4$). Changes in percentage osteolytic lesion (F) and average number of lesions (H) in the 5TGM1 tumour-bearing mice post-treated with ZA ($n=7$) or PBS ($n=7$) assessed 10 days post tumour cell injection. Age matched naïve tumour-free C57BL/KaLwRij mice injected with either PBS ($n=4$) or ZA ($n=5$) served as control. Mann-Whitney non-parametric test was used to compare the statistical difference between the mean in the PBS and the ZA treated groups with P value <0.05 as statistically significant * $P<0.05$, ** $P<0.01$, *** $P<0.001$.

5.4.2 THE EFFECT OF ZA TREATMENT ON TUMOUR BURDEN IN BONE DURING THE EARLY STAGES OF MYELOMA DEVELOPMENT

Flow cytometric analysis revealed no changes in 5TGM1-eGFP-DID cell burden in BM following ZA treatment assessed 10 day post tumour cell injection

From chapter 4, it was shown that 5TGM1-eGFP-DID cells could be identified in the BM as early as 3 days post tumour cell injection using flow cytometry. Therefore, flow cytometry was used to assess the effect of ZA pre or post-treatment on the number of DID⁺, eGFP⁺ and 5TGM1-eGFP-DID⁺ cells in the BM of mice injected. Figure 5.4-6 shows typical flow cytometry profiles of BM cell with 5TGM1-eGFP-DID cells with DID labelling on Y-axis and eGFP labelling on X-axis. BM cells from naïve tumour-free mice were used as negative controls to gate DID⁺ and eGFP⁺ fluorophore channel. Analysis revealed the presence of individual DID⁺, eGFP⁺ and dual labelled DID-eGFP⁺ population in the BM of tumour-bearing mice injected with 5TGM1 cells 10 day post tumour cell injection treated with VEH or ZA. Quantitative flow cytometry analysis showed no significant difference between VEH treated and ZA treated in the percentage DID⁺, eGFP⁺ and dual labelled DID-eGFP⁺ population in the BM (figure 5.4-7 A and B).

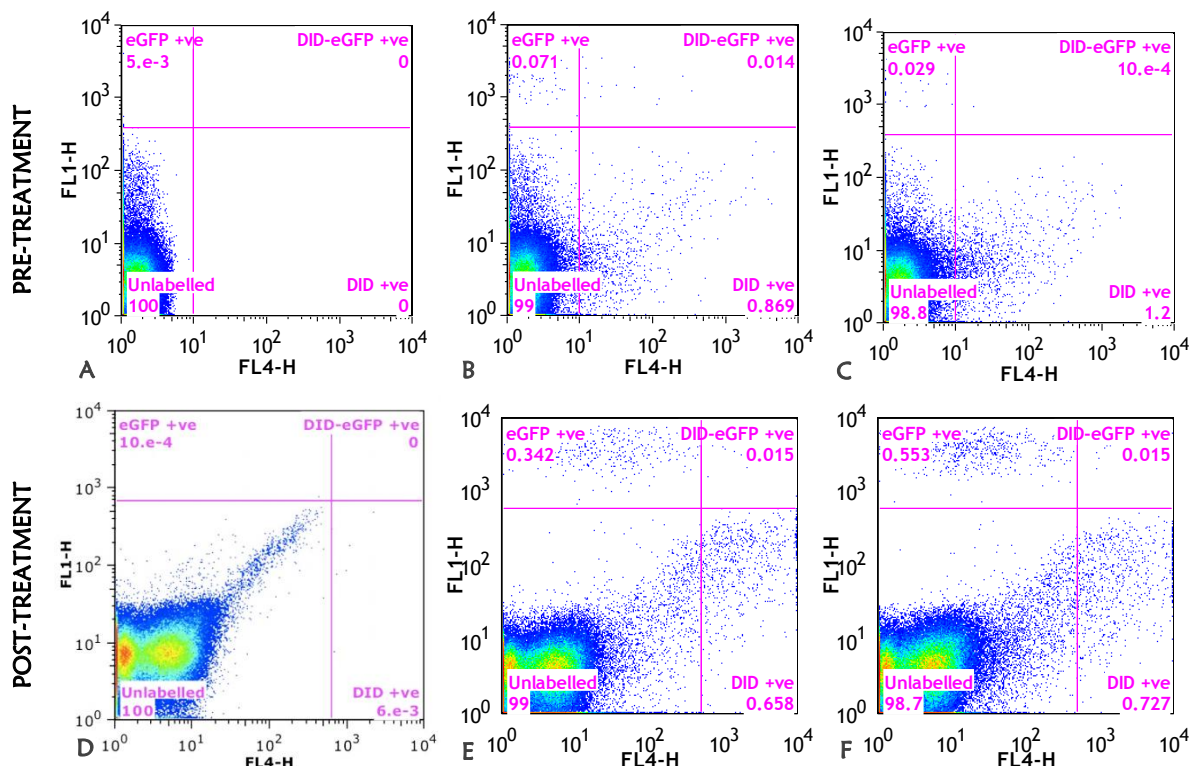


Figure 5.4-6: Flow cytometry profiles of BM cells from naïve C57BL/KaLwRij mice and 5TGM1 tumour-bearing mice treated with VEH or ZA.

Typical flow cytometric profiles of BM cells from mice injected with 5TGM1-eGFP-DID cells after 10 days post injection. BM profile from naïve tumour-free (**A**) and (**D**) mice was used to gate normal cells (negative controls). Profiles from 5TGM1 tumour-bearing mice after pre-treatment with VEH (**B**) or ZA (**C**) with FL1 (eGFP⁺) channel on Y axis and FL4 (DID⁺) channel on X-axis. BM profiles from 5TGM1 tumour-bearing mice after post-treatment with VEH (**E**) or ZA (**F**).

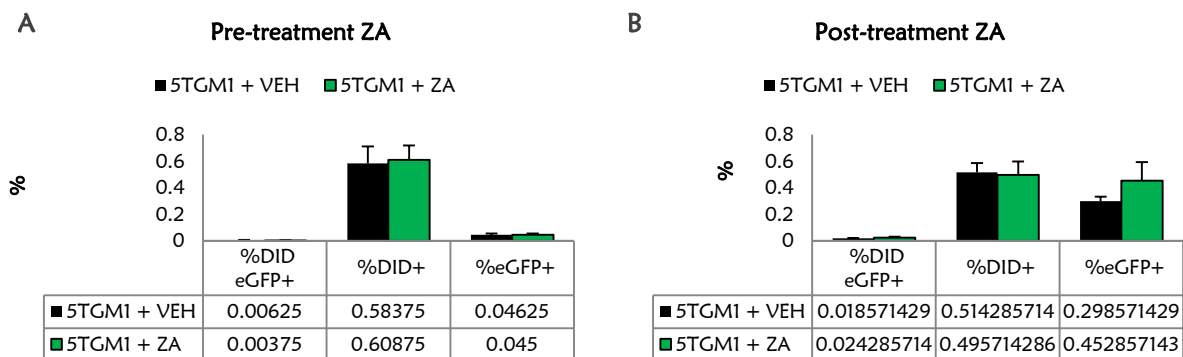


Figure 5.4-7: The effect of ZA treatment on tumour burden in the 5TGM1 model of myeloma assessed 10 days post tumour cell injection.

Flow cytometric analysis of changes in the percentage DID⁺, eGFP⁺ and DID-eGFP⁺ dual labelled 5TGM1 in tumour-bearing mice pre-treated (**A**) with ZA (n=8) or VEH (n=8) assessed 10 days post tumour cell injection. Flow cytometric analysis of changes in the percentage DID⁺, eGFP⁺ and DID-eGFP⁺ dual labelled 5TGM1 in tumour-bearing mice post-treated (**B**) with ZA (n=6) or VEH (n=7) assessed 10 days post tumour cell injection. Comparison was done between VEH or ZA treated groups in 5TGM1 tumour-bearing groups using a ‘non-parametric’ Mann Whitney-Wilcoxon test with P<0.05 as statistically significant. *P<0.05, **P<0.01, ***P<0.001.

ZA treatment showed no significant difference in the CD138 positive population in BM in the 5TGM1 tumour-bearing mice assessed 10 day post tumour cell injection.

Results showed that following pre-treatment with ZA no significant difference was observed in the number of CD138⁺ cells in BM of 5TGM1 tumour cell bearing mice when compared with VEH treated 5TGM1 tumour-bearing mice. Similarly there was no significant difference in the number of CD138⁺ cells in the tumour-free C57BL/KaLwRij mice following VEH or ZA treatment (figure 5.4-8 A). CD138⁺ colonies were expressed as percentage BM area occupied by CD138⁺ colonies. Results showed no significant difference in the percentage BM space occupied by CD138⁺ colonies between VEH and ZA pre-treatment assessed 10 days post tumour cell injection. There was no evidence of CD138⁺ colony formation in naive tumour-free C57BL/KaLwRij mice following VEH or ZA treatment (figure 5.4-8 B). Representative examples of CD138 stained BM from 5TGM1 tumour-bearing mice following VEH or ZA pre-treatment are shown in figure 5.4-9 A and B.

With ZA treatment post tumour cell injection, there was a significant reduction in the number of CD138⁺ tumour cells in the ZA treated tumour-free naïve C57BL/KaLwRij when compared with untreated tumour-free control group. However, no difference in the number of CD138⁺ cells were observed in the 5TGM1 tumour cell group treated with ZA when compared with VEH treated respective control groups (figure 5.4-8 B). Like the pre-treatment experiment, there was no evidence of CD138⁺ colony formation in the tumour-free mice and no significant difference was seen in the percentage BM space occupied by CD138⁺ colonies in the 5TGM1 tumour-bearing mice treated with ZA when compared to VEH treated group (figure 5.4-8 D). Representative examples of CD138 stained BM

from 5TGM1 tumour-bearing mice (10 days post tumour cell injection) following VEH or ZA post-treatment are shown in Figure 5.4-10 A and B.

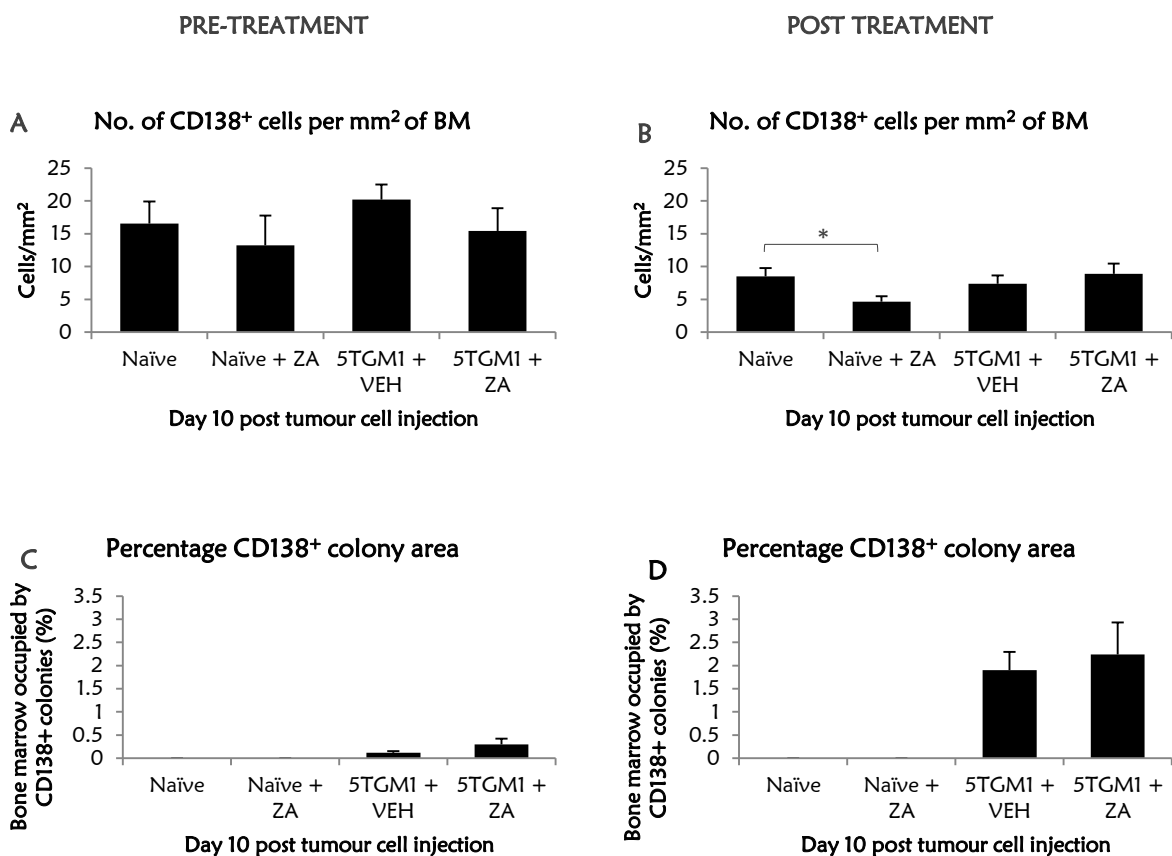


Figure 5.4-8: The effect of ZA treatment on CD138 positive colonies assessed by IHC, 10 days post tumour cell injection.

Changes in CD138⁺ population between 5TGM1 + VEH and 5TGM1 + ZA treated group was expressed as changes in individual number of CD138⁺ population and percentage BM space occupied by CD138⁺ colonies assessed 10 days post tumour cell injection. Changes in the number of CD138⁺ cells (**A**) and percentage CD138⁺ tumour colonies (**C**) in the 5TGM1 tumour-bearing mice pre-treated with ZA (n=8) or VEH (n=8) assessed 10 days post tumour cell injection. Tumour-free mice injected with either VEH (n=4) or ZA (n=4) served as controls. Changes in the number of CD138⁺ cells (**B**) and percentage CD138⁺ tumour colonies (**D**) in the 5TGM1 tumour-bearing mice post treated with ZA (n=7) or VEH (n=7) assessed 10 days post tumour cell injection. Tumour-free mice injected with either VEH (n=4) or ZA (n=5) served as controls. Mann-Whitney non-parametric test was used to compare the statistical difference between the VEH and the ZA treated groups with P value <0.05 as statistically significant *P<0.05, **P<0.01, ***P<0.001.

PRE-TREATMENT ZA STRATEGY

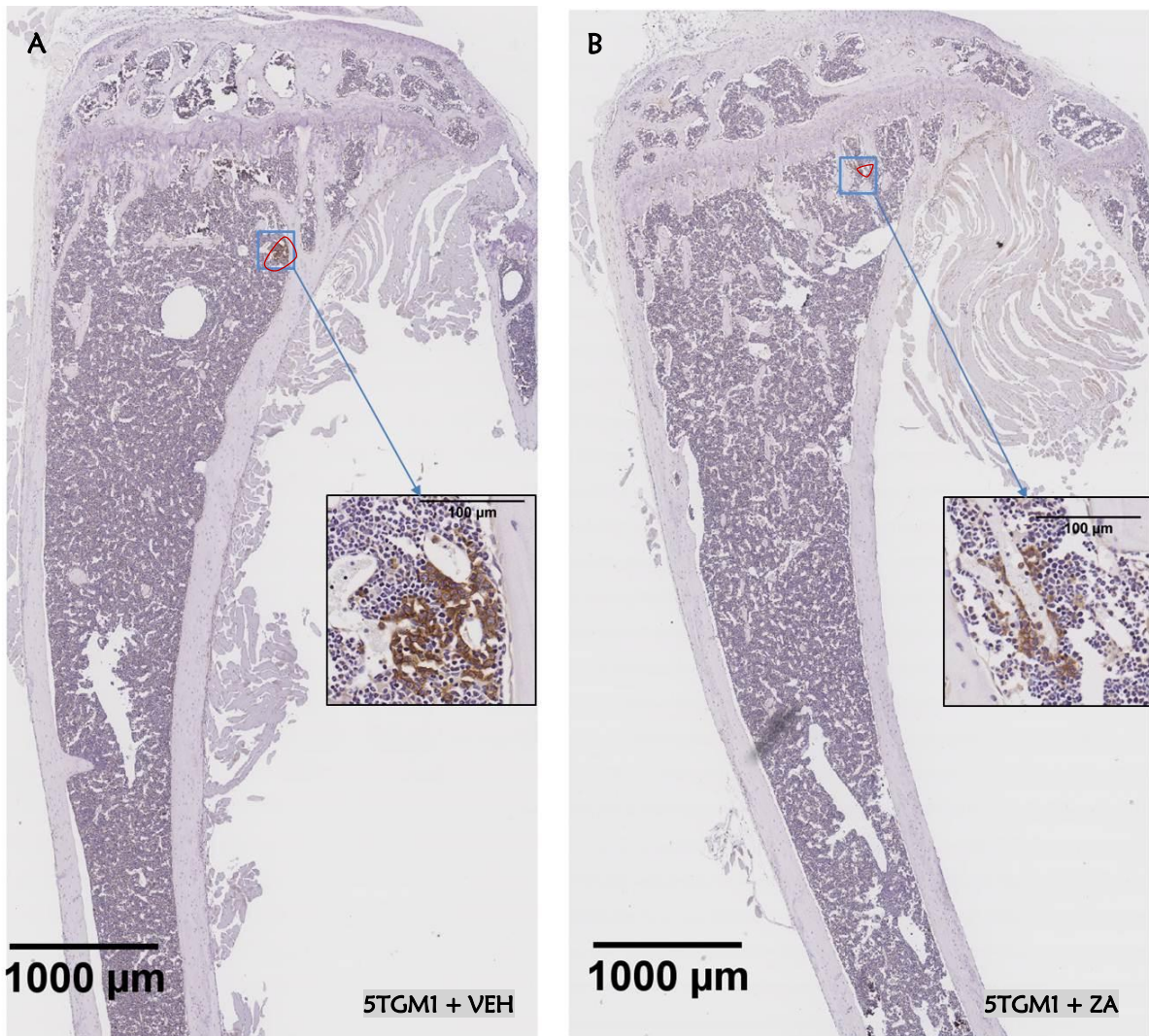


Figure 5.4-9: The effect of ZA pre-treatment on the CD138 positive tumour cell population 10 days post tumour cell injection.

Representative CD138 IHC stained sections of tibiae from mice bearing 5TGM1-eGFP-DID tumour cells (10 day post tumour cell injection) pre-treated with VEH (A) or ZA (B). Images are 2X magnified showing the proximal one third of the tibia (scale bar 1000 μ m) with magnification of CD138 $^{+}$ tumour colonies (inner box, 40X).

POST TREATMENT ZA STRATEGY

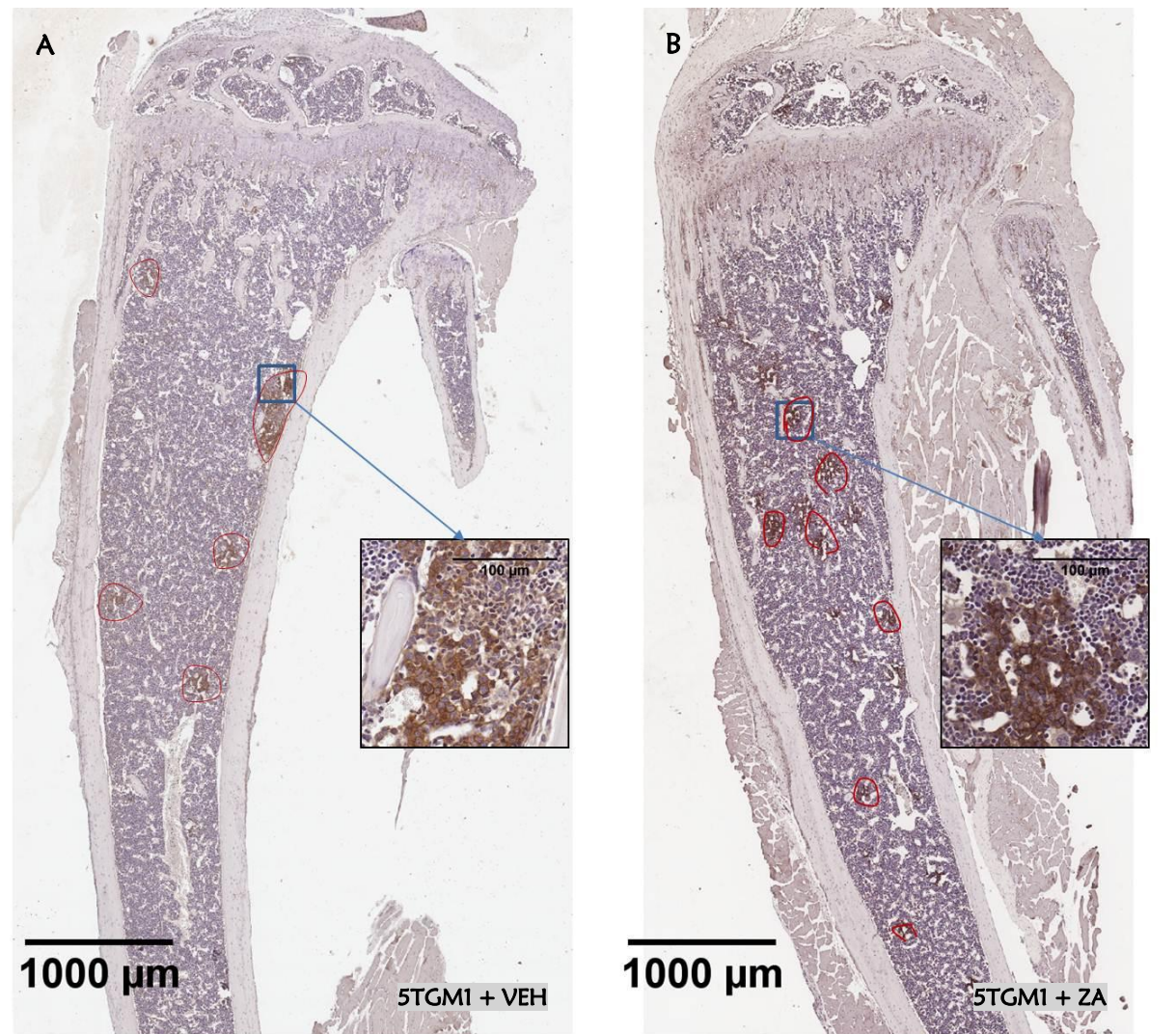


Figure 5.4-10: The effect of ZA post-treatment on the CD138 positive tumour cell population, 10 days post tumour cell injection.

Representative CD138 IHC stained sections of tibiae from mice bearing 5TGM1-eGFP-DID tumour cells (10 day post tumour cell injection) post-treated with VEH (A) or ZA (B). Images are 2X magnified showing the proximal one third of the tibia (scale bar 1000 μ m) with magnification of CD138 $^{+}$ tumour colonies (inner box, 40X).

Treatment with ZA initiated pre or post tumour cell injection showed no significant reduction in 5TGM1-DID⁺ tumour cells, 10 days post tumour cell injection

Multiphoton microscopy was used to quantify the tumour burden in the BM. Bone sections from tumour-free-control (both naïve and naïve + ZA; negative controls) were scanned using multiphoton microscope in order to determine the baseline fluorescence signals from the BM and was used to threshold the baseline bone and DID signals.

From chapter 4, it was clearly shown that only 5TGM1-DID⁺ were visualised in the BM 10 days post tumour cell injection, so, in this experiment the number of 5TGM1-DID⁺ cells was quantified. As expected 5TGM1-DID⁺ cells were clearly seen inside the BM and no evidence of eGFP⁺ signals were observed in both pre or post ZA treatment experiments. Figure 5.4-11 shows representative multiphoton microscopy images of naïve, naïve + ZA, 5TGM1 + VEH and 5TGM1 + ZA.

Representative examples of multiphoton images following pre or post ZA treatment showing the presence of 5TGM1-DID⁺ cells are shown in figure 5.4-12. Results were expressed as mean number of 5TGM1-DID⁺ cells present in mm³ of BM. Results showed that following ZA treatment, there was no significant difference in the number of 5TGM1-DID⁺ cells seen in the BM between VEH and ZA treated 5TGM1 tumour-bearing animals both after pre or post-treatment (figure 5.4-13 A and B).

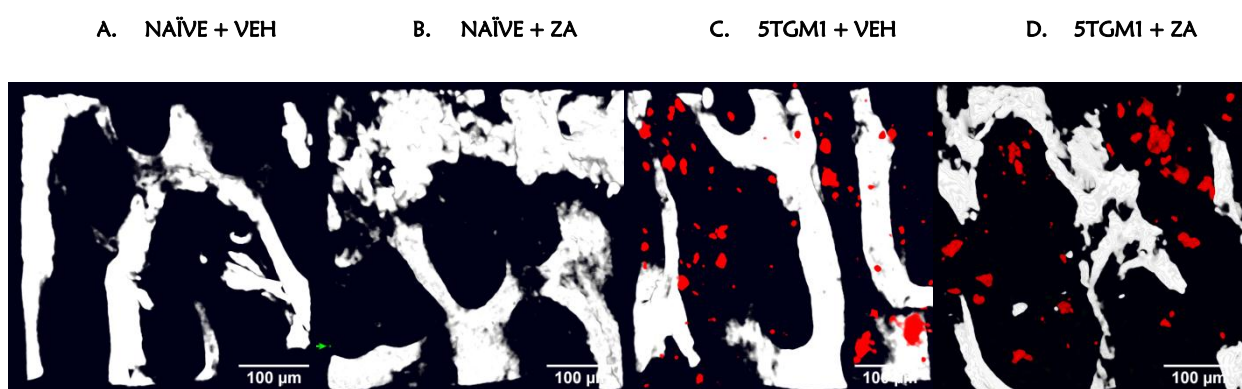


Figure 5.4-11: Representative examples of multiphoton images showing bone and 5TGM1-DID cells assessed 10 days post tumour cell injection.

Representative 2D multiphoton microscopic sections of tibiae (450 X 450 μm^2) of naïve, naïve + ZA, 5TGM1 + VEH and 5TGM1 + ZA showing bone (SHG) and DID⁺ signals, 10 days after 5TGM1-eGFP-DID tumour cell injection. Naïve (tumour-free) (**A**) and Naïve treated with ZA (**B**) were used as negative controls to determine baseline fluorescence of bone in order to threshold the images. (**C**) BM of mice injected with 5TGM1-eGFP-DID tumour cells treated with VEH and (**D**) mice injected with 5TGM1-eGFP-DID treated with ZA shows the presence of DID⁺ (red objects) 5TGM1 tumour cells in the BM.

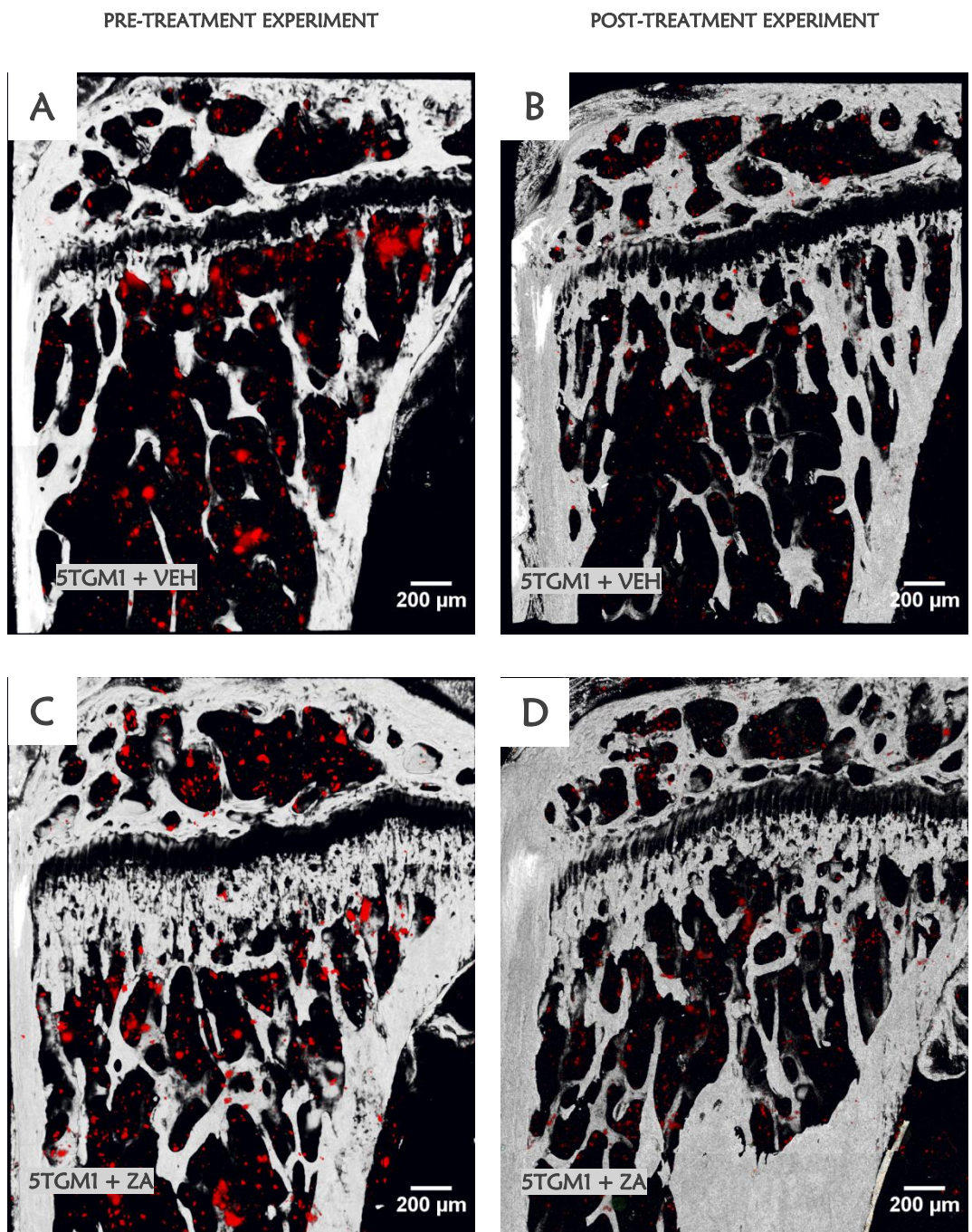
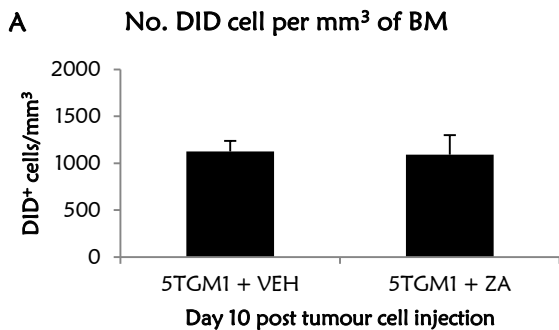


Figure 5.4-12: The effect of ZA pre or post-treatment on 5TGM1 tumour cell colonisation 10 days post tumour cell injection assessed by multiphoton microscopy.

Representative cross-sectional images of proximal metaphysis of tibia captured by multiphoton microscopy showing bone architecture and 5TGM1-DID⁺ cells (red) inside the BM following pre or post-treatment with ZA. Comparison of the effect of ZA (A) or VEH (C) treatment initiated prior to tumour cell injection on tumour load assessed by multiphoton microscopy assessed 10 days post tumour cell injection. Comparison of the effect of ZA (B) or VEH (D) treatment initiated after tumour cell injection assessed after 10 days post tumour cell injection.

PRE-TREATMENT EXPERIMENT



POST-TREATMENT EXPERIMENT

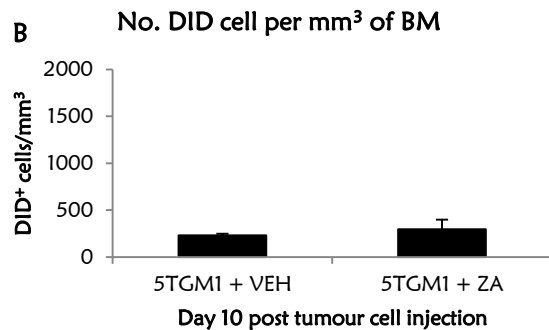


Figure 5.4-13: The effect of ZA on the early stages of myeloma development using multiphoton microscopy.

Changes in number of 5TGM1-DID⁺ per mm³ of BM (**A**) in the tumour-bearing mice pre-treated with ZA (n=8) or VEH (n=8) assessed 10 days post tumour cell injection. Changes in number of 5TGM1-DID⁺ per mm³ of BM (**B**) in the tumour-bearing mice post-treated with ZA (n=7) or VEH (n=7) assessed 10 days post tumour cell injection. A Mann-Whitney non-parametric test was used to compare the statistical difference between the mean in the VEH and the ZA treated groups with P value <0.05 as statistically significant *P<0.05, **P<0.01, ***P<0.001.

5.5 DISCUSSION

Studies on anti-myeloma therapeutics often neglect to focus the effect of chemotherapy on the early stage of disease development due to lack of sensitive methods to detect subtle changes following treatment. There is increasing evidence supporting the concept of the myeloma niche in the BM microenvironment playing a vital role in the development of myeloma. Targeting homing of tumour cells to bone by modification of the BM microenvironment during the early stages of disease diagnosis might offer alternative therapeutic strategies to those currently available which focus only on established disease.

To the best of my knowledge, this is the first study to show the effect of ZA treatment on the early events of tumour cell homing and colonisation in MM. In this chapter, the effect of ZA treatment on bone remodelling during myeloma development, development of osteolytic bone disease and tumour colonisation in the 5TGM1 murine myeloma model was tested 10 days after the tumour cell injection. In this study, ZA was administered in two different treatment strategies. In the first experiment, ZA treatment was initiated before tumour cell injection with a view that prior suppression of osteoclastic bone resorption would interfere with the homing and colonisation of the tumour cells to bone. In the second experiment a post-treatment strategy was used where ZA treatment was started after the tumour cells have homed to the BM.

Data from the present study shows that ZA treatment effectively suppresses osteoclastic bone resorption and osteoblastic bone formation irrespective of whether treatment was initiated prior to or after tumour cells had homed to bone. The study also provides strong evidence that both treatment strategies resulted in suppression of bone remodelling in a manner similar to tumour-free animals suggesting that the presence of tumour cells in bone did not alter the effects of ZA on bone remodelling. However, certain differences were observed between the two experiments. For example, following the pre-treatment of animals with ZA showed a significant increase in osteoclast number on the endocortical surface while in the ZA post-treatment experiment a significant decrease in osteoclast numbers was seen on the trabecular region. This difference may be due to the different age groups of mice used in the two studies. Furthermore, data on osteoclast numbers were quite varied even when compared with the tumour-free control mice. Secondly, in the pre-treatment experiment, no difference was seen in the P1NP levels of the 5TGM1 tumour-bearing mice following ZA treatment, whereas in the post-treatment experiment, prompt reduction was observed. This is particularly interesting because the P1NP levels in the 5TGM1 tumour-bearing mice following pre-treatment with ZA remained normal despite reduction in osteoblast numbers. The cause for this effect seen only in the pre-treatment and not in the post-treatment experiment is not known. In chapter 4, it is clearly shown that the presence of tumour cells in bone 10 days after tumour induction did not alter the indices of bone remodelling, which suggests smaller tumour foci during the early stages of myeloma development do not profoundly alter bone remodelling. Therefore, it is not surprising to see that ZA treatment initiated

before or after tumour cell injection showed similar suppression of bone remodelling because at the time of evaluation the presence of tumour cells in the BM did not affect the bone remodelling.

The effect of ZA treatment was tested on the development of myeloma-induced osteolytic lesion. According to the American Society Of Clinical Oncology (ASOC), induction of BP treatment in MM should commence only with the detection of lytic bone lesion on plain radiograph or evidence of spinal cord compression using imaging modalities (Kyle et al 2007). Moreover, several preclinical studies have also shown that cancer-induced osteolytic lesions were observed only during the late stages of disease development using x-ray radiography techniques. Data from chapter 4 showed that the development of osteolytic bone lesions commences as early as 10 days post tumour cell injection albeit with no significant changes in bone remodelling markers such as serum levels of bone turnover markers or changes in osteoclast or osteoblast numbers. Results from the present study showed that ZA significantly prevented the development of myeloma-induced osteolytic lesions and was independent of whether the treatment was initiated before or after tumour cell injection. Similar results were reported by Croucher et al (2003b) in the 5T2MM model where ZA treatment initiated at the time of tumour cell injection resulted in a complete protection against MBD, however when the treatment was initiated at the time of serum paraprotein detection it resulted only in partial protection. In their study the effect was tested on the late stages of disease where they showed increase in osteoclast number and suggested that this was responsible for lesion formation. In a recent clinical trial, Musto et al (2008) reported that ZA treatment in patients with asymptomatic myeloma resulted in significant reduction in skeletal related events at the time of progression. Interestingly, in the present study ZA treatment showed a significant reduction in the normal cortical pores in tumour-free naïve C57BL/KaLwRij mice. Compston et al (2011) showed that cortical bone morphology in humans with advancing age is associated with an increase in cortical porosity. This suggests that ZA treatment was not only associated with inhibition of osteoclastic bone resorption but was an extreme suppressor of bone remodelling preventing normal age-related bone loss. Taken together, the data from the present study suggests that clinically, MM induced osteolytic lesion are diagnosed well beyond the time of initiation of lesions in bone and due to the poor sensitivity in the methods used for diagnosis, treatments are only initiated with established bone disease. The study provides strong clinical rationale for the prophylactic commencement of ZA treatment in order to adequately prevent the development of MBD and preserve bone health.

Finally, the effect of ZA treatment was tested on the early stages of tumour homing and colonisation in bone in the 5TGM1 murine myeloma model using multiple methods (flow cytometry, CD138 IHC and multiphoton microscopy). Striking differences in the tumour load was observed in the CD138 IHC and multiphoton microscopy assessment between the two experiments. This may be because of using different age group of mice between the pre-treatment and post-treatment experiments. In addition, in the post-treatment experiment, multiphoton microscopy scanning was done at 512 X 512 pixel size which resulted in higher resolution images but longer time-frame (approx. 10 hr) for image acquisition.

Therefore there were high chances for photo bleaching due to prolonged exposure of the laser to the specimen. In order to reduce photo bleaching, in the pre-treatment experiment bone were scanned using low resolution 256 X 256 pixel images which shortened the scan time to approximately 3 hr compromising image quality and an improved detection of DID⁺ in the BM. This might also explain the observed difference in the tumour load between the two experiments when assessed by multiphoton microscopy.

Currently, there is not as much available published data where the effect of treatment was tested on the early stages of tumour cell colonisation in MM. Data from the present study demonstrates that ZA treatment, either initiated prior or after tumour cell homing to bone, did not significantly affect the tumour load in BM during the early stages (day 10 post tumour cell injection) of myeloma development. In contrast to the present study, reports by Daubiné et al (2007) showed weekly and daily ZA treatment initiated prior to tumour cell injection significantly inhibited homing of B02/GFP.2/luc⁺ breast cancer cell in BALB/c (nu/nu) athymic mice. In another study, van der Pluijm et al (2005) reported reduction in bone metastases in MDA-321-luc⁺/BALBc mice following olpadronate treatment. In both these studies ZA or olpadronate treatment was initiated one day before tumour cell injection and the doses of ZA used by Daubiné et al (2007) in their studies (100 µg/kg) were similar to what was used in the current study. Studies using *in vivo* breast cancer models have shown that ZA treatment prevented the development of early bone metastasis (Sasaki et al 1995; Brown 2012). Studies on breast cancer bone metastases show that cancer cells in the primary tumour site produce growth factors and chemokines such as VEGF, placental growth factor, SDF-1 resulting in a ‘pre-metastatic bone niche’ formation that attracts the tumour cells to bone. Moreover, tumour cells within the BM were also shown to enhance osteoclast activation, which in turn releases bone-derived growth factors such as TGF-β, IGF from the bone matrix promotes the survival of tumour cells. However, in the present study suppression of osteoclastic bone resorption by ZA showed no effect on the early stages of tumour load in the 5TGM1 model. Myeloma cells are derivatives of normal plasma cells which develop from HSCs which normally exist in the BM. This suggests that the early phase of tumour development in MM in 5TGM1 murine model is independent of the local changes in bone remodelling. BM is a complex environment capable of supporting a wide variety of cells including cancer cells. The functional interplay between the cellular compartments and liquid milieu comprised of bone derived growth factors, cytokines and chemokines within the BM offers a supportive environment not only for HSC but variety of tumour cells such as breast, prostate, MM, lung and kidney cancer cells (Manier et al 2012). *In vitro* studies have also shown that ZA treatment to inhibit tumour cell migration by inhibiting SDF-1/CXCR-4 chemotaxis mechanism (Denoyelle et al 2003).

To conclude, the current study shows that the presence of 5TGM1 tumour cells (10 day post tumour cell injection) in the BM did not significantly alter the bone remodelling indices except for preventing the onset of osteolytic bone disease. ZA treatment (pre or post-treatment strategies) in the 5TGM1 murine model of myeloma resulted only in suppression of bone remodelling similar that was observed

in tumour-free naïve mice. Contrary to the current perception where osteoclastic bone resorption plays an important role in the early homing and colonisation of myeloma cells to bone, results show that early treatment with ZA whether initiated prior to the introduction of myeloma cells or after established colony formation in bone in 5TGM1 murine myeloma model resulted only in prevention of the development of osteolytic bone disease but not the tumour load. This suggests that the on-going normal bone remodelling especially osteoclastic bone resorption may not play a role in the homing of myeloma cell to the bone. Although, the presence of 5TGM1 cells in bone triggers the onset of lytic lesion formation this is not sufficient to increase colony formation in this model. Treatment with ZA did suppress osteolytic lesion formation but did not affect colony formation, suggesting that the process of expansion from single cell to colonies was not reliant on a so called ‘vicious cycle’ in the 5TGM1 model.

CHAPTER 6 THE EFFECT OF ZOLEDRONIC ACID TREATMENT ON THE LATE STAGES OF MYELOMA DEVELOPMENT IN BONE

6.1 INTRODUCTION

Over the last few years, the NBPs such as ZA have been shown to be an effective anti-osteolytic agent and are now frequently used for the symptomatic management of hypercalcaemia of malignancy and cancer-induced bone disease in MM, breast and prostate cancer. Emerging evidence also suggests ZA has potential anti-tumour effects (Croucher et al 2003a). Several preclinical studies have demonstrated that ZA exerts anti-tumour effects in MM *in vitro* and *in vivo* directly or indirectly by altering bone remodelling, resulting in an overall reduction in tumour burden in several preclinical models of MM (Croucher et al 2003b; Clezardin et al 2005). Due to this, ZA is currently being considered for early inclusion with standard first-line chemotherapy in myeloma patients.

Recently, in a randomized phase III clinical trial (MRC Myeloma IX study) ZA inclusion with standard anti-myeloma chemotherapy showed a significant improvement in the OS by 5.5 months and a mild improvement in the PFS by 2 months when compared to CLO (Morgan et al 2010c). In a more recent phase III clinical trial, ZA inclusion with HDT followed by ASCT showed significant improvement in 10 years OS (61%) and PFS (66%) when compared to controls without ZA (Avilés et al 2013). The combination of ZA with thalidomide also showed significant anti-tumour response in asymptomatic MM patients (Witzig et al 2013). Despite all clinical evidence of ZA showing significant anti-tumour response in MM patients, initiation of ZA is not recommended for patients with MGUS or asymptomatic MM (Lacy et al 2006; Kyle et al 2007; Terpos et al 2009).

Although results from *in vivo* preclinical studies are encouraging, supporting significant anti-tumour response with early ZA treatment associated with reduction in tumour burden and improvement in disease-free survival (Croucher et al 2003b; Dairaghi et al 2012), no clear evidence has been offered to explain the mechanism behind the anti-myeloma effect with ZA. Several studies have shown that myeloma cells promote osteoclastogenesis which enhances osteoclastic bone resorption, thereby forming osteolytic bone disease which in turn releases bone derived factors which promote tumour progression (Michigami et al 2000). Furthermore, Abe et al (2004) also showed that osteoclasts not only support the growth and survival of myeloma cells but also renders them drug resistant to standard anti-cancer therapy such as doxorubicin. Therefore, it is expected that inhibiting osteoclastic bone resorption with ZA will inhibit tumour development by breaking the vicious cycle between osteoclastic bone resorption and tumour expansion. Although several studies have already shown the effect of ZA treatment on tumour burden in MM and other cancers, in this study ZA treatment was initiated before the tumour cells arrived in bone and to see whether this had additional benefits than when treatment was initiated at the time of clinical diagnosis. Furthermore, the effect of ZA treatment was also studied after the tumour cell colonised the BM in order to test whether ZA treatment affects the resident myeloma cells in bone. Finally the effect of ZA treatment was also studied on the development of signs of clinical morbidity in the 5TGM1 murine model of myeloma.

6.2 AIMS AND OBJECTIVES

The aims of this chapter were to test whether treatment with ZA initiated prior or after tumour cell injection will affect the late stages of tumour burden and development of the signs of clinical illness.

Hypotheses: ZA treatment initiated prior to tumour cell injection will inhibit the end-stage tumour burden and will delay the onset of development of signs of clinical illness.

The objectives were:-

1. To determine whether treatment with ZA pre or post-treatment injection of myeloma cells will significantly inhibit osteoclastic bone resorption and prevent the development of MBD.
2. To determine whether pre or post-treatment with ZA will reduce end-stage tumour burden in bone.
3. To determine whether ZA treatment will prolong the disease-free survival in the 5TGM1 murine model of myeloma.

6.3 MATERIALS AND METHODS

Detailed information on individual techniques performed is given in [Chapter 2: Materials and Methods.](#)

6.3.1 EXPERIMENTAL DESIGN TO STUDY THE EFFECT OF ZA TREATMENT INITIATED PRIOR TO TUMOUR CELL INJECTION ON THE LATE STAGES OF MYELOMA DEVELOPMENT IN BONE (PRE-TREATMENT EXPERIMENT)

9-12 week old male C57BL/KaLwRij mice were randomised, age matched and grouped as shown in figure 6.3-1. All mice were treated with either PBS (n=11) or ZA (n=11) (125 µg/kg subcutaneously twice-weekly) throughout the experiment. 7 days after the initiation of ZA or PBS treatment, animals in groups 3 and 4 were injected with 2×10^6 5TGM1-eGFP-DID labelled cells via the tail vein. All the animals were regularly monitored for signs of illness or the development of hind limb paralysis. In order to study the effect of ZA treatment on the late stages of disease, the study was continued until the first signs of clinical sickness (approximately 21 days post tumour cell injection). Naïve C57BL/KaLwRij mice treated with PBS (n=4) or ZA (n=4) were used as tumour-free controls. A schematic representation of the study design is given below.

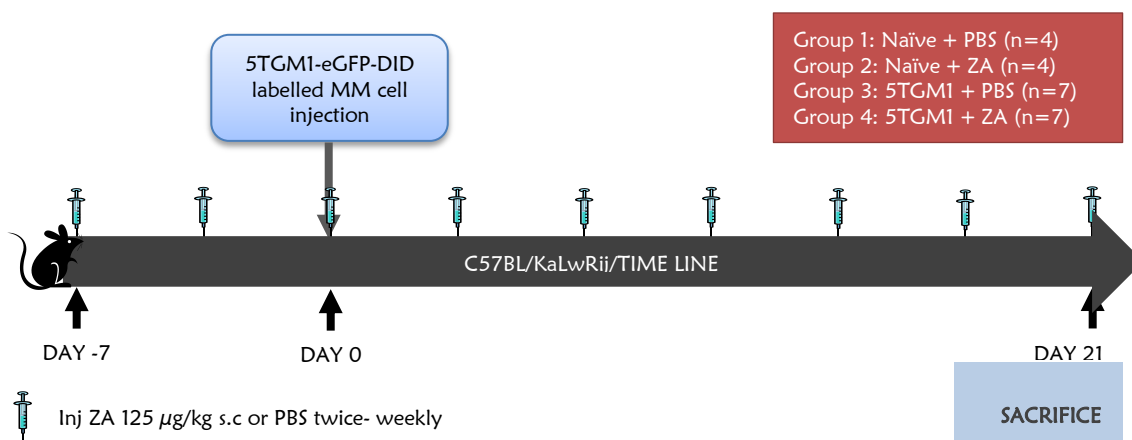


Figure 6.3-1: Experimental design to study the effect of ZA treatment initiated prior to tumour cell injection on the late stages of myeloma in bone.

ZA or PBS treatment was initiated in C57BL/KaLwRij mice (male, 9-12 weeks old) 7 days prior to tumour cell injection and continued throughout the experiment. 5TGM1 myeloma was induced by injecting mice with 2×10^6 5TGM1-eGFP-DID labelled cells on day 0. Mice were sacrificed on day 21 when the first mouse showed signs of clinical illness. Naïve C57BL/KalwRij mice treated with ZA or PBS served as tumour-free controls.

6.3.2 EXPERIMENTAL DESIGN TO STUDY THE EFFECT OF ZA TREATMENT INITIATED AFTER TUMOUR CELL INJECTION ON THE LATE STAGES OF MYELOMA DEVELOPMENT IN BONE (POST-TREATMENT EXPERIMENT)

6-9 week old female C57BL/KaLwRij mice were randomised, age matched and grouped as shown in figure 6.3-2. Mice were randomised, age matched and sequentially grouped to receive either PBS ($n=11$) or ZA ($n=10$). 3 days prior to ZA or PBS treatment, group 3 and 4 were injected with 2×10^6 5TGM1-eGFP-DID labelled cells via the tail vein. Animals were injected with either ZA 125 $\mu\text{g}/\text{kg}$ two doses three days apart or PBS every week. Mice were sacrificed after 21 days post tumour cell injection. Naïve C57BL/KaLwRij mice treated with PBS ($n=5$) or ZA ($n=5$) were used as tumour-free controls. A schematic representation of the study design is given below.

On the day of the sacrifice, all animals were starved 6 hr prior to the sacrifice in order to eliminate the circadian variation in the serum bone biomarkers. Mice were anaesthetised using 50-100 μl of pentobarbitone (intra-peritoneal injection) and blood samples were collected using cardiac puncture. Animals were culled by cervical dislocation while under deep non-recoverable anaesthesia and tissues were harvested.

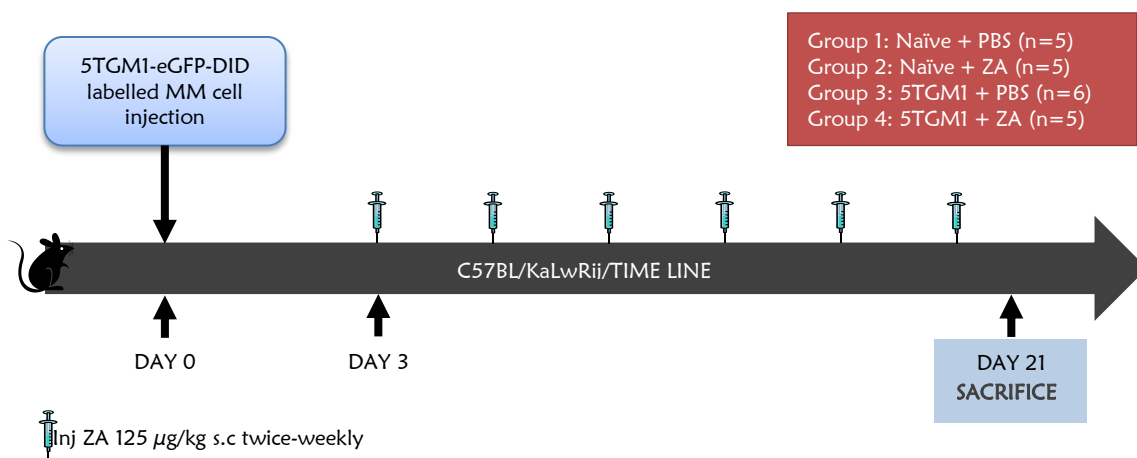


Figure 6.3-2: Experimental design to study the effect of ZA treatment initiated after the tumour cell injection on the late stages of myeloma development.

5TGM1 myeloma was induced by injecting C57BL/KaLwRij mice (female, 6-9 weeks old) with 2×10^6 5TGM1-eGFP-DID labelled cells on day 0. ZA or PBS treatment was initiated on day 3 post tumour cell injection and continued. Mice were sacrificed on day 21 when the first mouse showed signs of clinical illness. Naïve C57BL/KaLwRij mice treated with ZA or PBS served as tumour-free controls.

6.3.3 EXPERIMENTAL DESIGN TO STUDY THE EFFECT OF ZA TREATMENT ON DISEASE-FREE SURVIVAL

Mice were randomised into three experimental groups. Group A ($n=11$) mice were treated with PBS (100 μ l subcutaneously twice-weekly) 7 days prior and injected with 2×10^6 5TGM1-eGFP-DID labelled cell via the tail vein. PBS treatment was continued every week throughout the experiment until the development of signs of morbidity. Group B ($n=11$) mice received ZA treatment (125 μ g/kg s.c. twice-weekly) beginning with 2×10^6 5TGM1-eGFP-DID labelled cell injection and continued until the development of signs of morbidity. Group C ($n=11$) mice received ZA treatment (125 μ g/kg s.c. twice-weekly) 7 days prior to 2×10^6 5TGM1-eGFP-DID labelled cell injection and continued until the development of signs of morbidity. All animals were monitored regularly. A schematic representation of the study design is given in figure 6.3-3.

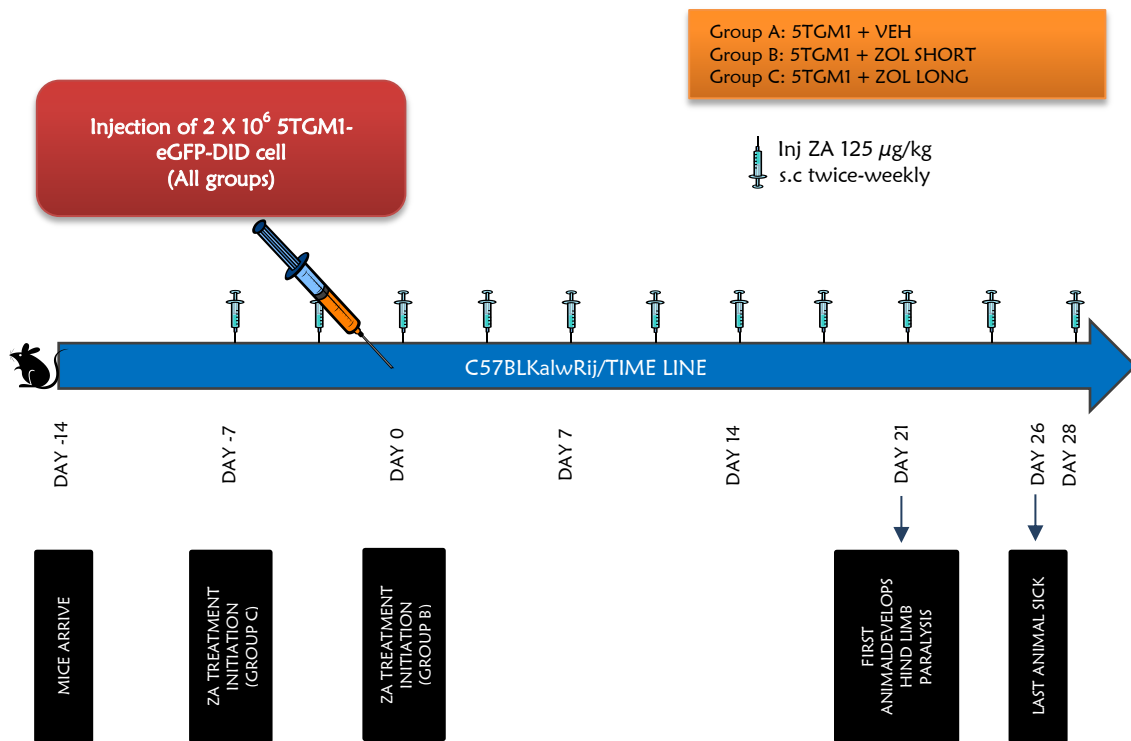


Figure 6.3-3: Schematic representation to study the effect of ZA treatment on the onset of illness.

C57BL/KaLwRij mice (female, 8-9 weeks old) were injected with 2×10^6 5TGM1-eGFP-DID labeled cells on day 0. ZA treatment was initiated on day -7 (ZOL LONG, Group C, $n=12$) and day 0 (ZOL SHORT, Group B, $n=12$). PBS treated 5TGM1 tumour-bearing mice (Group A, 5TGM1 + VEH, $n=11$) served as controls.

6.4 RESULTS

6.4.1 ZA TREATMENT EITHER PRE OR POST INJECTION OF 5TGM1 MURINE MYELOMA CELLS SIGNIFICANTLY SUPPRESSED BOTH OSTEOCLASTS AND OSTEOBLASTS IN THE 5TGM1 MURINE MYELOMA MODEL DURING THE LATE STAGE OF MYELOMA DEVELOPMENT

The effect of ZA treatment on osteoclast numbers assessed 21 day post tumour cell injection of 5TGM1 murine myeloma cells

Changes in Oc numbers following pre or post ZA treatment in the trabecular and endocortical region of the proximal tibial metaphysis in the 5TGM1 tumour-bearing mice (21 days post tumour cell injection) was assessed using static histomorphometry. In the pre-treatment experiment (ZA treatment initiated 7 days prior to 5TGM1 tumour cell injection), a significant reduction in the Oc number in both the trabecular and endocortical region was observed in the ZA treated 5TGM1 tumour-bearing mice when compared with PBS treated 5TGM1 tumour-bearing controls. However, no difference was observed in the number of Oc in the trabecular region between the PBS or ZA treated tumour-free naïve, age and sex matched C57BL/KaLwRij mice that were used as controls (figure 6.4-1 A and C). Interestingly, a significant increase in the number of Oc lining the endocortical surface in the 5TGM1 tumour-bearing mice when compared to tumour-free, naïve C57BL/KaLwRij control mice was observed (figure 6.4-1 C).

Following post-treatment (ZA treatment initiated 3 days after 5TGM1 tumour cell injection), a significant reduction in Oc number both in the trabecular and endocortical region was observed both in 5TGM1 tumour-bearing and tumour-free naïve controls when compared with age and sex matched PBS treated respective controls (figure 6.4-1 B and D). A significant increase in the number of Oc lining the endocortical surface in the 5TGM1 tumour-bearing mice when compared to tumour-free naïve controls was also seen at 21 days post tumour cell injection (figure 6.4-1 D).

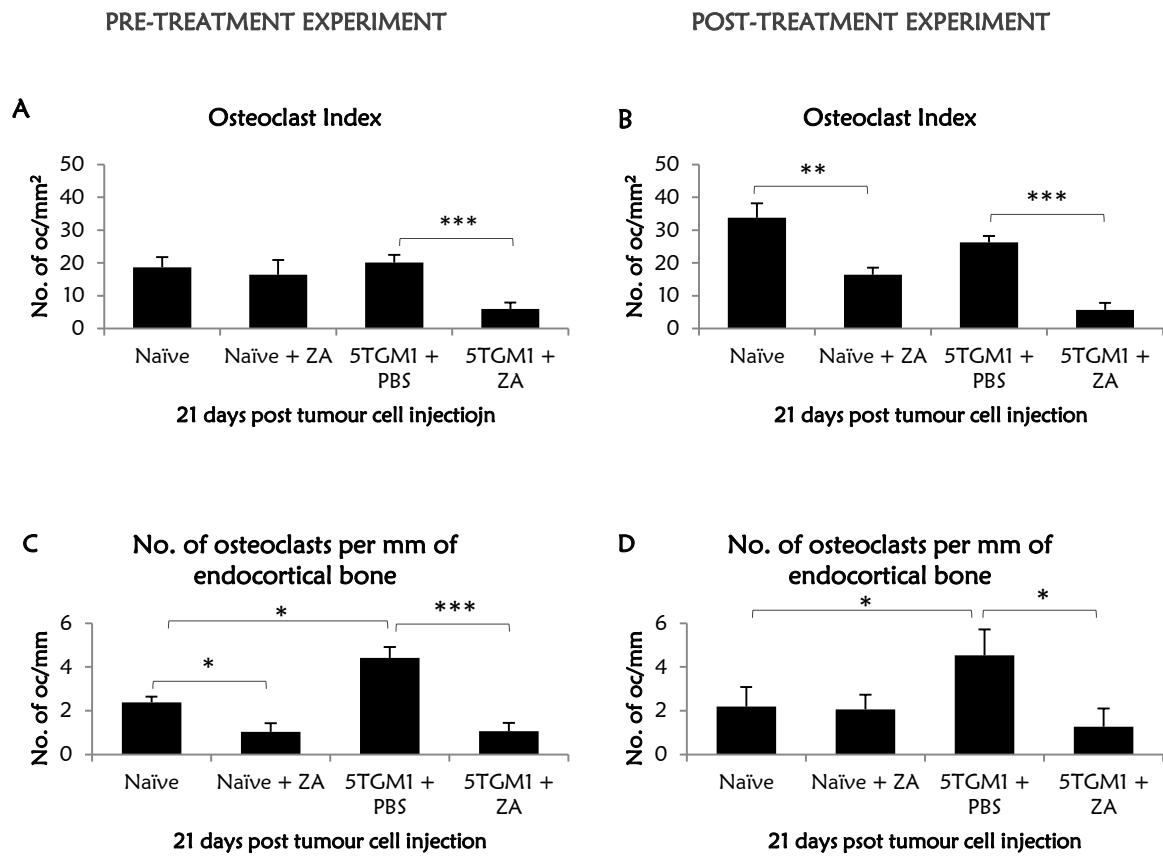


Figure 6.4-1: The effect of ZA treatment on Oc numbers in the 5TGM1 murine model of myeloma, 21 days post tumour cell injection.

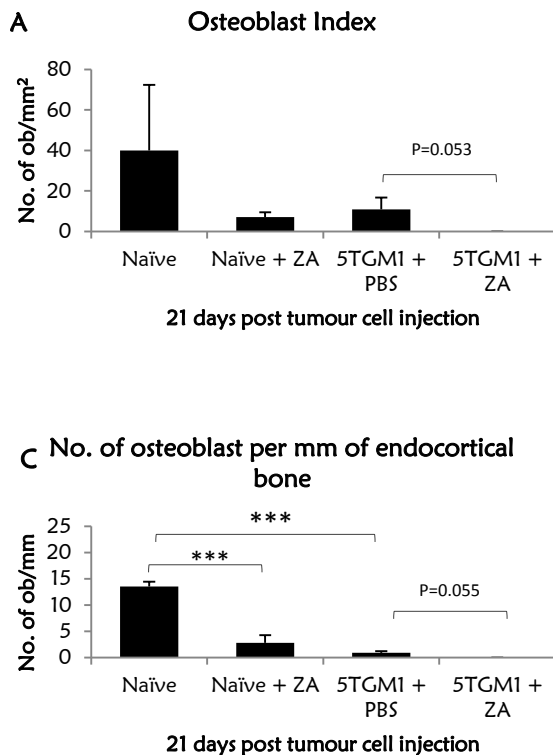
Histological analysis of Oc index (A) and number of Oc per mm of endocortical bone (C) in 5TGM1 tumour-bearing mice pre-treated for 7 days with ZA (n=7) or PBS (n=7) assessed 21 days post tumour cell injection. Tumour-free mice injected with either PBS (n=4) or ZA (n=4) served as controls. Changes in Oc index (B) and number of Oc per mm of endocortical bone (D) in 5TGM1 tumour-bearing mice treated with ZA (n=5) or PBS (n=6) 3 days after tumour injection, assessed 21 days post tumour cell injection. Tumour-free mice injected with either PBS (n=5) or ZA (n=5) served as controls. Comparison was done between PBS or ZA treated groups in both naïve tumour-free and 5TGM1 tumour-bearing groups using a one-tailed ‘non-parametric’ Mann Whitney-Wilcoxon test with P<0.05 as statistically significant. *P<0.05, **P<0.01, ***P<0.001.

The effect of ZA treatment on osteoblast numbers in the 5TGM1 murine model of myeloma assessed at 21 day post tumour cell injection

In 5TGM1 tumour-bearing mice pre-treatment with ZA significantly reduced the numbers of Ob both in the trabecular and endocortical region when compared to PBS 5TGM1 tumour-bearing mice. There was no statistically significant difference in Ob number in the naïve tumour-free mice treated with ZA or PBS assessed at 21 days post tumour cell injection ($P=0.05$; figure 6.4-2 A and C). However, there was a significant reduction in the number of Ob lining the endocortical region in the 5TGM1 tumour-bearing mice when compared with tumour-free control mice.

In the post-treatment experiment, a significant reduction in the number of Ob in the trabecular and endocortical region was observed in the 5TGM1 tumour-bearing mice 21 days post tumour cell injection when compared with tumour-free controls. Following ZA post-treatment, a significant reduction in trabecular Ob number was observed in the tumour-free PBS treated mice when compared with PBS treated groups. However, in the 5TGM1 tumour-bearing group following ZA treatment, a reduction in Ob number was observed but not statistically significant when compared to PBS treated tumour-bearing control groups (figure 6.4-2 B and D).

PRE-TREATMENT EXPERIMENT



POST-TREATMENT EXPERIMENT

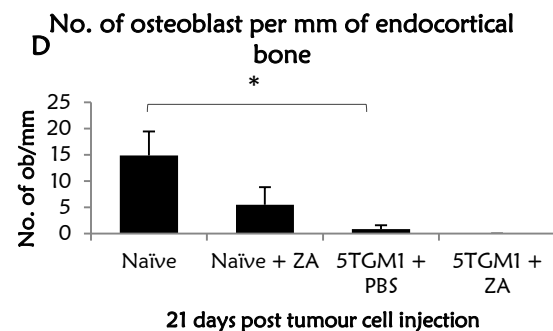
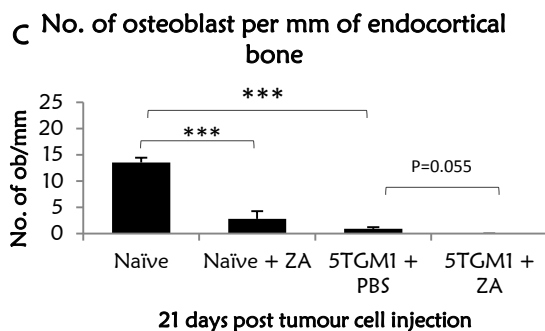
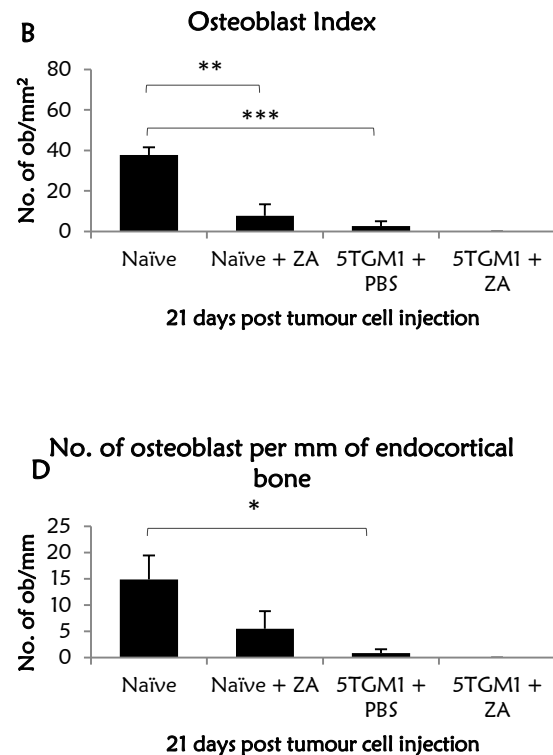


Figure 6.4-2: The effect of ZA treatment on Ob numbers in the 5TGM1 murine model of myeloma, 21 days post tumour cell injection.

Histological analysis of Ob index (A) and number of Ob per mm of endocortical bone (C) in 5TGM1 tumour-bearing mice pre-treated for 7 days with ZA (n=7) or PBS (n=7) assessed 21 days post tumour cell injection. Tumour-free mice injected with either PBS (n=4) or ZA (n=4) served as controls. Changes in Ob index (B) and number of Ob per mm of endocortical bone (D) in 5TGM1 tumour-bearing mice treated with ZA (n=5) or PBS (n=6) 3 days after tumour injection, assessed 21 days post tumour cell injection. Tumour-free mice injected with either PBS (n=5) or ZA (n=5) served as controls. Comparison was done between PBS or ZA treated groups in both naïve tumour-free and 5TGM1 tumour-bearing groups using a one-tailed ‘non-parametric’ Mann Whitney-Wilcoxon test with P<0.05 as statistically significant. *P<0.05, **P<0.01, ***P<0.001.

Treatment with ZA either pre or post injection of 5TGM1 murine myeloma cells preserved both trabecular and cortical bone volume in 5TGM1 model assessed 21 days post tumour cell injection

Representative microCT images of tibia following pre-treatment with PBS or ZA are shown in figure 6.4-3 A and B respectively. MicroCT analysis showed that there was a significant increase in cortical bone volume in both tumour-free and 5TGM1 tumour-bearing mice treated with ZA when compared to PBS treated respective control mice (figure 6.4-3 E). Similarly, greater trabecular bone volume (% BV/TV) was seen in the ZA treated tumour-free and 5TGM1 tumour-bearing animals when compared with respective PBS treated control groups (figure 6.4-3 G).

In the experiment where ZA treatment was initiated post tumour cell injection, there was a significant increase in cortical bone volume in both tumour-free and 5TGM1 tumour-bearing mice 21 days post tumour cell injection (figure 6.4-3 F). Similarly, increase in trabecular bone volume was seen in the ZA treated 5TGM1 tumour-bearing mice when compared with PBS treated tumour-bearing groups. Interestingly, a reduction in trabecular bone volume was observed in the 5TGM1 tumour-bearing mice when compared to tumour-free mice (figure 6.4-3 H). Representative microCT images of tibia following post-treatment with PBS or ZA are shown in figure 6.4-3 C and D respectively.

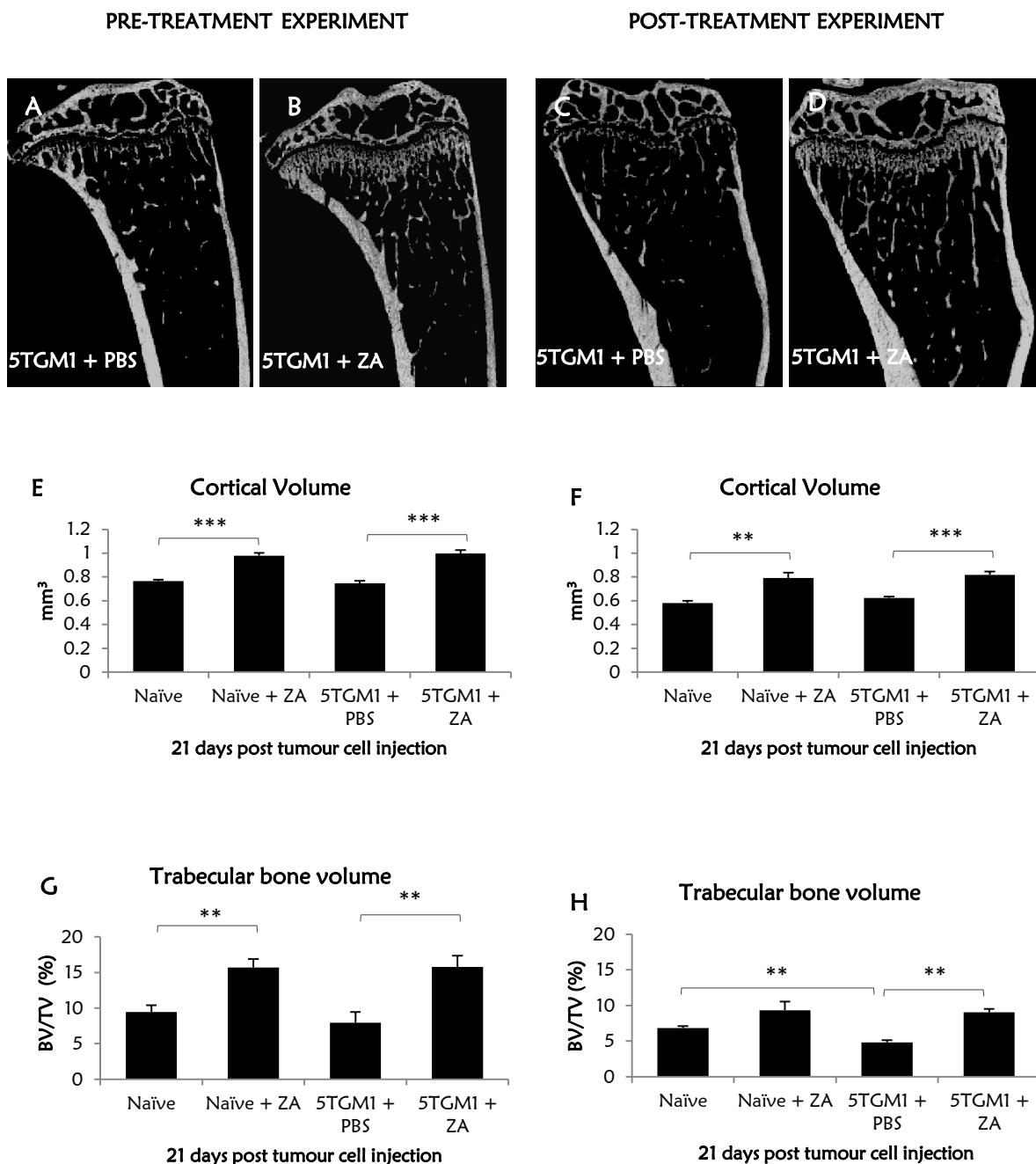


Figure 6.4-3: MicroCT analysis following pre and post ZA treatment in the 5TGM1 murine model of myeloma, 21 days post tumour cell injection

Representative micro CT longitudinal cross-section images of tibia from 5TGM1 tumour-bearing mice 21 day post tumour cell injection following pre (A, B) and post-treatment (C, D) with ZA or PBS respectively. Changes in Ct. V (E) and % BV/TV (G) in 5TGM1 tumour-bearing mice treatment initiated 7 days prior to tumour cell injection with ZA (n=7) or PBS (n=7) assessed 21 days post tumour cell injection. Tumour-free mice injected with either PBS (n=4) or ZA (n=4) served as controls. Changes in Ct. V (F) and % BV/TV (H) following post ZA treatment where treatment was initiated 3 days after tumour cell injection with ZA (n=5) or PBS (n=6). Tumour-free mice injected with either PBS (n=5) or ZA (n=5) served as controls. Comparison was done between PBS or ZA treated groups in both naïve tumour-free and 5TGM1 tumour-bearing groups using a one-tailed ‘non-parametric’ Mann Whitney-Wilcoxon test with P<0.05 as statistically significant. *P<0.05, **P<0.01, ***P<0.001.

Treatment of animals with ZA either pre or post injection of 5TGM1 murine myeloma cells reduced both serum levels of TRACP5b and P1NP assessed 21 days post tumour cell injection

Following ZA treatment prior to 5TGM1 tumour cell injection, a significant reduction in serum levels of TRACP5b in both 5TGM1 tumour-bearing mice and tumour-free naïve C57BL/KaLwRij mice was seen when compared to PBS treated respective control groups (figure 6.4-4 A). However, a significant reduction in serum levels of P1NP was observed only in the tumour-free naïve mice and not in the 5TGM1 tumour-bearing group 21 days post tumour cell injection when compared with respective PBS treated control group (figure 6.4-4 C). In the post-treatment experiment, a significant reduction in serum levels of TRACP5b and P1NP was observed in both 5TGM1 tumour-bearing mice and tumour-free naïve C57BL/KaLwRij mice with ZA treatment when compared to PBS treated control groups (figure 6.4-4 B and D). Interestingly, a significant increase in serum TRACP5b levels was observed in 5TGM1 tumour-bearing mice 21 days post tumour cell injection when compared with tumour-free control group ($P<0.001$).

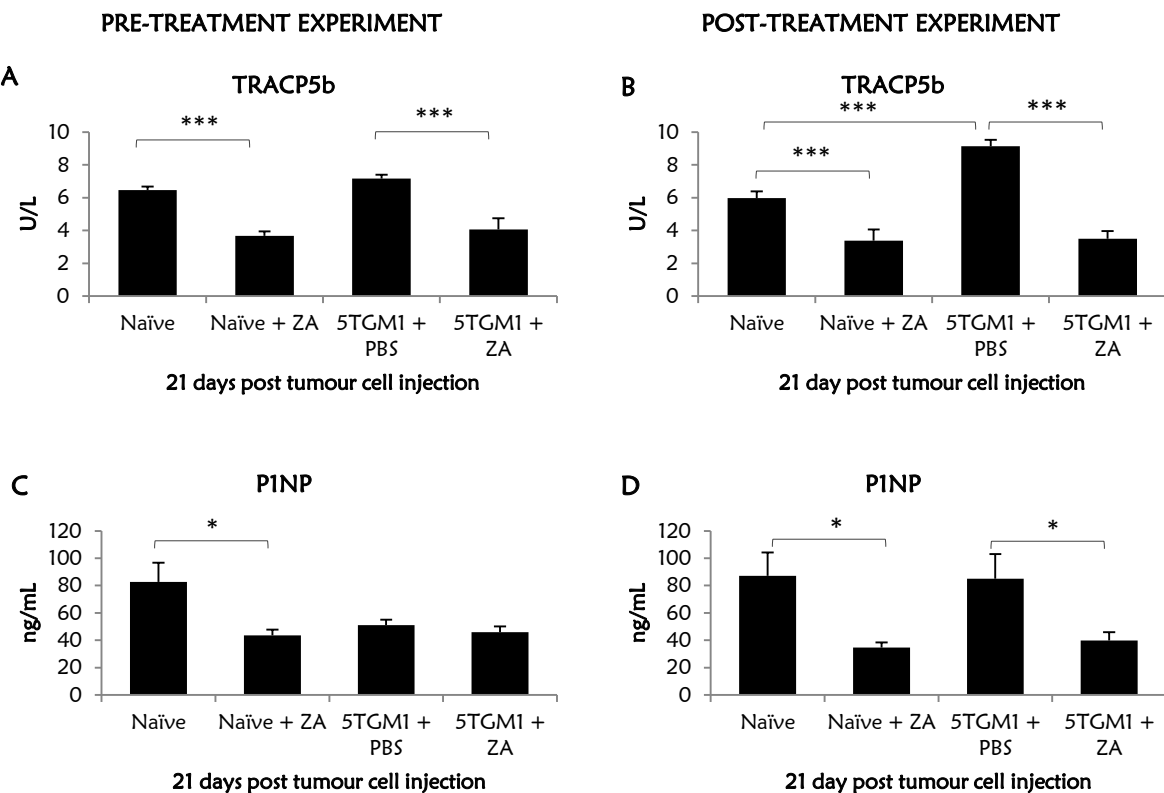


Figure 6.4-4: The effect of ZA treatment on serum bone turn over markers in the 5TGM1 murine model of myeloma 21 days post tumour cell injection.

Changes in serum levels of TRACP5b (A) and P1NP (C) respectively in 5TGM1 tumour-bearing mice pre-treated with ZA ($n=7$) or PBS ($n=7$) assessed 21 days post tumour cell injection. Age matched naïve tumour-free C57BL/KaLwRij mice injected with either PBS ($n=4$) or ZA ($n=4$) served as controls. Changes in serum levels of TRACP5b (B) and P1NP (D) respectively in 5TGM1 tumour-bearing mice post-treated with ZA ($n=5$) or PBS ($n=6$) assessed 21 days post tumour cell injection. Age matched naïve tumour-free C57BL/KaLwRij mice injected with either PBS ($n=5$) or ZA ($n=5$) served as controls. A one-tailed ‘non-parametric’ Mann Whitney-Wilcoxon test was used with $P<0.05$ as statistically significant. * $P<0.05$, ** $P<0.01$, *** $P<0.001$.

ZA prevents development of osteolytic lesions induced by myeloma cell growth, assessed 21 days post tumour cell injection

In the previous chapter (Chapter 5), it was shown that ZA treatment (both pre and post-treatment strategy) was effective in preventing the development of osteolytic bone lesion as early as 10 days post 5TGM1 tumour cell injection. Here the effect of ZA treatment was tested on the development of osteolytic lesions 21 days post 5TGM1 tumour cell injection when the animals showed signs of clinical illness. In the ZA pre-treatment experiment, there was a 540% increase ($0.25 \pm 0.03 \rightarrow 1.6 \pm 0.39$; $P<0.01$) in the percentage lesion area in the 5TGM1 tumour-bearing mice (21 days) when compared with tumour-free naïve control mice. However, following ZA treatment initiated prior to 5TGM1 tumour cell injection, a dramatic 92.5% reduction ($1.6 \pm 0.39 \rightarrow 0.12 \pm 0.03$; $P<0.001$) in the percentage lesion area was seen when compared with PBS treated 5TGM1 tumour-bearing mice (figure 6.4-5 E). Similar pattern was also observed in the average number of lesions with a 154% increase ($83.09 \pm 5.16 \rightarrow 211.7 \pm 27.2$; $P<0.01$) in the average number of osteolytic lesions in the 5TGM1 tumour-bearing mice when compared with tumour-free control group. Following ZA pre-treatment, 87.3% reduction ($211.7 \pm 27.2 \rightarrow 27.3 \pm 4.2$; $P<0.001$) in average lesion numbers was seen when compared with PBS treated 5TGM1 tumour-bearing mice (figure 6.4-5 G).

In the post ZA treatment experiment, there was a 250% increase ($0.32 \pm 0.06 \rightarrow 1.12 \pm 0.29$; $P<0.01$) in the percentage lesion area in the 5TGM1 tumour-bearing mice (21 days) when compared with tumour-free naïve control mice. However, following ZA treatment, a dramatic 91% reduction ($1.12 \pm 0.29 \rightarrow 0.10 \pm 0.01$; $P<0.001$) in the percentage lesion area in the percentage lesion area was seen when compared with PBS treated 5TGM1 tumour-bearing mice levels (figure 6.4-5 F). Similar pattern was also observed in the average number of lesions with a 123% increase ($108.3 \pm 6.41 \rightarrow 230.6 \pm 12.6$; $P<0.01$) in the average number of osteolytic lesions in the 5TGM1 tumour-bearing mice when compared with tumour-free control group. Following ZA pre-treatment, 90.9% reduction ($230.6 \pm 12.6 \rightarrow 20.9 \pm 4.07$; $P<0.001$) in average lesion numbers was seen when compared with PBS treated 5TGM1 tumour-bearing mice (figure 6.4-5 H).

Representative images showing the posterior surface of the tibia with cortical defects from 5TGM1 tumour-bearing mice pre or post treated with PBS or ZA are shown in figure 6.4-5 A, B, C and D respectively.

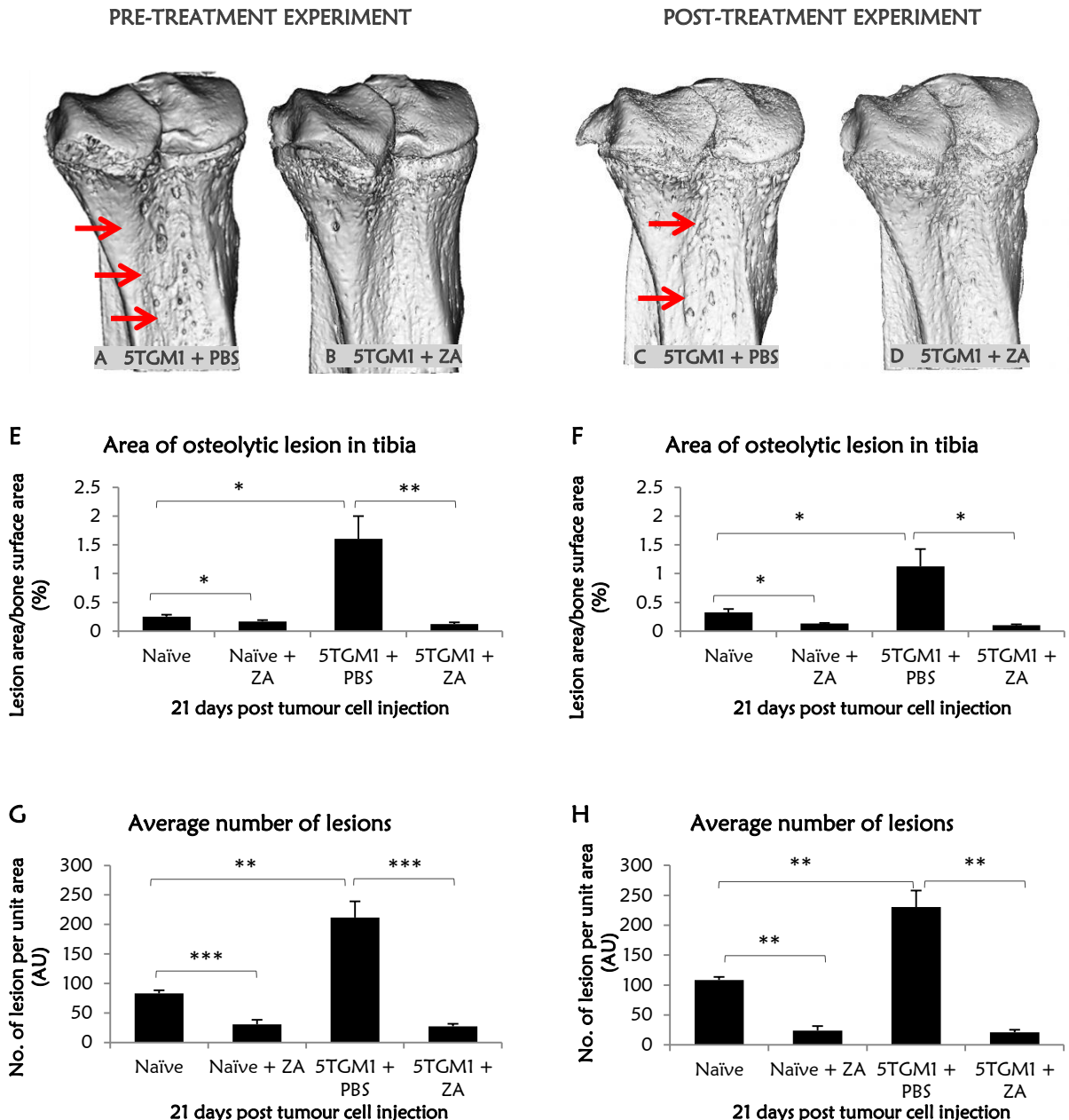


Figure 6.4-5: Effect of ZA treatment on the onset of tumour-induced osteolysis assessed 21 days post tumour cell injection.

Representative 3D models of proximal tibial metaphysis of 5TGM1 tumour-bearing mice following PBS or ZA treatment assessed 21 days post tumour cell injection showing osteolytic bone lesion (A), (B), (C) and (D). Osteolytic lesions (cortical defects) are shown in red arrows in the PBS treated 5TGM1 tumour-bearing mice. Changes in percentage osteolytic lesion (E) and average number of lesions (G) in the 5TGM1 tumour-bearing mice pre-treated with ZA (n=7) or PBS (n=7) assessed 21 days post tumour cell injection. Age matched naïve tumour-free C57BL/KaLwRij mice injected with either PBS (n=4) or ZA (n=4). Changes in percentage osteolytic lesion (F) and average number of lesions (H) in the 5TGM1 tumour-bearing mice post-treated with ZA (n=5) or PBS (n=3) assessed 21 days post tumour cell injection. Age matched naïve tumour-free C57BL/KaLwRij mice injected with either PBS (n=5) or ZA (n=5) served as control. Mann-Whitney non-parametric test was used to compare the statistical difference between the mean in the PBS and the ZA treated groups with P value <0.05 as statistically significant *P<0.05, **P<0.01, ***P<0.001.

6.4.2 THE EFFECT OF ZA TREATMENT ON TUMOUR BURDEN IN BONE DURING THE LATE STAGES OF MYELOMA DISEASE DEVELOPMENT

Flow cytometric analysis revealed no changes in 5TGM1-eGFP-DID cell burden in BM following ZA treatment assessed after 21 days post tumour cell injection

Flow cytometric analysis was used to quantify the number of DID⁺, eGFP⁺ and dual labelled 5TGM1-eGFP-DID⁺ tumour cell in the BM following pre and post ZA treatment. Figure 6.4-6 shows typical flow cytometry profiles of BM cell with 5TGM1-eGFP-DID cells with DID labelling on Y-axis and eGFP labelling on X-axis. BM cells from naïve tumour-free mice were used a negative controls to gate DID⁺ and eGFP⁺ fluorophore channels. Results showed no significant difference between VEH treated and ZA treated in the percentage DID⁺, eGFP⁺ and 5TGM1-eGFP-DID⁺ population in the BM 21 days post tumour cell injection both after pre or post ZA treatment experiments (figure 6.4-7).

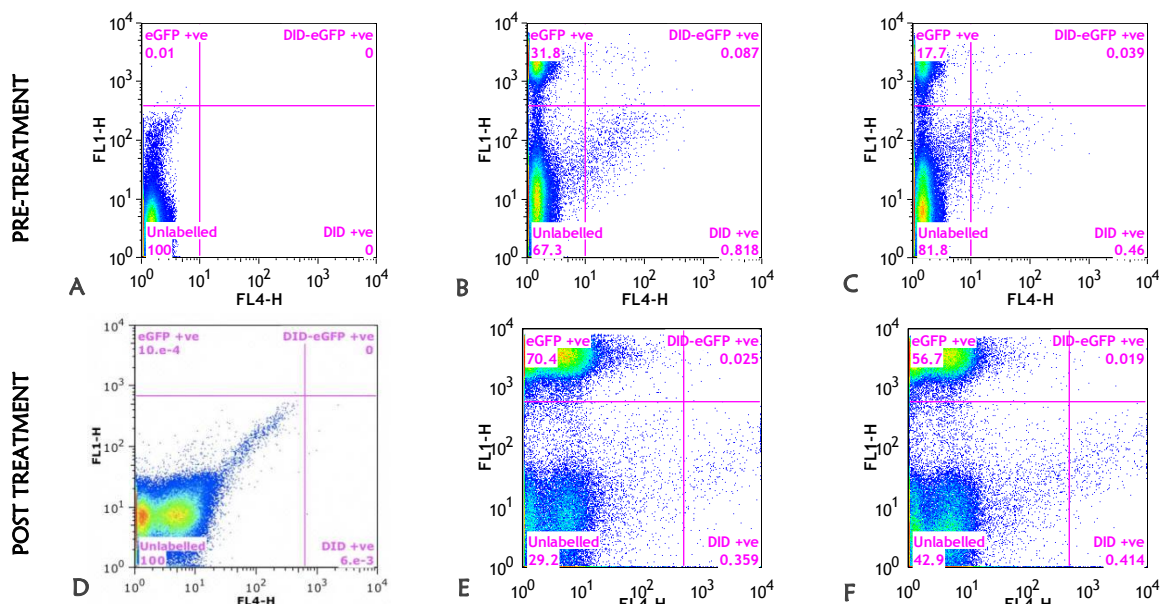


Figure 6.4-6: Flow cytometric profiles of BM cells positive for DID, eGFP and dual labelled 5TGM1-eGFP-DID cells

Typical flow cytometric profiles of BM cells from mice injected with 5TGM1-eGFP-DID after 21 days post injection. BM profile from naïve tumour-free (**A**) and (**D**) mice was used to gate normal cells. Profiles from 5TGM1 tumour-bearing mice after pre-treatment with VEH (**B**) or ZA (**C**) with FL1 (eGFP⁺) channel on Y axis and FL4 (DID⁺) channel on X-axis. BM profiles from 5TGM1 tumour-bearing mice after post-treatment with VEH (**E**) or ZA (**F**).

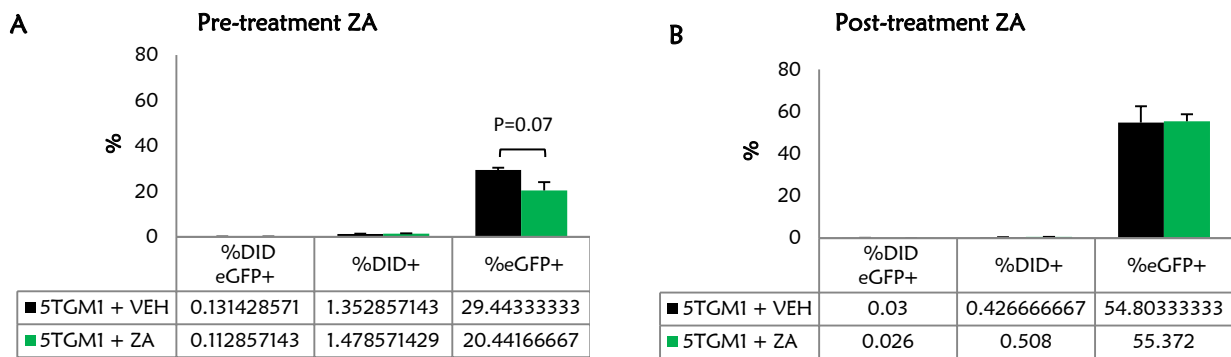


Figure 6.4-7: The effect of ZA treatment on 5TGM1 tumour burden 21 days post tumour cell injection.

Flow cytometric analysis of changes in the percentage DID⁺, eGFP⁺ and DID-eGFP⁺ dual labelled 5TGM1 in tumour-bearing mice pre-treated (**A**) with ZA (n=7) or VEH (n=7) assessed 21 days post tumour cell injection. Flow cytometric analysis of changes in the percentage DID⁺, eGFP⁺ and DID-eGFP⁺ dual labelled 5TGM1 in tumour-bearing mice post-treated (**B**) with ZA (n=5) or VEH (n=6) assessed 21 days post tumour cell injection. Comparison was done between VEH or ZA treated groups in the 5TGM1 tumour-bearing groups using a ‘non-parametric’ Mann Whitney-Wilcoxon test with P<0.05 as statistically significant. *P<0.05, **P<0.01, ***P<0.001.

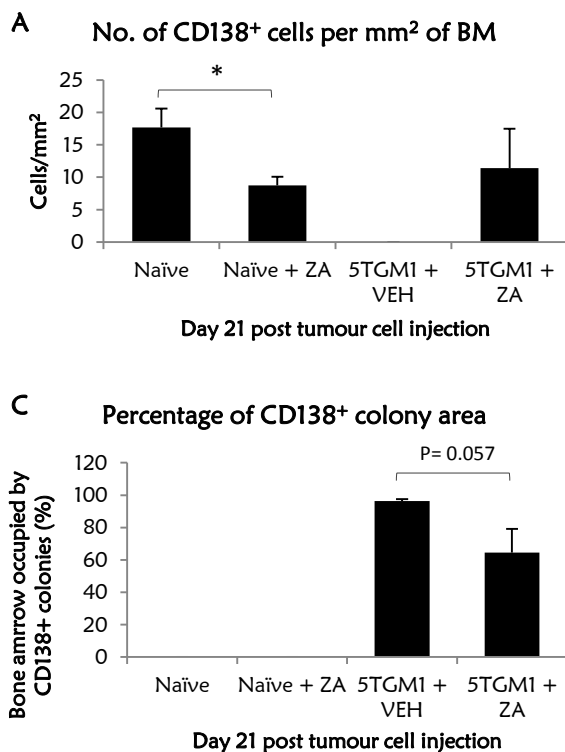
ZA treatment showed no significant difference in the CD138 positive cell population in BM of the 5TGM1 tumour-bearing mice

In chapter 5, it was shown that ZA treatment (pre or post-treatment) did not affect the CD138⁺ population in the BM following 10 days post 5TGM1 tumour cell injection. In this section, the effect of ZA treatment was tested on CD138⁺ population 21 days post 5TGM1 tumour cell injection. Results were expressed as number of CD138⁺ cell per mm² of BM in order to quantitate the individual cells and percentage BM space occupied by CD138⁺ colonies in order to quantitate the CD138⁺ colonies. In both experiments (pre or post-treatment), only individual CD138⁺ cells were seen mice and no there was no evidence of CD138⁺ colonies in tumour-free control (both VEH or ZA treated). In the pre-treatment experiment, a significant reduction in the number of CD138⁺ cells per mm² of BM was seen in ZA treated tumour-free control mice when compared with VEH treated tumour-free control (figure 6.4-8 A). However, no difference was observed between ZA and VEH treated tumour-free groups in the post-treatment experiment (figure 6.4-8 B). No evidence of individual CD138⁺ cells were seen in the 5TGM1 tumour-bearing mice (day 21) in both the experimental strategies. However, individual CD138⁺ cells were seen in ZA treated 5TGM1 tumour-bearing mice only in the pre-treatment experiment.

CD138⁺ tumour colonies were seen in 5TGM1 tumour-bearing mice (ZA or VEH treated) in both the experimental strategies. Following pre ZA treatment, although a 33.08 % (VEH vs. ZA, 96.37 ± 1.18 vs. 64.49 ± 14.64 ; P=0.057) reduction in the percentage BM space occupied by CD138⁺ colonies was observed when compared with VEH treated 5TGM1 tumour-bearing mice, it did not reach statistical significance (figure 6.4-8 C). Following post-treatment experiment, no significant difference was observed in the percentage BM space occupied by CD138⁺ colonies in the ZA treated 5TGM1 tumour-bearing group when compared with VEH treated control (figure 6.4-8 D).

Representative examples of CD138 stained BM sections from 5TGM1 tumour-bearing mice (21 days post tumour cell injection) following VEH or ZA treatment (pre and post) are shown in figure 6.4-9 and figure 6.4-10 respectively.

PRE-TREATMENT EXPERIMENT



POST-TREATMENT EXPERIMENT

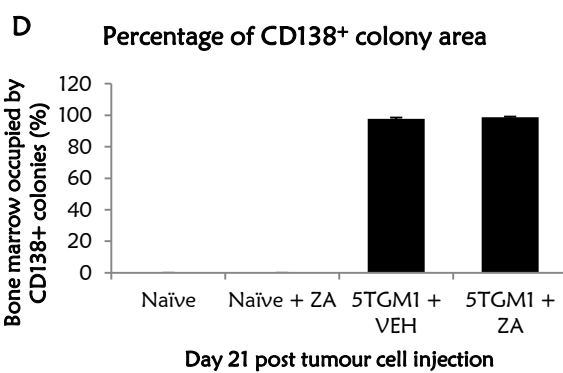
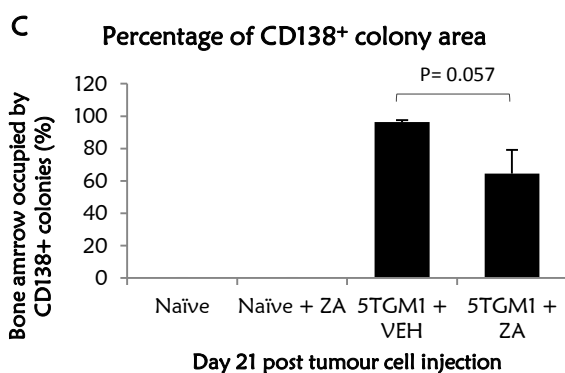
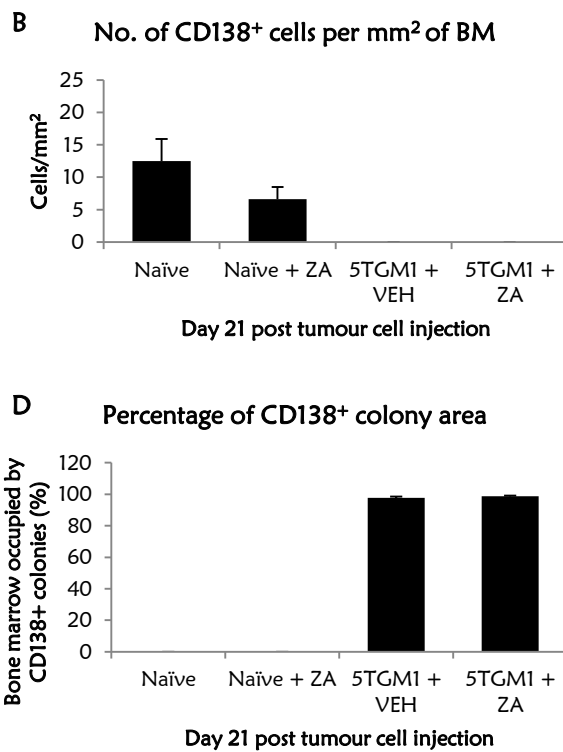


Figure 6.4-8: Effect of ZA on CD138 positive population on the late stages (21 day) of myeloma development in 5TGM1 murine model of myeloma.

Changes in CD138⁺ population between 5TGM1 + VEH and 5TGM1 + ZA treated group was expressed as changes in individual number of CD138⁺ population and percentage BM space occupied by CD138⁺ colonies assessed 21 days post tumour cell injection. Changes in the number of CD138⁺ cells (**A**) and percentage CD138⁺ tumour colonies (**C**) in the 5TGM1 tumour-bearing mice pre-treated with ZA (n=7) or VEH (n=7) assessed 21 days post tumour cell injection. Tumour-free mice injected with either VEH (n=4) or ZA (n=4) served as controls. Changes in the number of CD138⁺ cells (**B**) and percentage CD138⁺ tumour colonies (**D**) in the 5TGM1 tumour-bearing mice post treated with ZA (n=5) or VEH (n=6) assessed 21 days post tumour cell injection. Tumour-free mice injected with either VEH (n=5) or ZA (n=5) served as controls. Mann-Whitney non-parametric test was used to compare the statistical difference between the VEH and the ZA treated groups with P value <0.05 as statistically significant *P<0.05, **P<0.01, ***P<0.001.

PRE-TREATMENT ZA STRATEGY

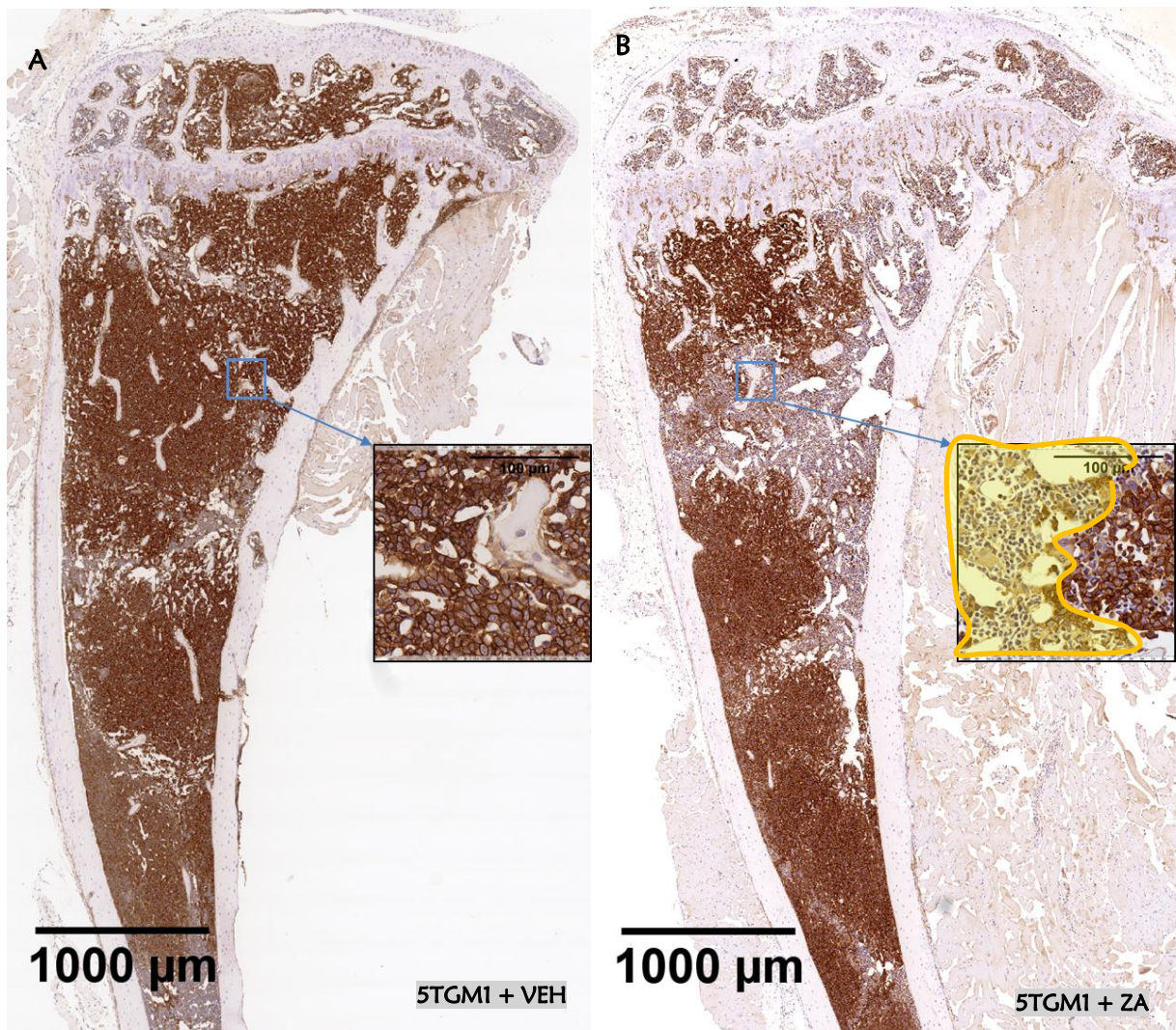


Figure 6.4-9: The effect of ZA pre-treatment on CD138 positive tumour cells 21 days post tumour cell injection.

Representative CD138 IHC stained images of tibia from mice bearing 5TGM1-eGFP-DID tumour cells (21 day post tumour cell injection) pre-treated with VEH (A) or ZA (B). Images are 2X magnified showing the proximal one third of the tibia (scale bar 1000 μ m) with magnification of CD138⁺ tumour colonies (inner box, 40X).

POST-TREATMENT ZA STRATEGY

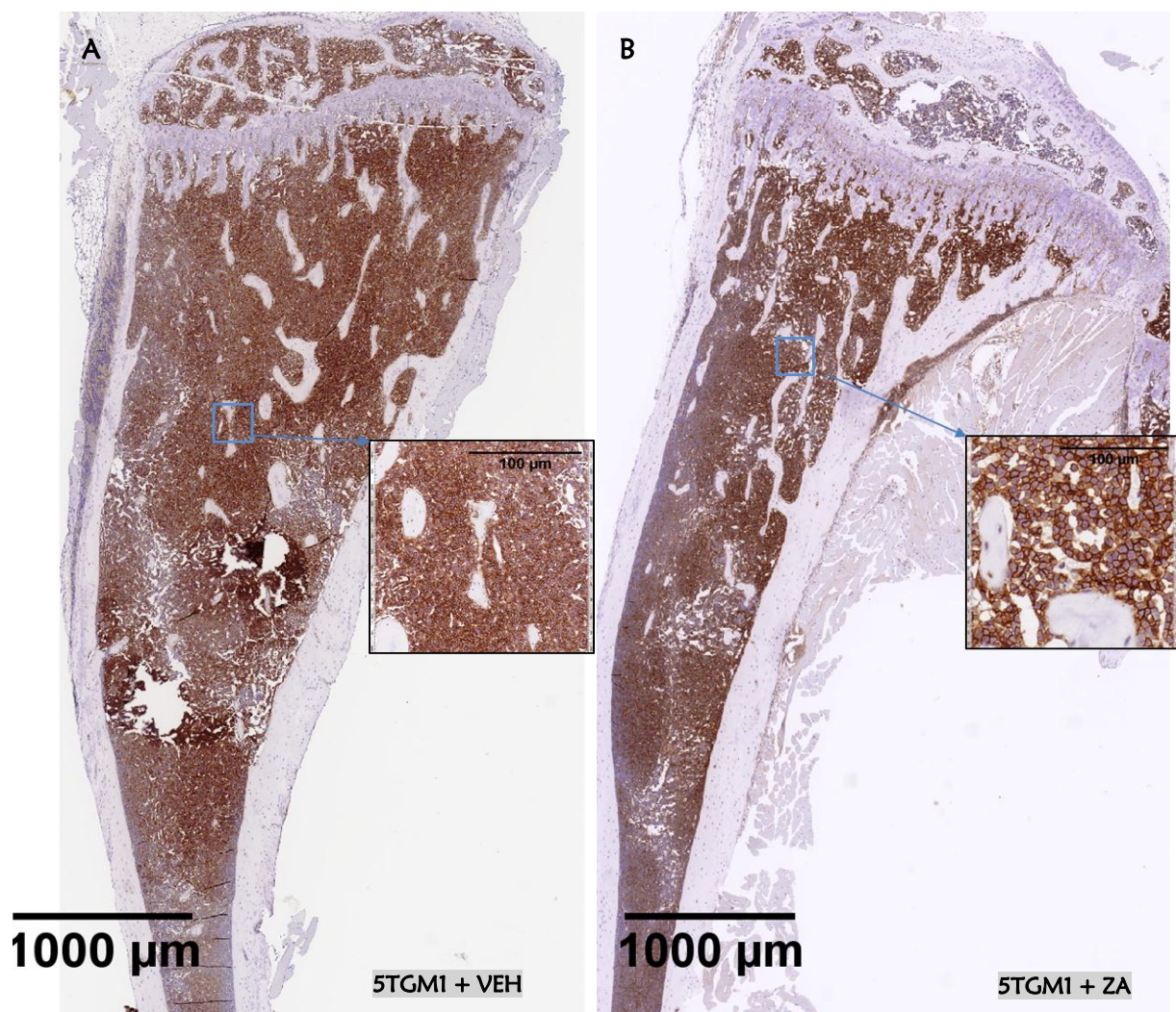


Figure 6.4-10: The effect of ZA post-treatment on CD138 positive cells 21 days post tumour cell injection.

Representative CD138 IHC stained of tibia from mice bearing 5TGM1-eGFP-DID tumour cells (21 day post tumour cell injection) post-treated with VEH (A) or ZA (B). Images are 2X magnified showing the proximal one third of the tibia (scale bar 1000 μm) with magnification of CD138⁺ tumour colonies (inner box, 40X).

Treatment of animals with ZA prior to 5TGM1-eGFP-DID murine myeloma cells showed significant reduction in 5TGM1-eGFP⁺ tumour colonies, 21 days post tumour cell injection

From chapter 5, it was clearly shown that using multiphoton microscopy 5TGM1-DID⁺ cell could be seen in the BM of mice injected with 5TGM1-eGFP-DID cells and ZA treatment (pre or post-treatment strategies) did not affect the number of 5TGM1-DID⁺ cells in the BM 10 days post tumour cell injection. In this section, the effect of ZA treatment (pre and post treatment strategies) on 5TGM1 murine model 21 days post tumour cell injection will be discussed. Multiphoton microscopy showed the presence of 5TGM1-DID⁺ tumour cells and 5TGM1-eGFP⁺ tumour colonies in the BM of mice injected with 5TGM1-eGFP-DID cells, 21 days post tumour cell injection. Figure 6.4-11 shows the representative multiphoton microscopy images of naïve, naïve + ZA, 5TGM1 + VEH and 5TGM1 + ZA showing the baseline fluorescent signals.

Results showed no significant difference in the number of 5TGM1-DID⁺ cells per mm³ of BM following pre and post-treatment with ZA when compared with VEH treated control 5TGM1 tumour-bearing mice, 21 days post tumour cell injection (figure 6.4-12 A and B). Interestingly, following pre-treatment with ZA, a significant 48.54 % reduction (VEH vs. ZA; 47.34 ± 6.03 vs. 24.36 ± 0.01 ; P<0.01) in the percentage 5TGM1-eGFP⁺ tumour colonies occupying the BM space (figure 6.4-12 C). However, no significant difference was observed with ZA post-treatment (figure 6.4-12 D). Representative multiphoton microscopy images of the proximal tibia metaphysis following pre or post ZA treatment are shown in figure 6.4-13 A, B, C and D.

In order to determine the effect of ZA treatment on the localisation of 5TGM1-DID⁺ cells in the BM, minimum distance of 5TGM1-DID⁺ cells to the nearest BM was quantitated. Following pre-treatment with ZA, a significant increase in the average minimum distance of 5TGM1-DID⁺ cells when compared to VEH treated 5TGM1 tumour-bearing mice 21 days post tumour cell injection (P<0.001) (figure 6.4-13 E). Strikingly, contradictory results were observed in the post ZA treatment experiment which showed a significant reduction in the average minimum distance of 5TGM1-DID⁺ cells to the nearest bone structure following ZA treatment when compared to VEH treated tumour-bearing mice (P<0.05) (figure 6.4-13 F).

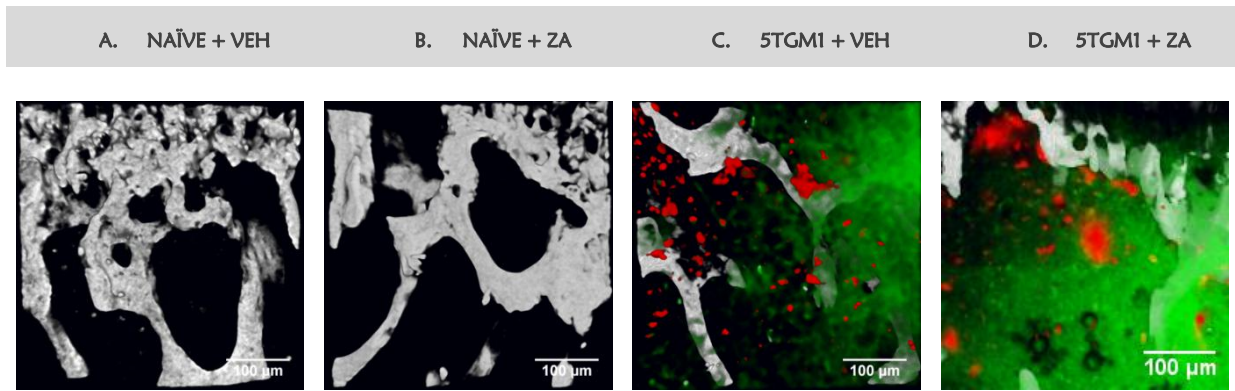


Figure 6.4-11: Multiphoton images of bones showing bone structures DID and eGFP labelling 21 days post tumour cell injection.

Representative 2D multiphoton microscopic images of tibiae ($450 \times 450 \mu\text{m}^2$) of naïve, naïve + ZA, 5TGM1 + VEH and 5TGM1 + ZA showing bone (SHG) DID^+ and eGFP^+ signals 21 days after 5TGM1-eGFP-DID tumour cell injection. Naïve (tumour-free) **(A)** and Naïve treated with ZA **(B)** were used as negative controls to determine baseline fluorescence of bone in order to threshold the images. **(C)** BM of mice injected with 5TGM1-eGFP-DID tumour cells treated with VEH and **(D)** mice injected with 5TGM1-eGFP-DID cells treated with ZA shows the presence of DID^+ 5TGM1 tumour cells (red objects), 5TGM1-eGFP $^+$ (green objects) myeloma colonies in the BM.

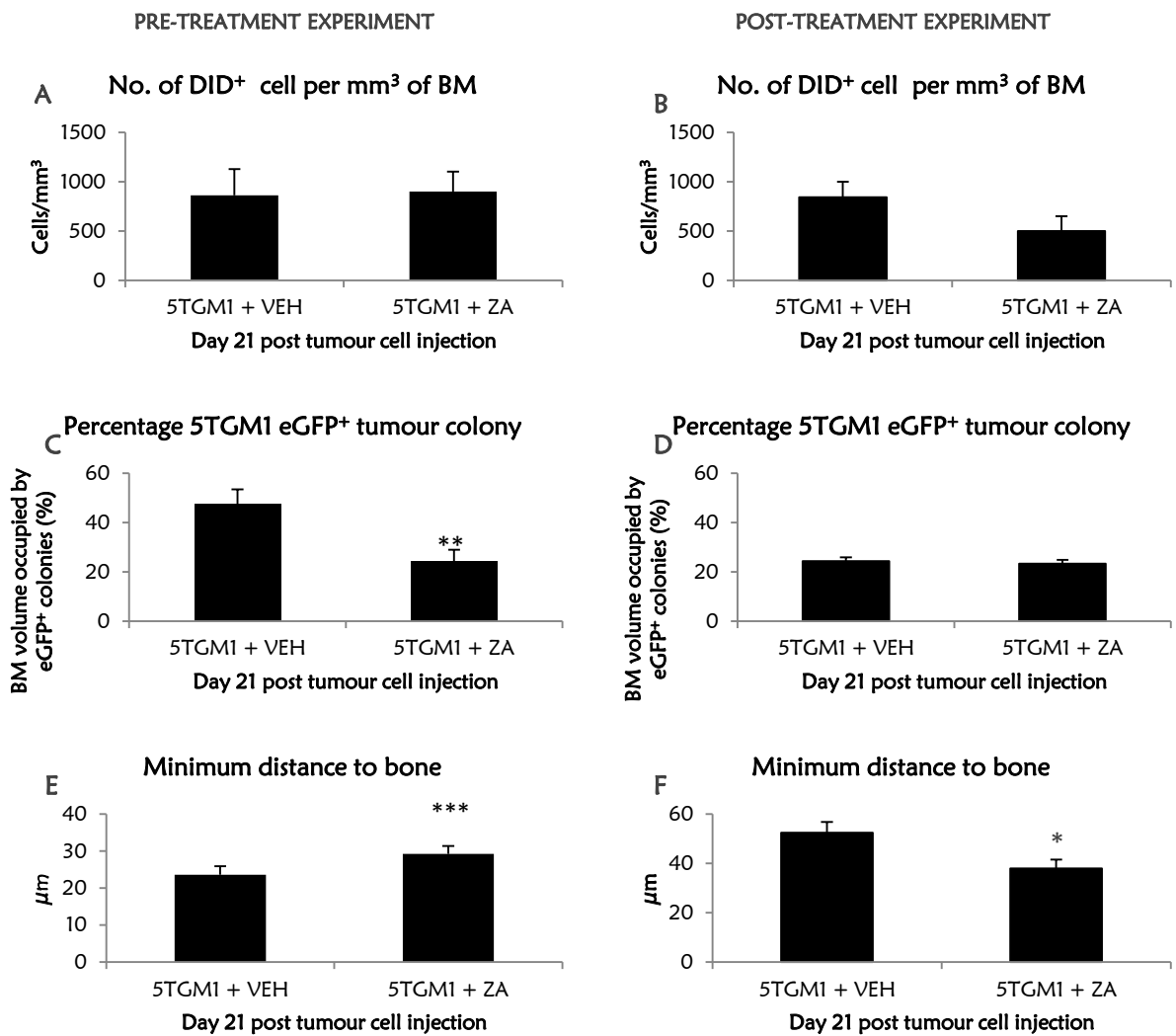


Figure 6.4-12: The effect of ZA on the late stages of myeloma development using multiphoton microscopy.

Changes in number of 5TGM1-DID⁺ per mm³ of BM (A), percentage BM occupied by 5TGM1-eGFP⁺ colonies (C) and the minimum distance (E) of 5TGM1-DID⁺ cells to the nearest bone in the 5TGM1 tumour-bearing mice pre-treated with ZA (n=7) or VEH (n=7) assessed 21 days post tumour cell injection. Tumour-free mice injected with either VEH (n=4) or ZA (n=4) served as controls. Changes in number of 5TGM1-DID⁺ per mm³ of BM (B), percentage BM occupied by 5TGM1-eGFP⁺ colonies (D) and the minimum distance (F) of 5TGM1-DID⁺ cells to the nearest bone in the 5TGM1 tumour-bearing mice post-treated with ZA (n=5) or VEH (n=4) assessed 21 days post tumour cell injection. Tumour-free mice injected with either VEH (n=5) or ZA (n=5) served as controls. A Mann-Whitney non-parametric test was used to compare the statistical difference between the mean in the VEH and the ZA treated groups with P value <0.05 as statistically significant *P<0.05, **P<0.01, ***P<0.001.

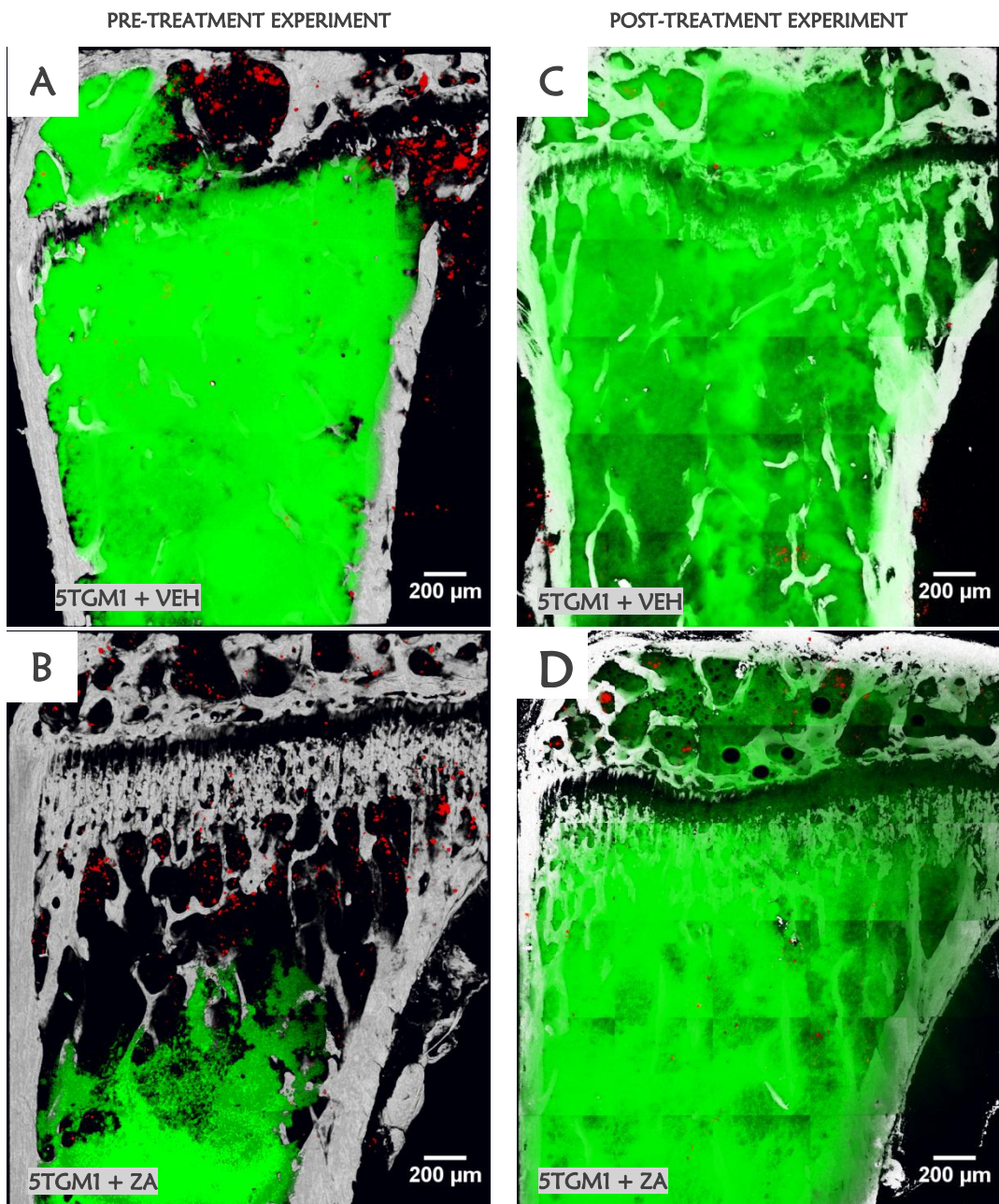


Figure 6.4-13: The effect of ZA pre or post-treatment on 5TGM1 tumour cell colonisation assessed 21 days post tumour cell injection.

Representative multiphoton cross-sectional images of proximal metaphysis of tibia captured by multiphoton microscopy showing bone architecture and 5TGM1-DID⁺ cells (red), 5TGM1-eGFP⁺ (green) myeloma colonies inside the BM following pre or post-treatment with ZA. Comparison of the effect of VEH (A) or ZA (B) initiated prior to tumour cell injection assessed 21 days post tumour cell injection. Comparison of the effect of VEH (B) or ZA (D) treatment initiated after tumour cell injection assessed after 21 days post tumour cell injection.

6.4.3 THE EFFECT OF ZA TREATMENT ON DISEASE-FREE SURVIVAL IN 5TGM1 TUMOUR-BEARING MICE

Result showed that continuous subcutaneous injection of ZA (125 µg/kg) significantly prolonged disease-free survival and delayed the onset of development of hind limb paralysis when compared with VEH treated 5TGM1 tumour-bearing control mice (figure 6.4-14). Interestingly there was no significant change in prolongation of disease-free survival when the ZA treatment was initiated prior or along with the tumour cell injection. Although the degree of delayed onset of morbidity was only 3 days when compared to the VEH treated 5TGM1 tumour-bearing animals, considering the severity and aggressiveness of the disease progression and symptoms development in the 5TGM1 murine model of myeloma and the treatment with ZA at dosages merely at the levels of bone disease management suggests that ZA treatment is responsible for delaying the onset of clinical signs of morbidity.

As all animals were sacrificed at the time of onset of morbidity, survival analysis was not performed due the limitation in the UK Home Office Project Licence Regulation (40/3096) demanding to sacrifice animals at the first sign of illness.

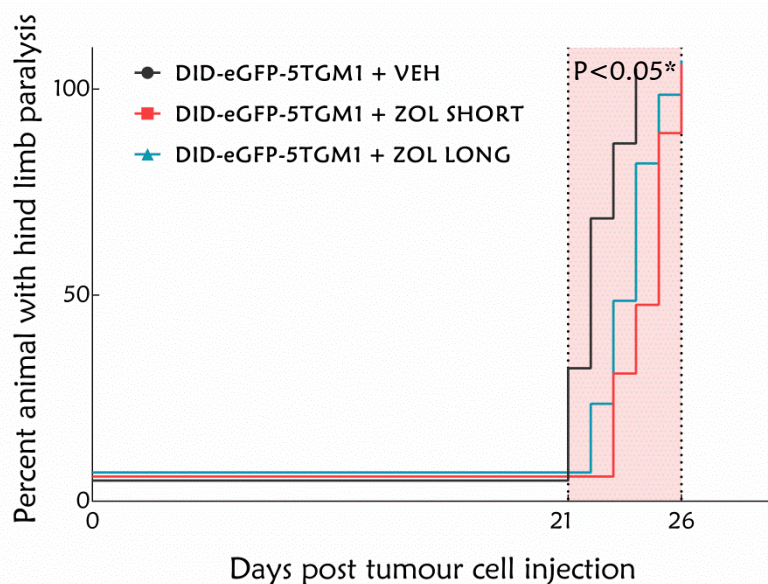


Figure 6.4-14: The effect of ZA treatment on the onset of morbidity.

A Kaplan Meir curve shows the effect of ZA treatment initiated prior to tumour cell injection (ZA LONG; n=11) and treatment initiated along with tumour cell injection (ZOL SHORT; n=11) on the onset of morbidity in the 5TGM1 murine model of myeloma when compared to VEH treated control group (n=11). Log-Rank (Mantel Cox) test was used with P<0.05* as statistically significant.

6.5 DISCUSSION

In this study, an *in vivo* model for myeloma growth in bone was developed by injecting the 5TGM1 murine myeloma cell line via the tail vein of C57BL/KaLwRij mice. This resulted in growth of myeloma cells in the BM, which gradually replaced the normal BM over a period of 21 days post tumour cell injection. Data from the present study showed that the development of 5TGM1 myeloma in the bone was associated with a significant increase in osteoclast numbers, increase in serum TRACP5b levels, reduction in osteoblast numbers, reduction in serum P1NP levels and formation of osteolytic bone lesion. Treatment with ZA either initiated prior to tumour cell homing (pre-treatment) or after tumour cell homing (post-treatment) resulted in significant reduction in both osteoclastic as well as osteoblastic activity with complete prevention of osteolytic bone disease. Results were in agreement with the previous studies where ZA or IBN administration resulted in the prevention of myeloma-induced osteolytic bone disease in the 5T2 and the 5TGM1 murine models of myeloma respectively (Dallas et al 1999; Croucher et al 2003b). Croucher et al (2003b) showed using 5T2MM murine model of myeloma that ZA treatment initiated after serum paraprotein detection only resulted in partial prevention of bone loss whereas ZA treatment initiated along with tumour cell injection resulted in complete prevention of myeloma-induced bone loss. This suggests that myeloma-induced osteoclastic activity begins early and ZA treatment initiated after established disease was not able to fully abrogate the myeloma-induced bone loss (Croucher et al 2003b). From chapter 4, it was clearly shown that until 3 days post tumour cell injection; there were no alterations in the indices of bone remodelling between the 5TGM1 tumour-bearing mice and the tumour-free control groups (figure 4.4-15 and figure 4.4-16). Therefore, in the present study, when ZA treatment was initiated either 7 days prior or 3 days after tumour cell injection, the bone remodelling in the 5TGM1 tumour-bearing mice was similar to the tumour-free control groups. This suggests that, if ZA treatment is initiated before onset of myeloma induced osteoclastic activity, it will completely prevent the development of tumour-induced bone loss.

Data from the current study showed that ZA treatment resulted in the reduction of tumour burden after 21 days post tumour cell injection in the 5TGM1 murine model of myeloma, only if initiated prior to tumour cell injection. The effect of ZA treatment on 5TGM1 tumour burden was assessed using flow cytometry, CD138 IHC and multiphoton microscopy. The data reported here shows that ZA treatment initiated prior to the 5TGM1 tumour cell injection reduced the number of 5TGM1-eGFP⁺ cells (30% reduction by flow cytometry; $P=0.07$) and CD138⁺ colonies in BM (33.13% reduction in tumour burden; $P=0.057$) although these were not statistically significant. However, using the 3D multiphoton microscopic technique, a significant 48.54% ($P<0.01$) reduction in 5TGM1-eGFP⁺ tumour colonies in BM was observed with ZA pre-treatment. The data presented here are in agreement with previous studies reported by Yacoby et al (2002) and Croucher et al (2003b) using ZA in the SCID/hu and 5T2MM murine myeloma models respectively. Interestingly, in the present study, no evidence of reduction of tumour burden was seen when ZA treatment was started after tumour cell homing to

bone. This was contrary to the reports of Croucher et al (2003b) where ZA (120 µg/kg) treatment initiated at the time of tumour cell injection or after detection of serum paraprotein (approx. 8 weeks after tumour cell injection) both resulted in significant reduction in tumour burden. The major difference between present study and the reports of Croucher et al (2003b) is that they used the 5T2MM murine model of myeloma whereas in this study 5TGM1 murine model of myeloma was used.

Data from the present study contradicts the reports of Dallas et al (1999) and Cruz et al (2001) who demonstrated that IBN, another potent BP effectively inhibited the development of osteolytic bone disease but not the tumour burden in the 5TGM1 and ARH77/SCID murine models of myeloma respectively. The differences in the BPs or the murine models used could also be responsible for the observed discrepancies. In both these studies, although IBN treatment was associated with inhibition of osteoclastic activity; there was no evidence of reduction in tumour burden. In both these studies IBN treatment was initiated along with tumour cell injection, unlike in the present study in which ZA treatment was initiated prior to tumour cell injection. This strongly implies that initiation of ZA treatment prior to tumour cell arrival in bone has definitive advantages in reducing the tumour burden during the late stages of disease development. Whether this was due to a direct inhibitory effect on the tumour cells when they home to the BM or an indirect effect mediated by inhibition of osteoclastic bone resorption is not clear from this experiment and warrants further investigation.

It has already been shown in Chapter 4 that a pool of dormant 5TGM1-DID⁺ cells existed in the BM even when the BM was completely replaced with proliferating tumour colonies. Myeloma cells arriving in the BM proliferate to form colonies and replace the entire BM over time. The presence of these subpopulations of dormant cell in BM proximal to the bone suggests that their preferential localisation near bone may play an important role in suppressing their ability to proliferate. Studies have shown that the endosteal niche which is seen adjacent to the trabecular bone plays an important role in maintaining the HSCs in a quiescent state. Whether these dormant 5TGM1-DID⁺ cells have hijacked the HSC niche and whether this mechanism is responsible for the quiescent nature of these cells are not known. Studies on HSCs suggest that osteoblasts are important components of the endosteal niche which maintains the HSCs in a quiescent state (Zhang et al 2003). Furthermore, Iriuchishima et al (2012) also showed that myeloma cells forms complexes with osteoblasts and osteoclasts near the endosteal regions. If the dormant tumour cells seen in this study were hijacking the endosteal niche, then ZA induced ablation of osteoblasts would result in the disruption of the niche, then it would be expected to result in mobilisation of these dormant cells. Contrastingly, Soki et al (2013) showed that ZA treatment was associated with an increase in the endosteal niche with concomitant increase in HSCs in the BM. In this study, ZA treatment was shown to increase the trabecular bone volume which in turn increases the endosteal niche sites in the bone. However, data from the present study showed that ZA treatment initiated pre or post tumour cell injection did not affect the number of these low cycling, persistently DID⁺ labelled 5TGM1 cells seen in the BM. Moreover, when ZA was initiated prior to 5TGM1-eGFP-DID tumour cell injection these cells were seen significantly further away from the bone,

whereas when ZA treatment was initiated after tumour cell injection these cells were seen closer to bone when compared to VEH treated controls (figure 6.4-12 E & F). This suggest that time of initiation of ZA treatment may play a crucial role on the distribution of these dormant myeloma cells inside the BM. The hypoxic nature of the endosteal niche is another factor shown to be responsible for the quiescent nature of the HSC in the endosteal niche (Noll et al 2012). Several studies have shown that ZA is able to inhibit angiogenesis by inhibiting endothelial cell proliferation or by blocking VEGF or FGF (Wood et al 2002). If this was the case, treatment with ZA should have reduced vascularity of the BM and induced more hypoxia, arresting more myeloma cells in a quiescent phase. However, ZA treatment (pre or post treatment experiments) did not modify the number of 5TGM1-DID⁺ cells seen in the BM when compared with VEH treated tumour-bearing controls. Techniques in the identification of dormant tumour cells and their proximity to bone using multiphoton microscopy are at their initial stages and require more studies using three-dimensional perfusion models to better understand the interactions between the myeloma cells and their putative endosteal niche sites.

It is interesting to speculate how pre-treatment with ZA inhibit colony formation but not the number of 5TGM1-DID⁺ cells arriving in the BM. Assuming that the myeloma colonies seen arises from the 5TGM1-DID⁺ cells observed at early time points after injection, ZA pre-treatment would appear to be suppressing the number of specific DID⁺ cells that are activated to form colonies or the survival of these cells. The number of 5TGM1-DID⁺ cells present in BM reduces over 21 days in animals that were studied (figure 4.4-13 A). This could be because some of the 5TGM1-DID⁺ cells were activated to form colonies, but equally this reduction could also represent the loss of cells via apoptosis or movement of these tumour cells out of the BM. The putative myeloma niche could have several roles: it could retain tumour cells in a dormant state in the same way HSCs are held, it could aid in the survival of single MM cells which then adapt to the new environment or it could act as a trap holding cells in the BM. If ZA pre-treatment reduces niche frequency, potential colony forming cells could die or lost and this might provide an explanation for the observed effects on colony formation at later time points.

In the present study, ZA treatment was also shown to prolong disease-free survival in the 5TGM1 murine model of myeloma. In untreated 5TGM1 tumour-bearing mice, the median time for the development of signs of morbidity was 21 days. With ZA treatment initiated 7 days prior to or at the time of tumour cell injection, the median time for the development of hind limb paralysis or sickness was 24 days ($P<0.05$). Similar results were shown by Croucher et al (2003b) in the 5T2MM model using single dose ZA where the median survival was 37 days compared to 35 days in untreated tumour controls. Development of hind limb paralysis is a sign of clinical disease and may reflect the onset of either extramedullary tumour development through vascular channels or collapse compression fracture of the vertebral column leading to spinal cord injury and paralysis. As ZA treatment showed clear evidence of prevention of development of osteolytic bone lesion in the tibia even after 21 days post tumour cell injection, it is less likely that collapse compression of vertebrae may happen at this stage. Therefore, haematogenous spread of the tumour cells to the spinal canal is more likely to be

responsible for the development of hind limb paralysis. This suggests that, the delay in the onset of hind limb paralysis or sickness associated with ZA treatment observed in the present study may be due to ZA induced inhibition of tumour development or spread. The results of the current study contradicts with reports of Dallas et al (1999) and Cruz et al (2001) who showed following IBM administration ($160\mu\text{g}/\text{kg}$) continuously in the 5TGM1 and ARH77/SCID model, although there was inhibition in development of bone disease there was no evidence of delay in the onset of paraplegia or prolongation of survival. This suggests that ZA exert anti-myeloma benefits in the 5TGM1 murine myeloma models in ways other than inhibiting osteoclastic bone resorption. However, the mechanisms are not known yet.

To conclude, the present study evaluated the effects of ZA on late stages of 5TGM1 murine model of myeloma in the absence of other anti-cancer therapeutics in an attempt to evaluate the anti-cancer potentials of the drug. ZA treatment (pre or post) was effective in inhibiting osteoclastic activity and preventing the development of osteolytic bone lesions in the 5TGM1 model, 21 days post tumour cell injection. ZA in a prophylactic strategy was effective in inhibiting myeloma tumour burden within the BM and prolonged disease-free survival.

CHAPTER 7 DISCUSSION

Despite modern advancements in the field of myeloma research, MM still remains incurable with majority of patients relapsing into a more drug-resistant type. With the introduction of high-dose chemotherapy (HDT) and autologous stem cell transplantation (ASCT) in the 1980s, extraordinary increase in survival outcomes have been made when compared to conventional chemotherapies (Durie 2010). Currently, the introduction of newer chemotherapeutic agents such as thalidomide, lenalidomide and bortezomib has resulted in dramatic improvements in the expected OS especially in newly diagnosed young myeloma patients (aged less than 45 years) (Brenner et al 2009). Although currently available treatments are successful in treating the condition in the short-term, they fail to cure the disease, resulting in relapse or refractory myeloma in almost all myeloma patients. Recently, it has been identified that the BM microenvironment plays an important role in the evolution of the disease contributing to proliferation, differentiation, migration, adhesion and chemoresistance of the myeloma tumour cell in the host BM (Manier et al 2012). The BM microenvironment is composed of stromal cells, endothelial cells, immune cells, osteoclasts and osteoblasts which interact with myeloma cells by close cell to cell contact. These interactions between the myeloma cells and the host BM microenvironment are discussed in detail in Chapter 1: Introduction. MM corresponds to the late stage continuum of MGUS, an asymptomatic premalignant phase during which malignant myeloma cells gradually homes, proliferates and replaces the BM with myeloma colonies, interacts with the BM cells and results in signs and symptoms of overt myeloma. It has been shown that myeloma cells reside in BM niches which not only promotes survival and colonisation but also protect these cancer cells against anti-myeloma chemotherapies (Meads et al 2008; Castells et al 2012; Manier et al 2012). There are two important considerations for clinical intervention in MM. Firstly, the presence of a premalignant phase offers a therapeutic window in which altering the BM may hinder early disease progression. Secondly, as myeloma cells were shown to evade treatment by hiding in specific BM niches, making the BM less conducive will result in increasing the susceptibility to the currently available treatments. Currently, research is already focussing on developing novel agents that target not only the cancer cells but also the BM microenvironment in order to completely eradicate tumour cells from the bone.

Work presented in this thesis has used a number of methods. Firstly, the effects of myeloma on bone remodelling during the different stages of disease development in order to determine the sequential development of tumour in bone from a single cell to established colonies over time has been studied. The effect of ZA treatment on the early and late stages of tumour development and the effect of ZA treatment on the onset of morbidity using the 5TGM1 murine model of myeloma has also been studied. As the main aim of thesis was to study the anti-tumour effects of ZA at different stages of myeloma development, initial studies were performed to understand the effects of short-term (125 µg/kg X 2) and continuous (125 µg/kg X 2 weekly, repeated every week) ZA treatment on normal bone remodelling in C57BL/KaLwRij mice (Chapter 3). The study provided strong evidence that ZA treatment, irrespective of whether it was short-term or continuous treatment, inhibited osteoclastic bone resorption and in addition inhibited osteoblastic bone formation. This was in agreement with previous studies where BPs and an anti-RANKL antibody (Denosumab), in addition to suppressing bone

resorption, markedly reduced bone formation (Pozzi et al 2009; Baron et al 2011). It is well established that bone remodelling is a tightly coupled process between bone resorption and formation with cross talk mechanisms between osteoclasts and osteoblasts in order to ensure balanced bone remodelling. Furthermore, it is also well established that osteoclasts regulates several osteoblast stimulating cytokines and the process of bone resorption releases bone matrix derived growth factors such as TGF- β , IGF and BMPs which promote osteoblast differentiation (Baron et al 2011). Therefore, disruption of one arm of the bone remodelling process is expected to alter the other. Moreover, Patntirapong et al (2012) also showed that ZA can directly inhibit osteoblast differentiation and suppress bone mineralisation. Taken together, this suggests that the inhibition of bone formation seen with ZA treatment might be a combined effect of direct ZA mediated cytotoxicity and indirect suppression of osteoclast. Data from the present study also showed that short-term ZA treatment resulted only in temporal and incomplete suppression of bone remodelling, whereas continuous treatment was required to profoundly suppress and maintain inhibition of bone remodelling over time. Chen et al (2002) showed that the anti-resorptive effects of ZA remain active in bone over a period of 28 days, even after a single dose. In contrast, the data presented here shows short-term ZA treatment was associated only with a temporal inhibition followed by a dramatic increase in osteoclast numbers and a thick band of primary spongiosa in the trabecular region parallel to the growth plate after 14 and 21 days post-treatment. Although uninterrupted reduction was seen in serum levels of TRACP5b after 14 and 21 days following the short-term ZA treatment, it only suggested that the osteoclasts were functionally less active and the existence of these elevated numbers of osteoclasts in the trabecular region after 14 and 21 days was the outcome of the short-term treatment. Similar observations were reported by Muderis et al (2007), where cyclical pamidronate treatment in children resulted in abnormal bands of opacities parallel to the growth plate in radiographs suggesting temporary cessation of osteoclastic activity with failure of primary spongiosa resorption following ZA treatment. This might primarily be a consequence of using young animals without skeletal maturity which are in their active phase of bone growth. As the majority of murine models of myeloma use young mice, short-term treatment with BPs will be ineffective in suppressing bone resorption over long-term and therefore a continuous dosage regimen will be required.

Chapter 4 reports the first longitudinal *in vivo* study describing the temporal and spatial development of myeloma in bone over time using the 5TGM1 murine model of myeloma. Work presented here shows the first comprehensive analysis of changes in bone remodelling, development of osteolytic lesions and tumour progression from the time of tumour cell injection to the development of overt myeloma colonies. The study provided strong evidence that tumour-induced changes in bone remodelling begins even before they can be clinically detected. For example, in this study, development of osteolytic bone disease following tumour cell injection was seen as early as 10 days post tumour cell injection. In the previous studies, the development of osteolysis following tumour development were seen only after established clinical disease such as the development of paraplegia or serum paraproteinemia (Alsina et al 1996; Vanderkerken et al 1997; Dallas et al 1999; Croucher et al 2003b). This might be due to the use of less sensitive techniques such as x-rays for the detection of

bone lesions in these studies. Recently, Berenson et al (2009) also showed evidence of bone loss and skeletal deformity in patients with MGUS and these patients might benefit from prophylactic bisphosphonate treatment. In the present study, an increase in osteoclast numbers and serum levels of TRACP5b and a reduction in osteoblast numbers and serum levels of P1NP were evident only during the later stages (day 21) of tumour development. Interestingly, changes in osteoclast and osteoblast numbers following myeloma development were noted only in the cortico-endosteal regions suggesting that bone cells may have heterogeneous responses depending on their location (trabecular or cortical) (Henriksen et al 2011). Bataille et al (1991) showed in myeloma patients, that an increase in both osteoclastic and osteoblastic activity was observed during the early stages of disease and increased osteoclastic but decreased osteoblastic activity was seen during late stages. The data from the present study agrees with the later stages as described by Bataille et al (1991) with increased osteoclastic activity but decreased osteoblastic activity in the 5TGM1 model (day 21). However, during the early stages (day 10) of myeloma development, indices of bone remodelling were similar to tumour-free control mice. This discrepancy might be due to the inherent differences between the myeloma patients and the murine models, especially the time taken for the development of overt myeloma. However, considering the time taken to evolve from MGUS to myeloma in humans, in the 5TGM1 murine model of myeloma which develops in 3 weeks this early asymptomatic stage may represent the MGUS stage in mice.

The thesis also provided evidence that myeloma progression is associated with a strong inhibition of osteoblastic bone formation activity and this may additionally contribute to the development of myeloma bone disease. In particular, the moderate increase in osteoclasts and serum levels of TRACP5b and an almost complete absence of osteoblasts and a reduction in the serum levels of P1NP observed during the later phase of the disease suggests uncoupling of bone remodelling. This was in agreement with the report of Hjorth-Hansen et al (1999) where partial inhibition of osteoclasts and complete absence of osteoblasts were seen in a SCID hu model using the JJN-3 cell line when the mice were sacrificed after the onset of hind-limb paralysis. Tian et al (2003) showed that in patients, myeloma cells produce DKK-1, an inhibitor of osteoblast function by paracrine mechanism. Besides, studies have also shown that myeloma cells inhibit osteoblast formation by suppressing Runx2 (an osteoblast transcription factor) activity in pre-osteoblasts as well as induce osteoblast apoptosis by inducing overexpression of Fas (cell surface death receptor) by the osteoblast (Heider et al 2005).

The present study is also the first comprehensive work to show the longitudinal development of myeloma in bone using the 5TGM1 murine model of myeloma. Previously, assessment of tumour burden in MM was made using indirect measures such as changes in tumour markers (e.g. serum paraprotein), development of spinal injury (morbidity), organ involvement and MRI which were evident only after established or late stage disease (Dallas et al 1999; Croucher et al 2003b; Dairaghi et al 2012). To detect changes in tumour burden following treatment, changes in serum levels of immunoglobulins (paraprotein) are routinely used which has relatively long plasma half-life (approx. 3

weeks). Although, few studies in the past used histomorphometric quantitation of tumour, CD138 IHC or flow cytometry in bone which represented direct measure of tumour burden also had their limitations (Croucher et al 2003b; Fryer et al 2013). For example, using histology although it was possible to identify tumour colonies based on morphology in bone at late stages, identification of single tumour cells during the early stages of myeloma development were impracticable. Likewise, the presence of CD138⁺ normal plasma cells and CD138⁻ myeloma cells in BM complicated the quantitation of tumour burden especially during the early stages of myeloma development using IHC or flow cytometry. Although Oyajobi et al (2007) successfully introduced the technique of direct tumour burden assessment by whole body fluorescence imaging using 5TGM1-eGFP cells, the technique allowed the detection of tumour burden only after established tumour colonies (approximately 2 weeks post tumour cell injection). In the present study, a syngeneic murine myeloma model was developed using 2 X 10⁶ 5TGM1-eGFP-DID labelled myeloma cells injected into the tail vein of immunocompetent C57BL/KaLwRij mice. This model is superior to the previously existing models for a number of reasons. Firstly, in this model, tumour cells were injected via the tail vein and they homed and colonised the BM similar to the human disease. Secondly, the course of the disease development mimicked human disease in which there was a brief asymptomatic phase followed by development of osteolytic bone disease and hind limb paralysis. Thirdly, the model allowed the detection of tumour burden even at a single cell stage by using combinations of methods such as flow cytometry, three-dimensional multiphoton microscopy and CD138 IHC. The ability to visualise the tumour cells in 3D may be useful to understand the complex interactions with the neighbouring BM cells. Finally, the model had a shorter time lag (3 weeks) for tumour development and allowed detection of minor changes in tumour burden which may be beneficial for testing anti-cancer therapy in the future.

Data presented here demonstrated the presence of MM cells in the proximal tibial metaphysis after 3 days post tumour cell injection. Similar observation were seen by Iriuchishima et al (2012) using U266-GFP labelled human myeloma cells in NOG-hMM (NOD/SCID/ γ c^{null}) mice, However, they showed that the myeloma cells were preferentially localised on the endosteal region of the bone whereas in this model the MM cells were randomly distributed throughout the metaphysis. Although flow cytometry and multiphoton microscopy confirmed the presence of MM cells in the BM as early as 3 days post tumour cell injection, CD138 IHC analysis revealed no difference in the number of CD138⁺ cells between 5TGM1 myeloma bearing mice and tumour-free control groups during early time-point (day 3 post tumour cell injection). This suggests that the 5TGM1-eGFP-DID cells present in the BM 3 days post tumour cell injection predominantly could have been CD138⁻ cells. This may be due to either a selective homing of the CD138⁻ cells to the BM or the 5TGM1-eGFP-DID cells injected into the mice could have predominantly been a CD138⁻ population. Zlei et al (2007) showed that during long-term *in vitro* culture of the human myeloma cell lines U266 and L363 resulted in the down regulation of CD138 expression. However, Matsui and colleagues (2004) showed that *in vitro* passaging of human myeloma cell lines such as RPMI 8226 and NCI-H929 contributed a less than 5% CD138⁻ population. This suggests that, in the present study, it is less likely that the 5TGM1-eGFP-DID cells injected to the

mice to be predominantly CD138⁻ population. Moreover, the same group also showed that, CD138⁻ myeloma cells were able to form colonies *in vitro* and engrafted murine long bones whereas CD138⁺ cells were not clonogenic *in vitro* and were incapable of forming tumours in mice. Furthermore, CD138⁻ myeloma cells both *in vitro* or *in vivo* produced CD138⁺ colonies (Matsui et al 2004). This correlated well with the present study, as the 5TGM1-eGFP-DID cells seen in the BM 3 days post tumour cell injection were CD138⁻, but there was an increase in number of single CD138⁺ cells and appearance of CD138⁺ tumour colonies (approx. 0.1% of the BM) in BM 10 days post tumour cell injection. This implicates that during the early stages of myeloma tumourigenesis, there is a selective homing of CD138⁻ tumour cells into the BM, but eventually leads to the development of CD138⁺ tumour colonies formed from these clonogenic CD138⁻ cells in BM in this murine model of myeloma. In agreement, Linlin Xu and colleagues (2013) using NCI-H929 human myeloma cell line reported that although the percentage of CD138⁻ cells (*in vitro*) were less than 4% in culture, there was significantly higher percentage (>50%) of CD138⁻ cells that homed to the BM when injected to NSG mice. Taken together, the data from the present study provides evidence for the preferentially homing of CD138⁻ cells to the BM, although the mechanisms are not known yet.

This study also provided strong evidence supporting the presence of inactive or cytokinetically quiescent tumour cells in BM (persistently DID labelled 5TGM1 cells) even after entire BM was replaced with myeloma colonies. The concept of tumour cell dormancy has been previously shown in a variety of solid tumours such as breast, thyroid and prostate which possibly explains late relapse in some patients declared disease-free (Uhr et al 2011). Several mechanisms were indicated to be responsible for the development of tumour dormancies such as epigenetic alterations in tumour cell, interaction of the tumour cells with the host BM microenvironment, angiogenic switching and anti-tumour immune surveillance (Gelao et al 2013). Evolving evidences suggests that these dormant populations may represent the MM-cancer stem cells (MM-CSC) which are limited in number, quiescent and capable of reinitiating tumour growth (Allan et al 2006). In addition, Matsui et al (2004) also demonstrated the presence of phenotypically heterogeneous populations in both patient myeloma cells and myeloma cell lines. They also showed that the MM-CSCs are a rare population (2 to 5%) of CD138⁻ cells which are highly clonogenic, immature and resemble mature B cells but not plasma cells. On the other hand, the CD138⁺ tumour cells which contributed to the tumour bulk were shown to be unable to form colonies both *in vitro* and *in vivo*. It has already been well established that tumour-host BM interactions play an important role in the propagation of myeloma in the BM. Tumour cells arriving at BM proliferate into overt colonies due to the stimulatory signals released upon close cell-cell contact and production of stimulatory cytokines and chemokines promoting tumour cell growth and tumour associated neovasculogenesis. However, those cells arriving at specific BM niches remains quiescent, especially in the case of the MM-CSCs with their unlimited self-renewal and their stem cell nature which renders them resistant to DNA damaging chemotherapy, making them potential targets responsible for relapse. Moreover, these quiescent MM-CSCs may not be a part of the tumour bulk and therefore could be independent of the tumour associated vascular supply and chemotherapy. Therefore, targeting tumour

angiogenesis might not affect these cells thereby making them resistant to chemotherapy treatments such as doxorubicin, lenalidomide or bortezomib (Naumov et al 2003). Furthermore, in the present study these dormant cells were found closer to the bone surface (endosteal and trabecular) when compared with 5TGM1-DID⁺ cells from earlier time points. It has already been suggested that the cross-talk between tumour cells and the host BM microenvironment may contribute to the quiescent nature of these cells (Gelao et al 2013). Recently studies have shown that MM cells and HSCs express similar cell surface molecules and share common signalling pathways within the BM microenvironment (Noll et al 2012). Quiescence in HSCs are attributed to the relative lower oxygen tension in specific sites within the BM referred to as ‘HSC niches’ which are identified to be closer to bone surface and far away from endothelial vasculature (Kubota et al 2008). Pre-osteoblasts also plays a very important role by β-catenin-N-cadherin complex formation between the osteoblasts and HSCs (Zhang et al 2003). This may suggest that MM-CSCs may hijack the HSC niche owing to the preservation of their stem cell characteristics and might contribute to the tumour re-initiating population. Further studies are required to understand the complex interactions between these quiescent cells and their niche environment especially using three-dimensional perfusion model may give further insights and newer potential targets.

Chapter 5 and 6 are the first novel and comprehensive studies to demonstrate the effects of early ZA treatment initiated 7 days prior (pre-treatment) or 3 days after (post-treatment) tumour cell injection on the early and late stages of tumour development (10 and 21 days post tumour cell injection respectively) in the 5TGM1 murine model of myeloma. Although several *in vivo* studies have previously established the anti-tumour effect of BPs in MM, in these studies treatment was only initiated after established disease similar to clinical scenarios (Dallas et al 1999; Choi et al 2001; Croucher et al 2003b). Even in human clinical trials, the treatment was initiated after the disease had clinical symptoms and the results were often compounded with the simultaneous use of other chemotherapeutic agents. Data from the present study indicates that initiation of ZA treatment prior to the tumour cell injection significantly prevented the early onset of tumour-induced osteolytic bone lesions and significantly inhibited tumour burden at the late stages (day 21) of disease. However, no effect was seen on the early stages (day 10) in this murine model of myeloma. In the other experiment where ZA treatment was initiated 3 days after the tumour cells were injected, although this prevented the early onset of tumour-induced bone disease, it had no effect on tumour burden at either the early or late stages of disease. In contrast to the data reported here, a study on breast cancer bone metastasis showed that ZA treatment either alone or in combination with doxorubicin effectively inhibited early and late tumour formation in bone (Brown 2012). Evolving evidence suggests that in breast cancer bone metastasis there is the development of pre-metastatic niche sites in bone owing to the release of signalling mechanisms from the primary tumour site promoting the homing and colonisation of tumour cells to bone (Kaplan et al 2005). However, in the case of MM, the myeloma cells are derived from malignant transformation of normal plasma cells which normally reside in bone. Therefore, it is probable that myeloma cells home to bone using similar mechanism to their non-malignant

counterparts and thus may be independent of the local changes in bone remodelling. In addition, in chapter 4 it has been clearly shown that the presence of tumour cells in BM at 10 days post tumour cell injection did not alter the bone remodelling which further suggests that tumour development during the early stages is independent of the local changes in bone remodelling. Interestingly, Croucher et al (2003b) reported that ZA treatment initiated at the time of tumour cell injection or after the detection of serum paraprotein (approximately 8 weeks after tumour cell injection) showed substantial reduction in tumour burden in bone in the 5T2MM murine model of myeloma. The reason for discrepancy between these studies may be due to the two different murine models used. Although, the 5T2 and 5TGM1 models evolved in C57BL/KaLwRij mice, the 5T2MM model takes about 3 months to develop compared to 3 weeks for the 5TGM1 model.

The concept of vicious cycle between the myeloma cells and the host BM cells has been of interest in the recent years. Several studies have shown that the myeloma cells interact with the BMSCs and osteoclasts thereby establishing a vicious cycle between myeloma expansion and bone disease (Abe et al 2004; Matsumoto et al 2006; Tanaka et al 2007). Data presented in the current study shows that the effect of ZA on myeloma tumour burden in bone is highly dependent on the time of initiation of treatment. ZA treatment initiated prior to tumour cell injection resulted in a reduction of bone tumour burden whereas treatment initiated after tumour cell injection did not. There could be several reasons to explain this phenomenon. In the pre-treatment experiment, mice received more dose of ZA compared with the post-treatment experiment suggesting that this could be a dosage dependent direct anti-tumour effect. Furthermore, in both these experiments ZA treatment resulted in a similar suppression of both osteoclastic bone resorption and osteoblastic bone formation which raises the possibility that the 5TGM1 model does not depend on the BM microenvironment for development. In agreement, Dallas et al (1999) showed that IBN treatment did not affect the tumour burden in the 5TGM1 model. However, recent reports from Dairaghi et al (2012) showed contrasting evidence that ZA treatment either initiated prior to tumour cell injection or after established disease significantly reduced tumour burden in the 5TGM1 model. However, in these experiments serum Ig levels were used as tumour burden indices which may not be accurate. Several *in vitro* studies have shown that ZA exerts cytotoxic effects on patient myeloma cells and myeloma cell lines (Aparicio et al 1998; Derenne et al 1999; Jagdev et al 2001). In addition, ZA inhibits BMSC mediated release of IL-6 which otherwise promotes myeloma cell growth (Derenne et al 1999). The availability of ZA in bone prior to the arrival of tumour cells may have resulted in a direct cytostatic effect of the tumour cells upon arrival. But, if ZA treatment was introduced after tumour cell homing to the bone, the myeloma cells would have already interacted with the cells of the BM microenvironment thereby evading treatment (Cheung et al 2001; Landowski et al 2003). Furthermore, ZA treatment was shown to inhibit tumour-associated angiogenesis *in vivo* (Croucher et al 2003b). However, the exact mechanism by which ZA exerts this anti-tumour effect only when the animals were treated prior to the homing of myeloma cells in bone is not yet clear and warrants further investigation.

Data from the current study provides strong clinical rationale to support the early use of bone modifying agents such as ZA which may be beneficial for both the prevention of tumour-induced bone disease as well as reduction in tumour burden. The present study showed that ZA treatment significantly extended disease-free survival and was not dependent on whether ZA treatment was initiated prior or at the time of tumour cell injection. Similar results were shown in both *in vivo* preclinical studies and human trials (Croucher et al 2003b; Morgan et al 2010c).

The present study is the first to show that anti-tumour effect of ZA in MM is dependent on the time of initiation of treatment. In this model, it is clearly shown that only ZA treatment initiated prior to tumour cell injection inhibited tumour burden (day 21) whereas treatment initiated after tumour cell injection did not, although both treatment strategies effectively suppressed bone remodelling. Moreover, both treatment strategies did not affect the process of tumour expansion from single cells to the formation of myeloma colonies during the early stages (day 10) of disease. The fact that no reduction in late stage tumour burden, despite effective suppression of osteoclastic bone resorption following ZA treatment, post tumour cell injection shows that the 5TGM1 model may not be dependent of the so called ‘vicious cycle’ for tumour expansion. Therefore, it is evident that the anti-tumour effect observed with ZA (pre-treatment) under this experimental condition is clearly due to the early induction of treatment prior to the tumour cell arrival in bone. However, the mechanisms responsible are not understood from the current experiment. Moreover, in the 5TGM1 model, development of osteolytic disease was seen as early as 10 days without any measurable alterations in bone remodelling such as an increase in osteoclastic bone resorption or a decrease in osteoblastic bone formation. However, it is well established that myeloma induced bone lesions are due to tumour-induced uncoupling of bone remodelling. This suggests that bone histomorphometry and serum levels of bone turn-over markers used in the present study may not have been sensitive enough to detect minor changes in bone remodelling and may need to be investigated further.

Future directions

In this study, the murine model of myeloma was developed by injecting 2×10^6 5TGM1-eGFP-DID cells into young (aged 6-12 weeks) C57BL/KaLwRij mice. The use of young mice in these experiments posed a major setback as MM is primarily a disease of the elderly. Young rodents are frequently used for the development of animal model of bone metastasis owing to high bone remodelling, active blood flow and a tortuous capillary network in the metaphysis of the long bones which promotes tumour cell retention and development (Rosol et al 2003). However, Glick et al (2013) showed that old mice (aged 18-20 months) supported the growth of myeloma better than young mice (aged 2-3 months) using 5T33MM cells injected in to wild type C57BL/6. Moreover, bone remodelling in young is high when compared to older rodents and this difference in the remodelling frequency may very well influence the bioavailability of bone-modifying agents such as ZA. Therefore, using older mice will be a better option for myeloma model development as it will be a better reflection of the clinical scenario with stable bone remodelling as MM is a disease of the elderly.

For the first time, subpopulations of ‘quiescent’ myeloma cells close to bone surfaces were identified during the late stages of tumour development. This suggests that within the BM specific niches exist which may render tumour cells dormant. It will therefore be interesting to characterise the ‘quiescent’ myeloma cells and define the niche they reside in the BM. For this purpose, the quiescent myeloma cells can be separated from the BM by fluorescently activated cell sorting (as the quiescent population were DID labelled) and analysed to determine whether these quiescent cells express cell surface markers similar to the HSC’s and therefore whether they hijack the HSC niches which rendering them in a quiescent state. To test the hypothesis that myeloma cells compete with HSCs to occupy endosteal niches, *in vivo* competitive engraftment assays between the myeloma cells and the HSCs can be performed to determine the cell type that preferentially localises to the BM endosteal niche. (Shiozawa et al 2011). Alternately, as HSC endosteal niches are made up of cells of the early osteoblastic lineage, using a conditional osteoblast knockout mouse (Col2.3 Δ -TK), it would be possible to ablate the osteoblasts and see whether this affects the homing of the myeloma cells to bone. Similar works were performed in a prostate cancer model by Shiozawa et al (2011). Finally, in the present study, it has been clearly shown that the quiescent myeloma cells resided closer to bone. It will be therefore interesting to define the location and components of these niches within the BM. As the cells are DID labelled, immunohistochemical techniques can be used to identify neighbouring cells such as osteoclasts, osteoblasts or HSCs by appropriate fluorophore labelled antibodies. Similar techniques were used by Iriuchishima et al (2012) who showed that myeloma cells form complexes with osteoclasts and osteoblasts in the endosteal region of the long bone.

In this study a novel multiphoton microscopy method was developed to visualise fluorescently tagged myeloma cells in bone. This technique can be further extended to determine whether ZA can directly inhibit myeloma cell growth *in vivo*. Although several studies have shown that ZA directly inhibit myeloma cell growth *in vitro*, whether ZA can be internalised by myeloma cells in bone is not known. Roelofs et al (2010) demonstrated the fluorescently labelled RIS are internalised into bone resorbing osteoclasts. Similar experiments may be helpful to determine whether ZA can be internalised by myeloma cells in the BM.

Finally, this thesis has clearly shown that ZA has anti-myeloma activity in the 5TGM1 murine model of myeloma if initiated prior to tumour cell injection. Previously, results from several preclinical and human clinical trials also suggested that ZA possessed anti-myeloma activity. In clinical scenarios, ZA is used as an adjunct along with standard myeloma chemotherapy. The effect of ZA in combination with other standard chemotherapeutic agents can be tested to see whether a combination treatment will evoke a better anti-tumour response in MGUS.

BIBLIOGRAPHY

- Abe, M., K. Hiura, J. Wilde, et al. (2002). "Role for macrophage inflammatory protein (mip)-1alpha and mip-1beta in the development of osteolytic lesions in multiple myeloma." *Blood* 100(6): 2195-2202.
- Abe, M., K. Hiura, J. Wilde, et al. (2004). "Osteoclasts enhance myeloma cell growth and survival via cell-cell contact: A vicious cycle between bone destruction and myeloma expansion." *Blood* 104(8): 2484-2491.
- Abe, M., S. Kido, M. Hiasa, et al. (2006). "Baff and april as osteoclast-derived survival factors for myeloma cells: A rationale for taci-fc treatment in patients with multiple myeloma." *Leukemia* 20(7): 1313-1315.
- Aiuti, A., I. J. Webb, C. Bleul, et al. (1997). "The chemokine sdf-1 is a chemoattractant for human cd34+ hematopoietic progenitor cells and provides a new mechanism to explain the mobilization of cd34+ progenitors to peripheral blood." *J Exp Med* 185(1): 111-120.
- Al Muderis, M., T. Azzopardi and P. Cundy (2007). "Zebra lines of pamidronate therapy in children." *J Bone Joint Surg Am* 89(7): 1511-1516.
- Allan, A. L., S. A. Vantyghem, A. B. Tuck, et al. (2006). "Tumor dormancy and cancer stem cells: Implications for the biology and treatment of breast cancer metastasis." *Breast Dis* 26: 87-98.
- Alsayed, Y., H. Ngo, J. Runnels, et al. (2007). "Mechanisms of regulation of cxcr4/sdf-1 (cxcl12)-dependent migration and homing in multiple myeloma." *Blood* 109(7): 2708-2717.
- Alsina, M., B. Boyce, R. Devlin, et al. (1996). "Development of an in vivo model of human multiple myeloma bone disease." *Blood* 87(4): 1495-1501.
- Amin, D., S. Cornell, S. Gustafson, et al. (1992). "Bisphosphonates used for the treatment of bone disorders inhibit squalene synthase and cholesterol biosynthesis." *J. Lipid Res.* 33(11): 1657-1663.
- Anderson, K. C. (2011). "New insights into therapeutic targets in myeloma." *ASH Education Program Book* 2011(1): 184-190.
- Aparicio, A., A. Gardner, Y. Tu, et al. (1998). "In vitro cytoreductive effects on multiple myeloma cells induced by bisphosphonates." *Leukemia* 12(2): 220-229.
- Asosingh, K., J. Radl, I. Van Riet, et al. (2000). "The 5tmm series: A useful in vivo mouse model of human multiple myeloma." *Hematol J* 1(5): 351-356.
- Asosingh, K., U. Gunthert, H. De Raeve, et al. (2001). "A unique pathway in the homing of murine multiple myeloma cells: Cd44v10 mediates binding to bone marrow endothelium." *Cancer Res* 61(7): 2862-2865.
- Avilés, A., M. Nambo, N. Neri, et al. (2007). "Antitumor effect of zoledronic acid in previously untreated patients with multiple myeloma." *Medical Oncology* 24(2): 227-230.
- Avilés, A., N. Neri, J. Huerta-Guzman, et al. (2013). "Randomized clinical trial of zoledronic acid in multiple myeloma patients undergoing high-dose chemotherapy and stem-cell transplantation." *Curr Oncol* 20(1): e13-20.

Axelrod, D. (1979). "Carbocyanine dye orientation in red cell membrane studied by microscopic fluorescence polarization." *Biophys J* 26(3): 557-573.

Barille, S., M. Collette, R. Bataille, et al. (1995). "Myeloma cells upregulate interleukin-6 secretion in osteoblastic cells through cell-to-cell contact but downregulate osteocalcin." *Blood* 86(8): 3151-3159.

Barille, S., C. Akhouri, M. Collette, et al. (1997). "Metalloproteinases in multiple myeloma: Production of matrix metalloproteinase-9 (mmp-9), activation of proMMP-2, and induction of MMP-1 by myeloma cells." *Blood* 90(4): 1649-1655.

Baron, R., S. Ferrari and R. G. G. Russell (2011). "Denosumab and bisphosphonates: Different mechanisms of action and effects." *Bone* 48(4): 677-692.

Bataille, R., D. Chappard, C. Marcelli, et al. (1991). "Recruitment of new osteoblasts and osteoclasts is the earliest critical event in the pathogenesis of human multiple myeloma." *J Clin Invest* 88(1): 62-66.

Baulch-Brown, C., T. J. Molloy, S. L. Yeh, et al. (2007). "Inhibitors of the mevalonate pathway as potential therapeutic agents in multiple myeloma." *Leuk Res* 31(3): 341-352.

Becker, N. (2011). "Epidemiology of multiple myeloma." Recent results in cancer research. *Fortschritte der Krebsforschung. Progres dans les recherches sur le cancer* 183: 25-35.

Benford, H. L., N. W. A. McGowan, M. H. Helfrich, et al. (2001). "Visualization of bisphosphonate-induced caspase-3 activity in apoptotic osteoclasts in vitro." *Bone* 28(5): 465-473.

Berardi, S., R. Ria, A. Reale, et al. (2013). "Multiple myeloma macrophages: Pivotal players in the tumor microenvironment." *Journal of Oncology* 2013: 6.

Berenson, J. R., A. Lichtenstein, L. Porter, et al. (1998). "Long-term pamidronate treatment of advanced multiple myeloma patients reduces skeletal events. Myeloma aredia study group." *J Clin Oncol* 16(2): 593-602.

Berenson, J. R., M. A. Dimopoulos and Y.-M. Chen (2006). "Zoledronic acid may improve survival compared to pamidronate in patients with mm and high balg levels: Univariate and multivariate models of hazard ratios." *ASH Annual Meeting Abstracts* 108(11): 3589-.

Berenson, J. R. and O. Yellin (2009). "Monoclonal gammopathy of undetermined significance: Why identification of these patients and assessment of their skeletons is important." *Clin Lymphoma Myeloma* 9(4): 311-315.

Bergstrom, J. D., R. G. Bostedor, P. J. Masarachia, et al. (2000). "Alendronate is a specific, nanomolar inhibitor of farnesyl diphosphate synthase." *Arch Biochem Biophys* 373(1): 231-241.

Blade, J., C. F. de Larrea and L. Rosinol (2012). "Extramedullary involvement in multiple myeloma." *Haematologica* 97(11): 1618-1619.

Boissier, S., S. Magnetto, L. Frappart, et al. (1997). "Bisphosphonates inhibit prostate and breast carcinoma cell adhesion to unmineralized and mineralized bone extracellular matrices." *Cancer Res* 57(18): 3890-3894.

Boissier, S., M. Ferreras, O. Peyruchaud, et al. (2000). "Bisphosphonates inhibit breast and prostate carcinoma cell invasion, an early event in the formation of bone metastases." *Cancer Res* 60(11): 2949-2954.

Brenner, H., A. Gondos and D. Pulte (2009). "Expected long-term survival of patients diagnosed with multiple myeloma in 2006-2010." *Haematologica* 94(2): 270-275.

Brocke-Heidrich, K., A. K. Kretzschmar, G. Pfeifer, et al. (2004). "Interleukin-6-dependent gene expression profiles in multiple myeloma ina-6 cells reveal a bcl-2 family-independent survival pathway closely associated with stat3 activation." *Blood* 103(1): 242-251.

Brown, H. K. (2012). "Tumour cell-bone cell interactions in breast cancer bone metastases; mechanisms and effects of therapies. Unpublished doctoral dissertation university of sheffield."

Buckle, C. H., E. De Leenheer, M. A. Lawson, et al. (2012). "Soluble rank ligand produced by myeloma cells causes generalised bone loss in multiple myeloma." *PLoS One* 7(8): e41127.

Bukowski, J. F., C. T. Morita, H. Band, et al. (1998). "Crucial role of tcr{gamma} chain junctional region in prenyl pyrophosphate antigen recognition by {gamma}{delta} t cells." *Journal of Immunology* 161(1): 286-293.

Capasso, L. L. (2005). "Antiquity of cancer." *International Journal of Cancer* 113(1): 2-13.

Carmeliet, P., L. Moons, R. Lijnen, et al. (1997). "Urokinase-generated plasmin activates matrix metalloproteinases during aneurysm formation." *Nat Genet* 17(4): 439-444.

Castells, M., B. Thibault, J. P. Delord, et al. (2012). "Implication of tumor microenvironment in chemoresistance: Tumor-associated stromal cells protect tumor cells from cell death." *Int J Mol Sci* 13(8): 9545-9571.

Catlett-Falcone, R., T. H. Landowski, M. M. Oshiro, et al. (1999). "Constitutive activation of stat3 signaling confers resistance to apoptosis in human u266 myeloma cells." *Immunity* 10(1): 105-115.

Chatterjee, M., T. Stuhmer, P. Herrmann, et al. (2004). "Combined disruption of both the mek/erk and the il-6r/stat3 pathways is required to induce apoptosis of multiple myeloma cells in the presence of bone marrow stromal cells." *Blood* 104(12): 3712-3721.

Chauhan, D., H. Uchiyama, Y. Akbarali, et al. (1996). "Multiple myeloma cell adhesion-induced interleukin-6 expression in bone marrow stromal cells involves activation of nf-kappa b." *Blood* 87(3): 1104-1112.

Chen, T., J. Berenson, R. Vescio, et al. (2002). "Pharmacokinetics and pharmacodynamics of zoledronic acid in cancer patients with bone metastases." *J Clin Pharmacol* 42(11): 1228-1236.

Cheung, W. C. and B. Van Ness (2001). "The bone marrow stromal microenvironment influences myeloma therapeutic response in vitro." *Leukemia* 15(2): 264-271.

Chim, C. S., R. Pang, T. K. Fung, et al. (2007). "Epigenetic dysregulation of wnt signaling pathway in multiple myeloma." *Leukemia* 21(12): 2527-2536.

Choi, S. J., J. C. Cruz, F. Craig, et al. (2000). "Macrophage inflammatory protein 1-alpha is a potential osteoclast stimulatory factor in multiple myeloma." *Blood* 96(2): 671-675.

Choi, S. J., Y. Oba, Y. Gazitt, et al. (2001). "Antisense inhibition of macrophage inflammatory protein 1-alpha blocks bone destruction in a model of myeloma bone disease." *J Clin Invest* 108(12): 1833-1841.

Cleazardin, P. (2005). "Anti-tumour activity of zoledronic acid." *Cancer Treat Rev* 31 Suppl 3: 1-8.

Cleazardin, P., F. H. Ebetino and P. G. Fournier (2005). "Bisphosphonates and cancer-induced bone disease: Beyond their antiresorptive activity." *Cancer Res* 65(12): 4971-4974.

Compston, J. (2011). "Age-related changes in bone remodelling and structure in men: Histomorphometric studies." *Journal of Osteoporosis Article ID 108324: 4 pages.*

Corso, A., E. Ferretti and M. Lazzarino (2005). "Zoledronic acid exerts its antitumor effect in multiple myeloma interfering with the bone marrow microenvironment." *Hematology* 10(3): 215-224.

Coscia, M., E. Quaglino, M. Iezzi, et al. (2010). "Zoledronic acid repolarizes tumour-associated macrophages and inhibits mammary carcinogenesis by targeting the mevalonate pathway." *Journal of Cellular and Molecular Medicine* 14(12): 2803-2815.

Coxon, F. P., M. H. Helfrich, R. Van't Hof, et al. (2000). "Protein geranylgeranylation is required for osteoclast formation, function, and survival: Inhibition by bisphosphonates and ggti-298." *Journal of Bone and Mineral Research* 15(8).

Coxon, J. P., G. M. Oades, R. S. Kirby, et al. (2004). "Zoledronic acid induces apoptosis and inhibits adhesion to mineralized matrix in prostate cancer cells via inhibition of protein prenylation." *BJU Int* 94(1): 164-170.

Crosgignani, V., A. Dvornikov, J. S. Aguilar, et al. (2012). "Deep tissue fluorescence imaging and in vivo biological applications." *J Biomed Opt* 17(11): 116023.

Croucher, P., S. Jagdev and R. Coleman (2003a). "The anti-tumor potential of zoledronic acid." *Breast* 12 Suppl 2: S30-36.

Croucher, P. I., C. M. Shipman, J. Lippitt, et al. (2001). "Osteoprotegerin inhibits the development of osteolytic bone disease in multiple myeloma." *Blood* 98(13): 3534-3540.

Croucher, P. I., H. De Raeve, M. J. Perry, et al. (2003b). "Zoledronic acid treatment of 5t2mm-bearing mice inhibits the development of myeloma bone disease: Evidence for decreased osteolysis, tumor burden and angiogenesis, and increased survival." *Journal of Bone and Mineral Research* 18(3): 482-492.

Cruz, J. C., M. Alsina, F. Craig, et al. (2001). "Ibandronate decreases bone disease development and osteoclast stimulatory activity in an in vivo model of human myeloma." *Experimental hematology* 29(4): 441-447.

Dabaja, B., F. L. Nasr, G. Y. Chahine, et al. (2004). "Estramustine, zoledronic acid and weekly docetaxel in metastatic androgen independent prostate cancer (maip)." *J Clin Oncol (Meeting Abstracts)* 22(14_suppl): 4706-.

Dairaghi, D. J., B. O. Oyajobi, A. Gupta, et al. (2012). "Ccr1 blockade reduces tumor burden and osteolysis in vivo in a mouse model of myeloma bone disease." *Blood* 120(7): 1449-1457.

Dallas, S. L., I. R. Garrett, B. O. Oyajobi, et al. (1999). "Ibandronate reduces osteolytic lesions but not tumor burden in a murine model of myeloma bone disease." *Blood* 93(5): 1697-1706.

Damaj, G., M. Mohty, N. Vey, et al. (2004). "Features of extramedullary and extraosseous multiple myeloma: A report of 19 patients from a single center." *European Journal Of Haematology* 73(6): 402-406.

Das, H., L. Wang, A. Kamath, et al. (2001). "Vgamma2vdelta2 t-cell receptor-mediated recognition of aminobisphosphonates." *Blood* 98(5): 1616-1618.

Daubiné, F., C. Le Gall, J. Gasser, et al. (2007). "Antitumor effects of clinical dosing regimens of bisphosphonates in experimental breast cancer bone metastasis." *Journal of the National Cancer Institute* 99(4): 322-330.

Deniset-Besseau, A., P. D. S. Peixoto, J. Duboisset, et al. (2010). Nonlinear optical response of the collagen triple helix and second harmonic microscopy of collagen liquid crystals, SPIE.

Denoyelle, C., L. Hong, J. P. Vannier, et al. (2003). "New insights into the actions of bisphosphonate zoledronic acid in breast cancer cells by dual rhoa-dependent and -independent effects." *Br J Cancer* 88(10): 1631-1640.

Derenne, S., M. Amiot, S. Barille, et al. (1999). "Zoledronate is a potent inhibitor of myeloma cell growth and secretion of il-6 and mmp-1 by the tumoral environment." *J Bone Miner Res* 14(12): 2048-2056.

Diel, I. J. (2000). "Antitumour effects of bisphosphonates: First evidence and possible mechanisms." *Drugs* 59(3): 391-399.

Diel, F., N. Gebbia, F. Poccia, et al. (2003). "Induction of gammadelta t-lymphocyte effector functions by bisphosphonate zoledronic acid in cancer patients in vivo." *Blood* 102(6): 2310-2311.

Dittel, B., J. McCarthy, E. Wayner, et al. (1993). "Regulation of human b-cell precursor adhesion to bone marrow stromal cells by cytokines that exert opposing effects on the expression of vascular cell adhesion molecule-1 (vcam-1)." *Blood* 81(9): 2272-2282.

Drach, J., J. Angerler, J. Schuster, et al. (1995). "Interphase fluorescence in situ hybridization identifies chromosomal abnormalities in plasma cells from patients with monoclonal gammopathy of undetermined significance." *Blood* 86(10): 3915-3921.

Dunford, J. E., K. Thompson, F. P. Coxon, et al. (2001). "Structure-activity relationships for inhibition of farnesyl diphosphate synthase in vitro and inhibition of bone resorption in vivo by nitrogen-containing bisphosphonates." *J Pharmacol Exp Ther* 296(2): 235-242.

Durie, B. G. (2010). "Role of new treatment approaches in defining treatment goals in multiple myeloma--the ultimate goal is extended survival." *Cancer Treat Rev* 36 Suppl 2: S18-23.

Erickson, L. D., L. L. Lin, B. Duan, et al. (2003). "A genetic lesion that arrests plasma cell homing to the bone marrow." *Proc Natl Acad Sci U S A* 100(22): 12905-12910.

Fauci , K. D. L., Longo D. L., Braunwald E, Hauser S. L., Jameson J. L and Loscalzo J. (2008). Harrison's internal medicine.

Ferlin, M., N. Noraz, C. Hertogh, et al. (2000). "Insulin-like growth factor induces the survival and proliferation of myeloma cells through an interleukin-6-independent transduction pathway." *British Journal of Haematology* 111(2): 626-634.

Fisch, P., M. Malkovsky, S. Kovats, et al. (1990). "Recognition by human v gamma 9/v delta 2 t cells of a groel homolog on daudi burkitt's lymphoma cells." *Science* 250(4985): 1269-1273.

Fooksman, D. R., T. A. Schwickert, G. D. Victora, et al. (2010). "Development and migration of plasma cells in the mouse lymph node." 33(1): 118-127.

Fournier, P., S. Boissier, S. Filleur, et al. (2002). "Bisphosphonates inhibit angiogenesis in vitro and testosterone-stimulated vascular regrowth in the ventral prostate in castrated rats." *Cancer Res* 62(22): 6538-6544.

Franchimont, N., S. Rydziel and E. Canalis (2000). "Transforming growth factor-[beta] increases interleukin-6 transcripts in osteoblasts." *Bone* 26(3): 249-253.

Fryer, R. A., T. J. Graham, E. M. Smith, et al. (2013). "Characterization of a novel mouse model of multiple myeloma and its use in preclinical therapeutic assessment." *PLoS One* 8(2): e57641.

Fuller, K., C. Murphy, B. Kirstein, et al. (2002). "Tnf{alpha} potently activates osteoclasts, through a direct action independent of and strongly synergistic with rankl." *Endocrinology* 143(3): 1108-1118.

Galson, D., S. D'Souza and G. D. Roodman (2013). Osteoclasts: Potential target for blocking microenvironmental support of myeloma. Advances in biology and therapy of multiple myeloma. N. C. Munshi and K. C. Anderson, Springer New York: 169-185.

Garrett, I. R., S. Dallas, J. Radl, et al. (1997). "A murine model of human myeloma bone disease." Bone 20(6): 515-520.

Gelao, L., C. Criscitiello, L. Fumagalli, et al. (2013). "Tumour dormancy and clinical implications in breast cancer." Ecancermedicalscience 7: 320.

Giuliani, N., R. Bataille, C. Mancini, et al. (2001). "Myeloma cells induce imbalance in the osteoprotegerin/osteoprotegerin ligand system in the human bone marrow environment." Blood 98(13): 3527-3533.

Giuliani, N., S. Colla, F. Morandi, et al. (2005). "Myeloma cells block runx2/cbfa1 activity in human bone marrow osteoblast progenitors and inhibit osteoblast formation and differentiation." Blood 106(7): 2472-2483.

Giuliani, N., F. Morandi, S. Tagliaferri, et al. (2006a). "Interleukin-3 (il-3) is overexpressed by t lymphocytes in multiple myeloma patients." Blood 107(2): 841-842.

Giuliani, N., V. Rizzoli and G. D. Roodman (2006b). "Multiple myeloma bone disease: Pathophysiology of osteoblast inhibition." Blood 108(13): 3992-3996.

Glass Li, D. A., P. Bialek, J. D. Ahn, et al. (2005). "Canonical wnt signaling in differentiated osteoblasts controls osteoclast differentiation." Developmental Cell 8(5): 751-764.

Glick, A., Y. Song, B. Hwang, et al. (2013). "Age matters: Young t lymphocytes offer better protection from myeloma proliferation." Immunity & Ageing 10(1): 1-9.

Gnant, M., B. Mlinaritsch, H. Stoeger, et al. (2010). "Mature results from abcsg-12: Adjuvant ovarian suppression combined with tamoxifen or anastrozole, alone or in combination with zoledronic acid, in premenopausal women with endocrine-responsive early breast cancer." J Clin Oncol (Meeting Abstracts) 28(15_suppl): 533-.

Green, J. R. (2003). "Antitumor effects of bisphosphonates." Cancer 97(S3): 840-847.

Green, J. R. (2005). "Zoledronic acid: Pharmacologic profile of a potent bisphosphonate." Journal of Organometallic Chemistry 690(10): 2439-2448.

Guenther, A., S. Gordon, M. Tiemann, et al. (2010). "The bisphosphonate zoledronic acid has antimyeloma activity in vivo by inhibition of protein prenylation." Int J Cancer 126(1): 239-246.

Gupta, D., S. P. Treon, Y. Shima, et al. (2001). "Adherence of multiple myeloma cells to bone marrow stromal cells upregulates vascular endothelial growth factor secretion: Therapeutic applications." Leukemia 15(12): 1950-1961.

Gutierrez, N. C., R. Garcia-Sanz and J. F. San Miguel (2007). "Molecular biology of myeloma." Clin Transl Oncol 9(10): 618-624.

Haas, W., P. Pereira and S. Tonegawa (1993). "Gamma/delta cells." Annual Review of Immunology 11(1): 637-685.

Halleen, J. M., S. L. Tiitinen, H. Ylipahkala, et al. (2006). "Tartrate-resistant acid phosphatase 5b (tracp 5b) as a marker of bone resorption." Clin Lab 52(9-10): 499-509.

Hallek, M., P. L. Bergsagel and K. C. Anderson (1998). "Multiple myeloma: Increasing evidence for a multistep transformation process." Blood 91(1): 3-21.

Hecht, M., I. von Metzler, K. Sack, et al. (2008). "Interactions of myeloma cells with osteoclasts promote tumour expansion and bone degradation through activation of a complex signalling network and upregulation of cathepsin k, matrix metalloproteinases (mmps) and urokinase plasminogen activator (upa)." *Exp Cell Res* 314(5): 1082-1093.

Heider, U., I. Zavrski, C. Jakob, et al. (2004). "Expression of receptor activator of nf-?B ligand (rankl) mrna in human multiple myeloma cells." *Journal of Cancer Research and Clinical Oncology* 130(8): 469-474.

Heider, U., L. C. Hofbauer, I. Zavrski, et al. (2005). "Novel aspects of osteoclast activation and osteoblast inhibition in myeloma bone disease." *Biochemical and Biophysical Research Communications* 338(2): 687-693.

Henriksen, K., M. Karsdal, J.-M. Delaissé, et al. (2003). "Rankl and vascular endothelial growth factor (vegf) induce osteoclast chemotaxis through an erk1/2-dependent mechanism." *Journal of Biological Chemistry* 278(49): 48745-48753.

Henriksen, K., J. Bollerslev, V. Everts, et al. (2011). "Osteoclast activity and subtypes as a function of physiology and pathology--implications for future treatments of osteoporosis." *Endocr Rev* 32(1): 31-63.

Hideshima, T., N. Nakamura, D. Chauhan, et al. (2001). "Biologic sequelae of interleukin-6 induced pi3-k/akt signaling in multiple myeloma." *Oncogene* 20(42): 5991-6000.

Hideshima, T., C. Mitsiades, G. Tonon, et al. (2007). "Understanding multiple myeloma pathogenesis in the bone marrow to identify new therapeutic targets." *Nat Rev Cancer* 7(8): 585-598.

Hjertner, Ö., G. Qvigstad, H. Hjorth-Hansen, et al. (2000). "Expression of urokinase plasminogen activator and the urokinase plasminogen activator receptor in myeloma cells." *British Journal of Haematology* 109(4): 815-822.

Hjorth-Hansen, H., M. F. Seifert, M. Borset, et al. (1999). "Marked osteoblastopenia and reduced bone formation in a model of multiple myeloma bone disease in severe combined immunodeficiency mice." *J Bone Miner Res* 14(2): 256-263.

Hobbs, J. R. (1969). "Immunochemical classes of myelomatosis. Including data from a therapeutic trial conducted by a medical research council working party*." *British Journal of Haematology* 16(6): 599-606.

Horie, N., H. Murata, S. Kimura, et al. (2007). "Combined effects of a third-generation bisphosphonate, zoledronic acid with other anticancer agents against murine osteosarcoma." *Br J Cancer* 96(2): 255-261.

Iguchi, T., Y. Miyakawa, K. Yamamoto, et al. (2003). "Nitrogen-containing bisphosphonates induce s-phase cell cycle arrest and apoptosis of myeloma cells by activating mapk pathway and inhibiting mevalonate pathway." *Cell Signal* 15(7): 719-727.

InternationalMyelomaWorkingGroup (2003). "Criteria for the classification of monoclonal gammopathies, multiple myeloma and related disorders." *Br J Haematol* 121(5): 749-757.

Iqbal, J., L. Sun, J. I. Mechanick, et al. (2011). "Anti-cancer actions of denosumab." *Curr Osteoporos Rep* 9(4): 173-176.

Iriuchishima, H., K. Takubo, Y. Miyakawa, et al. (2012). "Neovascular niche for human myeloma cells in immunodeficient mouse bone." *PLoS One* 7(2): e30557.

Jagdev, S. P., R. E. Coleman, C. M. Shipman, et al. (2001). "The bisphosphonate, zoledronic acid, induces apoptosis of breast cancer cells: Evidence for synergy with paclitaxel." *Br J Cancer* 84(8): 1126-1134.

Kaisho, T., J. Ishikawa, K. Oritani, et al. (1994). "Bst-1, a surface molecule of bone marrow stromal cell lines that facilitates pre-b-cell growth." *Proc Natl Acad Sci U S A* 91(12): 5325-5329.

Kaplan, R. N., R. D. Riba, S. Zacharoulis, et al. (2005). "Vegfr1-positive haematopoietic bone marrow progenitors initiate the pre-metastatic niche." *Nature* 438(7069): 820-827.

Kawabata, K., M. Ujikawa, T. Egawa, et al. (1999). "A cell-autonomous requirement for cxcr4 in long-term lymphoid and myeloid reconstitution." *Proc Natl Acad Sci U S A* 96(10): 5663-5667.

Kawano, M., T. Hirano, T. Matsuda, et al. (1988). "Autocrine generation and requirement of bsf-2/il-6 for human multiple myelomas." *Nature* 332(6159): 83-85.

Khokher, M. A. and P. Dandona (1989). "Diphosphonates inhibit human osteoblast secretion and proliferation." *Metabolism-Clinical and Experimental* 38(2).

Kim, J., R. A. Denu, B. A. Dollar, et al. (2012). "Macrophages and mesenchymal stromal cells support survival and proliferation of multiple myeloma cells." *British Journal of Haematology* 158(3): 336-346.

Klein, B. Y., H. Ben-Bassat, E. Breuer, et al. (1998). "Structurally different bisphosphonates exert opposing effects on alkaline phosphatase and mineralization in marrow osteoprogenitors." *J Cell Biochem* 68(2): 186-194.

Koenig, J., C. Ballantyne, A. Kumar, et al. (2002). "Vascular cell adhesion molecule-1 expression and hematopoietic supportive capacity of immortalized murine stromal cell lines derived from fetal liver and adult bone marrow." *In Vitro Cellular & Developmental Biology - Animal* 38(9): 538-543.

Komori, T. (2010). Regulation of osteoblast differentiation by runx2. *Osteoimmunology*. Y. Choi, Springer US. 658: 43-49.

Kong, Y.-Y., H. Yoshida, I. Sarosi, et al. (1999). "Opgl is a key regulator of osteoclastogenesis, lymphocyte development and lymph-node organogenesis." *Nature* 397(6717): 315-323.

Kubagawa, H., L. B. Vogler, J. D. Capra, et al. (1979). "Studies on the clonal origin of multiple myeloma. Use of individually specific (idiotype) antibodies to trace the oncogenic event to its earliest point of expression in b-cell differentiation." *The Journal of Experimental Medicine* 150(4): 792-807.

Kubista, B., K. Trieb, F. Sevelda, et al. (2006). "Anticancer effects of zoledronic acid against human osteosarcoma cells." *J Orthop Res* 24(6): 1145-1152.

Kubota, Y., K. Takubo and T. Suda (2008). "Bone marrow long label-retaining cells reside in the sinusoidal hypoxic niche." *Biochem Biophys Res Commun* 366(2): 335-339.

Kunzmann, V., E. Bauer, J. Feurle, et al. (2000). "Stimulation of gammadelta t cells by aminobisphosphonates and induction of antiplasma cell activity in multiple myeloma." *Blood* 96(2): 384-392.

Kyle, R. A., G. C. Yee, M. R. Somerfield, et al. (2007). "American society of clinical oncology 2007 clinical practice guideline update on the role of bisphosphonates in multiple myeloma." *Journal of Clinical Oncology* 25(17): 2464-2472.

Lacey, D. L., E. Timms, H. L. Tan, et al. (1998). "Osteoprotegerin ligand is a cytokine that regulates osteoclast differentiation and activation." *Cell* 93(2): 165-176.

Lacy, M. Q., A. Dispenzieri, M. A. Gertz, et al. (2006). "Mayo clinic consensus statement for the use of bisphosphonates in multiple myeloma." Mayo Clin Proc 81(8): 1047-1053.

Landowski, T. H., N. E. Olashaw, D. Agrawal, et al. (2003). "Cell adhesion-mediated drug resistance (cam-dr) is associated with activation of nf-[kappa]b (relb//p50) in myeloma cells." Oncogene 22(16): 2417-2421.

Lee, J. W., H. Y. Chung, L. A. Ehrlich, et al. (2004). "IL-3 expression by myeloma cells increases both osteoclast formation and growth of myeloma cells." Blood 103(6): 2308-2315.

Lee, M. V., E. M. Fong, F. R. Singer, et al. (2001). "Bisphosphonate treatment inhibits the growth of prostate cancer cells." Cancer Res 61(6): 2602-2608.

Libouban, H., M.-F. Moreau, M. F. Baslé, et al. (2003). "Increased bone remodeling due to ovariectomy dramatically increases tumoral growth in the 5t2 multiple myeloma mouse model." Bone 33(3): 283-292.

Lijnen, H. R., B. Van Hoef, F. Lupu, et al. (1998). "Function of the plasminogen/plasmin and matrix metalloproteinase systems after vascular injury in mice with targeted inactivation of fibrinolytic system genes." Arterioscler Thromb Vasc Biol 18(7): 1035-1045.

Linlin Xu, C. M., Hao Wu, Bradley Poteat, Colin D. Crean, Angelo A. Cardoso, John M Chirgwin, Helmut Hanenberg, Khalid S. Mohammad, Attaya Suvannasankha, and Edward F Srour. (2013). "Role of cd166 in multiple myeloma cell homing to the bone marrow microenvironment and disease progression." 2013 ASH Annual Meeting and Exposition.

Lopez-Anglada, L., N. C. Gutierrez, J. L. Garcia, et al. (2010). "P53 deletion may drive the clinical evolution and treatment response in multiple myeloma." Eur J Haematol 84(4): 359-361.

Luckman, S. P., D. E. Hughes, F. P. Coxon, et al. (1998). "Nitrogen-containing bisphosphonates inhibit the mevalonate pathway and prevent post-translational prenylation of gtp-binding proteins, including ras." J Bone Miner Res 13(4): 581-589.

Magnetto, S., S. Boissier, P. D. Delmas, et al. (1999). "Additive antitumor activities of taxoids in combination with the bisphosphonate ibandronate against invasion and adhesion of human breast carcinoma cells to bone." Int J Cancer 83(2): 263-269.

Manier, S., A. Sacco, X. Leleu, et al. (2012). "Bone marrow microenvironment in multiple myeloma progression." Journal of Biomedicine and Biotechnology 2012: 5.

Mariani, S., M. Muraro, F. Pantaleoni, et al. (2005). "Effector [gamma][delta] t cells and tumor cells as immune targets of zoledronic acid in multiple myeloma." Leukemia 19(4): 664-670.

Masarachia, P., M. Weinreb, R. Balena, et al. (1996). "Comparison of the distribution of 3h-alendronate and 3h-etidronate in rat and mouse bones." Bone 19(3): 281-290.

Massaia, M., S. Mariani, F. Pantaleoni, et al. (2009). Direct and indirect antitumor activity of zoledronic acid, Hematology Meeting Reports.

Mateos, M.-V., M.-T. Hernández, P. Giraldo, et al. (2013). "Lenalidomide plus dexamethasone for high-risk smoldering multiple myeloma." New England Journal of Medicine 369(5): 438-447.

Matsui, W., C. A. Huff, Q. Wang, et al. (2004). "Characterization of clonogenic multiple myeloma cells." Blood 103(6): 2332-2336.

Matsumoto, T. and M. Abe (2006). "Myeloma-bone interaction: A vicious cycle." IBMS BoneKEy 3(3): 8-14.

McCloskey, E. V., I. C. MacLennan, M. T. Drayson, et al. (1998). "A randomized trial of the effect of clodronate on skeletal morbidity in multiple myeloma. Mrc working party on leukaemia in adults." Br J Haematol 100(2): 317-325.

Meads, M. B., L. A. Hazlehurst and W. S. Dalton (2008). "The bone marrow microenvironment as a tumor sanctuary and contributor to drug resistance." Clin Cancer Res 14(9): 2519-2526.

Menu, E., K. Asosingh, I. Van Riet, et al. (2004). "Myeloma cells (5tmm) and their interactions with the marrow microenvironment." Blood Cells, Molecules, and Diseases 33(2): 111-119.

Mhaskar, R., J. Redzepovic, K. Wheatley, et al. (2012). "Bisphosphonates in multiple myeloma: A network meta-analysis." Cochrane Database Syst Rev 5: CD003188.

Michigami, T., N. Shimizu, P. J. Williams, et al. (2000). "Cell-cell contact between marrow stromal cells and myeloma cells via vcam-1 and $\alpha 4\beta 1$ -integrin enhances production of osteoclast-stimulating activity." Blood 96(5): 1953-1960.

Mitsiades, C. S., D. W. McMillin, S. Klipper, et al. (2007). "The role of the bone marrow microenvironment in the pathophysiology of myeloma and its significance in the development of more effective therapies." Hematology/Oncology Clinics of North America 21(6): 1007-1034.

Mohan, S. and D. J. Baylink (1991). "Bone growth factors." Clin Orthop Relat Res(263): 30-48.

Monkkonen, H., S. Auriola, P. Lehenkari, et al. (2006). "A new endogenous atp analog (appi) inhibits the mitochondrial adenine nucleotide translocase (ant) and is responsible for the apoptosis induced by nitrogen-containing bisphosphonates." Br J Pharmacol 147(4): 437-445.

Mönkkönen, H., P. D. Ottewell, J. Kuokkanen, et al. (2007). "Zoledronic acid-induced ipp/appi production in vivo." Life Sciences 81(13): 1066-1070.

Moreau, M. F., C. Guillet, P. Massin, et al. (2007). "Comparative effects of five bisphosphonates on apoptosis of macrophage cells in vitro." Biochem Pharmacol 73(5): 718-723.

Moreaux, J., E. Legouffe, E. Jourdan, et al. (2004). "Baff and april protect myeloma cells from apoptosis induced by interleukin 6 deprivation and dexamethasone." Blood 103(8): 3148-3157.

Morgan, G., F. Davies, W. Gregory, et al. (2010a). "Evaluating the effects of zoledronic acid (zol) on overall survival (os) in patients (pts) with multiple myeloma (mm): Results of the medical research council (mrc) myeloma ix study." J Clin Oncol (Meeting Abstracts) 28(15_suppl): 8021-.

Morgan, G. and A. Lipton (2010b). "Antitumor effects and anticancer applications of bisphosphonates." Semin Oncol 37 Suppl 2: S30-40.

Morgan, G. J., F. E. Davies, W. M. Gregory, et al. (2010c). "First-line treatment with zoledronic acid as compared with clodronic acid in multiple myeloma (mrc myeloma ix): A randomised controlled trial." The Lancet 376(9757): 1989-1999.

Musto, P., M. T. Petrucci, S. Bringhen, et al. (2008). "A multicenter, randomized clinical trial comparing zoledronic acid versus observation in patients with asymptomatic myeloma." Cancer 113(7): 1588-1595.

Mystakidou, K., E. Katsouda, E. Parpa, et al. (2005). "Randomized, open label, prospective study on the effect of zoledronic acid on the prevention of bone metastases in patients with recurrent solid tumors that did not present with bone metastases at baseline." Medical Oncology 22(2): 195-201.

Naumov, G. N., J. L. Townson, I. C. MacDonald, et al. (2003). "Ineffectiveness of doxorubicin treatment on solitary dormant mammary carcinoma cells or late-developing metastases." Breast Cancer Res Treat 82(3): 199-206.

Noel, A., C. Gilles, K. Bajou, et al. (1997). "Emerging roles for proteinases in cancer." *Invasion Metastasis* 17(5): 221-239.

Noll, J. E., S. A. Williams, L. E. Purton, et al. (2012). "Tug of war in the haematopoietic stem cell niche: Do myeloma plasma cells compete for the hsc niche[quest]." *Blood Cancer Journal* 2: e91.

Nordahl, J., G. Andersson and F. P. Reinholt (1998). "Chondroclasts and osteoclasts in bones of young rats: Comparison of ultrastructural and functional features." *Calcif Tissue Int* 63(5): 401-408.

Nyangoga, H., S. Blouin, H. Libouban, et al. (2010). "A single pretreatment by zoledronic acid converts metastases from osteolytic to osteoblastic in the rat." *Microsc Res Tech* 73(8): 733-740.

Ogata, A., D. Chauhan, G. Teoh, et al. (1997). "Il-6 triggers cell growth via the ras-dependent mitogen-activated protein kinase cascade." *Journal of Immunology* 159(5): 2212-2221.

Oshima, T., M. Abe, J. Asano, et al. (2005). "Myeloma cells suppress bone formation by secreting a soluble wnt inhibitor, sfrp-2." *Blood* 106(9): 3160-3165.

Oyajobi, B. O., G. Franchin, P. J. Williams, et al. (2003). "Dual effects of macrophage inflammatory protein-1alpha on osteolysis and tumor burden in the murine 5tgm1 model of myeloma bone disease." *Blood* 102(1): 311-319.

Oyajobi, B. O., S. Muñoz, R. Kakonen, et al. (2007). "Detection of myeloma in skeleton of mice by whole-body optical fluorescence imaging." *Molecular Cancer Therapeutics* 6(6): 1701-1708.

Pan, B., A. N. Farrugia, L. B. To, et al. (2004). "The nitrogen-containing bisphosphonate, zoledronic acid, influences rankl expression in human osteoblast-like cells by activating tnf-alpha converting enzyme (tace)." *J Bone Miner Res* 19(1): 147-154.

Papapoulos, S. E. (2006). "Bisphosphonate actions: Physical chemistry revisited." *Bone* 38(5): 613-616.

Parfitt, A. M., M. K. Drezner, F. H. Glorieux, et al. (1987). "Bone histomorphometry: Standardization of nomenclature, symbols, and units. Report of the asbmr histomorphometry nomenclature committee." *J Bone Miner Res* 2(6): 595-610.

Parmo-Cabañas, M., R. A. Bartolomé, N. Wright, et al. (2004). "Integrin [alpha]4[beta]1 involvement in stromal cell-derived factor-1[alpha]-promoted myeloma cell transendothelial migration and adhesion: Role of camp and the actin cytoskeleton in adhesion." *Experimental Cell Research* 294(2): 571-580.

Parmo-Cabañas, M., I. Molina-Ortiz, S. Matías-Román, et al. (2006). "Role of metalloproteinases mmp-9 and mt1-mmp in cxcl12-promoted myeloma cell invasion across basement membranes." *The Journal of Pathology* 208(1): 108-118.

Patntirapong, S., W. Singhatanadgit, C. Chanruangvanit, et al. (2012). Zoledronic acid suppresses mineralization through direct cytotoxicity and osteoblast differentiation inhibition.

Pearse, R. N., E. M. Sordillo, S. Yaccoby, et al. (2001). "Multiple myeloma disrupts the trance/osteoprotegerin cytokine axis to trigger bone destruction and promote tumor progression." *Proceedings of the National Academy of Sciences of the United States of America* 98(20): 11581-11586.

Ping Wu, F. E. D., Kevin Boyd, Karen Thomas, Sharon Dines, Radovan M. Saso, Mike N. Potter, Mark E. Ethell, Bronwen E. Shaw & Gareth J. Morgan (2009). "The impact of extramedullary disease at presentation on the outcome of myeloma." *Leukemia & Lymphoma* 50(2): 230-235.

Pozzi, S., S. Vallet, S. Mukherjee, et al. (2009). "High-dose zoledronic acid impacts bone remodeling with effects on osteoblastic lineage and bone mechanical properties." *Clinical Cancer Research* 15(18): 5829-5839.

Qiang, Y. W., Y. Chen, O. Stephens, et al. (2008). "Myeloma-derived dickkopf-1 disrupts wnt-regulated osteoprotegerin and rankl production by osteoblasts: A potential mechanism underlying osteolytic bone lesions in multiple myeloma." *Blood* 112(1): 196-207.

Radl, J., C. F. Hollander, P. van den Berg, et al. (1978). "Idiopathic paraproteinaemia. I. Studies in an animal model--the ageing c57bl/kalwrij mouse." *Clin Exp Immunol* 33(3): 395-402.

Raggatt, L. J. and N. C. Partridge (2010). "Cellular and molecular mechanisms of bone remodeling." *Journal of Biological Chemistry* 285(33): 25103-25108.

Rajkumar, S. V., M. A. Gertz, M. Q. Lacy, et al. (2003). "Thalidomide as initial therapy for early-stage myeloma." *Leukemia* 17(4): 775-779.

Rajkumar, S. V. (2005). "Mgus and smoldering multiple myeloma: Update on pathogenesis, natural history, and management." *ASH Education Program Book* 2005(1): 340-345.

Reinholz, G. G., B. Getz, L. Pederson, et al. (2000). "Bisphosphonates directly regulate cell proliferation, differentiation, and gene expression in human osteoblasts." *Cancer Research* 60(21).

Reszka, A. A. and G. A. Rodan (2003). "Mechanism of action of bisphosphonates." *Curr Osteoporos Rep* 1(2): 45-52.

Ria, R., A. M. Roccaro, F. Merchionne, et al. (2003). "Vascular endothelial growth factor and its receptors in multiple myeloma." *Leukemia* 17(10): 1961-1966.

Ribatti, D., B. Nico, D. Mangieri, et al. (2007). "Neridronate inhibits angiogenesis in vitro and in vivo." *Clinical Rheumatology* 26(7): 1094-1098.

Roelofs, A. J., F. P. Coxon, F. H. Ebetino, et al. (2010). "Fluorescent risedronate analogues reveal bisphosphonate uptake by bone marrow monocytes and localization around osteocytes in vivo." *J Bone Miner Res* 25(3): 606-616.

Rogers, M. J., J. C. Frith, S. P. Luckman, et al. (1999). "Molecular mechanisms of action of bisphosphonates." *Bone* 24(5, Supplement 1): 73S-79S.

Rogers, M. J., S. Gordon, H. L. Benford, et al. (2000). "Cellular and molecular mechanisms of action of bisphosphonates." *Cancer* 88(S12): 2961-2978.

Roodman, G. D. (2001). "Biology of osteoclast activation in cancer." *Journal of Clinical Oncology* 19(15).

Roodman, G. D. (2011). "Osteoblast function in myeloma." *Bone* 48(1): 135-140.

Rosol, T. J., S. H. Tannehill-Gregg, B. E. LeRoy, et al. (2003). "Animal models of bone metastasis." *Cancer* 97(S3): 748-757.

Rozemuller, H., E. van der Spek, L. H. Bogers-Boer, et al. (2008). "A bioluminescence imaging based in vivo model for preclinical testing of novel cellular immunotherapy strategies to improve the graft-versus-myeloma effect." *Haematologica* 93(7): 1049-1057.

Russell, R. G., N. B. Watts, F. H. Ebetino, et al. (2008). "Mechanisms of action of bisphosphonates: Similarities and differences and their potential influence on clinical efficacy." *Osteoporos Int* 19(6): 733-759.

Saad, F. (2008). "New research findings on zoledronic acid: Survival, pain, and anti-tumour effects." *Cancer Treat Rev* 34(2): 183-192.

Santini, D., B. Vincenzi, G. Avvisati, et al. (2002). "Pamidronate induces modifications of circulating angiogenetic factors in cancer patients." *Clinical Cancer Research* 8(5): 1080-1084.

Santini, D., B. Vincenzi, G. Dicuonzo, et al. (2003). "Zoledronic acid induces significant and long-lasting modifications of circulating angiogenic factors in cancer patients." *Clinical Cancer Research* 9(8): 2893-2897.

Sanz-Rodriguez, F., A. Hidalgo and J. Teixido (2001). "Chemokine stromal cell-derived factor-1 α modulates vla-4 integrin-mediated multiple myeloma cell adhesion to cs-1/fibronectin and vcam-1." *Blood* 97(2): 346-351.

Sasaki, A., B. F. Boyce, B. Story, et al. (1995). "Bisphosphonate risedronate reduces metastatic human breast cancer burden in bone in nude mice." *Cancer Res* 55(16): 3551-3557.

Sati, H. I. A., M. Greaves, J. F. Apperley, et al. (1999). "Expression of interleukin-1 β and tumour necrosis factor- α in plasma cells from patients with multiple myeloma." *British Journal of Haematology* 104(2): 350-357.

Sato, K., S. Kimura, H. Segawa, et al. (2005). "Cytotoxic effects of gammadelta t cells expanded ex vivo by a third generation bisphosphonate for cancer immunotherapy." *Int J Cancer* 116(1): 94-99.

Sato, M., W. Grasser, N. Endo, et al. (1991). "Bisphosphonate action. Alendronate localization in rat bone and effects on osteoclast ultrastructure." *J Clin Invest* 88(6): 2095-2105.

Scavelli, C., B. Nico, T. Cirulli, et al. (2008). "Vasculogenic mimicry by bone marrow macrophages in patients with multiple myeloma." *Oncogene* 27(5): 663-674.

Schenk, R., W. A. Merz, R. Mühlbauer, et al. (1973). "Effect of ethane-1-hydroxy-1,1-diphosphonate (ehdp) and dichloromethylene diphosphonate (cl 2 mdp) on the calcification and resorption of cartilage and bone in the tibial epiphysis and metaphysis of rats." *Calcif Tissue Res* 11(3): 196-214.

Schmidmaier, R., M. Simsek, P. Baumann, et al. (2006). "Synergistic antimyeloma effects of zoledronate and simvastatin." *Anticancer Drugs* 17(6): 621-629.

Senaratne, S. G., G. Pirianov, J. L. Mansi, et al. (2000). "Bisphosphonates induce apoptosis in human breast cancer cell lines." *Br J Cancer* 82(8): 1459-1468.

Senaratne, S. G., J. L. Mansi and K. W. Colston (2002). "The bisphosphonate zoledronic acid impairs ras membrane [correction of impairs membrane] localisation and induces cytochrome c release in breast cancer cells." *Br J Cancer* 86(9): 1479-1486.

Sezer, O., U. Heider, C. Jakob, et al. (2002). "Human bone marrow myeloma cells express rankl." *Journal of Clinical Oncology* 20(1): 353-354.

Shiozawa, Y., E. A. Pedersen, A. M. Havens, et al. (2011). "Human prostate cancer metastases target the hematopoietic stem cell niche to establish footholds in mouse bone marrow." *The Journal of Clinical Investigation* 121(4): 1298-1312.

Shipman, C. M., M. J. Rogers, J. F. Apperley, et al. (1997). "Bisphosphonates induce apoptosis in human myeloma cell lines: A novel anti-tumour activity." *Br J Haematol* 98(3): 665-672.

Shipman, C. M., P. I. Croucher, R. G. Russell, et al. (1998). "The bisphosphonate incadronate (ym175) causes apoptosis of human myeloma cells in vitro by inhibiting the mevalonate pathway." *Cancer Res* 58(23): 5294-5297.

Soki, F. N., X. Li, J. Berry, et al. (2013). "The effects of zoledronic acid in the bone and vasculature support of hematopoietic stem cell niches." *Journal of Cellular Biochemistry* 114(1): 67-78.

Solly, S. (1844). "Remarks on the pathology of mollities ossium; with cases." *Medico-chirurgical transactions* 27: 435.

Sordillo, E. M. and R. N. Pearse (2003). "Rank-fc: A therapeutic antagonist for rank-l in myeloma." *Cancer* 97(3 Suppl): 802-812.

Spencer, G. J., J. C. Utting, S. L. Etheridge, et al. (2006). "Wnt signalling in osteoblasts regulates expression of the receptor activator of nf{ κ }b ligand and inhibits osteoclastogenesis in vitro." *J Cell Sci* 119(7): 1283-1296.

Standal, T., C. Seidel, O. Hjertner, et al. (2002). "Osteoprotegerin is bound, internalized, and degraded by multiple myeloma cells." *Blood* 100(8): 3002-3007.

Stroh, M., J. P. Zimmer, D. G. Duda, et al. (2005). "Quantum dots spectrally distinguish multiple species within the tumor milieu in vivo." *Nat Med* 11(6): 678-682.

Tanaka, Y., M. Abe, M. Hiasa, et al. (2007). "Myeloma cell-osteoclast interaction enhances angiogenesis together with bone resorption: A role for vascular endothelial cell growth factor and osteopontin." *Clinical Cancer Research* 13(3): 816-823.

Tassone, P., S. Forciniti, E. Galea, et al. (2000). "Growth inhibition and synergistic induction of apoptosis by zoledronate and dexamethasone in human myeloma cell lines." *Leukemia* 14(5): 841-844.

Tassone, P., P. Neri, D. R. Carrasco, et al. (2005). "A clinically relevant scid-hu in vivo model of human multiple myeloma." *Blood* 106(2): 713-716.

Terpos, E., M. Politou, R. Szydlo, et al. (2003). "Serum levels of macrophage inflammatory protein-1 alpha (mip-1 α) correlate with the extent of bone disease and survival in patients with multiple myeloma." *British Journal of Haematology* 123(1): 106-109.

Terpos, E., O. Sezer, P. I. Croucher, et al. (2009). "The use of bisphosphonates in multiple myeloma: Recommendations of an expert panel on behalf of the european myeloma network." *Ann Oncol* 20(8): 1303-1317.

Theer, P. and W. Denk (2006). "On the fundamental imaging-depth limit in two-photon microscopy." *J Opt Soc Am A Opt Image Sci Vis* 23(12): 3139-3149.

Thomas, D. M., S. A. Johnson, N. A. Sims, et al. (2004). "Terminal osteoblast differentiation, mediated by runx2 and p27kip1, is disrupted in osteosarcoma." *The Journal of Cell Biology* 167(5): 925-934.

Thompson, K., M. J. Rogers, F. P. Coxon, et al. (2006). "Cytosolic entry of bisphosphonate drugs requires acidification of vesicles after fluid-phase endocytosis." *Molecular Pharmacology* 69(5): 1624-1632.

Tian, E., F. Zhan, R. Walker, et al. (2003). "The role of the wnt-signaling antagonist dkk1 in the development of osteolytic lesions in multiple myeloma." *N Engl J Med* 349(26): 2483-2494.

Trikha, M., R. Corringham, B. Klein, et al. (2003). "Targeted anti-interleukin-6 monoclonal antibody therapy for cancer." *Clinical Cancer Research* 9(13): 4653-4665.

Uchiyama, H., B. A. Barut, D. Chauhan, et al. (1992). "Characterization of adhesion molecules on human myeloma cell lines." *Blood* 80(9): 2306-2314.

Uchiyama, H., B. A. Barut, A. F. Mohrbacher, et al. (1993). "Adhesion of human myeloma-derived cell lines to bone marrow stromal cells stimulates interleukin-6 secretion." *Blood* 82(12): 3712-3720.

Uhr, J. W. and K. Pantel (2011). "Controversies in clinical cancer dormancy." *Proc Natl Acad Sci U S A* 108(30): 12396-12400.

Ullén, A., L. Lennartsson, K.-M. Kälkner, et al. (2008). "Zoledronic acid induces caspase dependent apoptosis in renal cancer cell lines." *Bone* 42(Supplement 1): S108-S109.

Uneda, S., H. Hata, F. Matsuno, et al. (2003). "Macrophage inflammatory protein-1 alpha is produced by human multiple myeloma (mm) cells and its expression correlates with bone lesions in patients with mm." *Br J Haematol* 120(1): 53-55.

Ural, A. U., M. I. Yilmaz, F. Avcu, et al. (2003). "The bisphosphonate zoledronic acid induces cytotoxicity in human myeloma cell lines with enhancing effects of dexamethasone and thalidomide." *Int J Hematol* 78(5): 443-449.

Vacca, A., D. Ribatti, M. Presta, et al. (1999). "Bone marrow neovascularization, plasma cell angiogenic potential, and matrix metalloproteinase-2 secretion parallel progression of human multiple myeloma." *Blood* 93(9): 3064-3073.

Vacca, A., R. Ria, F. Semeraro, et al. (2003). "Endothelial cells in the bone marrow of patients with multiple myeloma." *Blood* 102(9): 3340-3348.

Vachon, C. M., R. A. Kyle, T. M. Therneau, et al. (2009). "Increased risk of monoclonal gammopathy in first-degree relatives of patients with multiple myeloma or monoclonal gammopathy of undetermined significance." *Blood* 114(4): 785-790.

van Beek, E., E. Pieterman, L. Cohen, et al. (1999). "Farnesyl pyrophosphate synthase is the molecular target of nitrogen-containing bisphosphonates." *Biochem Biophys Res Commun* 264(1): 108-111.

van Beek, E. R., C. W. G. M. Löwik, F. H. Ebetino, et al. (1998). "Binding and antiresorptive properties of heterocycle-containing bisphosphonate analogs: Structure-activity relationships." *Bone* 23(5): 437-442.

van de Donk, N. W. C. J., H. M. Lokhorst and A. C. Bloem (2005). "Growth factors and antiapoptotic signaling pathways in multiple myeloma." *Leukemia* 19(12): 2177-2185.

van der Pluijm, G., H. Vloedgraven, E. van Beek, et al. (1996). "Bisphosphonates inhibit the adhesion of breast cancer cells to bone matrices in vitro." *The Journal of Clinical Investigation* 98(3): 698-705.

van der Pluijm, G., I. Que, B. Sijmons, et al. (2005). "Interference with the microenvironmental support impairs the de novo formation of bone metastases in vivo." *Cancer Res* 65(17): 7682-7690.

Van Driel, M., U. Gunthert, A. C. Van Kessel, et al. (2002). Cd44 variant isoforms are involved in plasma cell adhesion to bone marrow stromal cells. London, ROYAUME-UNI, Nature Publishing.

Van Riet, I., K. Vanderkerken, C. de Greef, et al. (1998). "Homing behaviour of the malignant cell clone in multiple myeloma." *Med Oncol* 15(3): 154-164.

Vande Broek, I., K. Asosingh, V. Allegaert, et al. (2004). "Bone marrow endothelial cells increase the invasiveness of human multiple myeloma cells through upregulation of mmp-9: Evidence for a role of hepatocyte growth factor." *Leukemia* 18(5): 976-982.

Vanderkerken, K., H. De Raeve, E. Goes, et al. (1997). "Organ involvement and phenotypic adhesion profile of 5t2 and 5t33 myeloma cells in the c57bl/kalwrij mouse." *Br J Cancer* 76(4): 451-460.

Vanderkerken, K., I. Vande Broek, D. L. Eizirik, et al. (2002). "Monocyte chemoattractant protein-1 (mcp-1), secreted by bone marrow endothelial cells, induces chemoattraction of 5t multiple myeloma cells." *Clin Exp Metastasis* 19(1): 87-90.

Vanderkerken, K., K. Asosingh, P. Croucher, et al. (2003a). "Multiple myeloma biology: Lessons from the 5tmm models." *Immunol Rev* 194: 196-206.

Vanderkerken, K., E. De Leenheer, C. Shipman, et al. (2003b). "Recombinant osteoprotegerin decreases tumor burden and increases survival in a murine model of multiple myeloma." *Cancer Research* 63(2): 287-289.

Varettoni, M., A. Corso, G. Pica, et al. (2010). "Incidence, presenting features and outcome of extramedullary disease in multiple myeloma: A longitudinal study on 1003 consecutive patients." *Annals of Oncology* 21(2): 325-330.

Virtanen, S. S., H. K. Vaananen, P. L. Harkonen, et al. (2002). "Alendronate inhibits invasion of pc-3 prostate cancer cells by affecting the mevalonate pathway." *Cancer Res* 62(9): 2708-2714.

Vordos, D., B. Paule, F. Vacherot, et al. (2004). "Docetaxel and zoledronic acid in patients with metastatic hormone-refractory prostate cancer." *BJU International* 94(4): 524-527.

Wahlgren, J., P. Maisi, T. Sorsa, et al. (2001). "Expression and induction of collagenases (mmp-8 and -13) in plasma cells associated with bone-destructive lesions." *The Journal of Pathology* 194(2): 217-224.

Wallace, P. K., J. D. Tario, Jr., J. L. Fisher, et al. (2008). "Tracking antigen-driven responses by flow cytometry: Monitoring proliferation by dye dilution." *Cytometry A* 73(11): 1019-1034.

Wei, Y. and J. Au (2005). "Role of tumour microenvironment in chemoresistance." *Integration/Interaction of Oncologic Growth* 15: 285-321.

Winter, M. C., I. Holen and R. E. Coleman (2008). "Exploring the anti-tumour activity of bisphosphonates in early breast cancer." *Cancer Treatment Reviews* 34(5): 453-475.

Witzig, T. E., K. M. Laumann, M. Q. Lacy, et al. (2013). "A phase iii randomized trial of thalidomide plus zoledronic acid versus zoledronic acid alone in patients with asymptomatic multiple myeloma." *Leukemia* 27(1): 220-225.

Wong, A. P., S. L. Cortez and W. H. Baricos (1992). "Role of plasmin and gelatinase in extracellular matrix degradation by cultured rat mesangial cells." *Am J Physiol* 263(6 Pt 2): F1112-1118.

Wood, J., K. Bonjean, S. Ruetz, et al. (2002). "Novel antiangiogenic effects of the bisphosphonate compound zoledronic acid." *Journal of Pharmacology and Experimental Therapeutics* 302(3): 1055-1061.

Yaccoby, S., R. N. Pearse, C. L. Johnson, et al. (2002). "Myeloma interacts with the bone marrow microenvironment to induce osteoclastogenesis and is dependent on osteoclast activity." *British Journal of Haematology* 116(2): 278-290.

Yamada, J., N. H. Tsuno, J. Kitayama, et al. (2009). "Anti-angiogenic property of zoledronic acid by inhibition of endothelial progenitor cell differentiation." *Journal of Surgical Research* 151(1): 115-120.

Yamaguchi, T., M. Yamauchi, T. Sugimoto, et al. (2002). "The extracellular calcium (Ca^{2+})-sensing receptor is expressed in myeloma cells and modulates cell proliferation." *Biochemical and Biophysical Research Communications* 299(4): 532-538.

Yang, Q., K. P. McHugh, S. Patntirapong, et al. (2008). "Vegf enhancement of osteoclast survival and bone resorption involves vegf receptor-2 signaling and beta3-integrin." *Matrix Biol* 27(7): 589-599.

Yin, L. (2005). "Chondroitin synthase 1 is a key molecule in myeloma cell-osteoclast interactions." *Journal of Biological Chemistry* 280(16): 15666-15672.

Yoneda, T. and T. Hiraga (2005). "Crosstalk between cancer cells and bone microenvironment in bone metastasis." *Biochemical and Biophysical Research Communications* 328(3): 679-687.

Yuasa, T., K. Sato, E. Ashihara, et al. (2009). "Intravesical administration of gammadelta t cells successfully prevents the growth of bladder cancer in the murine model." *Cancer Immunol Immunother* 58(4): 493-502.

Zandecki, M., V. Obein, F. Bernardi, et al. (1995). "Monoclonal gammopathy of undetermined significance: Chromosome changes are a common finding within bone marrow plasma cells." *Br J Haematol* 90(3): 693-696.

Zhang, J., C. Niu, L. Ye, et al. (2003). "Identification of the haematopoietic stem cell niche and control of the niche size." *Nature* 425(6960): 836-841.

Zipfel, W. R., R. M. Williams and W. W. Webb (2003). "Nonlinear magic: Multiphoton microscopy in the biosciences." *Nat Biotechnol* 21(11): 1369-1377.

Zlei, M., S. Egert, D. Wider, et al. (2007). "Characterization of in vitro growth of multiple myeloma cells." *Experimental hematology* 35(10): 1550-1561.